Synthesis and organometallic chemistry of rhodium and iridium complexes of macrocyclic PCP and POCOP pincer ligands

by

Baptiste Leforestier

A thesis submitted in partial fulfilment of the requirements for the degree of Doctor of Philosophy in Chemistry

University of Warwick, Department of Chemistry

January 2020

Table of Contents

Acknowledgements

Firstly extensive thanks go to Dr Adrian Chaplin for giving me this opportunity to work in this group and for his unwavering support during these four years, through the ups and downs and right until the very (very) end. Your sheer enthusiasm and your ability to come up with an endless supply of ideas even in the toughest spots have been a tremendous help in completing this thesis, and for that I am grateful.

Thanks are also owed to the support staff who have been essential in completing this thesis. Particular thanks must be given to Ivan Prokes and Rob Perry for their support and unwavering eagerness to help in carrying out NMR analyses. Thanks also go to Lijiang Song, Phil Aston and Jim Morrey for mass spectrometry analysis and advice.

To the Chaplin group; Caroline, you will be pleased to know that as it is finally my turn to say "it's finished, see you tomorrow!", I feel I can finally understand your accent. Korean Billy has certainly played a role in that achievement, but I suspect from the very beginning you have made many efforts to make that possible, for that I am so grateful. More seriously though, thank you for all the fun times there has been along these years, from demonstrating the feasibility of fitting in a locker, to getting lost in the streets of Tokyo and fortuitously ending up in the middle of the Tokyo Dome and an amusement park, to those weekends in the labs listening to the next Eurovision entries (Zee-e-e-e-e-ero graa-a-a-avity!!), it has been a blast. Jack, there has been much laughs, I could barely walk. Thank you so much for guiding me through the meanders of British politics and for teaching me about proper British good manners and etiquette. I can confidently say I had never seen a true excel spreadsheet before I met you. I know you are always "working on it" but I can tell you for sure that as a human and as a friend, you are doing amazing and I feel privileged to have the chance to know you

Tom, as it is time for me to sashay away, I realise from writing these lines just how much I have learned thanks to you. And that's not counting the discovery of the BA's test kitchens YouTube channel, which has eaten an inordinate amount of my time. Thank you for those late night discussions in the car on the way back from…. well anywhere really, and for being who you are. I feel that I have truly become a better person from meeting you. Gemma, I did not rank well at all on your scale of the most attractive men in the group, and you said I was also the rudest. Rude. I am still not over that. Just kidding!! It has been a lot of fun working with you as *colleagues* all these

years. Still kidding!! You are truly a friend and I am happy to have had so much fun in your company (not kidding).

Amy, Sam, I feel truly privileged to have had the opportunity to know you and work alongside you. Your presence in the group has been a breath of fresh air and fun and for that I am ever grateful. I very much look forward to reading your blog about your common passion for food. And condiments. For the record, I am definitely more shallots than red onions. Matt, a.k.a. Chemistry's Doctor Matthew Gyton, a.k.a. CDMG, a huge thank you for your help and supervision for the past four years, you have been a real role model. I have learned so much by just being at the next fume cupboard and shamelessly taking advantage of your encyclopaedic knowledge of chemistry, music, video games (have you bought that Switch yet?), the French revolution and Napoleonic wars (how?), the *feuerzangenbowle* (not quite right). Thank you for helping me understand the lyrics these whippersnappers play on Radio 1, and for teaching me about bogans and dropbears. This also means you have spent close to four years being the unfortunate guinea pig for all my jokes: for that, well done … and I'm Thorry (not Thorry). Ruth and Rhiann, with your guidance my vocabulary has grown tremendously in very short time and in unexpected ways. You have both made me feel very welcome in the group right from the very start, it would not have been the same without you. Finally to the newest members of the group, Jenifer, Alex and Matt, a.k.a. New Matt a.k.a impending coffee …. or was it coffee soon? It has been a pleasure to welcome you on the foreigners' side of the lab , although I am still mystified as to why you would move your car when… anyway. It has been a pleasure to meet you all and wish you all the best for the rest of your time in the group and beyond.

Julien, il aurait été impensable pour moi d'en arriver où j'en suis sans ton indéfectible soutien toutes ces années. Tu as réussi à me supporter dans tous les moments les plus difficiles (sans aucun doute le 13ème des travaux d'Hercule), tu as été présent dans tous les meilleurs et je ne pourrais jamais te remercier assez de m'avoir porté jusqu'ici. Où que l'avenir nous mène, je ne l'envisage pas un instant sans toi. Un immense merci également à Claire, ma meilleure amie. Quel chemin nous avons fait depuis Mme Mouton! Je suis fier de nous. A chaque fois qu'on se revoit, c'est comme si je n'étais jamais parti loin et j'attends avec impatience la prochaine pour qu'on fête tout ça. Et enfin maman, ou plutôt devrais-je épeler Maman, car ton soutien et ton cœur grand comme ça méritent bien une lettre capitale. Tu es incroyable, et je te dois tellement que la liste n'en finirait jamais… On a tous les deux fait un sacré bout de chemin, depuis, ne trouves-tu pas ?

Declaration of Collaborative and Published Work

This thesis is submitted to the University of Warwick in support of my application for the degree of Doctor of Philosophy. It has been composed by myself and has not been submitted in any previous application for any degree

The work presented (including data generated and data analysis) was carried out by the author except in the cases outlined below:

- Crystallographic analysis of all compounds, for which solid-state structures are described, was conducted by Dr Adrian B. Chaplin, Associate Professor, University of Warwick.
- Initial optimization of conditions for the preparation of compounds **1** and **2** was conducted by Dr Matthew R. Gyton, PDRA in the Chaplin group, as well as the initial synthetic work targeting **2•BH$_3$**, with the preparation of **8** and **8-Me** (Chapter 2).
- Acquisition of the NMR data for the measurement of spin-lattice relaxation times *T*1 for compounds M-15o,c was conducted by Dr Matthew R. Gyton (Chapter 3).
- Acquisition of VT-NMR data for **Rh-25o** and **^{13}C-Rh-25o** on high field NMR instruments was also conducted by Dr Matthew R. Gyton (Chapter 4).

Parts of this thesis have been published by the author:

B. Leforestier, M. R. Gyton, A. B. Chaplin, Synthesis and group 9 complexes of macrocyclic PCP and POCOP pincer ligands, *Dalton Trans.* **2020**, *in press*

Abbreviations

Ar	Aryl
Ar’	3,5-di-*tert*-butylphenyl
Ar^F	3,5-bis(trifluoromethyl)phenyl
ATR	Attenuated Total Reflection
BDE	Bond Dissociation Energy
br	Broad
calcd	Calculated
CCDC	Cambridge Crystallographic Data Centre
COD	1,5-cyclooctadiene
COE	cyclooctene
COSY	Correlation SpectroscopY
Cnt	Centroid
Cy	Cyclohexyl
DiFB	Difluorobenzene
DFT	Density Functional Theory
eq	Equivalents
ESI	Electrospray ionization
Et	Ethyl
fac	Facial
FPT	Freeze-pump-thaw
fwhm	Full width at half maximum
gem	Geminal
HMDS	Hexamethyldisilazane / bis(trimethylsilyl)amide

HMDSO	Hexamethyldisiloxane
HMBC	Heteronuclear Multiple Bond Correlation
HR	High Resolution
HSQC	Heteronuclear Single bond Quantum Coherence
*i*Pr	*iso*-propyl
IR	Infrared
LR	Low Resolution
Me	Methyl
mer	Meridional
MS	Mass Spectrometry
Ms	Mesyl / Methanesulfonic
m/z	Mass to charge ratio
NBD	Norbornadiene
NBE	Norbornene
*n*Bu	linear *n*-butyl
NHC	*N*-heterocyclic carbene
NMM	*N*-methylmorpholine
NMP	*N*-methyl-2-pyrrolidone
NMR	Nuclear Magnetic Resonance
o, m, p	*ortho, meta, para*
Ph	Phenyl
ppm	Part per million
Py	Pyridyl
r.t.	Room temperature

$t_{1/2}$	Half-life
*t*Bu	*tertio*-butyl
TBE	*tertio*-butylethylene
THF	Tetrahydrofuran
TLC	Thin Layer Chromatography
TMS	Tetramethylsilane
TOF	Turnover frequency
TON	Turnover number
UV-vis	UltraViolet-visible
VE	Valence Electron
VT	Variable temperature
XRD	X-ray diffraction

Abstract

Conferring high thermal stability and supporting a broad range of metal-based reactivity, *mer*-tridentate "pincer" ligands have become ubiquitous in contemporary organometallic chemistry and transformed homogeneous catalysis. Phosphine-based systems bearing a central aryl donor, derived from *meta*-xylene (PCP) or resorcinol (POCOP), are archetypical examples and complexes of rhodium and iridium have in particular found successful applications in inert bond activation reactions, with the catalytic dehydrogenation of alkanes most remarkable. Motived by the desire to further our understanding of these processes, the objective of this project was to explore the organometallic chemistry of macrocyclic PCP and POCOP pincer complexes featuring mechanically interlocked hydrocarbon substrates: [2]rotaxane and [2]catenanes. The interwoven topology of these systems was chosen as a means to circumvent problems associated with weak metal hydrocarbon interactions and provide a well-defined platform for interrogating their subsequent activation.

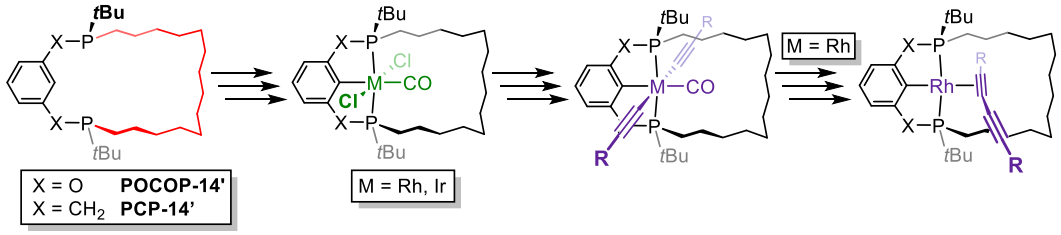

The multistep synthesis of macrocyclic **POCOP-14'** and **PCP-14'** proligands is reported herein, using racemic or asymmetric procedures, respectively. These proligands can be readily metalated and homologous series of $M^{I}(CO)$ and $M^{III}Cl_2(CO)$ derivatives (M = Rh, Ir) were isolated and fully characterised in solution and the solid state. The latter were critically evaluated as precursors for the construction of interlocked 1,3-diyne derivatives by Grignard-mediated alkynylation, decarbonylation, and C(sp)–C(sp) bond reductive elimination. Using this strategy, [Rh(POCOP-14)(Ar'C_4Ar')] (**Rh-25o**, Ar' = 3,5-tBu$_2$C$_6$H$_3$) was most notably isolated and its dynamic behaviour and reactivity comprehensively studied. This interlocked complex remarkably displays reversible C(sp)–C(sp) bond activation, but under carefully chosen conditions the axle can be reduced all the way to the corresponding 1,4-diarylbut-1-ene.

Chapter 1

Introduction

1.1. Overview of pincer ligands

Pincer ligands are tridentate ligands that generally favour a meridional coordination mode.[1] Both their κ^3-chelating nature as well as the relative inflexibility of their interaction with a metal centre confer very high thermal stability to their complexes. These ancillary ligands support reactions with strong ligands (CO, isocyanides) as well as strong oxidizing or reducing agents whilst retaining their pincer geometry, and have found wide applications in coordination chemistry and catalysis.[1–9]

Upon coordination, pincer ligands form a structure that consists of two fused metallacycles defined by two donor side arms and joined at a central donor atom. Inherently, there are endless possibilities to modulate each individual component of this scaffold which allows for tunable and precise control of the 1st and 2nd coordination spheres and therefore on the electronics and steric characteristics of the bound metal centre (Figure 1.1).

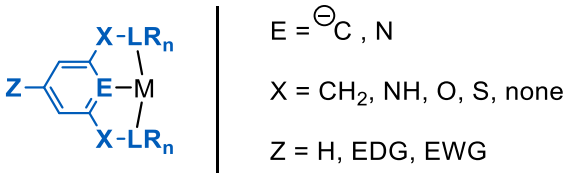

Figure 1.1. General structure of an aromatic pincer backbone.

In the case of the aromatic example depicted in Figure 1.1 variations on the central donor atom E as well as the nature of the L donors will largely affect the overall electron donating capability of the ligand, whilst leaving the sterics essentially untouched. Introducing various substituents on the aromatic cycle enables finer control on the electronic properties of the pincer as well. Conversely, the number and nature of R substituents on the flanking arms allow for a direct modification of the steric profile about the reactive metal centre and can be a platform for the introduction of chirality. Finally the size of the linker X, its nature, or even its absence will also subtly affect the properties of the complex through modification

of the metallacycle's size, its symmetry (C_2 / C_s) as well as the bite angle and flexibility of the scaffold.

Consequently, since the first monoanionic, phosphine-based examples reported by Shaw in 1976,[10] and particularly since the 1990s, pincer ligands have attracted considerable interest and a large number of structural variations have been published. In a recent review,[1] Crabtree and Peris developed a classification that is reflected in Figure 1.2, *i.e.* according to their symmetry, as well as their overall charge (in the ionic formalism).

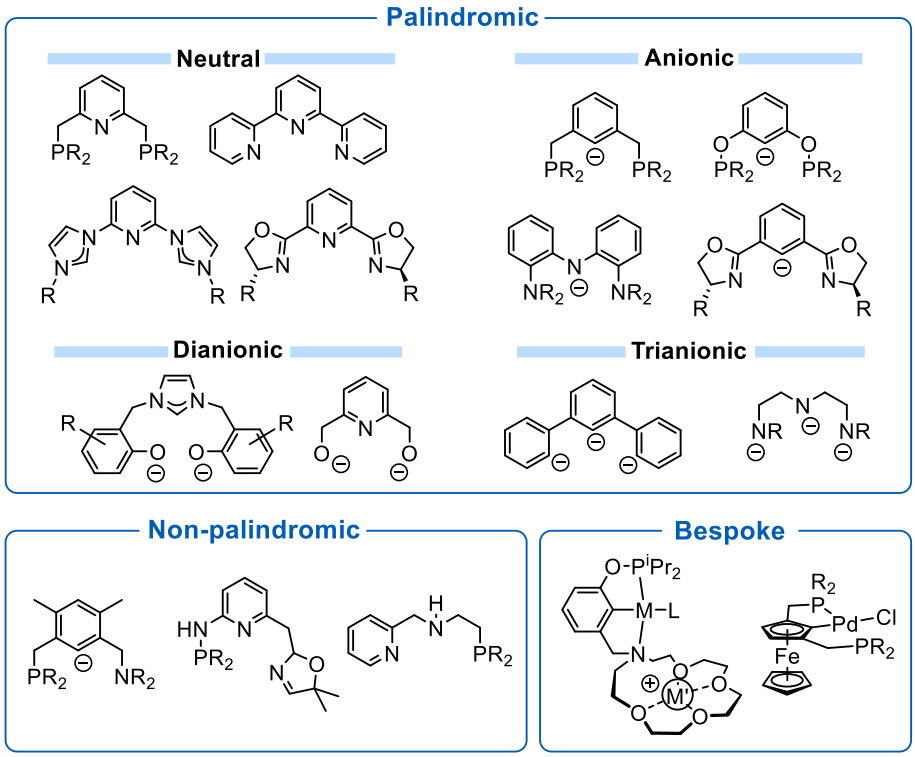

Figure 1.2. Examples of structural variations of the pincer scaffold.

Palindromic pincers are by far the most common, in particular monoanionic variants where the central donor bears a negative charge. Notable examples are based on the PCP and POCOP backbones first reported by Shaw *et. al.*[10] in 1976 and in 1999-2000 by the groups of Shibasaki, Jensen and Bedford,[11–14] respectively, and these scaffolds have found extensive application in catalysis and hydrogenation / dehydrogenation reactions (*vide infra*). Creation of NCN ligands using chiral oxazolines gave rise to applications in asymmetric catalysis, notably in asymmetric transfer hydrogenation reactions of ketones.[15–18] Neutral examples include the well-known PNP[19,20] and terpy[21] ligand scaffolds.

Dianionic and trianionic ligands are comparatively rarer and most commonly associated with the harder, more oxophilic early transition metals (Ti, Zr, Hf, Ta, Cr, W, Re).[22]

In recent years, more elaborate structural variations have been reported that go beyond simple tuning of sterics and electronics and aim to impart additional functionality to the second coordination sphere. For instance, pincer complexes incorporating a metallocene moiety have been reported whereby the metallocene moiety allows for the tunability of its catalytic properties through a smaller *pseudo*-bite angle (P-M-P), the nature of its central atom (Fe, Ru) or its redox state.[23–26] Other examples have been reported by the Miller group which feature an aza-crown ether as one of the donor arms that enables the tuning of the complex's catalytic properties *via* a cation controlled, reversible coordination of an ether moiety to the metal centre and/or through the introduction of a lewis acidic site in the second coordination sphere.[27–32]

As it is most relevant to the content in this thesis, this chapter will focus on monoanionic, phosphine-based, aromatic PCP and POCOP pincer ligands and the coordination chemistry and reactivity of their iridium and rhodium complexes.

1.2. Phosphine based pincer complexes of Rh and Ir.

Formation of PXCXP complexes normally involves metallation of the corresponding neutral proligands, involving phosphine-directed C–H bond activation. For rhodium and iridium, the metallation usually employs diene complexes as precursors, as these ligands are readily displaced by the two phosphorus donors that benefit from the chelate effect (Scheme 1.1).

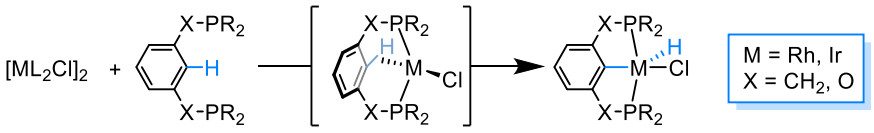

Scheme 1.1. Usual metallation pathway for PXCXP-based pincers via C–H bond activation.

After coordination of the two donor arms, the central aromatic C(sp^2)–H bond is pre-organised in close proximity to the metal centre, which kinetically facilitates the insertion and thereby of the new M–C σ-bond integrated in the two

metallacycles. This method is particularly attractive as it does not necessitate any pre-treatment of the pincer ligand in order to achieve the desired regioselectively.

Remarkably for Rh and Ir metal centres, this cyclometallation strategy could be expanded to C(sp^2)–C(sp^3) bonds, as shown by Milstein *et. al.* in the 1990s (Scheme 1.2).[33–36]

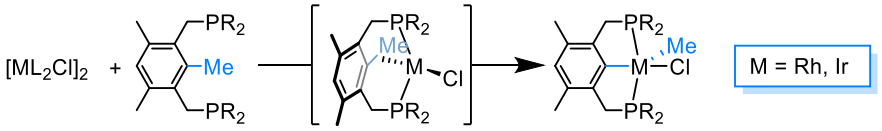

Scheme 1.2. Metallation of a PCP pincer ligand *via* C(sp^2)-C(sp^3) bond activation.

This result is particularly notable as the activation of C–C bonds by direct metal insertion has been shown to be both thermodynamically and kinetically less favourable than insertion into competing C–H bonds that are statistically more ubiquitous, less sterically encumbered and less directional.[37,38] In Milstein's approach, coordination of the pincer scaffold *via* its two phosphine arms allows for a well-defined preorganisation of the central C–C bond in close proximity to the metal, thereby essentially eliminating the entropic term associated with this reaction. The reaction is further favoured thermodynamically by the relief of the strain that was imposed upon coordination of the phosphine moieties and the enforced twisting of the aryl centre prior to C–C bond cleavage.

These very stable complexes have attracted significant attention in the past decades, in great part due to their demonstrated ability to cleave bonds which would otherwise be considered inert, namely C–H , C–C, C–O or C–X (X = F, Cl, Br, I). This reactivity as well as some selected catalytic applications are reviewed herein.

1.3. Inert bond activation by Rh and Ir complexes of PXCXP ligands.

The selective activation of inert bonds, such as single C–H and C–C bonds as found in alkanes, represents a major challenge of growing interest in light of the wide availability of low-cost, yet untapped, saturated petrochemical feedstocks.[39–41] Developments in this area, combined with the ubiquitous nature of these bonds in most compounds involved in the pharmaceutical and petrochemical industries,

have the potential to expand the possibilities for efficient substrate functionalization, for example to shorten multistep syntheses in the field of drug discovery or to provide useful building blocks for the polymer and materials industries.[42–44]

Current methods to convert saturated alkanes to value-added compounds usually require forcing conditions and are very energy-consuming.[45–49] Thus, the development of alternative solutions in the form of homogeneous catalysis involving transition metals has gained increasing attraction.[42,47,50,51] In this area, Rh and Ir complexes of PXCXP ligands (X = O, CH_2) have already shown promising results, of which selected examples are highlighted hereunder.

1.3.1. C–H bond activation

Direct C–H bond oxidative addition by pincer complexes usually requires the generation of a low-valent , highly reactive 14VE metal centre in oxidation state (I). Low-coordinate complexes (Scheme 1.3), can be generated by dehydrohalogenation of $M^{III}(H)(Cl)$ derivatives (top), or from the polyhydride/dihydrogen species in the presence of a sacrificial hydrogen acceptor (bottom).[6,52]

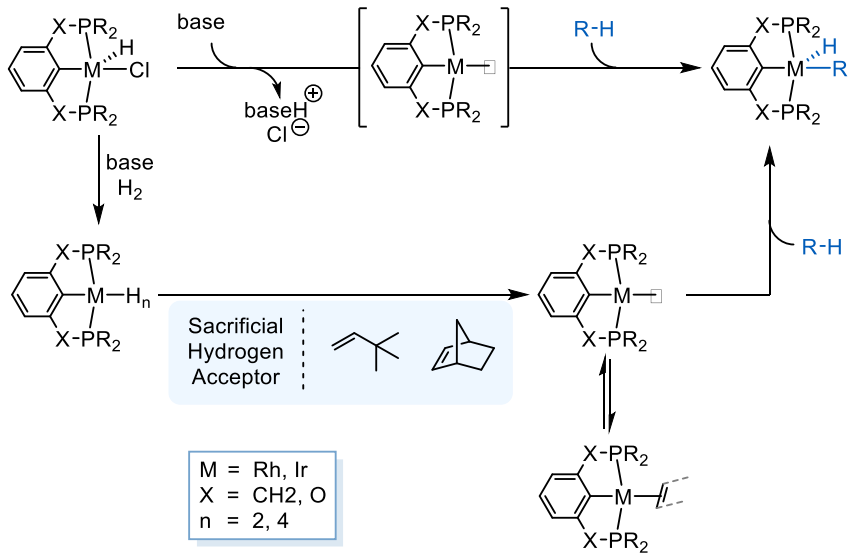

Scheme 1.3. Generation of low-valent 14VE complexes for subsequent C–H bond activation.

Astonishingly, very few examples of C–H bond activation mediated by {(PXCXP)Rh} fragments have been reported in the literature, with the exception of rather more acidic C(sp)–H bonds, in the context of alkyne dimerization

reactions (*vide infra*).[53] This is especially surprising, given the extensive chemistry established for non-pincer analogues such as the {Rh(PMe$_3$)$_2$Cl} fragment, which have been found to be very active in alkane dehydrogenation reactions for example.[54–56] Perhaps counterintuitively, calculations later showed that replacing a chloride ligand for a phenyl with a stronger *trans* influence disfavours oxidative addition of C–H bonds in the coordination plane, due to the significant weakening of the M–C and M–H bonds arising from such addition.[57]

On the other hand, reports of efficient alkane dehydrogenation reactivity by {(PCP)Ir} fragments in the late 1990's prompted a plethora of studies in the more general field of C–H bond activation by this system (Figure 1.3). In addition to the ability to activate C(sp^3)–H bonds inherent in the dehydrogenation of alkanes, the Goldman group reported in 2000 the facile oxidative addition of aryl and alkenyl C(sp^2)–H bonds to low-valent {(PCP)Ir} fragments generated from the corresponding dihydride species treated with a sacrificial hydrogen acceptor.[58]

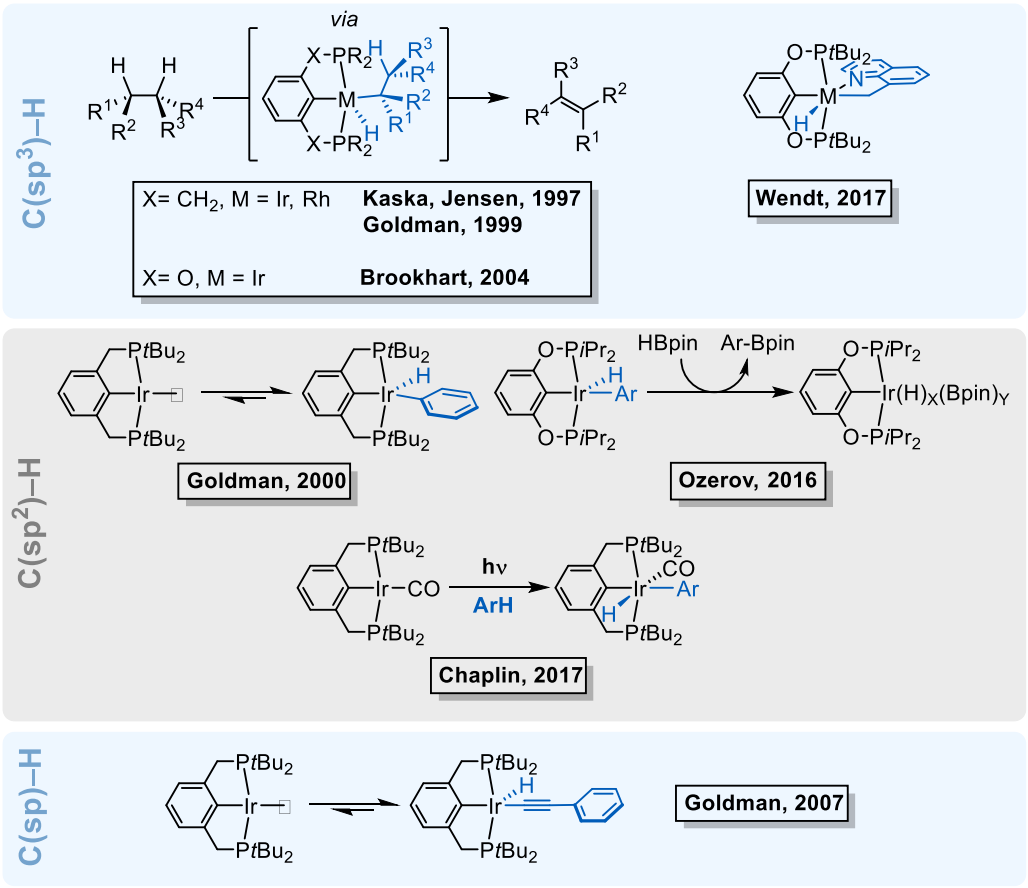

Figure 1.3. Selected examples of C–H bond activation reactions by {(PXCXP)Ir} fragments.

They note in particular the dynamic nature of such activations and their reversibility, as arene exchange was observed to occur very rapidly even on the NMR timescale. These findings were later substantiated by similar reports, with examples of directed activation of aromatic substrates bearing coordinating groups,[59] or an adamantyl-substituted PCP pincer with improved stability.[60]

The latter report on adamantyl-substituted backbones also highlighted the ability of {(POCOP)Ir} congeners to activate C(sp^2)–H and C(sp^3)–H bonds, building upon earlier reports by Brookhart and co-workers in 2004,[61] and later used in the context of borylation catalysis by Ozerov *et. al.*.[62] In 2017, the Chaplin group published an alternative approach to generating a 14VE fragments, whereby a square planar [(PCP)Ir(CO)] complex undergoes reversible C(sp^2)–H bond activation after photochemically promoted dissociation of the carbonyl ligand.[63]

Whilst the activation of C(sp^3)–H bonds is well established as a necessary requirement to alkane dehydrogenation reactions, few examples of isolated [(PXCXP)Ir(alkyl)(hydride)] complexes have been reported in the literature. A recent example by Wendt *et. al*. involves a cyclometallated 8-methylquinoline or 2-DMAP complex.[64] In this study supported with DFT calculations, the authors note that despite the presence of potential directing groups, the activation itself is not chelation assisted: precoordination of the pyridine moiety would result in the formation of 16VE complex upon which oxidative addition is not favoured.[65]

Finally, C(sp)–H bond activation was reported in 2007 by the Goldman group as well, with the isolation of a phenylalkynyl hydride complex which may further react with a second equivalent to promote the dimerization of phenylacetylene (*vide infra*).[66]

Whilst most organometallic chemistry pertaining to Rh and Ir complexes relies on oxidation states (I) and (III), it is worth mentioning that in the case of Ir the ability to reach higher oxidation states and the existence of Ir(V) complexes has been documented, either as reactive intermediates in the context of C–H activation processes or as isolated compounds.[67–71] In a recent example by the Goldman group, a double arene C–H activation was achieved by reacting a {(PCP)Ir} fragment with biphenyl or phenanthrene (Scheme 1.4).[72]

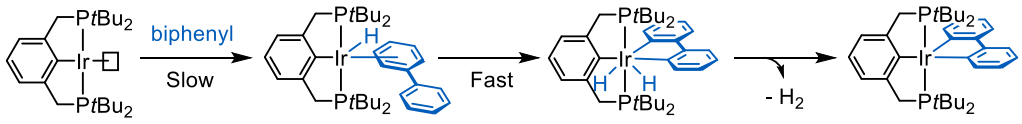

Scheme 1.4. Single and double C–H bond activation of biphenyl by a {(PCP)Ir} fragment.

After an initial (reversible) oxidative addition to give an Ir(III) aryl hydride, a second oxidative addition occurs even more rapidly to give an Ir(V) dihydride complex which rapidly loses H_2. This mechanism was substantiated by DFT calculations, which indicated the second oxidative addition was even easier than the first, as a result of the pre-positioning of the substrate and eliminating any entropic penalty otherwise associated with this reaction.

1.3.1.1. Application in alkane dehydrogenation reactions.

The first example of alkane dehydrogenation by a transition metal complex was reported by Crabtree in 1979 and established *tert*-butylethylene as a versatile H_2 acceptor (Scheme 1.5).[73] Indeed this alkene is generally too bulky to form stable π-complexes with reactive low coordinate metal centres and the absence of allylic protons and therefore of any possibility to isomerise further avoids any inhibition effect.

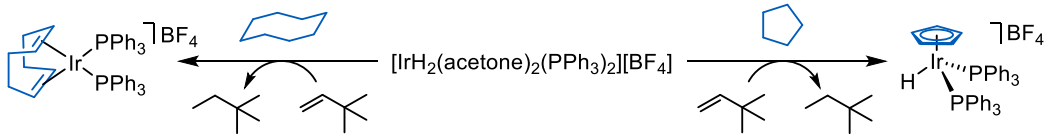

Scheme 1.5. Dehydrogenation reaction of cycloalkanes using *tert*-butylethylene as sacrificial hydrogen acceptor.

In the late 90s the first examples making use of PCP pincer complexes of Rhodium and Iridium were reported by Goldman, Kaska and Jensen, taking full advantage of this class of compounds' great thermal stability (Scheme 1.6).[74–77]

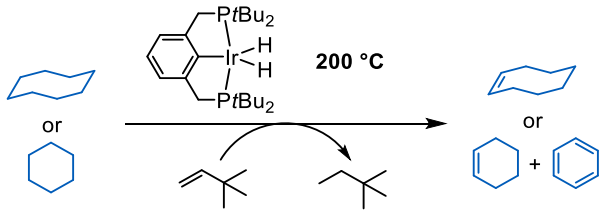

Scheme 1.6. Dehydrogenation reaction of cycloalkanes by a PCP-based pincer Ir complex.

An immediate comparison may be made between the two metals as in the dehydrogenation of COA in the presence of TBE. The reaction proceeds at a rate of 12 turnovers/min at 200 °C with little to no decomposition for the Iridium complex, but only 1.8 turnover/hour and significant decomposition was observed for the rhodium counterpart. These results may be rationalized in terms of general ability to shuttle between oxidation states (I) and (III) for both metals. For rapid catalysis, neither state (I) or (III) should be exceedingly favoured over the other. Thus, with an iridium centre that favours the M(III) oxidation state, a strong trans influence, anionic central donor is beneficial in disfavouring that same state. Whereas for its rhodium congener, which already naturally favours the +I oxidation state, a high trans influence ligand further tips the balance towards that same state by disfavouring even more the formation of Rh-H and Rh-C bonds. Accordingly, much greater performance in alkane dehydrogenation reactions could be obtained from carbazole based {(PNP)Rh} complexes (TON up to 340, TOF up to 500/h), *i.e.* with a weaker trans influence central donor.[78] Under the same conditions the {(PNP)Ir} analogue was found to be unreactive, the absence of high trans influence ligand causing the system to stop and rest in oxidation state +III as a dihydride complex. Consequently, most major developments pertaining to monoanionic ligand based pincer complexes mediating alkane dehydrogenation reactions used an iridium metal centre. Another landmark was achieved in 1997 as well, with the reports of catalysts [(*t*Bu$_4$-PCP)Ir(H)$_2$] and [(*i*Pr$_4$-PCP)Ir(H)$_2$] effectively promoting the alkane dehydrogenation reaction of cyclodecane to cyclodecene in the absence of a sacrificial hydrogen acceptor.[57] The reaction was carried out at 200 °C under reflux conditions, with the loss of gaseous hydrogen offsetting the unfavourable thermodynamics of the reaction.[57,79] The latter, less bulky catalyst proved more efficient exhibiting 1000 turnovers, a result further improved by installing electron-donating substituents in the *para*-position of the aryl scaffold.[80] The modularity of the pincer scaffold has subsequently led to improvements in catalytic performance in alkane dehydrogenation reactions (Figure 1.4). For instance in 2004, the bis(phosphinito) POCOP analogues with various substituents on the backbone were shown to enable turnover numbers up to 2200 with initial turnover frequencies up to 2.4/s (144/min) at 200 °C, significantly higher than the bis(phosphino) pincer complexes and with matching stability.[81–83]

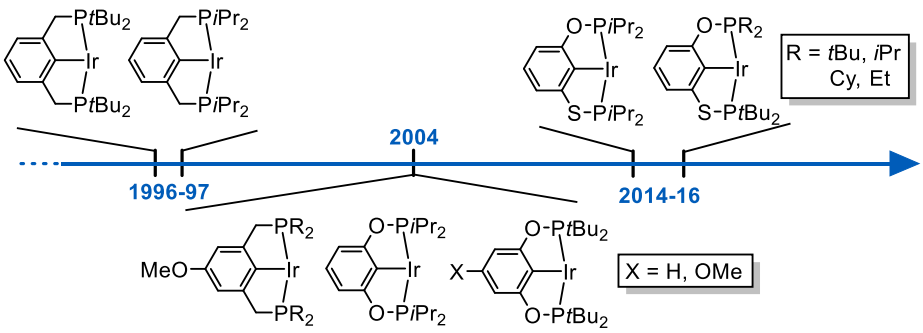

Figure 1.4. Structural variations for improved alkane dehydrogenation reaction catalysis.

More recently, Huang and co-workers reported the use of a non-palindromic (POCSP)Ir system which was demonstrated to be a very active dehydrogenation catalyst with TONs up to 5901 for the COA/TBE system, despite lower initial rates than POCOP analogues.[84,85] This system also showed higher activity in the dehydrogenation reaction of linear alkanes to form α-olefins, albeit with the concomitant isomerisation of the terminal alkenes to *trans*- and *cis*- internal alkenes, which decreased the overall regioselectivity for the transformation. This issue is also observed in PCP and POCOP complexes when applied to dehydrogenation of linear alkanes, with the isomerisation unavoidable under the reaction conditions required to promote dehydrogenation (Scheme 1.7).[86] In that regard the {(POCSP)Ir} system also improved upon its predecessors, with Huang *et. al*. showing that performing the reaction at a reduced temperature of 100 °C the system retained appreciable activity for the n-octane/TBE transfer dehydrogenation whilst completely avoiding any isomerisation product with 14 TONs.

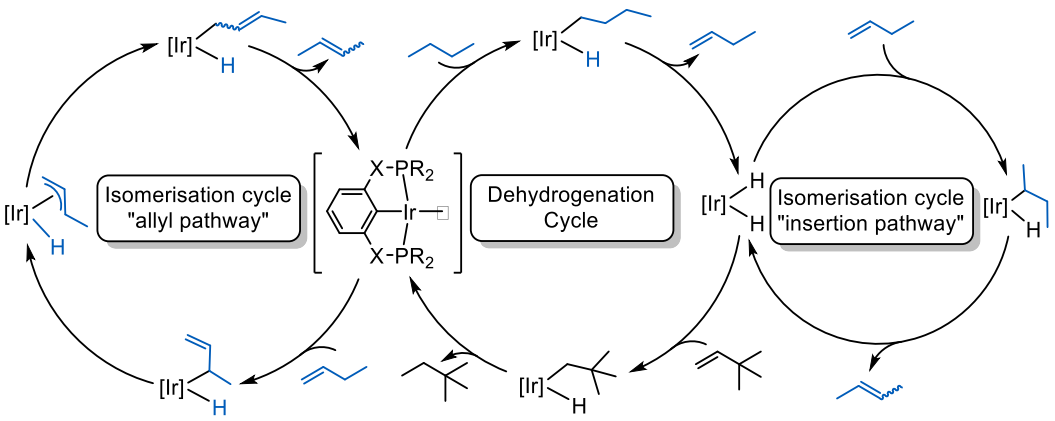

Scheme 1.7. Mechanistic cycles for the pincer iridium-catalysed n-alkane/TBE transfer dehydrogenation and terminal alkene isomerisation. Illustrated here with n-butane.

1.3.1.2. Application in terminal alkyne coupling

The facile cleavage of *sp*-hybridized C–H bonds as well as the established ability of unsaturated substrates to insert into a M–H bond (M = Rh, Ir) paves the way for applications in C–C bond forming reactivity. In 2007, the (PCP)Ir system was successfully applied in the context of alkyne dimerization (Scheme 1.8).[66] The reaction proceeds *via* activation of a first equivalent of alkyne to yield an alkynyl hydride complex. Subsequent insertion of a second equivalent of alkyne into the Ir–H bond yields a *E*-alkenyl alkynyl or *gem*-alkenyl alkynyl complex, which can undergo reductive elimination to yield the corresponding enynes, depending on the geometry and sterics around the reactive centre. Indeed for this specific example, the head-to-tail insertion product does not undergo reductive elimination, most likely as a result of unfavourable orientation of the alkenyl ligand orbitals with regards to the alkynyl. On the other hand, the head-to-head insertion product undergoes a facile reductive elimination. Together with the reversibility of the insertion step, this system is able to yield the *E*-enyne selectively.

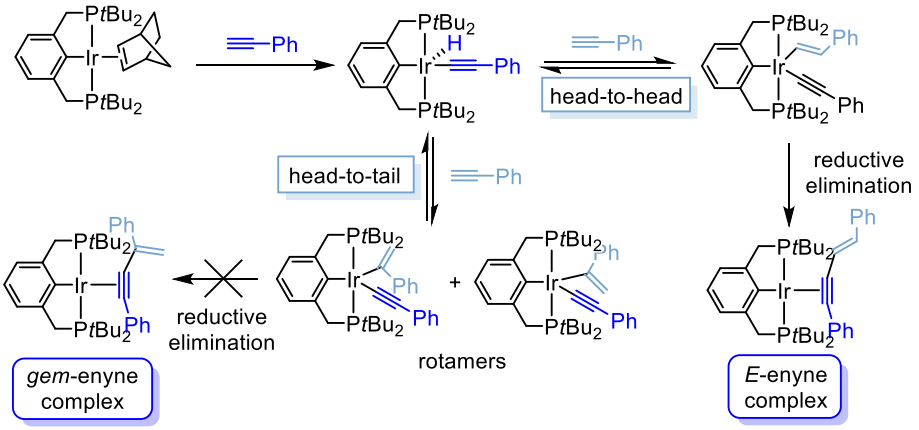

Scheme 1.8. Mechanism of {(PCP)Ir} mediated phenylacetylene dimerization reaction.

The scope of catalysts was expanded in 2014 by Ozerov and co-workers to {(PXCXP)Rh} systems.[53] Whilst these catalysts also promote the dimerization of alkynes in near quantitative conversion, they proved much less selective than the previously described {(PCP)Ir} system, yielding a mixture of *gem*-, *E*-enynes as well as oligomers (Table 1.1). Crucially, it was observed that the selectivity as well

as the rate were largely dependent on the nature of the backbone (POCOP vs PCP), the substituents on the phosphine donors (*t*Bu vs *i*Pr) and the alkyne substrate but no clear trend could be established.

Table 1.1. *gem*- / *E*-enyne ratios for (PXCXP)Rh-based dimerization catalysts.

	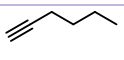	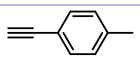	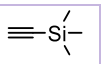
{(iPr$_4$-POCOP)Rh}	3.8	0.42	1.8
{(tBu$_4$-POCOP)Rh}	5.3	0.15	3.2
{(iPr$_4$-PCP)Rh}	3.6	0.39	0.25

1.3.2. C–C bond activation

The activation of C–C bonds remains a challenge as direct metal insertion has been shown to generally be thermodynamically and kinetically less favourable than insertion into competing C–H bonds. The latter are statistically more ubiquitous, less sterically encumbered and less directional.[37,38] In many cases, this results in a substantially greater activation energy barrier to oxidative addition and the reverse reaction pathway, the reductive elimination, is frequently thermodynamically favoured.[87] As a result, most examples pertain to C–C bonds that are subjected to strain, as can be found in small ring systems of 4 or less atoms, the relief of which becomes a driving force for the reaction as illustrated in 2014 by Goldman et. al. using a biphenylene C–C bond (Scheme 1.9, A).[88] After generation of the reactive 14VE species {(PCP)Ir}, an initial C–H bond oxidative addition occurs selectively before fully converting to the C-C addition product upon heating to 125 °C (*t*Bu) or at room temperature (*i*Pr).

In 2016, Jones *et. al.* reported that a similar reaction is possible with the 5 membered ring of fluorenone to give a carbonyl biphen complex (Scheme 1.9, B).[89] The (POCOP)Ir system was also reported to enable C–C bond activation in a recent study by Koridze et. al.,[90] who showed that EtOH (and primary alcohols) are readily decarbonylated to form a stable carbonyl hydrido methyl complex as a mixture of isomers (Scheme 1.9, C). Further mechanistic investigations suggested that instead of a direct C–C oxidative addition, EtOH is first dehydrogenated to acetaldehyde, which can undergo C–H oxidative addition to form an acetyl hydride complex before decarbonylating.

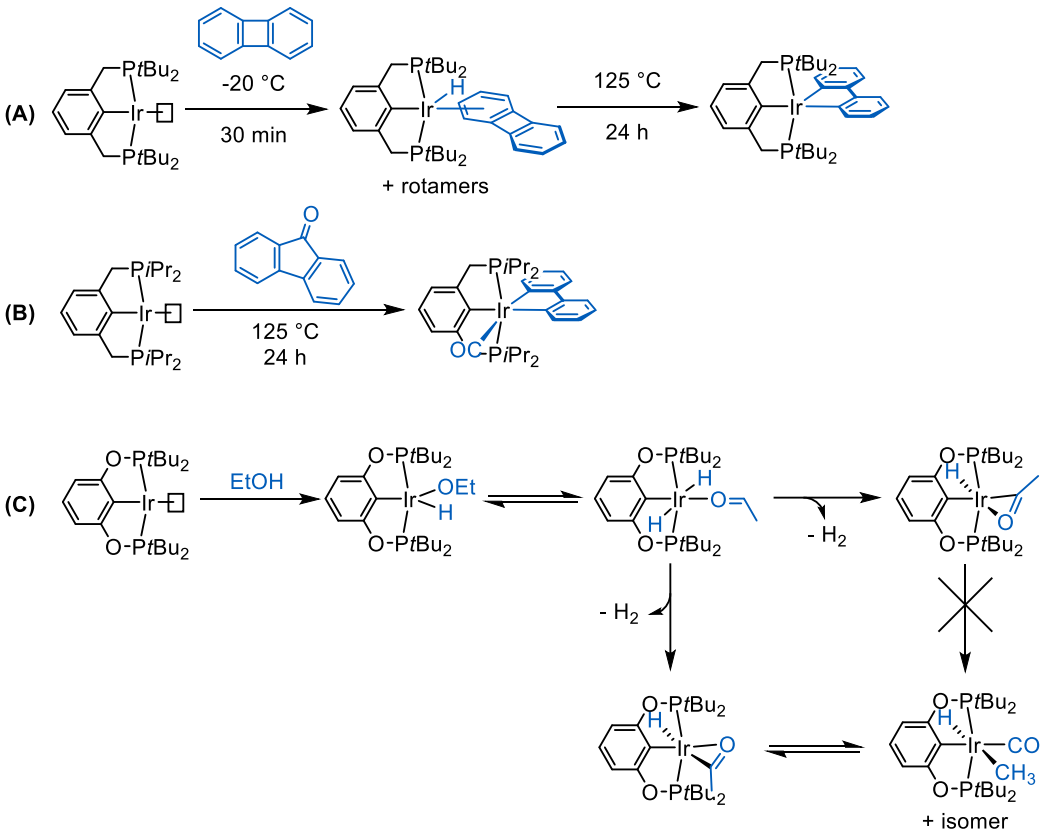

Scheme 1.9. Examples of C–C bond activation reaction mediated by (PXCXP)Ir systems.

1.3.3. Other inert bond activations

Pincer fragments of the formula {(PXCXP)M} (where X = CH_2, O and M = Rh, Ir) have also been shown to activate carbon-halogen bonds, although they represent perhaps less of a challenge than C–H and C–C bonds, partly on account of their lower average bond dissociation energies (selected BDEs in kJ/mol: C–H, 415; C–C , 345; C–Cl, 330; C–Br, 275; C–I, 240).[91] Indeed some examples may be found in the literature, even for the Rh-based pincers that were relatively ineffective at activating C–H bonds, namely {(POCOP)Rh}[92–96] and {(PCP)Rh},[97–100] in addition to Ir-based complexes {(POCOP)Ir} and {(PCP)Ir}.[66,87,101] A remarkable result was published in *Science* in 2011 by Goldman and Krogh-Jespersen and showed the net oxidative addition of C(sp^3)-F bonds (BDE 460 kJ/mol).[91,102] However the barrier for the direct oxidative addition to the Ir(I) centre is prohibitively high, with an alternative pathway consisting of an initial reversible C-H activation followed by α-fluorine migration to generate a methylidene complex and hydride migration to regenerate the alkyl (Scheme 1.10). Another example was reported

in 2017 with the *ortho*- C(sp2)–F addition of fluorinated aryl ketones to a {(PCP)Ir} centre, whereby a mechanistic proposal employed a direct (chelate assisted) oxidative addition step.[103]

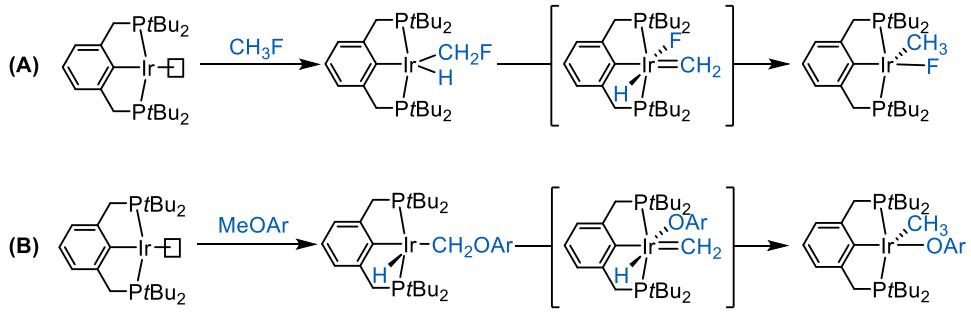

Scheme 1.10. C–F (top) and C–O (bottom) bond activation reactions by a (PCP)Ir system.

Finally, {(PCP)Ir} centres were also reported to activate the C–O bonds (BDE 350 kJ/mol)[91] in ethers and esters, in a mechanism very similar to the one depicted in Scheme 1.10 for C(sp^3)–F bonds, with an initial C–H activation promoting a subsequent α-migration of the OAr group and completed by hydride migration.[104,105]

1.4. Aims and objectives

The overarching aim of this project is to study and further our understanding of processes pertaining to alkane dehydrogenation reactions and activation of inert bonds by PXCXP-based Rh and Ir pincer complexes.

The approach will use a mechanically interlocked hydrocarbon-ligand topology as a kinetic trap, in the hope to counterbalance the unfavourable thermodynamics associated with such reactions by holding the hydrocarbon substrate in close proximity to the metal centre. More specifically, the synthesis of [2]catenanes and [2]rotaxanes comprising a macrocyclic PXCXP pincer ligand and interlocked cycloalkane or alkyl chain terminated with bulky stopper groups, respectively (Scheme 1.11).

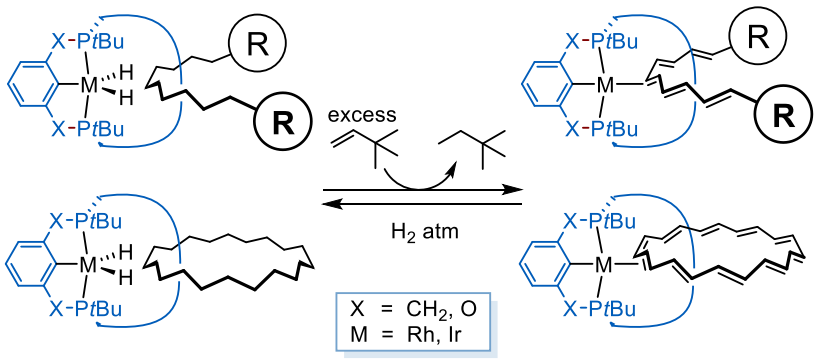

Scheme 1.11. Proposed interlocked topologies for the study of Rh and Ir reactions with hydrocarbons.

To this end, the first objective was the synthesis of macrocyclic PXCXP pro-ligands. In particular, the presence of two asymmetrically substituted phosphines means synthetic routes may provide two diastereomers, *anti*- or *syn*-substituted with respect to the coordination plane (Figure 1.5). Of these, only the *anti*-substituted isomer allows the full advantage of the presence of the macrocycle, which would be on average positioned in the coordination plane of a square planar complex. Therefore methodologies needed to target the isolation of the proligands as pure *anti*-isomers. The size of the macrocycle was set to 14 carbons, building on the established chemistry previously developed in the group with NHC-based CNC complexes featuring a 12-membered alkyl tether with either end attached to an additional nitrogen atom *alpha* to the coordinating position (Figure 1.5).

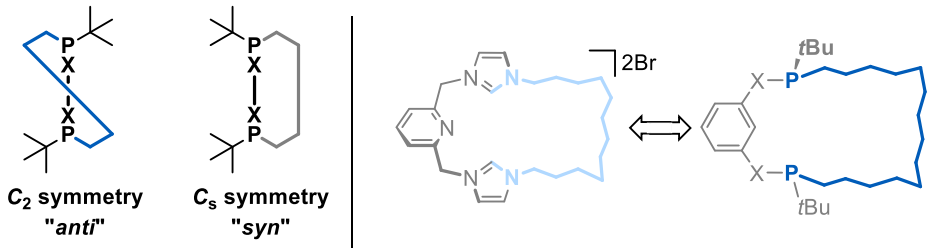

Figure 1.5. *anti* and *syn* stereoisomers of the target proligands (left) and comparison to previously developed CNC-12 proligands (right).

Next, metallation conditions were assessed with a view to preparing complexes suitable for different templating strategies for constructing interlocked derivatives. To this end, both passive and active metal templation techniques could be envisioned, either through simple coordination of an axle and capping or by C-C bond forming reactivity, respectively. The reactivity of such interlocked complexes in the context of C-H and C-C bond activation as well as hydrogenation reactions was finally investigated.

In addition to the potential development of new, selective methods for alkane transformation, this work could also serve as a platform in the long term to probe the possibilities for reversible hydrogen storage in the solid state in a safe fashion, *via* the reversible conversion of unsaturated hydrocarbons to their saturated counterparts.

1.5. Chelating macrocyclic ligands in the literature.

The expansion of acyclic ligands to their macrocyclic analogues is an approach that has attracted some attention since the late 1960s.[106–109] Indeed macrocyclic ligands tend to exhibit enhanced stability due to their intrinsic geometry which pre-orients the donors for coordination and removes any entropic penalty that would otherwise arise from significant geometrical rearrangements, in addition to usual considerations associated with the chelate effect. They have found limited applications in homogeneous catalysis.[110–112] Some structural variations have been reported in the last decade featuring both phosphine and NHC ligands and their coordination chemistry to late-transition metals.[113–115]

1.5.1. NHC-based CNC macrocyclic ligands

The inclusion of NHC-based tridentate donor sets in macrocycles has been reported on several occasions in the last decade,[116,117] and only one featured a macrocycle completed by an alkyl tether to form a 14 membered ring.[115,118] However, it must be noted that the latter is not able to adopt a tridentate coordination mode as a result of the ring strain that stems from the short hexyl tether (Figure 1.6, left). The Chaplin group further expanded this ligand class by preparing a variety of NHC-based macrocyclic ligands and their Pd, Mo, Ni and Rh complexes. Structural variations include the length of the alkyl tether (n = 8, 10, 12, 14, 16) as well as variants without a methylene bridge which directly affects the flexibility, dynamics and reactivity of the resulting scaffold (Figure 1.6, right).[119–125]

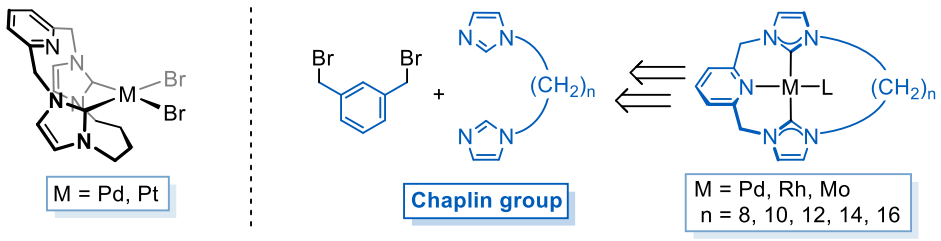

Figure 1.6. Literature examples of NHC-based CNC macrocyclic ligands.

The macrocyclic CNC ligand scaffolds are accessed starting from bis-*N*-(imidazolyl)alkanes; reaction with 2,6-bis(bromomethyl)pyridine in dilute

conditions affords the desired target ligands as bromide salts. Classic metallation conditions involve the deprotonation and *in situ* generation of the Ag(I) derivatives and transmetallation with the metal of interest. This method was diversified in 2016 and it was found that both Ag and Cu were suitable transfer agents for the synthesis of Ni, Rh and Pd macrocycles in good to excellent yields.[122] Alternatively, the target complexes may be accessed by first preparing terminal alkene functionalised acyclic pro-ligands, then metalation (Scheme 1.12). At this point, ring closing metathesis using Grubbs' first generation catalyst is facilitated by the preorganisation/templation provided by the pincer backbone. Subsequent hydrogenation affords the desired complex with an entirely saturated alkyl tether.[120]

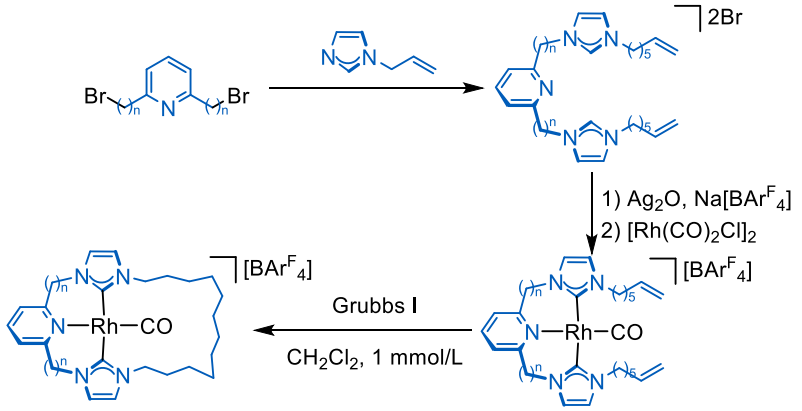

Scheme 1.12. Alternative synthetic pathway for Rh carbonyl macrocycles

Complexes of these macrocyclic CNC ligands have served as a platform to observe contrasting reactivities, notably in terminal alkyne coupling (TAC) reactions described in Scheme 1.13.[124] In this study, TAC was successfully employed to access a series of metallo-rotaxanes. Interesting results were obtained in terms of rate and selectivity when changing parameters such as the ring size, or in comparison to the acyclic analogue, the reaction affording *E*-enynes selectively for the smaller macrocycles and exclusively *gem*-enynes for their acyclic counterpart.

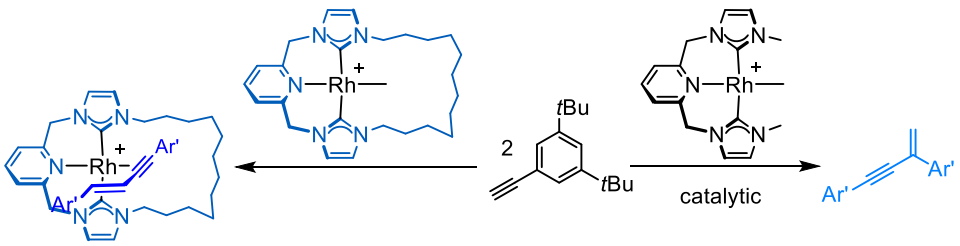

Scheme 1.13. Contrasting selectivity observed with macrocyclic *vs* acyclic NHC-based CNC Rh pincer complexes in terminal alkyne coupling reactions.

Importantly in the context of this thesis, treatment of these interlocked complexes with strong ligands such as CO showed that the axle was not displaced, which indicates both the presence of a robust mechanical bond and that the size of the Ar' stopper group is sufficiently bulky to prevent simple dethreading.

1.5.2. Applications in supramolecular chemistry

Since the first reported synthesis of a rotaxane in 1967,[126] which relied on the statistical probability of two "halves" to react through a macrocycle, the methodology for accessing these mechanically interlocked molecules has evolved considerably by the use of templating strategies. Examples include the use of intermolecular interactions such as hydrophobic,[127,128] π–π stacking,[129,130] or hydrogen bonding interactions[131,132] in order to favour a "pseudo-rotaxane" or "pseudo-catenane" geometry that may subsequently lead to a rotaxane through introduction of bulky stopper groups, or to a catenane through macrocyclization, respectively.

The well-defined coordination geometries of transition metal complexes of multidentate ligands have allowed their use as versatile templates for macrocyclization and capping reactions.[133] Sauvage's group was the first to report an example of passive metal templated synthesis of a catenane in 1983.[134] His strategy involved a Cu(I) centre as a template, which bound two bidentate phenanthroline based ligands in a tetrahedral geometry (Scheme 1.14).

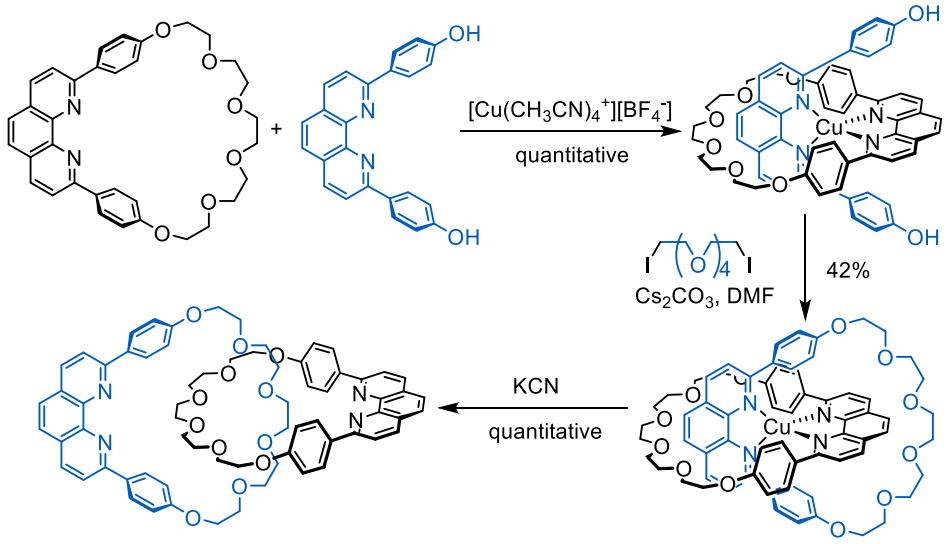

Scheme 1.14. Sauvage's Cu(I) mediated passive template methodology for the synthesis of a [2]catenane.

Subsequent alkylation of the phenoxy- moieties with bis-alkyl-iodides yielded the cyclised metallo-catenane, which can be readily converted to the free catenane by treatment with potassium cyanide.

This passive metal-template approach, which only involves a coordination event to achieve the correct positioning of the different fragments, was further developed with pyridine based square planar palladium complexes by Sauvage in the early 2000s, as well as by the Leigh group in 2005 with a Grubbs catalyst (1st generation) mediated ring closing metathesis.[135,136] But the Leigh group has also been particularly active in demonstrating the feasibility of active metal templating strategies, whereby the reactivity of the metal centre is utilized to construct and lock the threaded system. They have notably made use of CuAAC "click" reactions to obtain threaded disubstituted triazoles in excellent yields.[137] Another example of Copper mediated active templation was reported that same year by Saito et. al. using a Glaser terminal alkyne homocoupling reaction (Scheme 1.15).[138,139]

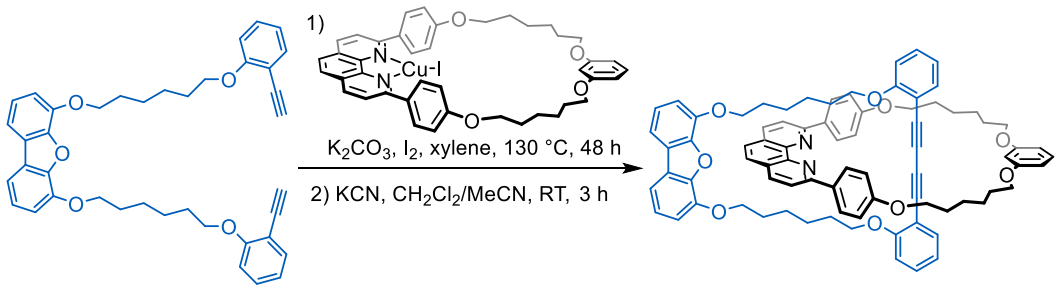

Scheme 1.15. Saito's approach to synthesising [2]catenanes *via* a Cu(I) mediated Glaser coupling.

More recently, the Leigh group reported a procedure involving Nickel catalysed $C(sp^3)$–$C(sp^3)$ bond coupling as a way to achieve interlocking within a Pybox based macrocyclic pincer ligand (Scheme 1.16).[140] This approach is currently under investigation in the Chaplin group for the construction of interlocked pure hydrocarbon catenanes and rotaxanes.

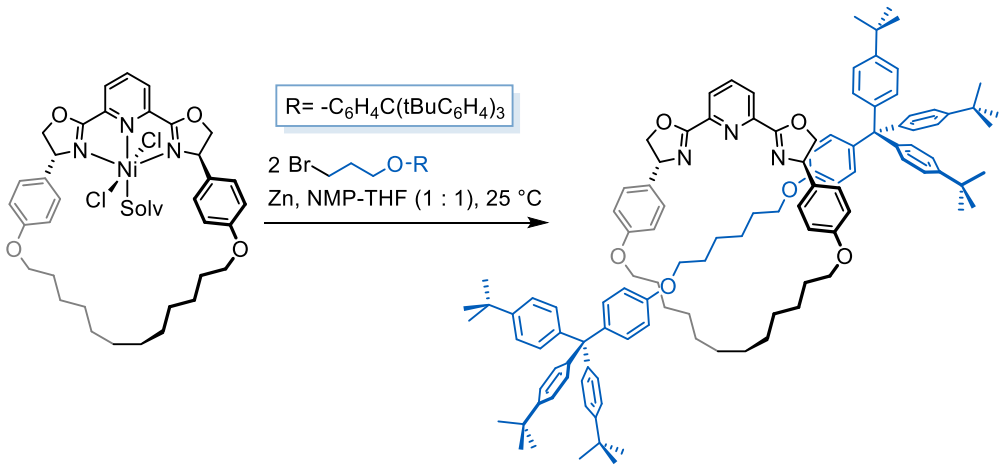

Scheme 1.16. Application of Ni-mediated unactivated sp^3-carbon homocoupling to [2]rotaxane synthesis by Leigh et. al.

1.6. References

[1] E. Peris, R. H. Crabtree, *Chem. Soc. Rev.* **2018**, 1959–1968.
[2] *Pincer Compounds: Chemistry and Applications*, Elsevier, Waltham, MA, **2018**.
[3] M. A. W. Lawrence, K.-A. Green, P. N. Nelson, S. C. Lorraine, *Polyhedron* **2018**, *143*, 11–27.
[4] D. Pugh, A. A. Danopoulos, *Coord. Chem. Rev.* **2007**, *251*, 610–641.
[5] D. Morales-Morales, in *Chem. Pincer Compd.*, Elsevier Science B.V., Amsterdam, **2007**, pp. 151–179.
[6] H. Valdés, E. Rufino-Felipe, D. Morales-Morales, *J. Organomet. Chem.* **2019**, *898*, 120864.
[7] M. Albrecht, G. van Koten, *Angew. Chem. Int. Ed.* **2001**, *40*, 3750–3781.
[8] M. Albrecht, M. M. Lindner, *Dalton Trans.* **2011**, *40*, 8733–8744.
[9] A. Kumar, T. M. Bhatti, A. S. Goldman, *Chem. Rev.* **2017**, *117*, 12357–12384.
[10] C. J. Moulton, B. L. Shaw, *J. Chem. Soc., Dalton Trans.* **1976**, 1020–1024.
[11] F. Miyazaki, K. Yamaguchi, M. Shibasaki, *Tetrahedron Lett.* **1999**, *40*, 7379–7383.
[12] D. Morales-Morales, C. Grause, K. Kasaoka, R. Redón, R. E. Cramer, C. M. Jensen, *Inorg Chim Acta* **2000**, *300–302*, 958–963.
[13] D. Morales-Morales, R. Redón, C. Yung, C. M. Jensen, *Chem. Commun.* **2000**, 1619–1620.
[14] R. B. Bedford, S. M. Draper, P. Noelle Scully, S. L. Welch, *New J. Chem.* **2000**, *24*, 745–747.
[15] J. Ito, T. Shiomi, H. Nishiyama, *Adv. Synth. Catal.* **2006**, *348*, 1235–1240.
[16] J. Ito, S. Ujiie, H. Nishiyama, *Chem. Commun.* **2008**, 1923.
[17] J. Ito, S. Ujiie, H. Nishiyama, *Organometallics* **2009**, *28*, 630–638.
[18] J. Ito, R. Asai, H. Nishiyama, *Org. Lett.* **2010**, *12*, 3860–3862.
[19] D. Hermann, M. Gandelman, H. Rozenberg, L. J. W. Shimon, D. Milstein, *Organometallics* **2002**, *21*, 812–818.
[20] E. Ben-Ari, M. Gandelman, H. Rozenberg, L. J. W. Shimon, D. Milstein, *J. Am. Chem. Soc.* **2003**, *125*, 4714–4715.
[21] C. Wei, Y. He, X. Shi, Z. Song, *Coord. Chem. Rev.* **2019**, *385*, 1–19.
[22] M. E. O'Reilly, A. S. Veige, *Chem Soc Rev* **2014**, *43*, 6325–6369.
[23] E. J. Farrington, E. Martinez Viviente, B. S. Williams, G. van Koten, J. M. Brown, *Chem. Commun.* **2002**, 308–309.
[24] A. A. Koridze, S. A. Kuklin, A. M. Sheloumov, M. V. Kondrashov, F. M. Dolgushin, A. S. Peregudov, P. V. Petrovskii, *Russ. Chem. Bull.* **2003**, *52*, 2754–2756.
[25] A. A. Koridze, S. A. Kuklin, A. M. Sheloumov, F. M. Dolgushin, V. Yu. Lagunova, I. I. Petukhova, M. G. Ezernitskaya, A. S. Peregudov, P. V. Petrovskii, E. V. Vorontsov, M. Baya, R. Poli, *Organometallics* **2004**, *23*, 4585–4593.
[26] A. Labande, N. Debono, A. Sournia-Saquet, J.-C. Daran, R. Poli, *Dalton Trans.* **2013**, *42*, 6531.
[27] M. R. Kita, A. J. M. Miller, *J. Am. Chem. Soc.* **2014**, *136*, 14519–14529.
[28] J. Grajeda, M. R. Kita, L. C. Gregor, P. S. White, A. J. M. Miller, *Organometallics* **2016**, *35*, 306–316.
[29] L. C. Gregor, J. Grajeda, M. R. Kita, P. S. White, A. J. Vetter, A. J. M. Miller, *Organometallics* **2016**, *35*, 3074–3086.
[30] A. J. M. Miller, *Dalton Trans.* **2017**, *46*, 11987–12000.
[31] L. C. Gregor, J. Grajeda, P. S. White, A. J. Vetter, A. J. M. Miller, *Catal. Sci. Technol.* **2018**, *8*, 3133–3143.
[32] C. Yoo, H. M. Dodge, A. J. M. Miller, *Chem. Commun.* **2019**, *55*, 5047–5059.
[33] M. Gozin, A. Weisman, Y. Ben-David, D. Milstein, *Nature* **1993**, *364*, 699–701.
[34] B. Rybtchinski, A. Vigalok, Y. Ben-David, D. Milstein, *J. Am. Chem. Soc.* **1996**, *118*, 12406–12415.
[35] B. Rybtchinski, D. Milstein, *Angew. Chem. Int. Ed.* **1999**, *38*, 870–883.
[36] M. Gandelman, A. Vigalok, L. Konstantinovski, D. Milstein, *J. Am. Chem. Soc.* **2000**, *122*, 9848–9849.
[37] J. R. Norton, *Acc. Chem. Res.* **1979**, *12*, 139–145.
[38] R. H. Crabtree, *Chem. Rev.* **1985**, *85*, 245–269.
[39] Q. Wang, X. Chen, A. N. Jha, H. Rogers, *Renew. Sustain. Energy Rev.* **2014**, *30*, 1–28.
[40] J. L. Schnoor, *Environ. Sci. Technol.* **2012**, *46*, 4686–4686.

[41] N. López-Cortés, A. Beloqui, A. Ghazi, M. Ferrer, in *Handb. Hydrocarb. Lipid Microbiol.* (Ed.: K.N. Timmis), Springer Berlin Heidelberg, Berlin, Heidelberg, **2010**, pp. 2841–2858.
[42] S. R. Golisz, T. Brent Gunnoe, W. A. Goddard, J. T. Groves, R. A. Periana, *Catal. Lett.* **2011**, *141*, 213–221.
[43] X. Tang, X. Jia, Z. Huang, *Chem. Sci.* **2018**, *9*, 288–299.
[44] M. M. Bhasin, D. W. Slocum, Eds. , *Methane and Alkane Conversion Chemistry*, Springer US, Boston, MA, **1995**.
[45] Z. Zakaria, S. K. Kamarudin, *Renew. Sustain. Energy Rev.* **2016**, *65*, 250–261.
[46] J. A. Martens, A. Bogaerts, N. De Kimpe, P. A. Jacobs, G. B. Marin, K. Rabaey, M. Saeys, S. Verhelst, *ChemSusChem* **2017**, *10*, 1039–1055.
[47] N. J. Gunsalus, A. Koppaka, S. H. Park, S. M. Bischof, B. G. Hashiguchi, R. A. Periana, *Chem. Rev.* **2017**, *117*, 8521–8573.
[48] R. H. Crabtree, *Chem. Rev.* **1995**, *95*, 987–1007.
[49] P. Schwach, X. Pan, X. Bao, *Chem. Rev.* **2017**, *117*, 8497–8520.
[50] A. E. Shilov, G. B. Shul'pin, *Russ. Chem. Rev.* **1987**, *56*, 442–464.
[51] G. A. Olah, A. Goeppert, G. K. S. Prakash, *Beyond Oil and Gas: The Methanol Economy*, Wiley, **2009**.
[52] J. Choi, A. H. R. MacArthur, M. Brookhart, A. S. Goldman, *Chem. Rev.* **2011**, *111*, 1761–1779.
[53] C. J. Pell, O. V. Ozerov, *ACS Catal.* **2014**, *4*, 3470–3480.
[54] J. A. Maguire, W. T. Boese, A. S. Goldman, *J. Am. Chem. Soc.* **1989**, *111*, 7088–7093.
[55] J. A. Maguire, A. S. Goldman, *J. Am. Chem. Soc.* **1991**, *113*, 6706–6708.
[56] J. A. Maguire, A. Petrillo, A. S. Goldman, *J. Am. Chem. Soc.* **1992**, *114*, 9492–9498.
[57] W. Xu, G. P. Rosini, K. Krogh-Jespersen, A. S. Goldman, M. Gupta, C. M. Jensen, W. C. Kaska, *Chem. Commun.* **1997**, 2273–2274.
[58] M. Kanzelberger, B. Singh, M. Czerw, K. Krogh-Jespersen, A. S. Goldman, *J. Am. Chem. Soc.* **2000**, *122*, 11017–11018.
[59] B. Punji, T. J. Emge, A. S. Goldman, *Organometallics* **2010**, *29*, 2702–2709.
[60] X. Zhang, M. Kanzelberger, T. J. Emge, A. S. Goldman, *J. Am. Chem. Soc.* **2004**, *126*, 13192–13193.
[61] I. Göttker-Schnetmann, P. S. White, M. Brookhart, *Organometallics* **2004**, *23*, 1766–1776.
[62] L. P. Press, A. J. Kosanovich, B. J. McCulloch, O. V. Ozerov, *J. Am. Chem. Soc.* **2016**, *138*, 9487–9497.
[63] S. A. Hauser, J. Emerson-King, S. Habershon, A. B. Chaplin, *Chem. Commun.* **2017**, *53*, 3634–3636.
[64] D. A. Ahlstrand, A. V. Polukeev, R. Marcos, M. S. G. Ahlquist, O. F. Wendt, *Chem. - Eur. J.* **2017**, *23*, 1748–1751.
[65] K. Krogh-Jespersen, M. Czerw, K. Zhu, B. Singh, M. Kanzelberger, N. Darji, P. D. Achord, K. B. Renkema, A. S. Goldman, *J. Am. Chem. Soc.* **2002**, *124*, 10797–10809.
[66] R. Ghosh, X. Zhang, P. Achord, T. J. Emge, K. Krogh-Jespersen, A. S. Goldman, *J. Am. Chem. Soc.* **2007**, *129*, 853–866.
[67] P. J. Alaimo, R. G. Bergman, *Organometallics* **1999**, *18*, 2707–2717.
[68] S. R. Klei, T. D. Tilley, R. G. Bergman, *J. Am. Chem. Soc.* **2000**, *122*, 1816–1817.
[69] K. Kawamura, J. F. Hartwig, *J. Am. Chem. Soc.* **2001**, *123*, 8422–8423.
[70] K. J. H. Young, O. A. Mironov, R. A. Periana, *Organometallics* **2007**, *26*, 2137–2140.
[71] T. J. Hebden, K. I. Goldberg, D. M. Heinekey, X. Zhang, T. J. Emge, A. S. Goldman, K. Krogh-Jespersen, *Inorg. Chem.* **2010**, *49*, 1733–1742.
[72] D. A. Laviska, T. Zhou, A. Kumar, T. J. Emge, K. Krogh-Jespersen, A. S. Goldman, *Organometallics* **2016**, *35*, 1613–1623.
[73] R. H. Crabtree, J. M. Mihelcic, J. M. Quirk, *J. Am. Chem. Soc.* **1979**, *101*, 7738–7740.
[74] M. Gupta, W. C. Kaska, C. M. Jensen, *Chem. Commun.* **1997**, 461–462.
[75] M. Gupta, C. Hagen, W. C. Kaska, R. E. Cramer, C. M. Jensen, *J. Am. Chem. Soc.* **1997**, *119*, 840–841.
[76] K. Wang, M. E. Goldman, T. J. Emge, A. S. Goldman, *J. Organomet. Chem.* **1996**, *518*, 55–68.
[77] M. Gupta, C. Hagen, R. J. Flesher, W. C. Kaska, C. M. Jensen, *Chem Commun* **1996**, 2083–2084.
[78] D. Bézier, C. Guan, K. Krogh-Jespersen, A. S. Goldman, M. Brookhart, *Chem. Sci.* **2016**, *7*, 2579–2586.

[79] F. Liu, A. S. Goldman, *Chem. Commun.* **1999**, 655–656.
[80] K. Zhu, P. D. Achord, X. Zhang, K. Krogh-Jespersen, A. S. Goldman, *J. Am. Chem. Soc.* **2004**, *126*, 13044–13053.
[81] D. Morales-Morales, R. Redón, C. Yung, C. M. Jensen, *Inorg Chim Acta* **2004**, *357*, 2953–2956.
[82] I. Göttker-Schnetmann, M. Brookhart, *J. Am. Chem. Soc.* **2004**, *126*, 9330–9338.
[83] I. Göttker-Schnetmann, P. White, M. Brookhart, *J. Am. Chem. Soc.* **2004**, *126*, 1804–1811.
[84] W. Yao, Y. Zhang, X. Jia, Z. Huang, *Angew. Chem. Int. Ed.* **2014**, *53*, 1390–1394.
[85] W. Yao, X. Jia, X. Leng, A. S. Goldman, M. Brookhart, Z. Huang, *Polyhedron* **2016**, DOI 10.1016/j.poly.2016.02.044.
[86] F. Liu, E. B. Pak, B. Singh, C. M. Jensen, A. S. Goldman, *J. Am. Chem. Soc.* **1999**, *121*, 4086–4087.
[87] R. Ghosh, T. J. Emge, K. Krogh-Jespersen, A. S. Goldman, *J. Am. Chem. Soc.* **2008**, *130*, 11317–11327.
[88] D. A. Laviska, C. Guan, T. J. Emge, M. Wilklow-Marnell, W. W. Brennessel, W. D. Jones, K. Krogh-Jespersen, A. S. Goldman, *Dalton Trans* **2014**, *43*, 16354–16365.
[89] M. Wilklow-Marnell, W. W. Brennessel, W. D. Jones, *Polyhedron* **2016**, *116*, 38–46.
[90] A. V. Polukeev, P. V. Petrovskii, A. S. Peregudov, M. G. Ezernitskaya, A. A. Koridze, *Organometallics* **2013**, *32*, 1000–1015.
[91] Y.-R. Luo, Y.-R. Luo, *Comprehensive Handbook of Chemical Bond Energies*, CRC Press, Boca Raton, **2007**.
[92] S. D. Timpa, C. M. Fafard, D. E. Herbert, O. V. Ozerov, *Dalton Trans.* **2011**, *40*, 5426.
[93] S. D. Timpa, C. J. Pell, J. Zhou, O. V. Ozerov, *Organometallics* **2014**, *33*, 5254–5262.
[94] S. D. Timpa, J. Zhou, N. Bhuvanesh, O. V. Ozerov, *Organometallics* **2014**, *33*, 6210–6217.
[95] S. D. Timpa, C. J. Pell, O. V. Ozerov, *J. Am. Chem. Soc.* **2014**, *136*, 14772–14779.
[96] H. Salem, Y. Ben-David, L. J. W. Shimon, D. Milstein, *Organometallics* **2006**, *25*, 2292–2300.
[97] M. E. van der Boom, C. L. Higgitt, D. Milstein, *Organometallics* **1999**, *18*, 2413–2419.
[98] C. M. Frech, Y. Ben-David, L. Weiner, D. Milstein, *J. Am. Chem. Soc.* **2006**, *128*, 7128–7129.
[99] E. Kossoy, B. Rybtchinski, Y. Diskin-Posner, L. J. W. Shimon, G. Leitus, D. Milstein, *Organometallics* **2009**, *28*, 523–533.
[100] C. M. Frech, D. Milstein, *J. Am. Chem. Soc.* **2006**, *128*, 12434–12435.
[101] J. Yang, M. Brookhart, *J. Am. Chem. Soc.* **2007**, *129*, 12656–12657.
[102] J. Choi, D. Y. Wang, S. Kundu, Y. Choliy, T. J. Emge, K. Krogh-Jespersen, A. S. Goldman, *Science* **2011**, *332*, 1545–1548.
[103] M. Wilklow-Marnell, W. W. Brennessel, W. D. Jones, *Organometallics* **2017**, *36*, 3125–3134.
[104] J. Choi, Y. Choliy, X. Zhang, T. J. Emge, K. Krogh-Jespersen, A. S. Goldman, *J. Am. Chem. Soc.* **2009**, *131*, 15627–15629.
[105] S. Kundu, J. Choi, D. Y. Wang, Y. Choliy, T. J. Emge, K. Krogh-Jespersen, A. S. Goldman, *J. Am. Chem. Soc.* **2013**, *135*, 5127–5143.
[106] G. A. Melson, *Coordination Chemistry of Macrocyclic Compounds*, New York, **1979**.
[107] C. D. Swor, D. R. Tyler, *Coord. Chem. Rev.* **2011**, *255*, 2860–2881.
[108] D. K. Cabbiness, D. W. Margerum, *J. Am. Chem. Soc.* **1969**, *91*, 6540–6541.
[109] P. G. Edwards, F. E. Hahn, *Dalton Trans.* **2011**, *40*, 10278.
[110] M. Ranocchiari, A. Mezzetti, *Organometallics* **2009**, *28*, 1286–1288.
[111] C. Röhlich, K. Köhler, *Adv. Synth. Catal.* **2010**, *352*, 2263–2274.
[112] R. Bigler, A. Mezzetti, *Org. Lett.* **2014**, *16*, 6460–6463.
[113] F. E. Hahn, V. Langenhahn, T. Lügger, T. Pape, D. Le Van, *Angew. Chem. Int. Ed.* **2005**, *44*, 3759–3763.
[114] A. Flores-Figueroa, T. Pape, K.-O. Feldmann, F. E. Hahn, *Chem Commun* **2010**, *46*, 324–326.
[115] C. Radloff, H.-Y. Gong, C. Schulte to Brinke, T. Pape, V. M. Lynch, J. L. Sessler, F. E. Hahn, *Chem. - Eur. J.* **2010**, *16*, 13077–13081.
[116] K. Meyer, A. F. Dalebrook, L. J. Wright, *Dalton Trans.* **2012**, *41*, 14059.
[117] S. Saito, I. Azumaya, N. Watarai, H. Kawasaki, R. Yamasaki, *HETEROCYCLES* **2009**, *79*, 531.
[118] A. Biffis, M. Cipani, E. Bressan, C. Tubaro, C. Graiff, A. Venzo, *Organometallics* **2014**, *33*, 2182–2188.

[119] R. E. Andrew, A. B. Chaplin, *Dalton Trans.* **2013**, *43*, 1413–1423.
[120] R. E. Andrew, A. B. Chaplin, *Inorg. Chem.* **2015**, *54*, 312–322.
[121] R. E. Andrew, D. W. Ferdani, C. A. Ohlin, A. B. Chaplin, *Organometallics* **2015**, *34*, 913–917.
[122] R. E. Andrew, C. M. Storey, A. B. Chaplin, *Dalton Trans.* **2016**, *45*, 8937–8944.
[123] S. L. Apps, R. E. Alflatt, B. Leforestier, C. M. Storey, A. B. Chaplin, *Polyhedron* **2017**, DOI 10.1016/j.poly.2017.08.001.
[124] C. M. Storey, M. R. Gyton, R. E. Andrew, A. B. Chaplin, *Angew. Chem. Int. Ed.* **2018**, *57*, 12003–12006.
[125] M. R. Gyton, B. Leforestier, A. B. Chaplin, *Organometallics* **2018**, *37*, 3963–3971.
[126] I. Thomas. Harrison, Shuyen. Harrison, *J. Am. Chem. Soc.* **1967**, *89*, 5723–5724.
[127] J. F. Stoddart, *Angew. Chem. Int. Ed.* **1992**, *31*, 846–848.
[128] H. Murakami, A. Kawabuchi, K. Kotoo, M. Kunitake, N. Nakashima, *J. Am. Chem. Soc.* **1997**, *119*, 7605–7606.
[129] W. R. Dichtel, O. Š. Miljanić, J. M. Spruell, J. R. Heath, J. F. Stoddart, *J. Am. Chem. Soc.* **2006**, *128*, 10388–10390.
[130] O. Š. Miljanić, W. R. Dichtel, S. Mortezaei, J. F. Stoddart, *Org. Lett.* **2006**, *8*, 4835–4838.
[131] C. A. Hunter, *J. Am. Chem. Soc.* **1992**, *114*, 5303–5311.
[132] F. Vögtle, S. Meier, R. Hoss, *Angew. Chem. Int. Ed. Engl.* **1992**, *31*, 1619–1622.
[133] G. Gil-Ramírez, D. A. Leigh, A. J. Stephens, *Angew. Chem. Int. Ed.* **2015**, *54*, 6110–6150.
[134] C. O. Dietrich-Buchecker, J. P. Sauvage, J. P. Kintzinger, *Tetrahedron Lett.* **1983**, *24*, 5095–5098.
[135] C. Hamann, J.-M. Kern, J.-P. Sauvage, *Dalton Trans.* **2003**, 3770–3775.
[136] A.-M. L. Fuller, D. A. Leigh, P. J. Lusby, A. M. Z. Slawin, D. B. Walker, *J. Am. Chem. Soc.* **2005**, *127*, 12612–12619.
[137] V. Aucagne, K. D. Hänni, D. A. Leigh, P. J. Lusby, D. B. Walker, *J. Am. Chem. Soc.* **2006**, *128*, 2186–2187.
[138] S. Saito, E. Takahashi, K. Nakazono, *Org. Lett.* **2006**, *8*, 5133–5136.
[139] Y. Sato, R. Yamasaki, S. Saito, *Angew. Chem. Int. Ed.* **2009**, *48*, 504–507.
[140] S. M. Goldup, D. A. Leigh, R. T. McBurney, P. R. McGonigal, A. Plant, *Chem. Sci.* **2010**, *1*, 383–386.

Chapter 2

Synthesis of macrocyclic POCOP and PCP proligands

This chapter describes the development of two synthetic routes for the preparation of novel phosphine-based macrocyclic proligands. Both C_2-symmetric proligands feature a tetradecamethylene linker that joins the two phosphine donors that are appended to a central resorcinol (**POCOP-14'**) or *m*-xylene (**PCP-14'**) backbone. Phosphine-based PONOP-14 and PNP-14 analogues bearing a 2,6-dihydroxypyridine or a lutidine backbone (respectively) are being developed concurrently in the group.

A racemic synthetic route is first described which provides racemic **POCOP-14'** and the diastereomeric *syn* congener. The unavoidable formation of the *syn* isomer *via* this route, as well as its challenging separation, prompted the development of an alternative asymmetric route, which was applied to the enantio- and diastereoselective synthesis of *anti* (*R*,*R*)-**PCP-14'**.

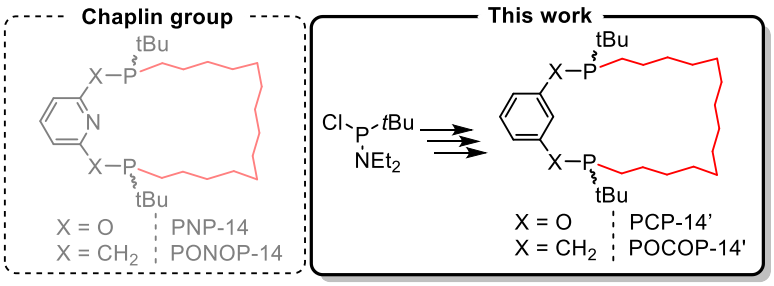

Part of the work described in this chapter has been published:

B. Leforestier, M. R. Gyton and A. B. Chaplin *Dalton Trans*. 2020, *in the press,* doi.org/10.1039/c9dt04835a

2.1. Introduction

2.1.1. General methods for the synthesis of PCP and POCOP proligands

The synthesis of phosphine based pincers most commonly employs well established organophosphorus chemistry. POCOP ligands are mostly obtained via nucleophilic substitution of the halogen atom of R_2PCl with a deprotonated resorcinol. Deprotonation may be achieved through the use of various bases, including triethylamine, n-butyllithium, KHMDS or sodium hydride (Scheme 2.1(a)). The PCP backbone on the other hand is typically obtained by reduction of R_2PCl with Li metal, which can then undergo nucleophilic substitution on 1,3-bis-(halogenomethyl)benzene (Scheme 2.1(b,i)). Alternatively, secondary phosphines are nucleophilic enough to substitute the halogen in the 1,3-bis-(halogenomethyl)benzene to form the phosphonium salt, which are in turn readily deprotonated to give the desired neutral phosphine donor (Scheme 2.1(b,ii)).[1–3]

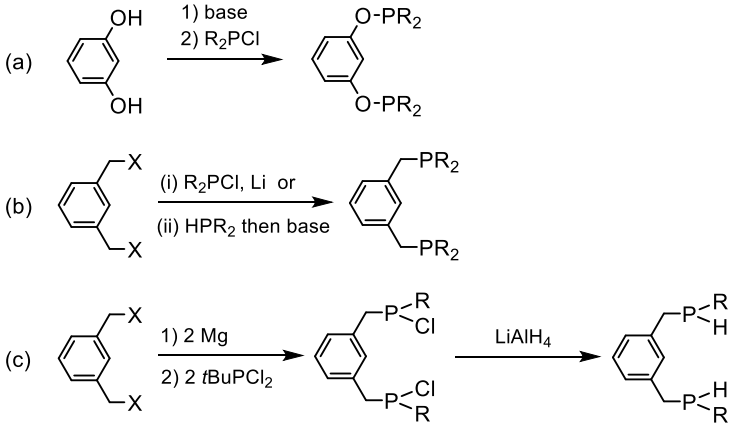

Scheme 2.1. Common synthetic pathways for phosphine-based pincer proligands.

Specifically for method (b.ii), the introduction of the phosphine donors may be carried out sequentially, allowing for the installation of non-palindromic and structurally more diverse PCP ligands.[4] More recently, a halogen xylyl derivative was used to generate the corresponding bis-Grignard, which subsequently undergoes nucleophilic substitution on $PRCl_2$ (Scheme 2.1(c)). Further treatment with $LiAlH_4$ affords the corresponding secondary diphosphine. The latter may be recrystallized as a racemic mixture of diastereomers, allowing for an easy access to substitution patterns with C_2 or C_s symmetry.[5] The straightforward deprotonation of these secondary phosphines gives an additional opportunity to introduce structural diversity in the proligand's backbone.

2.1.2. Asymmetric phosphine synthesis

The above methods would lead to a racemic mixture of *syn* and *anti* diastereoisomers for our target ligands, which would need to be separated. Therefore, an alternative synthetic route using adapted literature methods that enable the selective preparation of a single enantiomer for our phosphorus centres could make it possible to avoid the formation of the *syn* isomer altogether and simplify the purification of our target compounds.

The usual methods to prepare phosphines, whose chirality stems purely from a chiral phosphorus centre, historically rely on the resolution of phosphine oxides or quaternary phosphinates by using a chiral acid (*e.g.* tartaric acid)[6–8] or by stereoselective synthesis using chiral auxiliaries, with menthol the earliest example.[9,10] The desired phosphines are commonly obtained by addition of Grignard reagents and subsequent reduction of the phosphine oxides or nucleophilic displacement of the chiral auxiliary. Methods developed more recently employed asymmetric catalysis, with examples featuring Pd,[11] Pt,[12,13] or Ru-based catalysts the most notable.[14]

Of particular relevance to the work described herein, the preparation of P-stereogenic phosphines using chiral aminoalcohol auxiliaries offers an inexpensive and convenient synthetic route to a variety of asymmetrically substituted ligands. The Jugé group, in particular, developed what is referred to today as the "ephedrine method" (Scheme 2.2).[15]

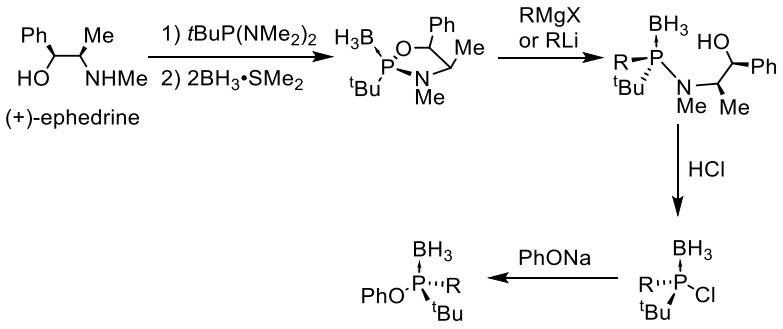

Scheme 2.2. Asymmetric phosphinite synthesis *via* the "ephedrine method".

The first step involves the diastereoselective preparation of a heterocyclic oxazaphospholidine and its protection, here as a borane adduct. Regio- and stereoselective ring-opening upon substitution with a nucleophile such as an organomagnesium or lithium reagent enables the formation of a chiral

phosphanamine. Eventually, the chiral auxiliary may be cleaved off by subsequent acidolysis. In this case hydrochloric acid affords the chloride substituted phosphine borane,[16] which was reported to undergo nucleophilic substitution with sodium phenoxide to afford the desired chiral phosphinite.

A disadvantage inherent to this method is the use and difficulty to procure ephedrine, which is a restricted drug precursor. To address this issue, alternative auxiliaries have been developed with work by Verdaguer *et. al.* involving (±)-cis-1-amino-2-indanol most notable (Scheme 2.3).[17–19]

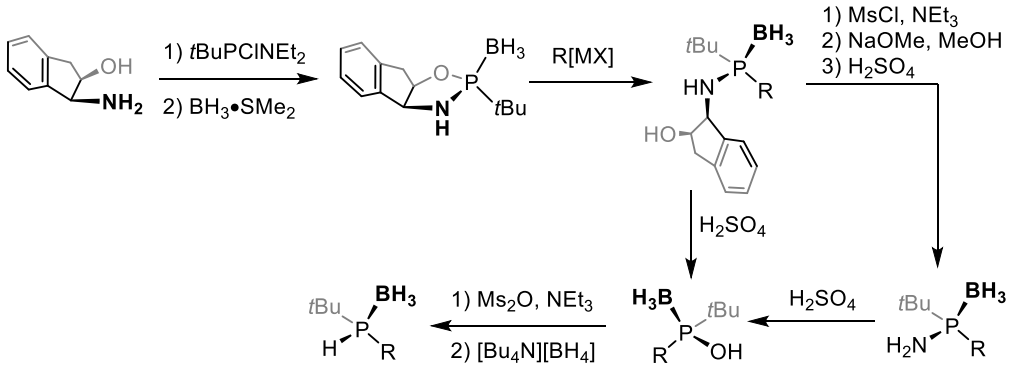

Scheme 2.3. Alternative to the "ephedrine method" employing (+)-cis-1-amino-2-indanol.

The principle remains very similar to the ephedrine method described above, in that an oxazaphospholidine borane is prepared and crystallised diastereoselectively and then ring opened with a Grignard reagent to give a phosphanamine borane. Cleavage of the chiral auxiliary was first achieved in a sequential manner by mesylating the hydroxyl group, allowing elimination by treatment with NaOMe to form an iminophosphine borane, which is followed by acidic hydrolysis to give the corresponding aminophosphine borane. Further hydrolysis then leads to the borane protected phosphinous acid, which can also be obtained directly from acidolysis of the auxiliary by treatment with H_2SO_4 in a methanol/water mixture. The mesylated phosphinous acid borane can be accessed by treatment with Ms_2O, although the reaction mixture must be kept at or below -20°C to avoid racemization. The mesyl group is a sufficiently good leaving group to be displaced by nucleophilic substitution reactions with a variety of primary amines or a hydride source to provide the optically pure phosphine borane.

The chiral information is fully retained throughout, with the enantiomeric excess for each intermediate shown in Scheme 2.3 determined to be >99%.

2.2. Development of a racemic route

2.2.1. Retrosynthetic strategy

The macrocyclic nature of our target proligands implies a ring-closing step in the synthetic pathway. We proposed the use of well-established Grubbs-mediated ring-closing metathesis to mediate this step.[20,21] This in turns requires the introduction of an octenyl substituent on the phosphines, so a 14-carbon ring is obtained after metathesis (Scheme 2.4). In order to take advantage of known literature procedures to access pincer scaffolds, the next disconnection is made at the P–X bond (X = O, CH_2), so as to use commercially available resorcinol and 1,3-bis(bromomethyl)benzene together with a chlorophosphine or a secondary phosphine, respectively. Finally, the *tert*-butylchloro(oct-7-en-yl)phosphine or *tert*-butyl(oct-7-en-yl)phosphine were prepared *via* nucleophilic substitution by a Grignard reagent on commercially available *tert*-butyldichlorophosphine.

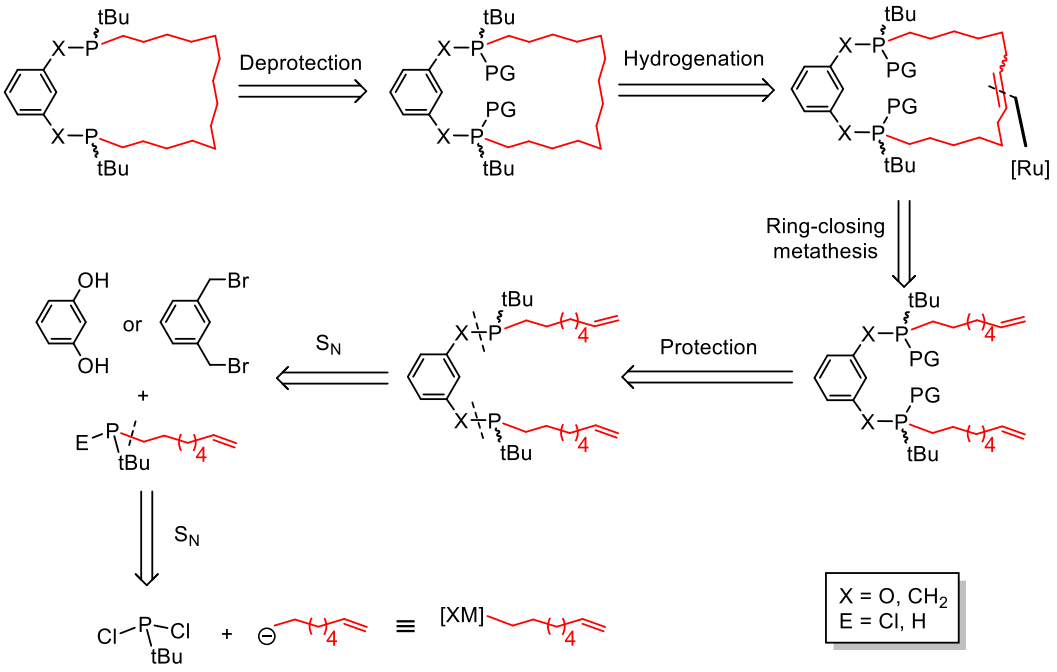

Scheme 2.4. Retrosynthetic scheme for the preparation of target proligands.

*2.2.2. Preparation of tert-butylchloro(oct-7-en-1-yl)phosphine **2**.*

The investigation into the synthesis of the target macrocyclic pincer ligand started with the adaptation of known organophosphorus chemistry and previous work within the Chaplin group (M. R. Gyton) developing methodology for the

preparation of *tert*-butylchloro(oct-7-en-1-yl)phosphine. It was found that direct treatment of *tert*-butyldichlorophosphine with 1 equivalent of the appropriate Grignard reagent does not allow for the selective instalment of only one octenyl chain at the phosphorus centre, instead yielding a mixture of unreacted starting material and mono- and disubstituted phosphines **2** and **2'** (Scheme 2.5).

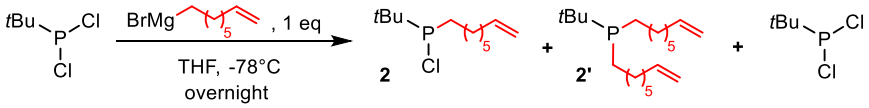

Scheme 2.5. Attempted direct synthesis of **2**.

To obviate the formation of **2'**, a literature procedure was used to prepare phosphanamine P(*t*Bu)(NEt_2)Cl in excellent yield by treatment with 2 equivalents of diethylamine in hexane (Scheme 2.6).[22] This asymmetrically substituted phosphine then enabled the desired monosubstitution using one equivalent of oct-1-enyl magnesium bromide to afford octenyl-substituted phosphanamine **1** in 91 % yield.

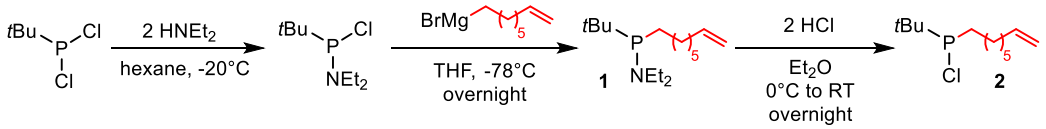

Scheme 2.6. Preparation of **2**.

Subsequent treatment of **1** with HCl (2 eq.) in ether afforded chlorophosphine **2** in very good yield. The reaction was carried out using high solvent volumes with dropwise addition of HCl so that stirring remains effective throughout the reaction. Indeed the formation of the ammonium salt fine precipitate was otherwise found to impede homogeneous stirring, which in turn resulted in a less clean reaction mixture as observed by ^{31}P NMR spectroscopy, stemming from the concurrent formation of protonated **2-H**$^+$. A pure sample could be obtained after filtration and several successive purification steps by vacuum transfer. Alternatively, quantification of **2'** by NMR spectroscopy and treatment with a stoichiometric amount of base enables the isolation of pure **2**.[23]

*2.2.3. Protection strategies and preparation of **POCOP-14'**.*

With **2** in hand, it was subjected to nucleophilic substitution at the P-centre with half an equivalent of resorcinolate, which was generated by deprotonation with sodium hydride following literature procedures evoked above (Scheme 2.7).[1] This protocol afforded pre-macrocyclic pincer proligand **3** as a colourless oil in excellent yield and 94% purity. Further purification of this compound proved challenging as it is non-volatile and its air sensitivity is problematic for chromatography-based purification methods. Therefore **3** was reacted on without further purification.

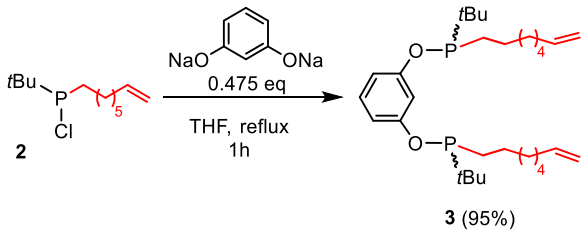

Scheme 2.7. Preparation of **3**.

With pre-macrocyclic **3** in hand, attention turned to protection strategies. A commonly employed method for protecting phosphines is to convert them to the corresponding phosphine sulfide with the deprotection effected at a later stage by reduction with Raney nickel or silanes.[24,25] This protection strategy was being developed concurrently in the group (M. R. Gyton), applied to the preparation of the PONOP backbone, and proved effective in shielding the phosphine groups in the transition-metal catalysed ring-closing metathesis and hydrogenation steps.

Thus, compound **3** was reacted with elemental sulfur to afford **3·S$_2$** in 66% yield after straightforward purification by silica chromatography (Scheme 2.8).

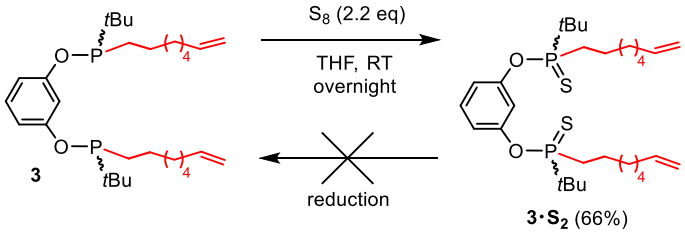

Scheme 2.8. Attempted protection/deprotection of **3** with sulfur.

To assess the feasibility of the usual deprotection strategies at this point, several reduction methods were trialled. Treatment with Raney nickel in methanol, acetonitrile or DMF all resulted in the complete decomposition of the ligand into an intractable and complex mixture of compounds. Phosphine transfer with excess tri-*iso*-propylphosphite yielded no product either, even upon prolonged heating, and decomposition of the starting material occurred above 80°C, putatively as a result of P–O bond cleavage, weakened by the electron-depleting P(V) centre as well as the aromatic backbone. Hence a milder protection/deprotection method was required and attention turned to the use of borane.[26,27]

Treatment of **3** with a slow addition of borane dimethylsulfide at -78°C enabled the formation of **4** with limited loss of the terminal alkene groups (Scheme 2.9). The borane proved to be a suitable alternative to sulfide protection in terms of stability in air and on silica, and borane protected pre-macrocyclic proligand **4** was isolated in 79% yield after column chromatography, as a 1:1 mixture of diastereoisomers, that could be deprotected later (*vide infra*).

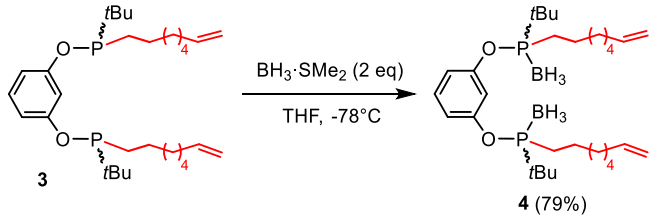

Scheme 2.9. Protection of **3** as the borane adduct **4**.

With borane-protected pre-macrocyclic ligand **4** in hand, ring-closing metathesis using Grubbs' 1st generation catalyst was achieved in 94% yield to afford cyclised **5**, as shown in Scheme 2.10. A concentration of 5 mmol.L^{-1} was found suitable to promote the intramolecular cyclisation and avoid polymerisation altogether. The monomeric nature of **5** was unambiguously established by X-ray crystallography on a later derivative (*vide infra*). As for the previous step, **5** could be purified by silica chromatography and was isolated as a 1:1 mixture of diastereomers and alkene isomers, however, no noticeable difference was observed between the behaviours of both diastereoisomers and the desired *anti* isomer could not be separated from its *syn* congener by chromatography.

Initial attempts at hydrogenating **5** using 10 mol% Pd/C resulted only in a partial hydrogenation of the alkene moieties even with heating and prolonged reaction times, putatively as a consequence of a more facile adsorption of the *Z*- over *E*-isomer or conversely a greater stability of the *E*- over *Z*-isomers formed in the previous step. The reaction also yielded several otherwise unidentified byproducts. Instead, **5** was cleanly hydrogenated using Wilkinson's catalyst (5 mol%) under an atmosphere of H_2 to afford **6** as a 1:1 mixture of diastereoisomers, ***anti*-6** and ***syn*-6**.

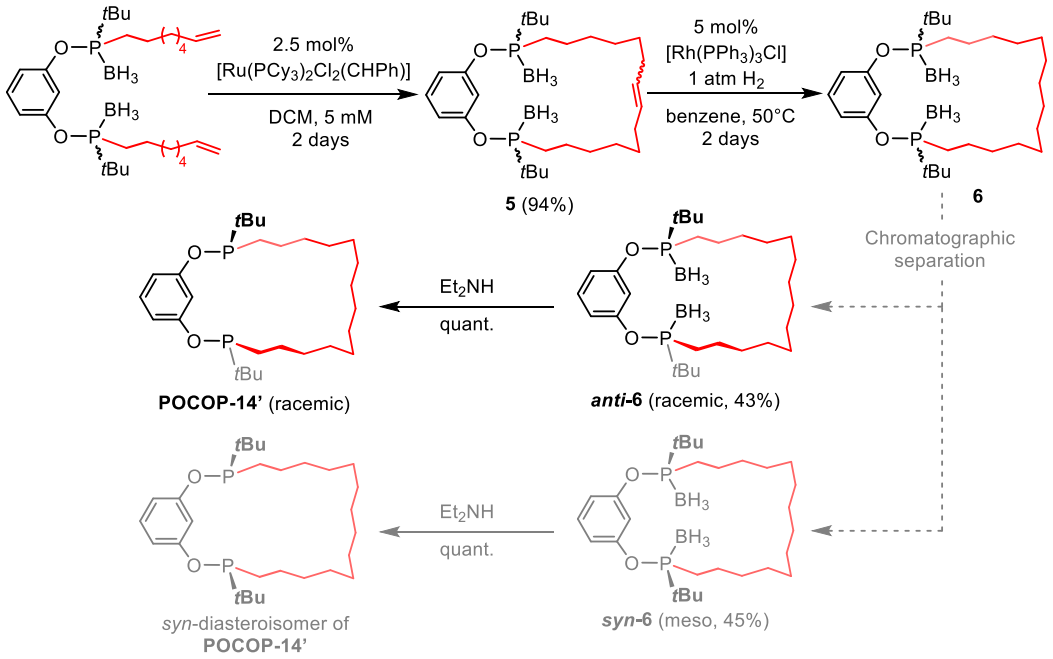

Scheme 2.10. Final steps of the preparation of **POCOP-14'**.

Product **6** is stable on silica and can be purified by column chromatography. Crucially, it was observed for the first time that the two diastereomers do not co-elute by TLC, with R_f values of 0.45 and 0.42 in 10% EtOAc in hexane. Purification by silica chromatography was carried out, albeit with great effort and difficulty. Indeed, direct separation of the two diastereomers on a 2 g scale was found to be impossible and coelution invariably occurred, even with very high silica loading and regardless of the polarity of the eluent. Analytically pure samples could only be obtained by performing repeated columns sequentially to yield increasingly diastereomerically enriched fractions until satisfactory purity was established by ^{1}H NMR spectroscopy. Although their respective ^{1}H NMR spectrum are significantly different, notably in the aromatic region (Figure 2.1), the stereochemistry of each could not be determined with certainty at this point.

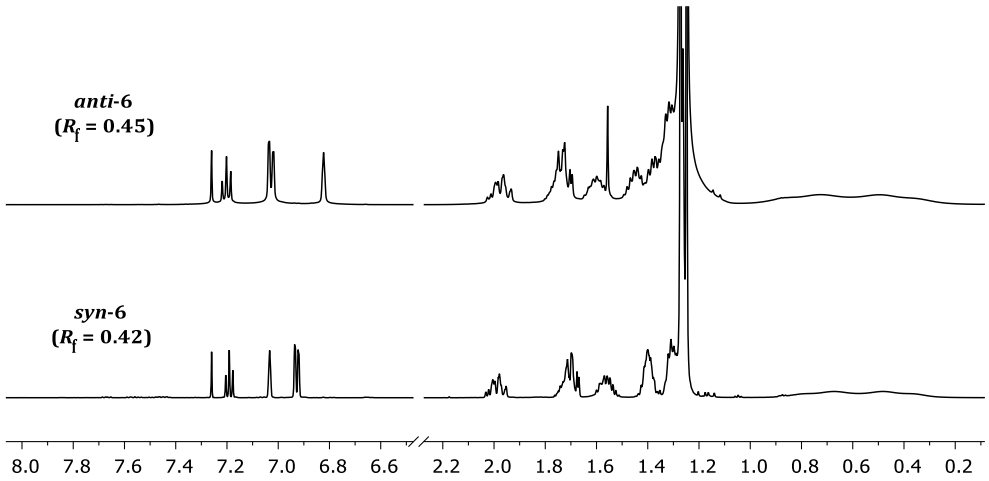

Figure 2.1. ^{1}H NMR spectra of ***anti*-6** (top) and ***syn*-6** (bottom).

Fortunately, crystals of both borane-protected diastereomers could be obtained by slow evaporation in hexane and the second fraction was unambiguously assigned to be the *syn*-isomer, ***syn*-6** (Figure 2.2, left), while the first was assigned to be the *anti*-isomer, ***anti*-6** (Figure 2.2, right). The P–B bond lengths (***syn*-6**, P2–B2, 1.915(8); P3–B3, 1.896(7); ***anti*-6**, B2–P2, 1.908(2); B3–P3, 1.905(2), B12–P12, 1.901(2); B13–P13, 1.904(2)) are very similar between the two isomers and are in line with previously reported phosphinite borane adducts in the literature (*viz.* P–B bond distances: (MesO)PH_2·BH_3, 1.882(6); (MesO)PhPH·BH_3, 1.894(3); (MesO) Ph_2P·BH_3, 1.917(5)).[28] Perhaps more surprisingly, the P–O bond distance in those reported compounds with a good leaving group are shorter than those found in ***syn*-6** and ***anti*-6** (***syn*-6**, P2–O107, 1.617(4); P3–O108, 1.630(4); ***anti*-6** P2–O107, 1.6323(9); P3–O108, 1.6270(9), P12–O207, 1.6284(10); P13–O208, 1.6274(10) vs (MesO)PH_2·BH_3, 1.597(3); (MesO)PhPH·BH_3, 1.6117(13); (MesO)Ph_2P·BH_3, 1.629(3)). This may be the indication of a rather weakened P–O bond in this scaffold, stemming from electron depletion both from the borane moiety and the phosphinite borane substituted aromatic cycle.

Finally, deprotection was achieved by dissolving these compounds in neat diethylamine over 7 days at room temperature. Monitoring by ^{31}P NMR spectroscopy showed the reaction to slow down progressively, as might be expected with an increase in the quantity of free phosphine in solution competing with diethylamine to re-form a borane adduct. Heating to 50°C allowed for complete and quantitative conversion after 2 days, and isolation of pure samples of **POCOP-14'** and its *syn* isomer.

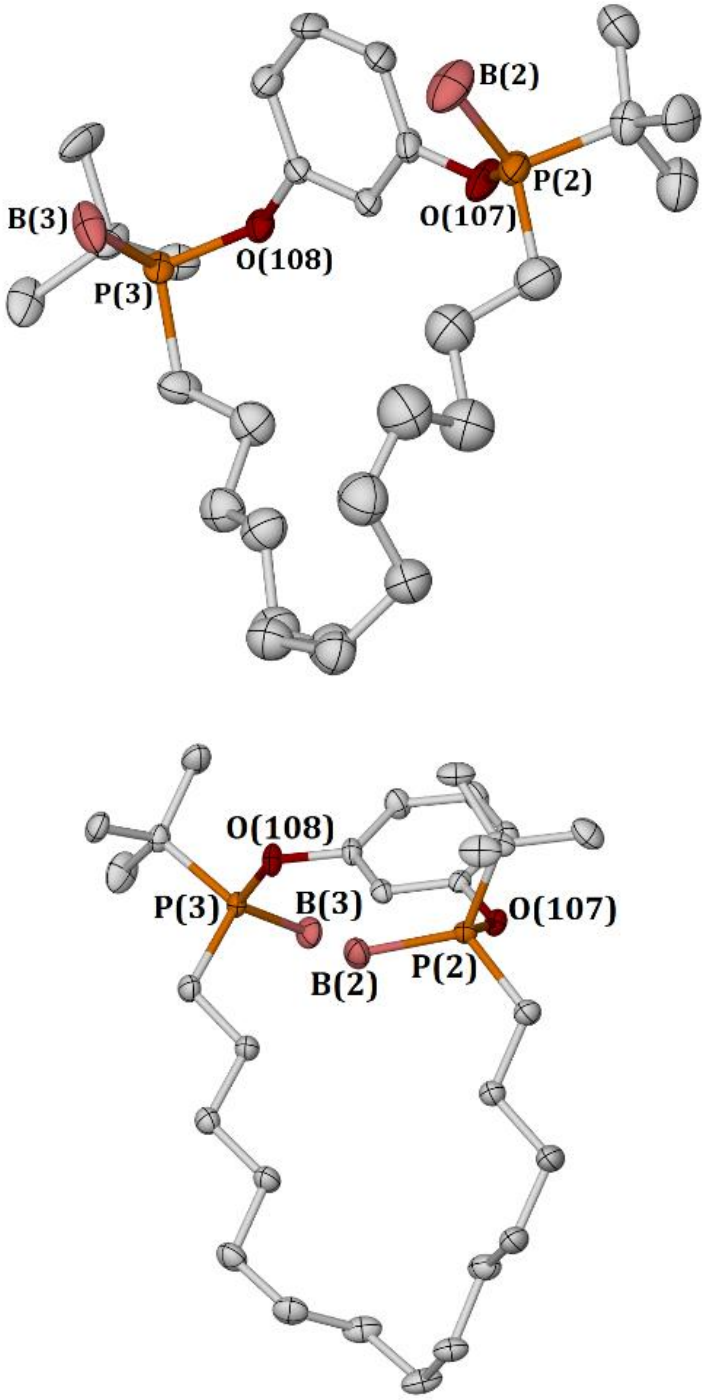

Figure 2.2. Solid-state structures of ***syn*-6** (top) and ***anti*-6** (bottom; one unique molecule, *Z*′ = 2). Thermal ellipsoids drawn at 40% and 50% probability, respectively; minor disordered components omitted (***syn*-6**; *t*Bu groups and methylene chain). Selected bond lengths (Å): ***syn*-6**, P2–B2, 1.915(8); P3–B3, 1.896(7); P2–O107, 1.617(4); P3–O108, 1.630(4); ***anti*-6**, B2–P2, 1.908(2); B3–P3, 1.905(2); P2–O107, 1.6323(9); P3–O108, 1.6270(9); B12–P12, 1.901(2); B13–P13, 1.904(2); P12–O207, 1.6284(10); P13–O208, 1.6274(10).

2.3. Development of an asymmetric route

2.3.1. Preparation of an enantiopure (oct-7-en-1-yl) substituted precursor

The difficulty in obtaining **POCOP-14'** as a pure diastereomer led us to develop an alternative, asymmetric synthetic route by adapting the literature methods developed by the Verdaguer group (*vide supra*).

Oxazaphospholidine **7** was prepared following a literature procedure from (–)-*cis*-1-amino-2-indanol and *tert*-butyldichlorophosphine. Compound **8** was successfully obtained in 91 % yield upon treatment with octenyl-magnesium bromide (Scheme 2.11). Unfortunately, subsequent reaction with hydrochloric acid in any proportion and concentration failed to provide phosphine chloride **2·BH$_3$**, leaving the starting material untouched. Amine methylation, bringing our system closer to the "ephedrine method", was successfully undertaken within the group (M. R. Gyton) to afford **8-Me**, but unfortunately also proved unreactive towards hydrochloric acid.

Thus, another method to cleave the chiral auxiliary was trialled instead involving concentrated sulfuric acid in a water/methanol mixture to afford the corresponding phosphinous acid borane **9** (Scheme 2.12). Subsequent mesylation provided a good leaving group for reaction with nucleophiles.[18]

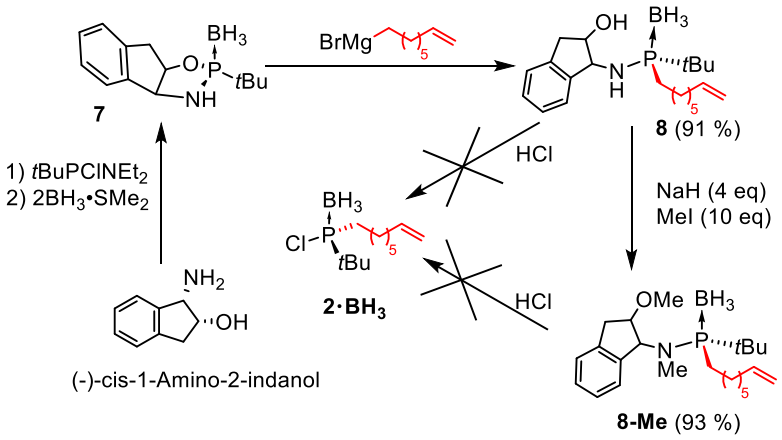

Scheme 2.11. Ring-opening of **7** with oct-7-en-1-yl magnesium bromide and attempted acidolysis of **8**/**8-Me** with HCl.

An adaptation of the literature conditions developed by Verdaguer *et. al.*[18] was necessary in this case as poor solubility of our starting material was found using the reported conditions – a 2:1 mixture of MeOH in water – which made the

reaction sluggish and unselective. The borane adduct may be cleaved under forcing conditions, which results in rapid tautomerisation to form the corresponding phosphine oxide; indeed prolonged heating at 80°C resulted in complete conversion of **8** to the corresponding phosphine oxide. On the other hand, a 20:1 MeOH to water mixture is adequate to dissolve the starting material, but promotes the formation of a greater amount phosphine oxide, with respect to the original 2:1 mixture. Optimal conditions were found to be a 3:1 MeOH to water mixture and heating at 70 °C for 4 days, however, formation of the phosphine oxide could not be entirely avoided. As opposed to the procedure reported in the literature, **9** was found to be slightly unstable on silica, further decomposing into the oxide. However, a short plug of silica in CH_2Cl_2 was sufficient to enable the isolation of the product in >95 % purity. This procedure was found to afford **9** in 87 % yield reproducibly.

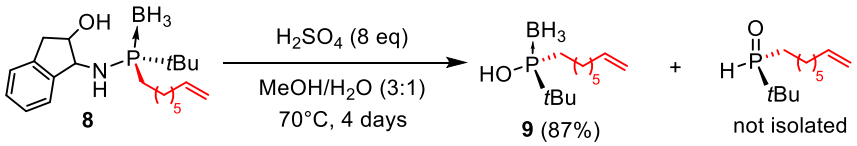

Scheme 2.12. Acidolysis of **8** using H_2SO_4.

2.3.2. Attempted asymmetric synthesis of the POCOP scaffold

Unfortunately, several attempts at reacting the mesylate of **9** with aromatic nucleophiles were unsuccessful, as highlighted in Table 2.1. Resorcinol was found to be unreactive under the literature conditions,[18] *i.e.* with an excess mesic anhydride with respect to **9**. Preliminary deprotonation with sodium hydride did not give any trace of product, nor did 2,6-diaminopyridine. It was envisioned that with the literature conditions the excess of mesic anhydride may react with the various nucleophiles to form unwanted mesylates, therefore losing their nucleophilic character. However, reducing the amount of mesic anhydride to stoichiometric proportions, with respect to **9**, did not afford any product either. Finally, even a more nucleophilic substrate like aniline did not yield any of the expected nucleophilic substitution product.

Table 2.1. Mesylation of **9** and reactions with various aromatic nucleophiles.

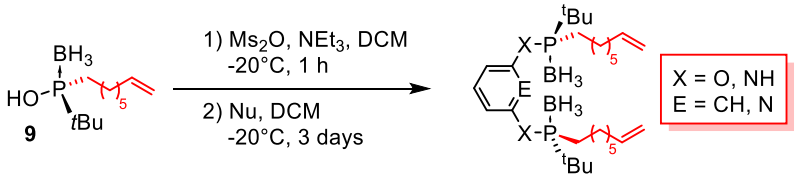

Nu	eq. of **9**	eq Ms_2O	yield (%)
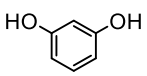	3	4.5	-
	3	3	-
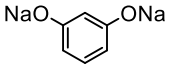	3	4.5	-
	3	3	-
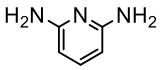	3	4.5	-
	3	3	-
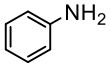	0.3	0.45	-

Alternatively, deprotonating **9** with LiHMDS, NaH or KHMDS generated the corresponding lithium, sodium or potassium salts. However, these substrates were not nucleophilic enough to promote S_NAr of fluorinated aromatic substrates (1,3-difluorobenzene, 2,6-difluoropyridine), failing to afford precursors to POCOP or PONOP macrocyclic pro-ligands (Scheme 2.13.). Thereafter, efforts to obtain a pincer ligand via this asymmetric route were focused on the PCP scaffold only.

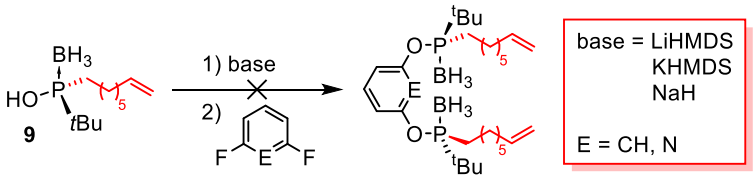

Scheme 2.13. Attempted synthesis of the POCOP/PONOP backbones *via* S_NAr.

*2.3.3. Preparation of tert-butyl(oct-7-en-1-yl)phosphine borane **10**.*

With phosphinous acid borane **9** in hand, attention turned to its conversion to the phosphine borane analogue. A range of conditions were trialled based on the

literature procedure reported by Verdaguer *et. al.*,[19] which are summarised in Table 2.2. An initial test on an NMR scale was carried out following the literature conditions, using tetrabutylammonium borohydride as reducing agent. With our system, these resulted in a 71% conversion to a new species with a ^{31}P shift of 22.3 ppm and attributed to be the product, in good agreement with literature values for similar compounds.[29] Unfortunately, no product could be isolated in any appreciable quantity at this step after workup and chromatography (entry 1). The reaction was repeated with a longer reaction time of 16 h, resulting in complete conversion of the starting material observed both by NMR spectroscopy and TLC (Entry 2). Column chromatography enabled the isolation of the desired product but in only 5% isolated yield. Simultaneously, another product was isolated which showed a complete loss of the terminal alkene signals by ^{1}H NMR spectroscopy. This result was initially attributed to the *in situ* generation of an equivalent of borane from the borohydride moiety, which can in turn add to the alkene double bond and be hydrolysed during the acidic work up to form the alkane.

Table 2.2. Optimization of conditions for the preparation of **10**.

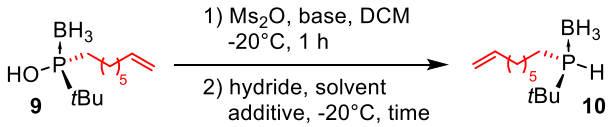

	Base (eq)	H⁻ source (eq)[a]	Add. (eq)	t (h)[b]	Conv.[c] / isol. yield **10**
1	NMM (1.25)	$[Bu_4N][BH_4]$ (3)	-	2	71% / -
2	NMM (1.25)	$[Bu_4N][BH_4]$ (3)	-	16	100% / 5%
3	NMM (1.25)	$[Bu_4N][BH_4]$ (3)	1-hexene (50)	16	18% / 15%
4	NMM (1.25)	$[Bu_4N][BH_4]$ (3)	1-hexene (10)	16	72% / 41%
5	NMM (1.25)	$[Bu_4N][BH_4]$ (3)	1-hexene (20)	16	65% / 56%
6	NEt_3 (2.5)	AlH_3 (4)	-	16	100% / 52%
7	NEt_3 (2.5)	AlH_3 (4)	-	3	100% / 59%
8	NEt_3 (2.5)	$[Bu_4N][BH_4]$ (1)	-	16	100% / 79%

(a) when $[Bu_4N][BH_4]$, reaction carried out in DCM. For AlH_3, in Et_2O; (b) reaction time after hydride source addition; (c) by ^{31}P NMR spectroscopy.

The reaction was therefore repeated in entry 3 with a large excess (50 eq) of 1-hexene chosen to be a sacrificial alkene to react with the generated borane equivalent. Unfortunately such a large excess made the reaction sluggish,

resulting in 18% conversion after 16 h, albeit effectively preventing the formation of the over reduced product and with **10** isolated in 15% yield. Reducing the excess of sacrificial alkene yielded better although still incomplete conversions with overall improved yields (41% and 56%, entries 4 and 5 respectively), however with 10 – 13% isolated yield of the over reduced product.

Using alane as an alternative reducing agent dramatically improved the conversion up to 100%, with the product representing 93% of the crude mixture by integration of the $^{31}P\{^{1}H\}$ NMR spectrum (entry 6). The rest was attributed to the formation of a phosphine oxide, putatively as a result of borane deprotection with the excess base and rapid tautomerisation. However, the product **10** was isolated pure in only 52% yield, hinting at the possibility of another, yet unidentified decomposition pathway. Repeating the reaction with the same conditions and monitoring by TLC showed complete conversion could be achieved within 3 h, and the product was isolated with a marginally improved yield of 59%.

Serendipitously, it was observed at this point that a pure, dried sample kept at room temperature overnight was not stable, the initially clear oil becoming more opaque and very viscous. Analysis of this product showed >80% loss of the desired product by ^{31}P NMR spectroscopy, converted to a new species with a ^{31}P shift of 29.9 ppm, consistent with a tertiary phosphine borane product.[29] Upon consulting the literature, this decomposition process was attributed to the uncatalysed hydrophosphination of alkenes with secondary phosphine boranes previously reported in the literature to occur under mild conditions and even at room temperature,[30] in our case either intramolecularly in a macrocyclization reaction or through intermolecular oligomerisation. Thus, **10** needs to be prepared and used immediately or alternatively must be stored as a dilute solution at or below -30°C.

This conclusion prompted a re-evaluation of our initial conditions using tetrabutylammonium borohydride. It was hypothesized that using an excess of triethylamine would also inhibit further reactivity with *in situ* generated BH_3. It was also discovered that complete conversion could be achieved using a stoichiometric amount of reducing agent instead of 3 equivalents. Consequently, the best conditions for the preparation of **10** are shown in entry 8, with excess NEt_3 and using stoichiometric tetrabutylammonium borohydride as a convenient

reducing agent at -20°C for 16 h. This enabled the isolation of **10** in 79% after work up and column chromatography.

2.3.4. Asymmetric synthesis of the PCP scaffold.

Phosphine borane **10** was readily deprotonated with *n*BuLi and reacted with bis(bromomethyl)benzene to afford pre-macrocyclic, borane protected pro-ligand **11** in excellent yield (Scheme 2.14).

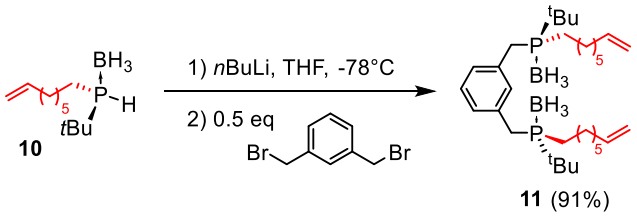

Scheme 2.14. Lithiation of **10** and preparation of **11**.

At this point, an initial deprotection test was carried out by dissolving **11** in neat diethylamine. Satisfyingly, complete removal of the borane group was observed after 3 days of heating to 50°C. Consequently, the remaining steps of the synthesis were carried out in a similar way to the previously described synthesis of **POCOP-14'** (Scheme 2.15). Ring closing metathesis was achieved under the same dilute conditions and using Grubbs' 1st generation catalyst to afford **12** in 91% yield after column chromatography, followed by hydrogenation using Wilkinson's catalyst yielding **13** in 88% isolated yield. Quantitative deprotection to afford **PCP-14'** was achieved in neat diethylamine with heating at 50°C in a sealed vessel for 4 days.

The considerably longer time it takes to fully deprotect **PCP-14'** than for **POCOP-14'** is consistent with the individual phosphine moiety in **PCP-14'** being more electron rich than its phosphinite counterpart in **POCOP-14'**, and it is therefore able to form a stronger borane adduct.

The presence of only one singlet for **PCP-14'** after the deprotection was a strong indication that only one diastereoisomer was formed *via* this synthetic route (*viz.* $\Delta\delta$ = 1.1 ppm by ^{31}P NMR spectroscopy for **POCOP-14'**).

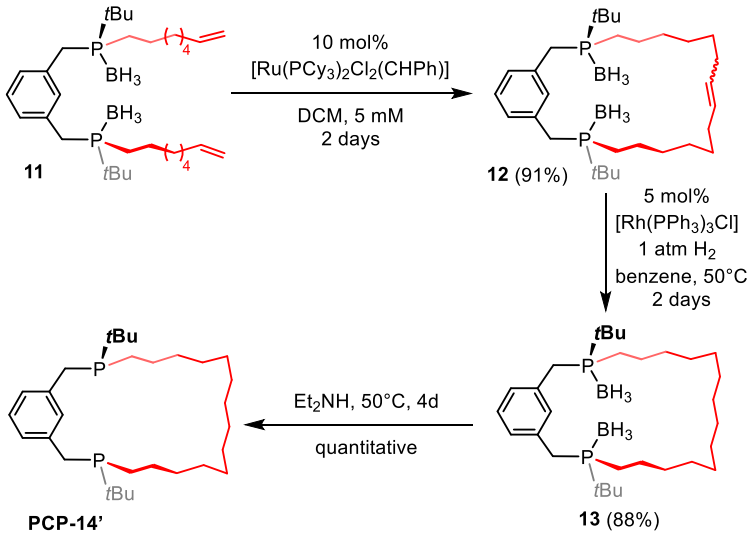

Scheme 2.15. Final steps for the synthesis of **PCP-14'**.

2.3.5. Enantiopurity determination

Methods to assess then stereopurity of an organophosphorus compound include the use of chiral derivatization agents in the view of distinguishing signals pertaining to the newly formed diastereomers by NMR, direct analysis by chiral HPLC or the use of chiral shift reagents that make use of Van der Waals or hydrogen bond interactions to form diastereomeric pairs in solution that are distinguishable by NMR. [31,32] Given the well-defined backbone of **PCP-14'** and **POCOP-14'** (which does not allow further chemical derivatization) as well as their air-sensitive character, the latter method was chosen. More specifically, a method published in 1985 by Kagan and co-workers using a chiral amide, (−)-3,5-dinitro-*N*-(1-phenylethyl)benzamide, as chiral shift agent was employed to determine the enantiopurity of various phosphine oxides.[33,34]

Following a literature method,[35] **PCP-14'** and **POCOP-14'** were successfully oxidized cleanly to **PCP-14'·O$_2$** and **POCOP-14'·O$_2$** in 84% and 95% yield after treatment with 3 Å molecular sieves to remove the water and hydrogen peroxide adducts (Scheme 2.16). Care was taken to limit the reaction time of **POCOP-14'·O$_2$** with molecular sieves, as prolonged exposure (>16 h) resulted in appreciable decomposition. This possibly stems from the mildly acidic character of zeolites, which can promote acid catalysed P–O bond cleavage, specially in this case as these bonds are weakened by both the aromatic substituent at the oxygen and the electron deficient P(V) oxide centre in **POCOP-14'·O$_2$**.

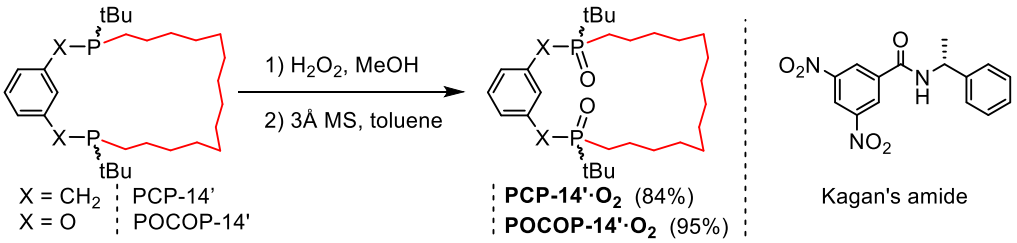

Scheme 2.16. Preparation of oxides **PCP-14'·O₂** and **POCOP-14'·O₂** (left) and Kagan's amide chiral shift agent (right).

In order to fully dissolve the chiral shift agent as well as maximise hydrogen bonding, CD_2Cl_2 was chosen as the solvent then 1, 2 and 5 equivalents of chiral shift agent were added. In the case of **POCOP-14'·O₂**, an increasing amount of chiral shift agent resulted in a visible splitting of the $^{31}P\{^1H\}$ singlet peak into two peaks of equal intensity (Figure 2.3), as well as distinct, albeit ill-defined changes in the alkyl region in the ^1H NMR spectrum. This is fully consistent with the preparation of **POCOP-14'** *via* a racemic route, in which the desired *anti* diastereomer is obtained as a racemate.

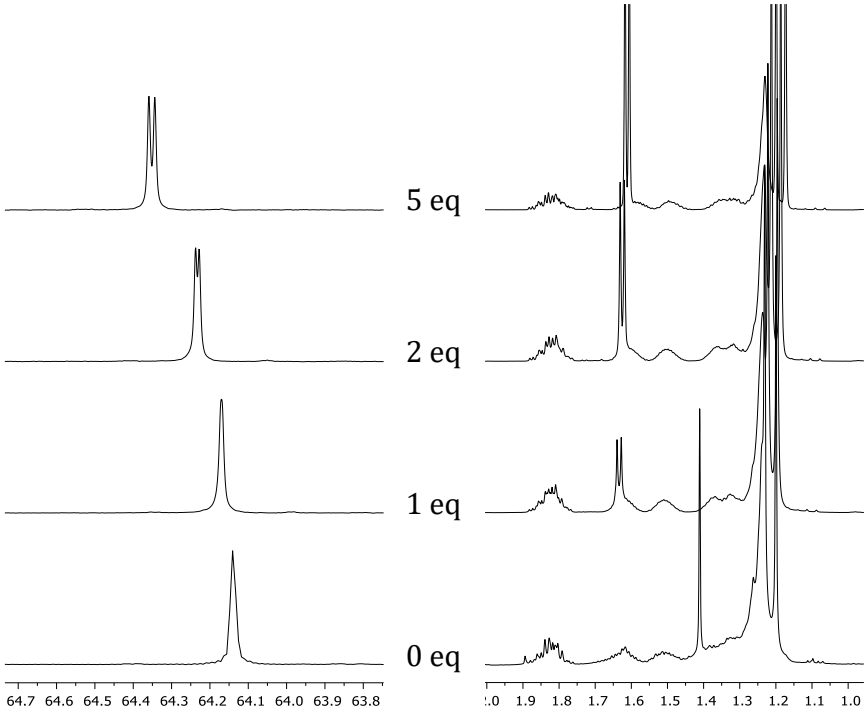

Figure 2.3. $^{31}P\{^1H\}$ (left) and ^1H NMR (right) spectra of **POCOP-14'·O₂** with 0, 1, 2 and 5 equivalents of chiral shift agent (CD_2Cl_2; 0 eq,162/500MHz; 1, 2 and 5 eq, 243/600 MHz).

A sample of **PCP-14'·O₂** was likewise treated with 1, 2 and 5 equivalents of chiral shift agent (Figure 2.4), and did not show any noticeable splitting or broadening of the singlet peak in the $^{31}P\{^1H\}$ NMR spectrum despite a pronounced downfield

shift (*ca*. 1.2 ppm). In addition, no changes in the splitting pattern pertaining to the backbone's methylene bridges could be observed, as opposed to the 4-6 Hz splitting commonly seen in structurally related phosphine oxide compounds in the literature.[33] This result, in conjunction with the absence of other NMR signals being observed during the deprotection step as well as the absence of separable diastereomers at any point, allowed the conclusion that **PCP-14'** was obtained in >95% ee, *i.e.* with an overall retention of the chiral information throughout the synthetic route.

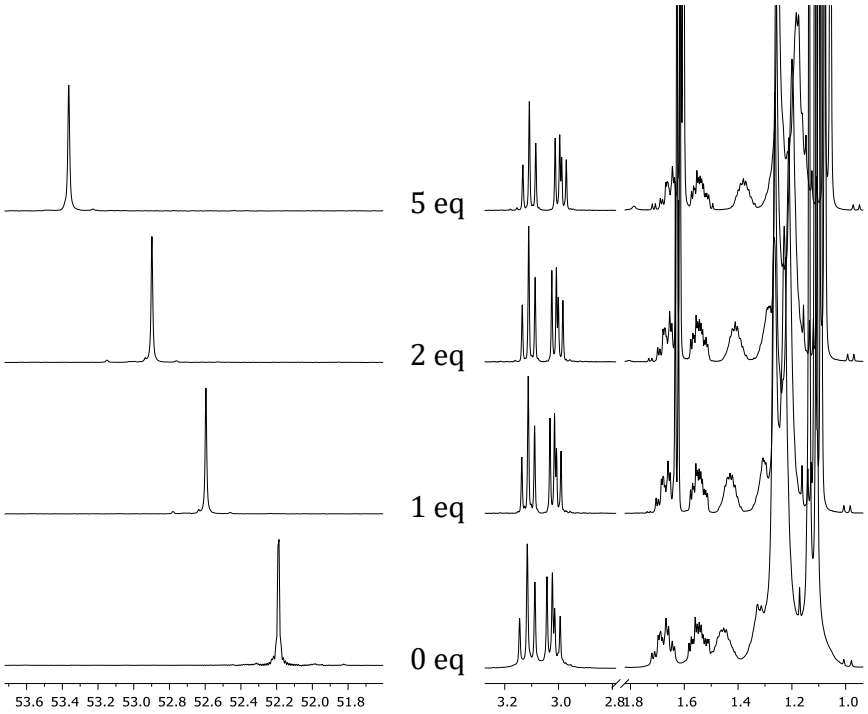

Figure 2.4. $^{31}P\{^{1}H\}$ (left) and ^{1}H NMR (right) spectra of **PCP-14'·O$_2$** with 0, 1, 2 and 5 equivalents of chiral shift agent (CD_2Cl_2; 0 eq,162/500MHz; 1, 2 and 5 eq, 243/600 MHz).

2.4. References

[1] D. Morales-Morales, in *Chem. Pincer Compd.*, Elsevier Science B.V., Amsterdam, **2007**, pp. 151–179.
[2] D. Benito-Garagorri, V. Bocokić, K. Mereiter, K. Kirchner, *Organometallics* **2006**, *25*, 3817–3823.
[3] S. Murugesan, B. Stöger, M. Weil, L. F. Veiros, K. Kirchner, *Organometallics* **2015**, *34*, 1364–1372.
[4] S. Kundu, Y. Choliy, G. Zhuo, R. Ahuja, T. J. Emge, R. Warmuth, M. Brookhart, K. Krogh-Jespersen, A. S. Goldman, *Organometallics* **2009**, *28*, 5432–5444.
[5] J. S. Ritch, D. Julienne, S. R. Rybchinski, K. S. Brockman, K. R. D. Johnson, P. G. Hayes, *Dalton Trans.* **2014**, *43*, 267–276.
[6] A. Grabulosa, J. Granell, G. Muller, *Coord. Chem. Rev.* **2007**, *251*, 25–90.
[7] L. Horner, H. Winkler, A. Rapp, A. Mentrup, H. Hoffmann, P. Beck, *Tetrahedron Lett.* **1961**, *2*, 161–166.
[8] K. M. Pietrusiewicz, M. Zablocka, *Chem. Rev.* **1994**, *94*, 1375–1411.
[9] Olaf. Korpiun, Kurt. Mislow, *J. Am. Chem. Soc.* **1967**, *89*, 4784–4786.
[10] Olaf. Korpiun, R. A. Lewis, James. Chickos, Kurt. Mislow, *J. Am. Chem. Soc.* **1968**, *90*, 4842–4846.
[11] J. R. Moncarz, N. F. Laritcheva, D. S. Glueck, *J. Am. Chem. Soc.* **2002**, *124*, 13356–13357.
[12] C. Scriban, D. S. Glueck, *J. Am. Chem. Soc.* **2006**, *128*, 2788–2789.
[13] I. Kovacik, D. K. Wicht, N. S. Grewal, D. S. Glueck, C. D. Incarvito, I. A. Guzei, A. L. Rheingold, *Organometallics* **2000**, *19*, 950–953.
[14] V. S. Chan, I. C. Stewart, R. G. Bergman, F. D. Toste, *J. Am. Chem. Soc.* **2006**, *128*, 2786–2787.
[15] M. Dutartre, J. Bayardon, S. Jugé, *Chem. Soc. Rev.* **2016**, *45*, 5771–5794.
[16] E. B. Kaloun, R. Merdès, J.-P. Genêt, J. Uziel, S. Jugé, *J. Organomet. Chem.* **1997**, *529*, 455–463.
[17] T. León, A. Riera, X. Verdaguer, *J. Am. Chem. Soc.* **2011**, *133*, 5740–5743.
[18] S. Orgué, A. Flores-Gaspar, M. Biosca, O. Pàmies, M. Diéguez, A. Riera, X. Verdaguer, *Chem. Commun.* **2015**, *51*, 17548–17551.
[19] E. Salomó, S. Orgué, A. Riera, X. Verdaguer, *Synthesis* **2016**, *48*, 2659–2663.
[20] S. Monfette, D. E. Fogg, in *Green Metathesis Chem.* (Eds.: V. Dragutan, A. Demonceau, I. Dragutan, E.Sh. Finkelshtein), Springer Netherlands, Dordrecht, **2010**, pp. 129–156.
[21] P. A. Chase, M. Lutz, A. L. Spek, G. P. M. van Klink, G. van Koten, *J. Mol. Catal. Chem.* **2006**, *254*, 2–19.
[22] E. V. Avtomonov, N. A. Ustynyuk, D. A. Lemenovskii, V. V. Kotov, *Z. Für Naturforschung B* **2014**, *56*, 812–822.
[23] T. M. Hood, M. R. Gyton, A. B. Chaplin, *Dalton Trans.* **2020**, DOI 10.1039/C9DT04474D.
[24] L. D. Quin, *A Guide to Organophosphorus Chemistry*, Wiley, New York, **2000**.
[25] M. Peruzzini, L. Gonsalvi, *Phosphorus Compounds: Advanced Tools in Catalysis and Material Sciences*, Springer Science & Business Media, **2011**.
[26] P. Pellon, *Tetrahedron Lett.* **1992**, *33*, 4451–4452.
[27] D. B. G. Williams, H. Lombard, M. Van Niekerk, P. P. Coetzee, *Phosphorus Sulfur Silicon Relat. Elem.* **2002**, *177*, 2115–2116.
[28] E. Rivard, A. J. Lough, I. Manners, *J. Chem. Soc. Dalton Trans.* **2002**, 2966–2972.
[29] N. Oohara, T. Imamoto, *Bull. Chem. Soc. Jpn.* **2002**, *75*, 1359–1365.
[30] D. Mimeau, O. Delacroix, A.-C. Gaumont, *Chem. Commun.* **2003**, 2928.
[31] *P-Stereogenic Ligands in Enantioselective Catalysis:*, Royal Society Of Chemistry, Cambridge, **2010**.
[32] O. I. Kolodiazhnyi, *Asymmetric Synthesis in Organophosphorus Chemistry: Synthetic Methods, Catalysis, and Applications*, Wiley-VCH Verlag GmbH & Co. KGaA, Weinheim, Germany, **2016**.
[33] E. Duñach, H. B. Kagan, *Tetrahedron Lett.* **1985**, *26*, 2649–2652.
[34] *Tetrahedron Asymmetry* **2003**, *14*, 1459–1462.
[35] C. R. Hilliard, N. Bhuvanesh, J. A. Gladysz, J. Blümel, *Dalton Trans* **2012**, *41*, 1742–1754.

Chapter 3

Synthesis of Rh and Ir complexes of macrocyclic POCOP-14 and PCP-14

With macrocyclic **POCOP-14'** and **PCP-14'** in hand, this chapter describes the metallation of these pincer proligands with iridium and rhodium centres. The focus will be placed, in particular, on the preparation of hydrido chloride species followed by their use as a platform to access polyhydride complexes. The corresponding M(I) carbonyl complexes were also targeted, with a view to using the carbonyl as a reporter group to assess the differences in electron density at the metal centre and gauge the net donor ability of our ligands. The preparation of $M^{III}(CO)(Cl)_2$ congeners was also investigated, which ultimately proved to be the most useful precursors.

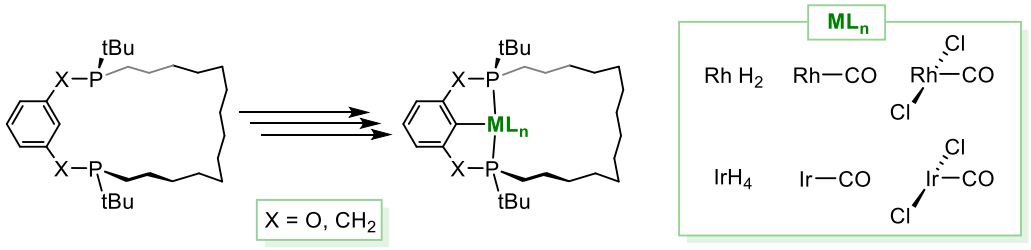

Note: in this chapter, both **PCP-14** and **POCOP-14** are drawn as a single *anti* enantiomer for clarity. However, in the case of **POCOP-14**, both enantiomers are always present and reacted as the racemate, i.e. (*R*,*R*)-**POCOP-14** and (S,S)-**POCOP-14**.

Part of the work described in this chapter has been published:

B. Leforestier, M. R. Gyton and A. B. Chaplin *Dalton Trans*. 2020, *in the press*, doi.org/10.1039/c9dt04835

3.1. Introduction

3.1.1. Synthesis of polyhydride pincer complexes

As was highlighted in Chapter 1, the vast majority of the reactivity accessible with group 9 pincer compounds requires the generation of 14VE low coordinate species, which may be accessed *via* the treatment of the hydridochloride complex with a base, or more commonly by reacting a polyhydride species with a sacrificial hydrogen acceptor.

Since the first synthesis of [(*t*Bu$_4$-PCP)Rh(H)(Cl)] and [(*t*Bu$_4$-PCP)Ir(H)(Cl)] by Shaw in 1976, these complexes have most commonly been prepared under fairly demanding conditions. The protocol they developed involved the direct use of the hydrated chloride salts $MCl_3 \cdot xH_2O$ (M = Rh, Ir) in a propanol/water mixture and reflux for 20 h (Figure 3.1).[1] The use of alkene-based precursors such as $[Ir(COE)_2Cl]_2$ was only reported in 2002, but similarly reflux conditions are necessary for metallation *via* C–H bond activation to go to completion.[2] Similarly, the metallation of POCOP-based scaffolds using $[M(alkene)_2Cl]_2$ precursors in toluene is often reported to occur in sealed vessels heated up to 150 °C for a prolonged time (5 to 18 h).[3–9] It is likely that the conformational freedom of the proligand may inhibit the metallation step: the instalment of bulky substituents (R' = *t*Bu, -CF_3) in positions 4, 6 on the aromatic backbone allowed the metallation step for POCOP scaffolds to be completed in 45 min in refluxing benzene.[10,11] The presence of these substituents effectively directs the phosphine groups so that they are pre-organised in a pincer-like fashion. The use of this steric aid was also shown to prevent the formation of undesired species such as coordination polymers, although in the context of the metallation of R$_4$-POCOP (R= *t*Bu, *i*Pr) with $[Ir(CO)_2Cl(p\text{-toluidine})]$.[12] An interesting alternative was reported in 2011 specifically for the metallation of *i*Pr$_4$-POCOP with $[Rh(COD)Cl]_2$: the reaction was carried out in pyridine to afford the hydrido chloride pyridine complex at room temperature in only 3 h, the desired hydrido chloride complex being generated by treatment with $BF_3 \cdot OEt_2$ to remove the pyridine moiety.[5]

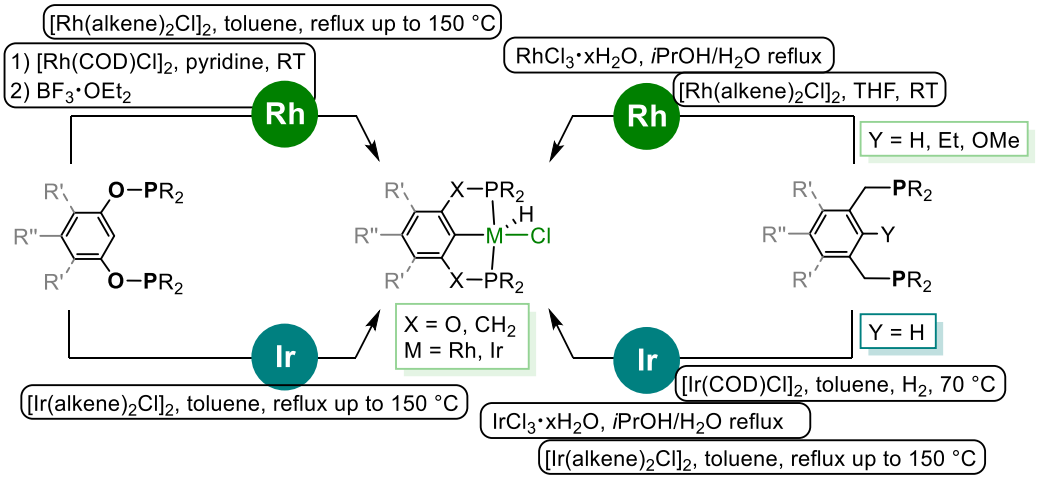

Figure 3.1. Various reagents and conditions employed for the preparation of PXCXP-based hydrido chloride complexes.

Among the four complexes in the (PXCXP)M series, the (PCP)Rh combination is the one that has benefitted from the greatest variety of synthetic protocols to access the hydrido chloride complex. Whilst it can be accessed through the methods reported above, notably by reaction of the proligand with $[Rh(COE)_2Cl]_2$, it was found that the reaction proceeded quantitatively in seconds in THF at room temperature.[13] Building on this system's ability to metallate *via* C-H and C-C bond activation, the Milstein group reported in 1998 a similar result with ethyl substituted pro-ligands. After an initial C-C activation step that affords the rhodium ethyl chloride complex, β-hydride elimination provides the hydrido chloride complex with loss of ethylene.[14,15] A similar procedure involving an initial C-O bond activation was reported earlier that same year, which occurs at room temperature and is accompanied by loss of formaldehyde.[16]

Polyhydride complexes can also be easily prepared in one step from the corresponding hydridochloride complexes (Scheme 3.1). The transformation is most readily achieved by treatment with $LiBHEt_3$ as a hydride source, the precipitation of LiCl constituting a strong driving force for the process, under an atmosphere of H_2 for the iridium complexes (Scheme 3.1).[6,17] Alternatively, a variety of bases have been shown to be effective in removing HCl to promote the formation of the polyhydride species under an atmosphere of H_2.[2,4,7,18–22]

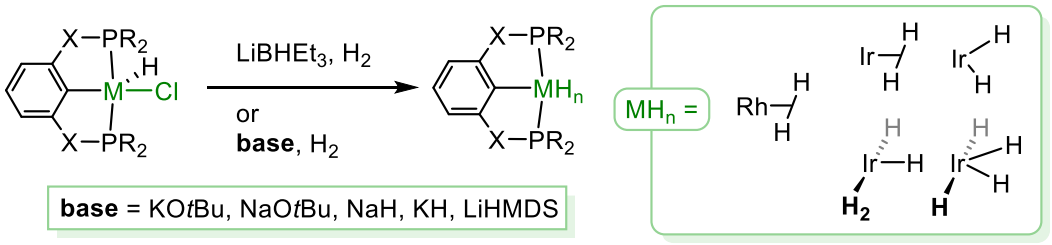

Scheme 3.1. Usual conditions for the preparation of PXCXP-based polyhydride species.

A major difference immediately appears between iridium and rhodium polyhydride complexes. Whilst the latter commonly coordinate only one equivalent of dihydrogen in a σ-bound fashion, their iridium counterparts are unstable with respect to oxidative addition of H_2. They have also been shown to subsequently bind a second equivalent of dihydrogen, and such complexes spontaneously form tetrahydride or dihydride dihydrogen complexes when placed under an atmosphere of H_2. In fact, generation of the dihydride species in iridium's case requires prolonged exposure to vacuum with or without heating in order to promote the loss of H_2.

3.1.2. Characterisation of polyhydride complexes

The presence of hydrides can be established by observation of a distinctly upfield resonances by ^{1}H NMR spectroscopy, or by IR spectroscopy with ν(M-H) bands usually between 1600 to 2200 cm^{-1} with varying intensity.[23] But the structural formulation of such complexes is not always straightforward: conventional NMR methods do not allow the determination of the classical or nonclassical nature of hydride ligands (Figure 3.2). This may sometimes be determined unequivocally by X-ray crystallography or more ideally by neutron diffraction.[24–28] Deuteration can be employed in order to observe the $^1J_{HD}$ coupling constant, the value of which decreases the more classical the hydride. This method is however limited to systems where no fluxionality is present, a feature that is unfortunately omnipresent in metal polyhydride species.[29]

To help distinguish between classical and nonclassical formulations, Crabtree developed an NMR method in 1987 which has been used extensively since. This method relies on the hypothesis that hydrogen nuclei that are classically

coordinated will relax much slower than hydrogen nuclei involved in a nonclassical coordination mode.[30] The spin lattice relaxation time T_1 is measured

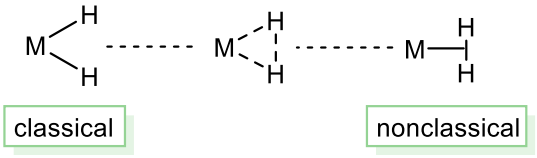

		Thresholds	
^{1}H MHz	B (T)	nonclassical	classical
250	5.874	< 80 ms	> 150 ms
300	7.049	< 96 ms	> 180 ms
400	9.398	< 128 ms	> 240 ms
500	11.747	< 160 ms	> 300 ms
600	14.095	< 193 ms	> 360 ms

Figure 3.2. Representations of classical and nonclassical hydride formulations for a generic MH_2 fragment (top) and table summarising T_1 value thresholds for their assignment (bottom).

by inversion recovery methodology at different temperatures to locate its minimal value. This was used to define what is now referred to as the "T_1 criterion", i.e. classical hydrides are characterized by T_1(min) values greater than 150 ms at 250 MHz, with non-classical hydrides exhibiting T_1(min) values lower than 80 ms. This criteria is generalizable to any machine as a result of T_1 being directly proportional to the field strength, and some corresponding values are reported in Figure 3.2.[30,31] Using this methodology, the T_1(min) values in [(tBu$_4$-PXCXP)M(H)$_n$] were determined to be 23 ms (X=O, M=Rh, n=2, 222 K, 500 MHz), 26 ms (X=CH$_2$, M=Rh, n=2, 228 K, 400 MHz), 110 ms (X=O, M=Ir, n=4, 220 K, 500 MHz) and 130 ms (X=CH$_2$, M=Ir, n=4, 220 K, 500 MHz).[22,23,32] On the basis of these, all rhodium complexes are straightforwardly assigned as non-classical σ-bound dihydrogen species, whilst the measurements for the iridium complexes leave a degree of ambiguity. Consequently, these two compounds were investigated further by Goldman's group, in a study that employs a combination of NMR, IR spectroscopy and computational methods.[23] This paper highlighted that different formulation as tetrahydride or dihydride dihydrogen complex are both possible (Scheme 3.2), and indeed were calculated to be nearly isoenergetic and linked by very low energy barriers for interconversion. Thus all the experimental measurements in the solid-state or in solution are best reconciled

by the description of these systems as dynamic in nature with a combination of classical and nonclassical characteristics.

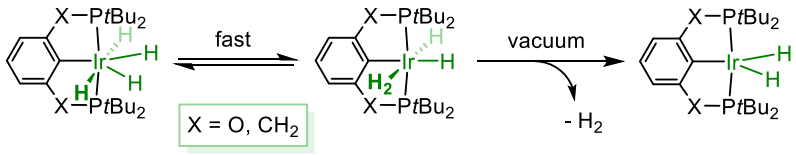

Scheme 3.2. Rapid exchange between tetrahydride and dihydride dihydrogen formulations and possible loss of dihydrogen for PXCXP-based iridium complexes.

3.1.3. Carbonyl complexes; synthesis and use of CO as a reporter group

The installation of carbonyl ligand on a pincer complex is facile and rapid on account of it being a strongly coordinating; it is an excellent π-acceptor which allows for a strong interaction with low-valent, late-transition-metal centres. In particular the extent of π-backbonding into the CO ligand is directly reflected by its solid-state (notably bond length) and spectroscopic properties, with IR spectroscopy the most practical. An approach that is all the more practical as the IR stretching band, ν(CO), is usually intense and conveniently located in the range 2150–1850cm^{-1} for singly bound terminal carbonyls, down to 1750 cm^{-1} for bridging carbonyls, an area of the spectrum that is relatively unperturbed by most other functional groups. The use of CO as a reporter group is well documented in the literature, with Tolman's electronic parameter (TEP) the quintessential example.[33,34] This parameter was initially based on the carbonyl stretching frequencies of complexes of the form [Ni(CO)$_3$L], but other less toxic examples have been employed involving most notably *cis*-[MCl(CO)$_2$L] (M = Rh, Ir).[35–39] Computational approaches have also provided useful complementary tools,[40] with an example applied to phosphines reported by Gusev in 2009.[41] In particular, the DFT method employed showed an excellent correlation between calculated gas-phase ν(CO) and experimental values, thereby allowing the accurate prediction of TEPs for phosphines not previously studied by Tolman as well as a wide variety of two electron donor ligands.[41,42]

The application of such methodology was extended to pincer chemistry only recently, with a 2015 study by Ozerov focused on diarylamido-based complexes of the formula [Rh(PNL)CO], where L is an imine or a phosphonite donor.[43] In

2019, the approach was employed by Langer *et. al.* to probe the donor strength of various main group fragments as the central donor of a PYP phosphine-based pincer, and complementarily by the Chaplin group to examine the variations in net donor abilities of different pincer backbones with an identical central donor (Figure 3.3).

Consequently, the formation of carbonyl complexes of rhodium and iridium for our ligands is of particular interest to provide a basis for the comparison of the net donor strength across the series. In the literature, such complexes are most commonly prepared by straightforward ligand substitution. Carbon monoxide is able to easily displace any other weaker L-type ligand in the coordination plane

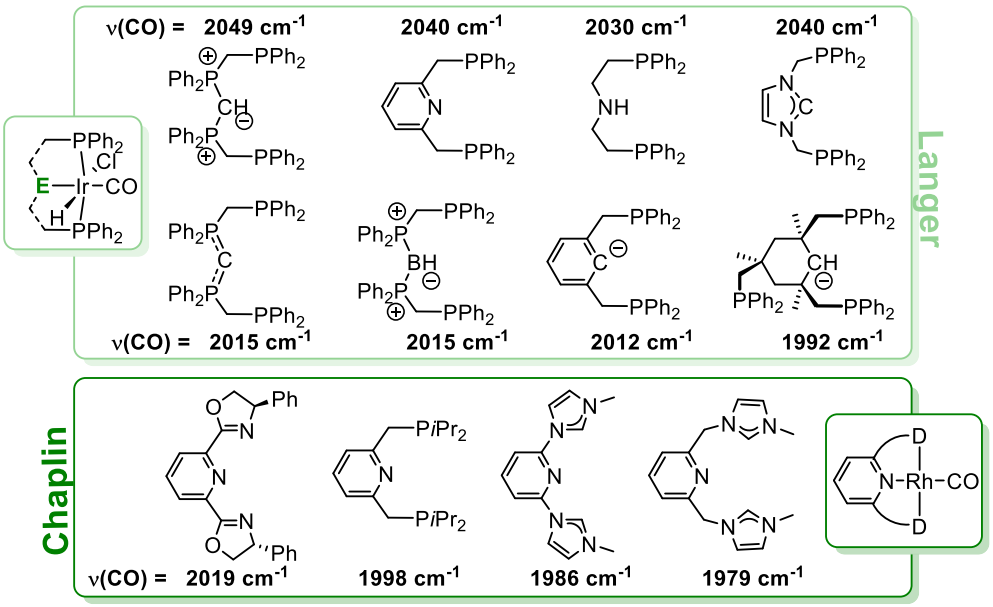

Figure 3.3. Literature examples for the use of CO as a reporter group to probe the net donor characteristics of pincer complexes.

quantitatively and in minutes (Scheme 3.3).[2,4,44–52] Variations around this procedure have been reported, by reacting the hydrido chloride complex with (i) CO and (ii) treatment with a base (or the reverse: (ii) then (i)),[7,19,53,54] or in the case of {(PCP)Ir} by treatment of the dihydride with methanol: O–H bond activation followed by β-hydride elimination affords a dihydride compound which readily loses H_2 to release the steric strain of the carbonyl ligand in that position.[55]

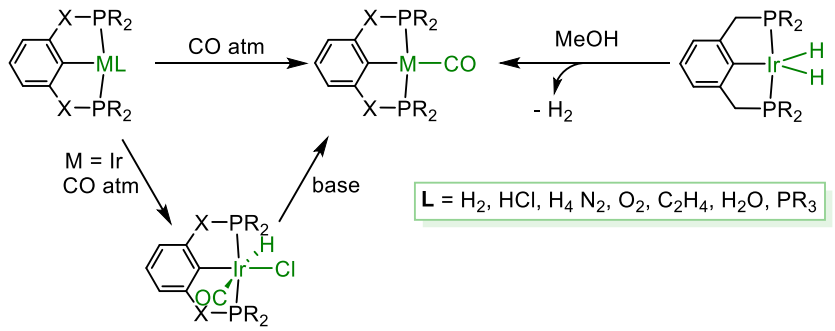

Scheme 3.3. Usual conditions for the preparation of PXCXP-based carbonyl complexes of rhodium(I) and iridium(I).

Alternatively, carbonyl complexes may be accessed directly as products of proligand metallation, by employing [Ir(CO)$_2$Cl(p-toluidine)] as the metal precursor. This approach was shown in a study from 2015 by the Goldman group, which also highlighted the effect of sterics (Scheme 3.4).[12] Metallation of the *i*Pr$_4$-POCOP proligand afforded a somewhat expected carbonyl hydrido chloride complex, with subsequent dehydrohalogenation with a base affording the carbonyl complex. Conversely, under the same conditions *t*Bu$_4$-POCOP afforded the Ir(I) carbonyl complex directly.[56]

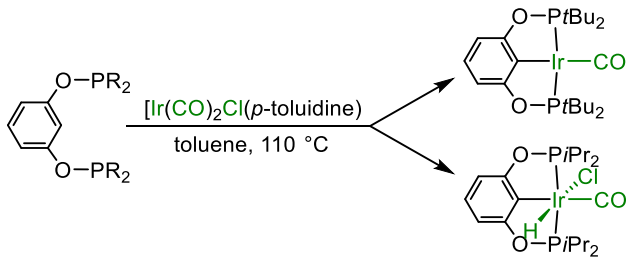

Scheme 3.4. P-substituent dependent metallation reactions.

Based on literature precedents, the synthesis of polyhydride species and carbonyl complexes of our ligands were investigated, for which we expected to access a spectrum in terms net donor strengths and reactivity across the series {(POCOP)Rh}, {(PCP)Rh}, {(POCOP)Ir}, {(PCP)Ir}.

3.2. Metallation and synthesis of polyhydride derivatives

3.2.1. Attempted synthesis of $M^{III}(H)(Cl)$ complexes

With proligands **POCOP-14'** and **PCP-14'** in hand, attention turned to investigating the metallation conditions with iridium precursors. Initial attempts at a direct adaptation of literature conditions for acyclic variants, *i.e.* with $[Ir(COD)Cl]_2$ in toluene at 150 °C for 12 h, unfortunately resulted in intractable mixtures of compounds as well as decomposition when applied to **POCOP-14'**, as observed by ^{31}P NMR spectroscopy. It was hypothesized that the elevated temperature promotes adverse reactions leading to the fragmentation of the POCOP backbone, and milder conditions were studied. Using the acyclic *t*Bu$_4$-POCOP proligand as a model, conditions developed by Goldman's group in 2004 were tested, whereby the metallation step is carried out at a lower temperature of 70 °C but under a H_2 atmosphere.[57] Satisfyingly, Goldman's study showed near complete conversion to the hydrido chloride complex was observed after 2 days at 70 °C under H_2 as indicated by a ^{31}P resonance at δ 174.9,[6] when less than 20% conversion was achieved in a control experiment under Ar (Scheme 3.5).

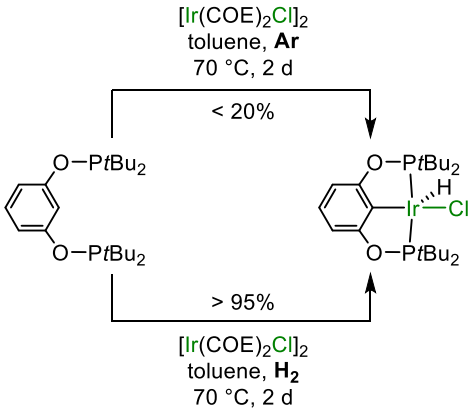

Scheme 3.5. Milder metallation conditions for the metallation of *t*Bu$_4$-POCOP.

Thus, metallation of **POCOP-14'** was attempted using the aforementioned conditions, with $[Ir(COE)_2Cl]_2$ (Scheme 3.6). Upon mixing in toluene, a colour change from orange to yellow was immediately observed, possibly indicating the displacement of the precursor's olefin ligands by the phosphines. The sample was degassed, placed under H_2 (1 atm) and heated to 70 °C for 1 h, which resulted in the formation of a thick orange gel. Heating to 110 °C dissolved the gel but

ultimately resulted in the formation of a dark orange precipitate which was found to be insoluble in most solvents (toluene, benzene, DCM, MeCN, acetone, chloroform, EtOH, water). Analysis of the mixture by NMR spectroscopy showed a complete loss of all ^{31}P resonances with the exception of a very weak signal at δ 164.7 which was later assigned as a polyhydride species (*vide infra*). Repeating the reaction under Ar at 70 °C afforded the same results. Similar behaviour has been reported in the literature during the formation of bis(phosphite) Ir and Pd complexes and was attributed to the ability of these ligands to bridge between metal centres and form insoluble polymeric materials.[12,58]

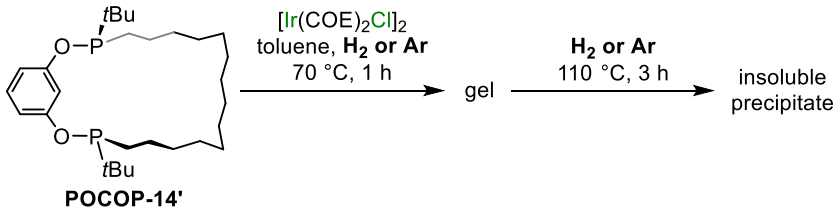

Scheme 3.6. Initial metallation attempt for **POCOP-14'** with $[Ir(COE)_2Cl]_2$.

The use of $[Ir(COD)Cl]_2$ as an alternative iridium precursor was trialled next. Gratifyingly the reaction with **POCOP-14'** did not form a gel or a precipitate and instead afforded a deep red solution after 18 h at 120 °C (Scheme 3.7). In the $^{31}P\{^1H\}$ NMR spectrum the appearance of one main species was observed at 170.3 ppm, along with very broad signals between 130 and 160 ppm. In the ^{1}H NMR spectrum, an upfield resonance was observed as a triplet ($^2J_{PH}$ = 14.3 Hz) at -32.74 ppm, characteristic of a hydride ligand *trans* to a vacant site in addition to alkene signals associated with free COD. Although distinctly downfield compared to the acyclic variant's hydride signal (*viz.* [(*t*Bu$_4$-POCOP)Ir(H)(Cl)] in d_2-DCM, δ(^{1}H) -41.39 (t, $^2J_{PH}$ = 13.1 Hz); δ(^{31}P) 175.8), the very similar coupling pattern of this resonance as well as the ^{31}P shift allowed the assignment of this new species as the hydrido chloride compound **Ir-14o**. Further heating at 120 °C for a total of 4 days resulted in the disappearance of the species associated with the broad signals and further conversion to **Ir-14o**, albeit with the concomitant formation of 2 new species, hereafter referred to as **Ir-20o** and **Ir-23o**. These species are characterised by a loss of C_2 symmetry, the presence of an additional hydride resonance for **Ir-23o** and were later identified as products of intramolecular C–H

bond activation (*vide infra*, section 3.4). The experiment was repeated under an atmosphere of H_2, with heating for 3 days which afforded complete conversion by NMR spectroscopy to **Ir-14o** as well as the formation of the previously observed species with a sharp ^{31}P resonance at 164.7 ppm, later identified as **Ir-15o**. Unfortunately, isolation of **Ir-14o** proved elusive, with decomposition to an intractable mixture of compounds occurring on prolonged exposure to vacuum and its very high solubility in alkanes and TMS afforded only oily residues on attempted crystallisation.

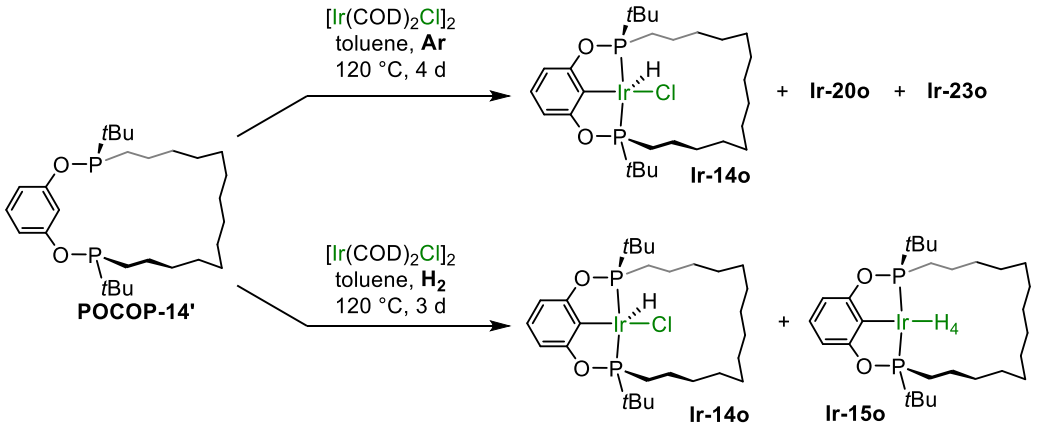

Scheme 3.7. Metallation of **POCOP-14'** with $[Ir(COD)Cl]_2$.

The same methods were applied to the metallation of **PCP-14'** with iridium precursors. Again, straightforward heating to 150 °C in the presence of 0.5 eq. of $[Ir(COE)_2Cl]_2$ in toluene resulted in an intractable mixture of compounds. Alternatively, repeating the reaction at 70 °C under H_2 gave a single compound after 18 h. It is characterized by a broad ^{31}P resonance at 42.4 ppm, therefore possibly dynamic in nature, and was putatively formulated as **pre-Ir-14c** (Scheme 3.8). In addition, the absence of hydride signals in the ^1H NMR spectrum as well as the presence of a singlet in the aromatic region unequivocally indicate that no cyclometallation occurred in these conditions. Further heating to 110 °C for 1.5 h resulted in little change to the reaction mixture, notwithstanding the appearance of minor broad signals in the $^{31}P\{^1H\}$ NMR spectrum with no associated hydride resonances by ^1H NMR.

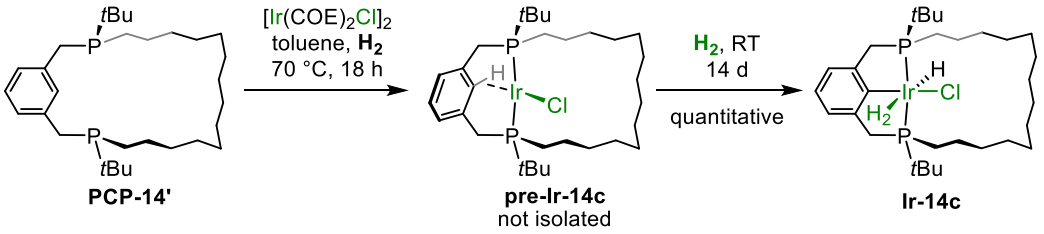

Scheme 3.8. Metallation of **PCP-14'** with $[Ir(COE)_2Cl]_2$.

Surprisingly, on one occasion, leaving the sample at room temperature for 14 days resulted in the complete and clean formation of a new asymmetric species characterised by two doublets in the $^{31}P\{^1H\}$ spectrum and a large $^2J_{PP}$ coupling constant of 312 Hz consistent with *trans*-coordinated phosphines as well as a hydride resonance at δ -21.79 (Figure 3.4). This signal is not as upfield as could be expected for a hydride *trans* to a vacant site, which could be explained by the (weak) coordination of a H_2 to complete the coordination sphere. This formulation is further supported by the observation of a very broad resonance centred at δ -2.84 (fwhm = 230 Hz) in the ^1H NMR spectrum, which would be consistent with a rapid exchange with dihydrogen in solution on the NMR timescale. This hypothesis is consistent with the observed asymmetry in the $^{31}P\{^1H\}$ NMR spectrum, thus conferred by the strictly C_2 symmetric nature of the ligand combined with a non-symmetric coordination sphere. Asymmetry is also observed in the ^1H NMR spectrum with the presence of two doublets in the alkyl region integrating to 9H each, coupling constants of 13.1 Hz and 13.9 Hz, respectively, and which may be assigned to the two P*t*Bu groups in the pincer. This spectroscopic evidence lead to the assignment of this species as **Ir-14c**. Switching to an Ar atmosphere through freeze-pump-thaw degassing resulted in the immediate loss of the signal at -2.84 ppm, and was accompanied by a significant broadening of the ^{31}P resonances as well. The compound could be recovered by freeze-pump-thaw degassing and placing the solution back under H_2. Similarly to **Ir-14o**, all attempts to isolate **Ir-14c** as a clean compound were unsuccessful, due to decomposition under vacuum and inaptitude for crystallisation. Unfortunately, this result could not be reproduced: any subsequent attempt at metallation with the same method gave only the intermediate compound **pre-Ir-14c**. It cannot be ruled out that the presence of adventitious moisture or oxygen upon prolonged storage at room temperature might have catalysed the metallation process, a hypothesis that could not be confirmed, however.

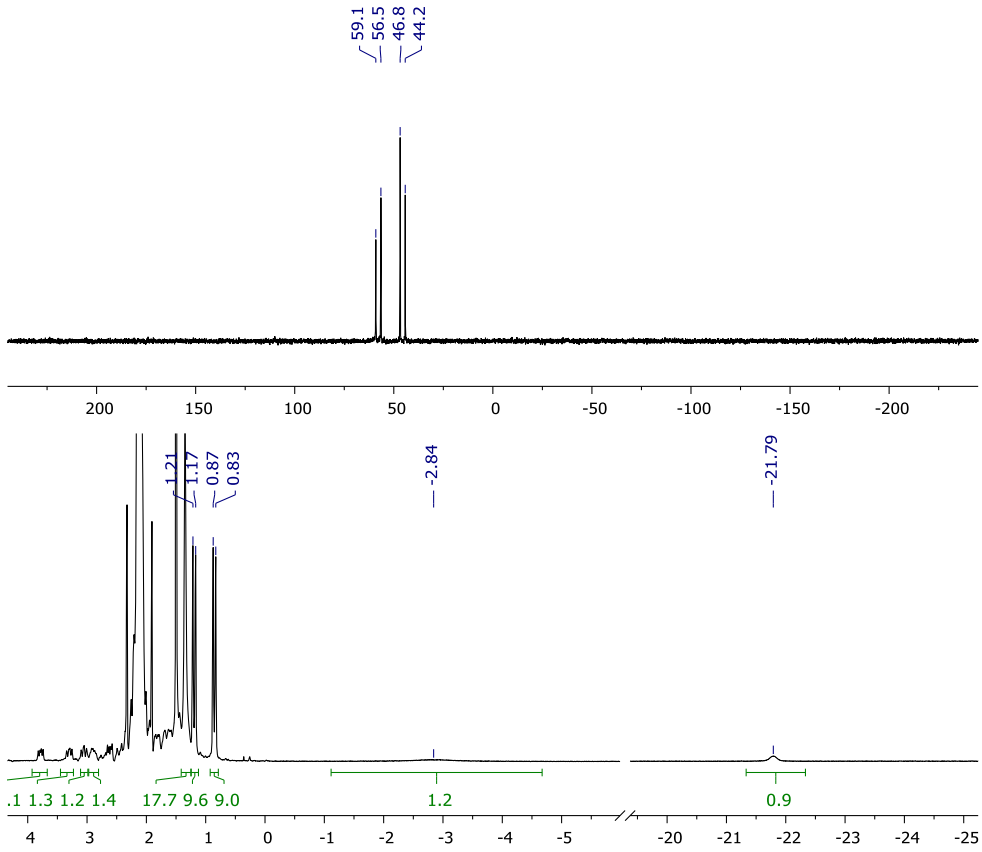

Figure 3.4. $^{31}P\{^{1}H\}$ (top) and ^{1}H (bottom) spectra of **Ir-14c** in toluene-d_0 (with C_6D_6 capillary) at 121 MHz and 300 MHz, respectively.

As opposed to the two cases with Ir described above, metallation of **PCP-14'** with $[Rh(COE)_2Cl]_2$ was found to be more straightforward. Heating a mixture of the ligand and the precursor at 100 °C in toluene for 18 h afforded a single species by ^{31}P NMR spectroscopy, asymmetric in nature with a large $^{2}J_{PP}$ coupling of 386 Hz that confirmed the *mer* coordination mode of the pincer scaffold. In the ^{1}H NMR spectrum, a corresponding hydride signal was observed at -21.50 ppm as a ddd due to the coupling to the Rh centre ($^{1}J_{RhH}$ = 31.9 Hz) and a different coupling constant for each phosphorus centre ($^{2}J_{PH}$ = 15.6, 10.8 Hz). Hence this species could be attributed to compound **Rh-14c** (Scheme 3.9), which also showed poor stability under vacuum and once again, all attempts at isolation resulted in an intractable mixture of compounds that could not be separated by usual methods. The reaction was repeated under an atmosphere of H_2 at 110 °C and afforded complete conversion overnight to **Rh-14c** as well as *ca.* 5 % of a new, C_2-symmetric species at 70.4 ppm (d, $^{1}J_{RhP}$ = 153 Hz), later identified as the dihydrogen complex **Rh-15c** (*vide infra*).

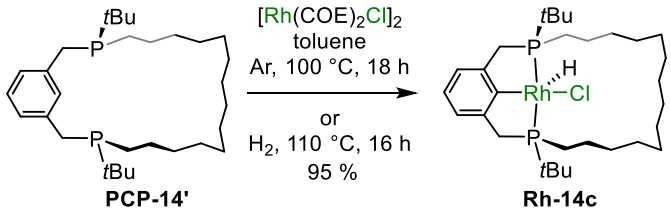

Scheme 3.9. Metallation of **PCP-14'** with $[Rh(COE)_2Cl]_2$.

Finally, the focus turned to the metallation of **POCOP-14'** with Rh precursors (Scheme 3.10). The ligand was treated with 0.5 eq $[Rh(COE)_2Cl]_2$ and heated to 120 °C in toluene for 18 h, which resulted in the formation of one main species, which was attributed to the hydrido chloride compound **Rh-14o**. Similarly to its Ir congener, **Rh-14o** exhibits a single signal by ^{31}P NMR spectroscopy with a $^{1}J_{RhP}$ coupling constant consistent with a Rh(III) centre ($\delta(^{31}P)$ 185.3, d, $^{1}J_{RhP}$ = 120 Hz), and is associated with an upfield hydride resonance at -23.53 ppm (dt, $^{1}J_{RhH}$ = 32.7 Hz, $^{2}J_{PH}$ = 13.1 Hz), only marginally downfield from reported acyclic variants (viz. -P*t*Bu$_2$, δ -27.13, $CDCl_3$; -P*i*Pr$_2$, δ -25.19).[3] Other species could be observed in the $^{31}P\{^{1}H\}$ NMR spectrum as broad signals and are likely to be non cyclometallated species. Indeed, heating to 120 °C for a total of 2 days resulted in the complete disappearance of these signals, albeit with the formation of a new species (15% of the mixture by integration) which showed a loss of C_2 symmetry, a *trans* $^{2}J_{PP}$ coupling constant (257 Hz) as well as significantly larger $^{1}J_{RhP}$ coupling constants of 157 and 159 Hz, respectively, consistent with a yet unidentified Rh(I) species. For consistency, the reaction was also repeated under a H_2 atmosphere and afforded a similar conversion to **Rh-14o**, however, further heating to 120 °C gave rise to the formation of a C_2-symmetric, Rh(I) species (d, $^{1}J_{RhP}$ = 165 Hz) at 198.4 ppm instead, which was later characterised as the dihydrogen complex **Rh-15o** (*vide infra*). This was thought to occur either *via* displacement and loss of gaseous HCl by solvated H_2 in excess, or *via* hydrogenation of the unidentified species. Compound **Rh-14o** displayed the same stability issues as its congeners which also precluded its isolation as a pure compound.

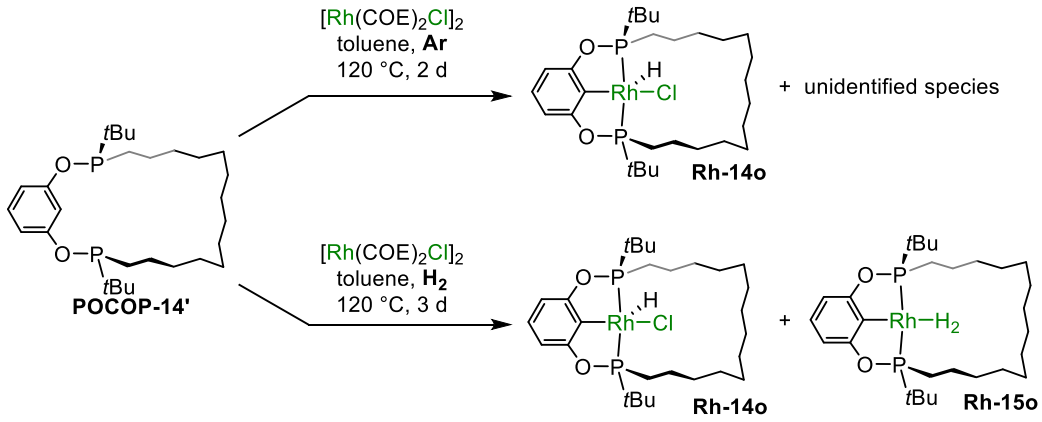

Scheme 3.10. Metallation of **POCOP-14'** with $[Rh(COE)Cl]_2$.

3.2.2. One-pot synthesis of polyhydride derivatives

As the hydridochloride complexes **M-14o,c** proved difficult to prepare and could not be isolated as clean compounds, other metal derivatives were explored. The aforementioned observation of the polyhydride complexes, as well as literature precedent for their use as useful organometallic precursors, prompted us to investigate the possibility to form these complexes directly in a one pot procedure, following initial metallation.

Satisfyingly, rhodium dihydrogen complexes **Rh-15o** and **Rh-15c** could be prepared in quantitative spectroscopic yield *via* metallation with $[Rh(COE)_2Cl]_2$ under H_2 under the conditions developed previously, followed by direct treatment with KO*t*Bu at 120 °C under a dihydrogen atmosphere (Scheme 3.11). Both **Rh-15o** and **Rh-15c** could be characterized *in situ* by NMR spectroscopy and adopt time-averaged C_2 symmetry with ^{31}P resonances at δ 198.4 (d, $^1J_{RhP}$ = 165 Hz) and 70.4 (d, $^1J_{RhP}$ = 153 Hz), with the large coupling constants to Rh indicative of a +I oxidation state, and broad hydride resonances at δ -2.87 (**Rh-15o**) / -4.36 (**Rh-15c**), respectively. The latter's more upfield signal may be explained by an expected higher net donating ability offered by a {(PCP)Rh} fragment than a {(POCOP)Rh} fragment, resulting in a slightly more activated H_2 and greater hydridic character.

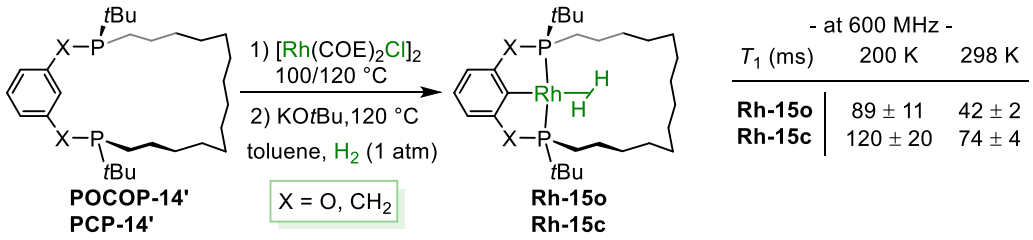

Scheme 3.11. Preparation of **Rh-15o** and **Rh-15c** and associated T_1 relaxation times.

The structural formulations of these complexes are supported by short spin-lattice relaxation times at 200 K under Ar (T_1^{200K} = 89 ± 11 ms, **Rh-15o**; T_1^{200K} = 120 ± 20 ms, **Rh-15c**; 600 MHz), consistent with nonclassical hydrides, with the higher value for the (PCP)Rh complex in agreement with its more electron-rich centre.[22,32,59] The measurements repeated at 298 K unexpectedly gave significantly shorter relaxation times (T_1^{298K} = 42 ± 2 ms, **Rh-15o**; T_1^{298K} = 74 ± 4 ms, **Rh-15c**; 600 MHz), which could indicate that exchange between coordinated and dissolved H_2 is fast on the NMR timescale, thereby artificially shortening the measured relaxation time. This suggests and supports the observed poor stability of these complexes under an Ar atmosphere and vacuum.

In a similar manner to that employed for the rhodium complexes, iridium tetrahydride complexes **Ir-15o** and **Ir-15c** were prepared by metallation with $[Ir(COD)Cl]_2$ and $[Ir(COE)_2Cl]_2$, respectively, in toluene under the previously developed conditions and subsequent treatment with KO*t*Bu at 120 °C under H_2 (Scheme 3.12).

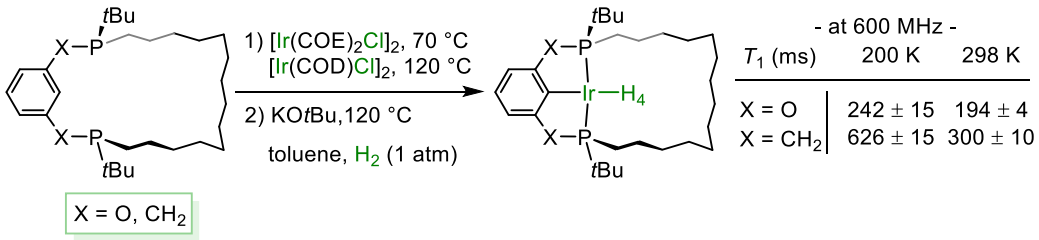

Scheme 3.12. Preparation of **Ir-15o** and **Ir-15c** and T_1 relaxation times.

These complexes adopt time-averaged C_2 symmetry with sharp ^{31}P singlet resonances at 165.0 and 49.9 ppm, respectively. In the ^1H NMR spectrum these complexes show a relatively sharp triplet, integrating to 4H at δ -8.26 ($^2J_{PH}$ = 9.9 Hz, **Ir-15o**) and δ -8.99 ($^2J_{PH}$ = 9.8 Hz, **Ir-15c**) at 298 K, and which broaden

slightly on cooling to 200 K. Spin-lattice relaxation times were determined at 200 K (T_1^{200K} = 242 ± 15 ms, **Ir-15o**; T_1^{200K} = 626 ± 15 ms, **Ir-15c**; 600 MHz) and are consistent with structures with a significantly more pronounced classical hydride character (at 600MHz, classical hydrides T_1 > 360 ms, nonclassical hydrides T_1 < 193 ms).[30,31] The T_1^{200K} for **Ir-15c** is indicative of an Ir(V) tetrahydride structure, whilst the T_1^{200K} for **Ir-15o** does not allow it to be classified as either. The T_1 values at 298 K were likewise measured and found to be significantly shorter (T_1^{298K} = 194 ± 4 ms, **Ir-15o**; T_1^{298K} = 300 ± 10 ms, **Ir-15c**; 600 MHz). Therefore once again loss of H_2 in solution and dynamic exchange cannot be ruled out, ultimately the structures for **Ir-15o,c** are best described as fluxional in nature, where dynamic interconversion between classical tetrahydride and dihydride dihydrogen formulations occurs rapidly on the NMR timescale (Scheme 3.13). Such behaviour was also noted by Goldman's group in 2010 for the *t*Bu-substituted acyclic variants of our complexes.[23]

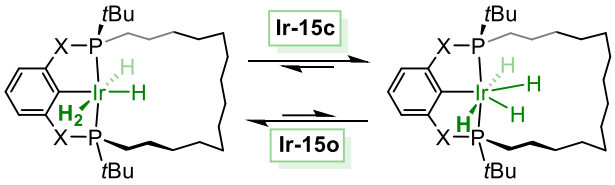

Scheme 3.13. Proposed rapid interconversion between tetrahydride and dihydride dihydrogen formulations for **Ir-15o,c**.

Complexes **Ir-15o,c** displayed very poor stability under both Ar atmosphere and reduced pressure, which precluded their isolation and they could only be used *in situ* thereafter. Further complicating their characterisation in solution, particularly in the case of **Ir-15o**, rapid H/D exchange was noted in deuterated solvents at several positions in the complex, even at room temperature, namely at the hydride position, on the alkyl chain, the *t*Bu groups and on the aromatic backbone (Figure 3.5). This deuteration occurred too quickly in the case of **Ir-15o** for its characterisation to be carried out in toluene-d_8, C_6D_6 or even cyclohexane-d_{12}, and characterisation was therefore carried out in *proteo*-toluene. Conversely, this work highlights the ability of this class of pincer complexes to catalyse hydrogen isotope exchange in mild conditions, which could find applications in the preparation of relevant isotopically labelled compounds. The

latter are critical in drug development processes or more generally in studying reaction mechanisms.[60,61] Whilst the ability of Ir pincer complexes to catalyse H/D exchange with on hydrocarbons with solvent as a deuterium source has been documented previously by the groups of Hartwig,[62] Grubbs,[63] or more recently Wendt,[64] they remain limited to unsaturated hydrocarbons under mild conditions, unactivated alkanes requiring higher temperatures up to 150 °C. Only one recent example of a {(PCP)Ir} complexe was reported by Smith *et. al.* to catalyse H/D exchange on linear alkanes under mild conditions.[65]

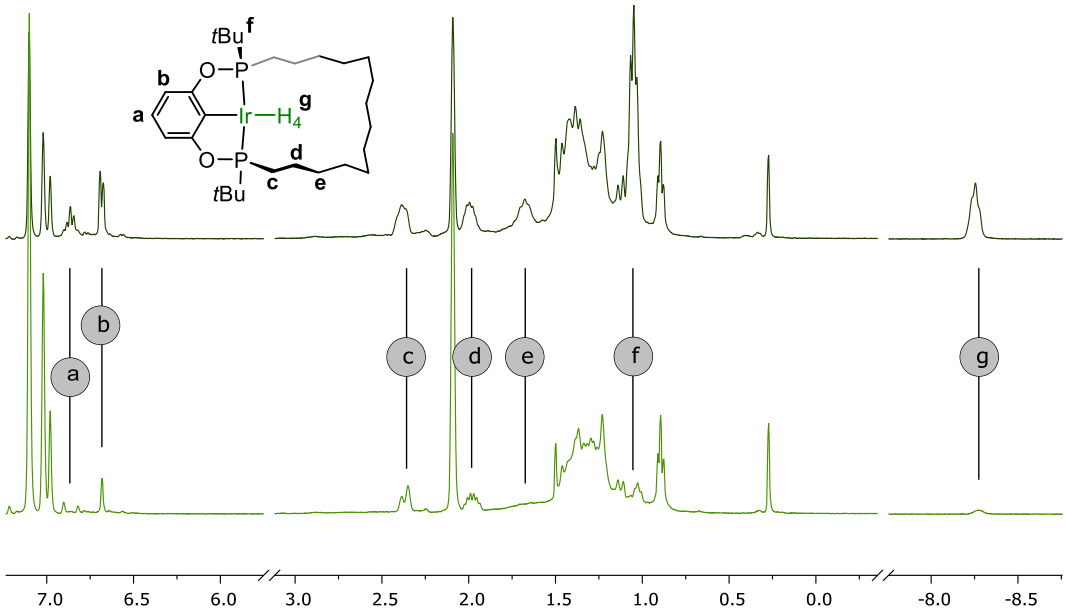

Figure 3.5. ^{1}H NMR spectra (400 MHz) of **Ir-15o** in toluene-d_8 under H_2 atmosphere after 5 min at room temperature (top) and after 14 h at room temperature (bottom).

Further studies would be required in order to ascertain the mechanisms for the observed H/D exchange with the various deuterated solvents used. Nevertheless, it is likely that **Ir-15o,c**'s ability to quickly and reversibly dehydrogenate its alkyl chain intramolecularly (*vide infra*) is a key step in the process, as it provides both unsaturated moieties able to insert into M–(H/D) bonds as well as the flexibility in the coordination sphere required to open the coordination space for bond-activating interaction with the deuterated solvent or $(H/D)_2$. The latter may also be achieved *via* reductive elimination at the pincer backbone's aryl position, although the possibility of an Ir(V) intermediate cannot be ruled out either.

Whilst the intramolecular processes evoked above account for the H/D exchange reactions at the alkyl chain's and the *tert*-butyl groups' positions, the partial deuteration of the aromatic backbone suggests the presence of additional intermolecular processes which favour H/D exchange at the less hindered position (Figure 3.5, (a)).

3.3. Metal carbonyl complexes

3.3.1. Synthesis of carbonyl complexes

With pure polyhydride species **M-15o,c** able to be generated in toluene solution, attention turned to the preparation of the corresponding metal carbonyl complexes which offer a spectroscopic handle to quantify the net donor ability and enhance the prospect for isolation from solution.

Toluene solutions of iridium complexes **Ir-15o,c** were therefore degassed and immediately placed under CO atmosphere. In accordance with the dynamic behaviour described in section in 3.2.2, one equivalent of H_2 was rapidly displaced by CO to form *cis*-dihydride Ir(III) species ***cis*-Ir-16o,c** evidenced by loss of C_2 symmetry, large *trans* $^2J_{PP}$ coupling constants and two hydride resonances each integrating to 1H (***cis*-Ir-16o**, δ(^{1}H) –9.82 (t), –10.75 (dd); δ(^{31}P) 160.4, 154.6 ($^2J_{PP}$ = 305 Hz); ***cis*-Ir-16c**, δ(^{1}H) –10.66 (ddd), –11.59 (td); δ(^{31}P) 51.0, 45.8 ($^2J_{PP}$ = 286 Hz)). Heating to 120 °C under CO for several days resulted in a mixture of three species, ***cis*-Ir16o,c**, a new C_2-symmetric species assigned to ***trans*-Ir-16o,c** and an additional species characterised by a singlet by ^{31}P NMR spectroscopy, **Ir-17o,c**. The latter was notably observed to be moderately sharp under a full atmosphere of CO but broad under partial atmosphere of CO. Additional heating in the presence of *tert*-butylethylene under CO ultimately resulted in the formation of the latter species exclusively. Upon repeated degassing and placing the samples under an Ar atmosphere, the signals for **Ir-17o,c** sharpened to singlets (**Ir-18o**, δ(^{31}P) 186.7; **Ir-18c**, δ(^{31}P) 68.1).

The assignment of **Ir-18o,c** as Ir(I) carbonyl complexes was later confirmed by solid-state characterisation, in which case the initially formed species that were observed as broad signals in the ^{31}P{^{1}H} NMR spectrum may only arise from coordination of a second CO ligand to form bis(carbonyl) complexes of either distorted trigonal bipyramidal geometry (likely for **Ir-17o**) or distorted square pyramidal geometry (likely for **Ir-17c**).[66] Unfortunately, isolation of both carbonyl complexes at this point was prevented by their unexpected instability upon concentration in vacuo or their excellent solubility in all tested organic solvents (DCM, hexane, cyclohexane, HMDSO, TMS).

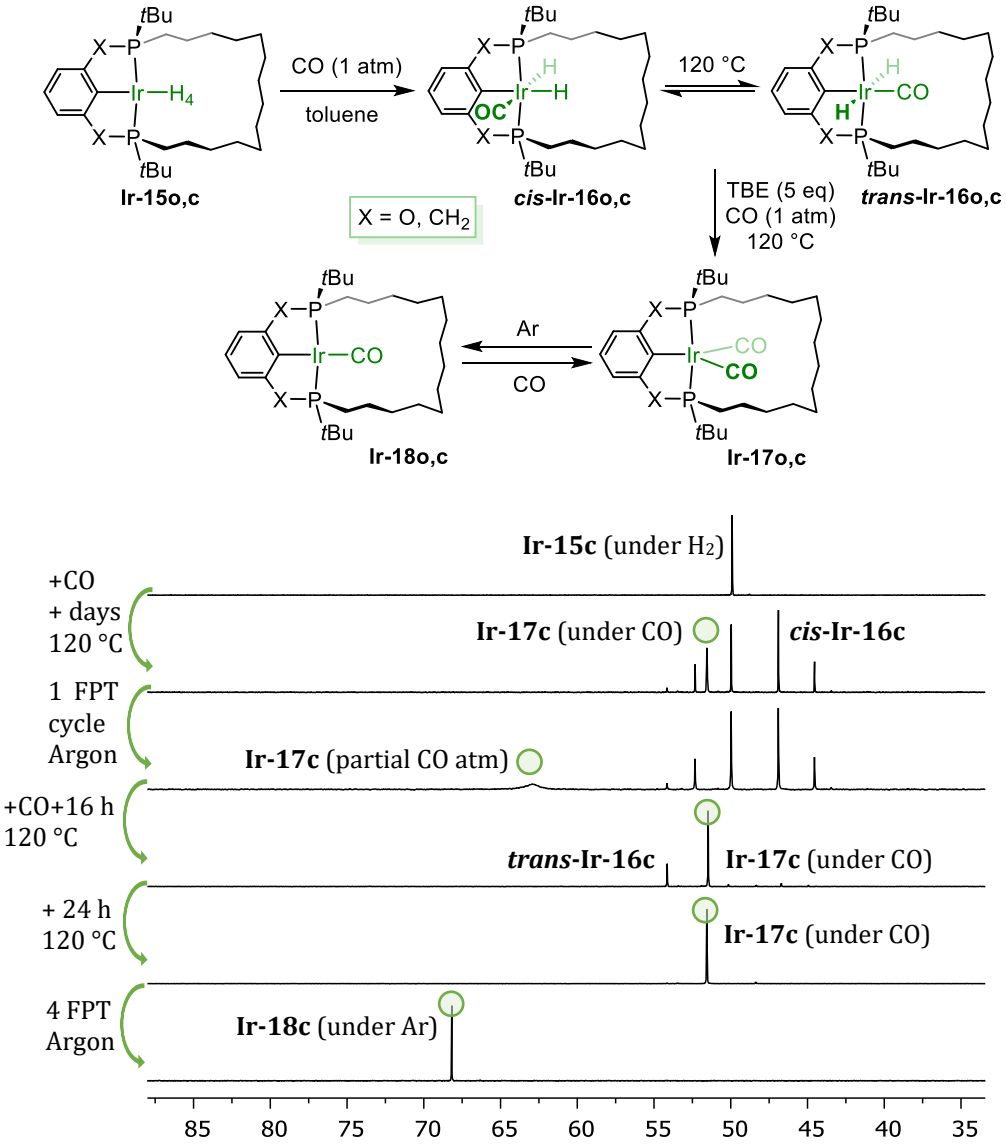

Figure 3.6. (top) Synthetic scheme for the preparation of **Ir-18o,c**; (bottom) selected $^{31}P\{^{1}H\}$ NMR spectra recorded *in situ* **Ir-18c**. The green circles denote the purely carbonyl complexes **Ir-17c** and **Ir-18c**. *Tert*-butylethylene is present in 5 equivalents in all steps.

In agreement with their earlier formulation as σ-bound dihydrogen complexes, placing solutions of **Rh-15o,c** under an atmosphere of CO resulted in an immediate change of colour from orange to bright yellow. Analysis by ^{1}H NMR spectroscopy showed the absence of any hydridic signals and indicated the rapid displacement of H_2 by one equivalent of CO to form **Rh-18o,c** (Scheme 3.14). These complexes are characterised by a time-averaged C_2 symmetry, as evidenced by a single doublet ^{31}P resonance with large $^{1}J_{RhP}$ coupling constants in line with a Rh(I) centre assignment (**Rh-18o**, δ(^{31}P) 201.6, $^{1}J_{RhP}$ = 156 Hz; **Rh-18c**, δ(^{31}P) 75.0, $^{1}J_{RhP}$ = 146 Hz).

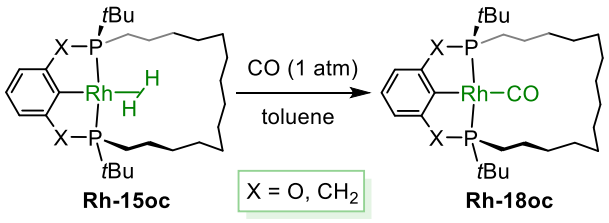

Scheme 3.14. Preparation of **Rh-18o,c**.

Purification to remove byproducts from earlier steps (cyclooctane, unidentified metal species) was impeded by the excellent solubility of these complexes in all tested organic solvents (MeOH, DCM, hexane, cyclohexane, HMDSO, TMS), and recrystallisation or chromatography methods failed to yield purer samples and, in the latter case, resulted in significant decomposition on silica or alumina.

3.3.2. Isolation and oxidation of metal carbonyls

Oxidation of **M-18o,c** to their octahedral, coordinatively saturated counterparts **M-19o,c** was targeted to facilitate their isolation, inspired by similar chemistry that was carried out in the group on macrocyclic [(CNC)Rh(CO)] complexes.[67] This oxidation was readily achieved across the series by reacting **M-18o,c** with a suspension of $PhICl_2$ and slowly thawing the reaction from -78 °C to room temperature (Scheme 3.15). Initial trials at room temperature resulted in the formation of a greater quantity of byproducts which putatively stem from competing oxidative addition of C–I or C–H bonds, especially in the case of the iridium complexes, or perhaps from the formation of *cis*-dichloride complexes. Formation of the desired complexes was confirmed by the observation of C_2-symmetry and reduction in the $^1J_{RhP}$ coupling constants measured by ^{31}P NMR spectroscopy (**Ir-19o**, δ(^{31}P) 144.4; **Ir-19c**, δ(^{31}P) 33.8; **Rh-19o**, δ(^{31}P) 181.0, $^1J_{RhP}$ = 92 Hz; **Rh-19c**, δ(^{31}P) 87.0, $^1J_{RhP}$ = 87 Hz).

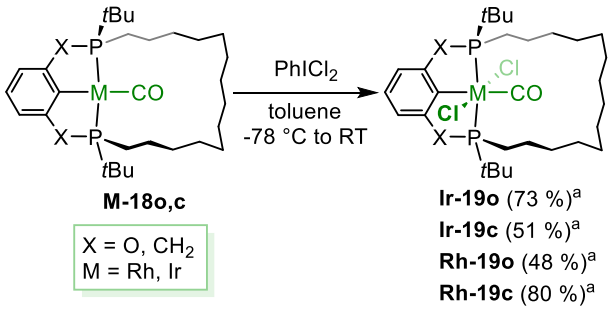

Scheme 3.15. Oxidation **M-18o,c** with $PhICl_2$ in toluene. (a) yields reported for the one-pot multistep preparation of **M-19o,c** from the corresponding ligand.

A common feature in the ^{1}H NMR spectra of all four complexes is the presence of an alkyl signal shifted significantly downfield and integrating as 2H (Figure 3.7, left). This resonance was assigned to the first methylene in the macrocyclic linker with the aid of COSY and HSQC experiments. The unusual deshielding of these nuclei is thought to arise from diamagnetic anisotropy induced by the proximity of the chloride ligands,[68,69] with one of the methylene protons being conformationally maintained in a direction pointing towards them (Figure 3.7, right). This conformational lock therefore makes both protons in the methylene inequivalent, and by use of selective ^{31}P decoupling experiments, these signals were deconvoluted to doublet (coupling to *geminal*-CH) of triplet (coupling to α-CH_2) of virtual triplet from the coupling to the two phosphorus atoms.

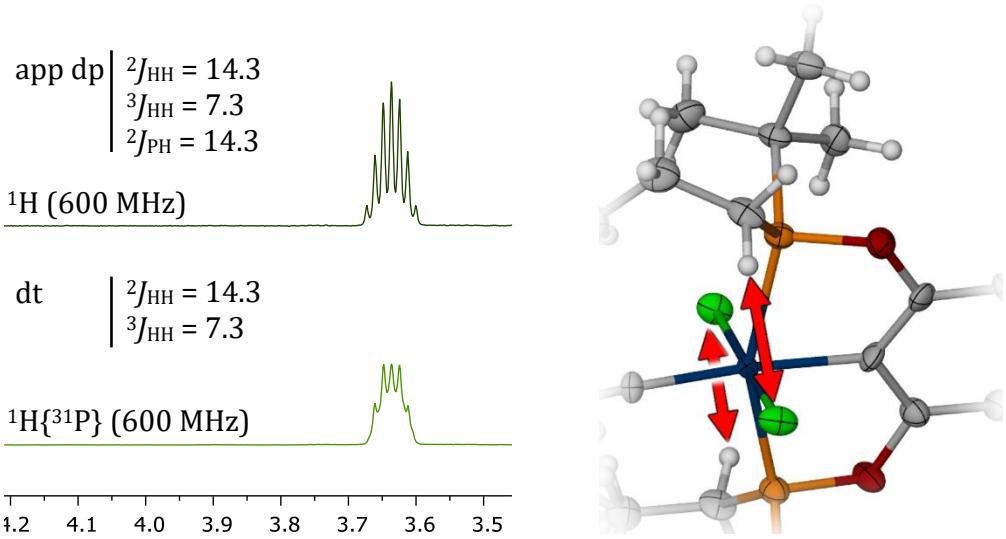

Figure 3.7. Stacked ^{1}H NMR and $^{1}H\{^{31}P\}$ NMR spectra showing the PCH_2 resonance in **Ir-19o** (C_6D_6, 600 MHz) (left); Selected part of the solid-state structure of **Ir-19o** highlighting their spatial proximity with the Cl ligands. Selected distances: Cl6-H13A, 2.733(2), Cl7-H11S, 2.685(2) (right).

Satisfyingly, **M-19o,c** were all found to be stable in air and could be purified by silica chromatography. In addition, the full series was found to crystallize readily upon solvent removal allowing determination of their solid-state structures by single-crystal X-ray diffraction (Figure 3.8). A difference must be noted however, in that loss of CO was observed in the case of **Rh-19o,c** particularly with **Rh-19c** upon extended storage in toluene solution. This was apparent by a distinct colour change from a bright yellow to a light orange and by ^{31}P NMR spectroscopy with the appearance of new C_2-symmetric resonances. Placing those samples back

under CO atmosphere or bubbling of CO in solution resulted in the immediate recovery of pure **Rh-19o,c**. Although not isolated, these new species are likely $Rh^{III}(Cl)_2$ complexes, with a square-based pyramidal coordination geometry.

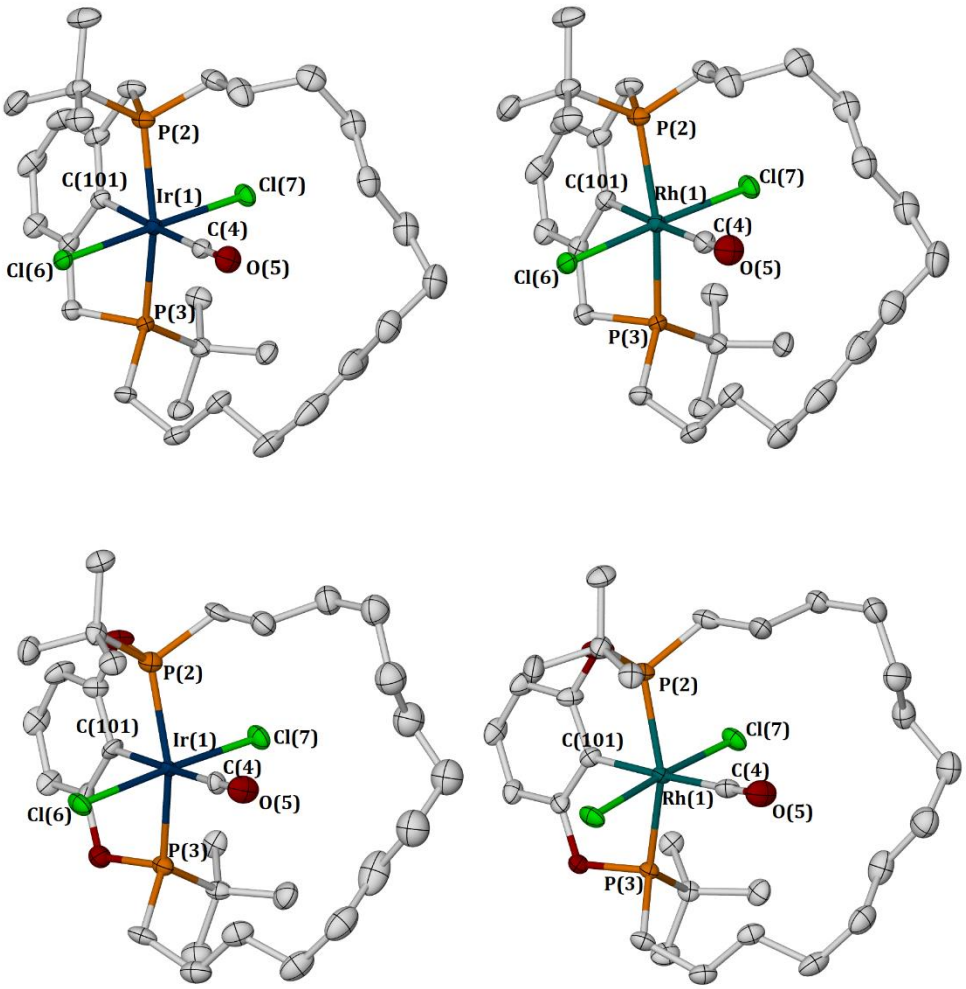

Figure 3.8. Solid-state structure of complexes **Ir-19c** (top left), **Ir-19o** (bottom left), **Rh-19c** (top right) and **Rh-19o** (bottom right). Thermal ellipsoids at 50% probability. Hydrogen atoms and minor disorder components omitted for clarity.

During later investigations towards transmetallation reactions on these complexes (see Chapter 4), it was found that alkyl Grignard reagents were very effective reducing agents for the reduction of **M-19o,c**. Indeed, all 4 complexes are readily converted to their M(I) analogues in quantitative spectroscopic yield in 4 h at room temperature by treatment with *i*PrMgCl·LiCl (3 eq) in THF. Further quenching of the excess Grignard with a protic solvent (EtOH, MeOH), followed by filtration and concentration *in vacuo* allowed the isolation of analytically pure

samples of **Rh-18o,c**, and X-ray quality crystals could be grown from slow evaporation of TMS solutions (Figure 3.9).

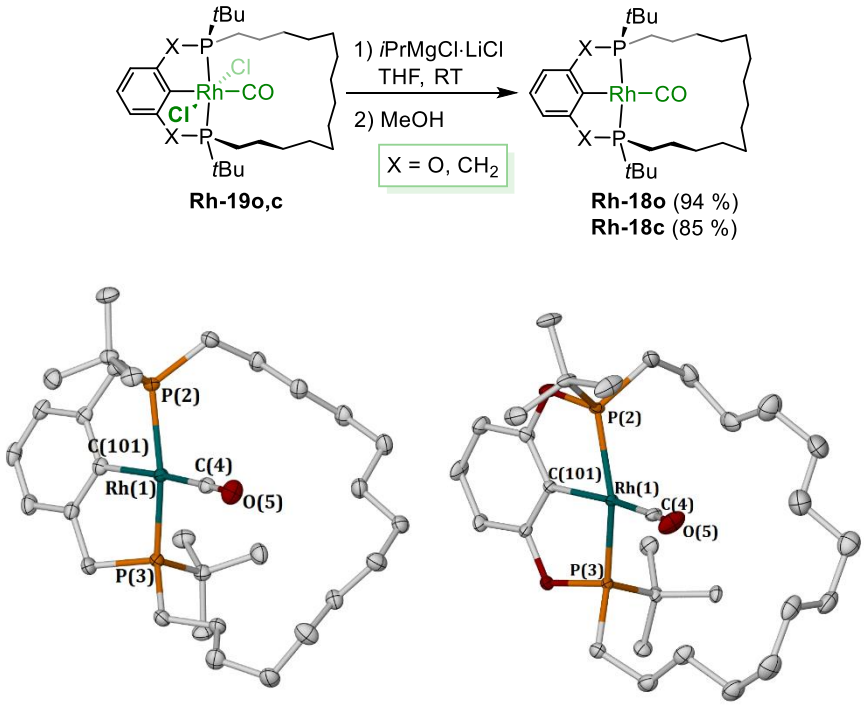

Figure 3.9. Synthetic scheme for the reduction of **Rh-19o,c** (top); Solid-state structure of complexes **Rh-18o** (right) and **Rh-18c** (left) (bottom). Thermal ellipsoids at 50% probability. Hydrogen atoms and minor disorder components omitted for clarity.

Conversely, quenching the excess Grignard reagent with a protic solvent in the case of **Ir-19o,c** resulted in an immediate decomposition to several unidentified products. The presence of hydride signals as well as the very asymmetric nature of the products observed by ^{31}P NMR spectroscopy may suggest the intramolecular addition of a macrocyclic C–H bond. Whilst the addition of C–H bonds to square planar four-coordinate complexes is rare, it is not unprecedented as was exemplified in 2014 in a report by Goldman *et. al.* showing the facile acid catalysed oxidative addition of an alkynyl C(sp)–H bond.[70,71] In our case, the additional challenge to activate a C(sp^3)–H may be offset by the intramolecular nature of the process and therefore the reduction of any entropic penalty. In the case of **Ir-19o,c**, the C–H bond activation could occur either on the flexible alkyl tether or on a *t*Bu group. The latter was shown to occur for iridium complexes of both PCP[18,72] and POCOP[73] scaffolds; in POCOP's case the reaction was mediated by protic acids.

The isolation of the Ir(I) carbonyl complexes **Ir-18o,c** in a clean fashion would have been challenging *via* this route in any case, on account of the instability noted previously when extended time is needed to rigorously dry the samples *in vacuo*. With this caveat in mind, our attention turned to the use of various other reducing agents that would not require quenching, and ideally in a very volatile solvent. Taking advantage of the excellent solubility of **Ir-19o,c** in alkanes, pentane was selected for its volatility. Zn powder (10 eq) was trialled first which did not afford any product by ^{31}P NMR spectroscopy. Magnesium powder was tested next in the same excess and whilst it did promote the desired reduction, the rate was very low and less than 10 % product was observed after a week stirring at room temperature. Heating at reflux increased the reaction rate, albeit with the concomitant formation of unknown impurities. A suitable alternative was found with KC_8 also using 10 equivalents, which brought about the clean reduction of **Ir-19o,c** to **Ir-18o,c** in two days at room temperature (Figure 3.10). Subsequent filtration and removal of the volatiles afforded analytically pure samples of **Ir-18o,c**, which satisfyingly provided X-ray suitable crystals by slow evaporation of TMS (**Ir-18o**) or neopentane (**Ir-18c**) solutions.

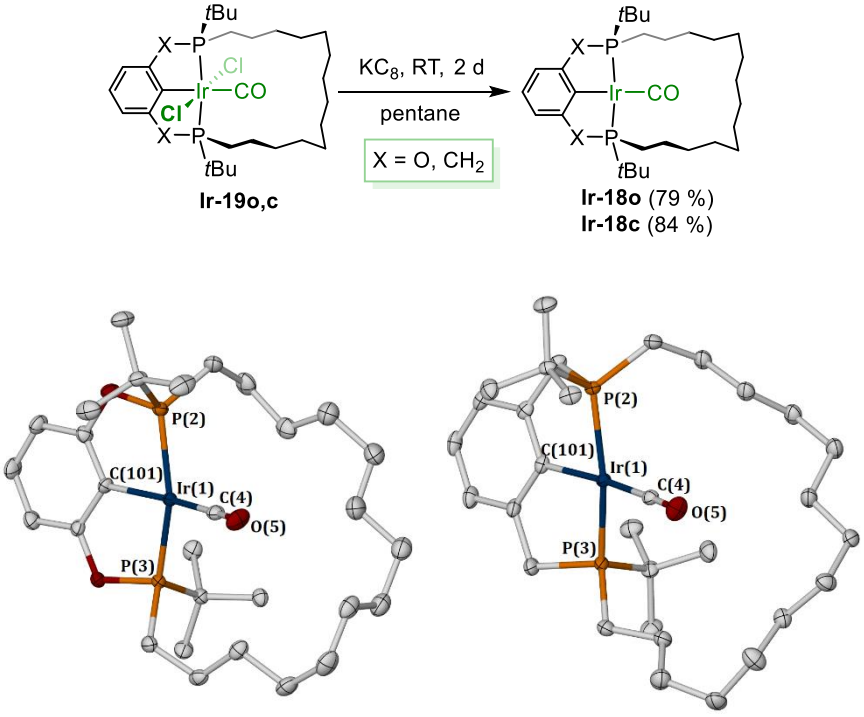

Figure 3.10. (top) synthetic scheme for the reduction of **Ir-19o,c**; (bottom) Solid-state structure of complexes **Ir-18o** (left) and **Ir-18c** (right). Thermal ellipsoids at 50% probability. Hydrogen atoms and minor disorder components omitted for clarity.

Finally, isolated of samples of **Ir-18o** and **Ir-18c** were degassed and placed under an atmosphere of H_2 in toluene-d_8 to afford clean samples of ***cis*-Ir16o,c** for solution state characterisation (Scheme 3.16). The preparation of clean samples of ***trans*-Ir16o,c** was, however, not possible as prolonged heating at 120 °C of a *cis*- sample under H_2 did not yield full conversion to the isomerised product, suggesting the presence of an equilibrium.

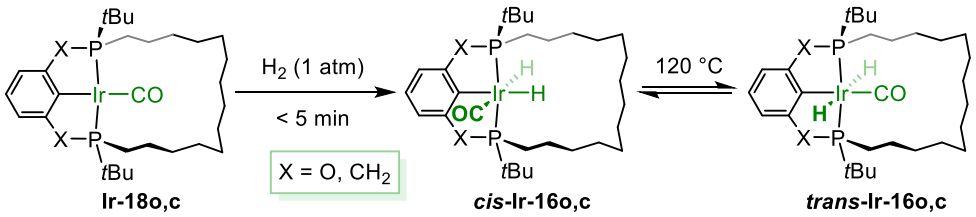

Scheme 3.16. Preparation of ***cis*-Ir-16o,c** from **Ir-18o,c** and their subsequent isomerisation.

*3.3.3. Solid-state structures of **M-18** and **M-19***

The solid-state structures of **M-18/19o,c** shown above in figures 3.8, 3.9 and 3.10 demonstrate the adoption of distorted square planar / octahedral metal coordination geometries, with the tetradecamethylene linker of the pincer ligands considerably skewed to one side of the coordination plane conferring overall C_1 symmetry and inducing an appreciable deviation of the C101–M1–C4 angles from linearity (table 3.1); especially in the case of the phosphinite pincer (171.38(10) °, **Rh-18c**; 165.3(3) °, **Rh-18o**; 171.91(10) °, **Ir-18c**; 165.6(2) °, **Ir-18o**). The methylene chains of the macrocycles are also non-symmetrically positioned in the M(III) congeners, but in this case contortion is counteracted by buttressing with the ancillary chloride ligands and more ideal C101-M1-C4 angles are observed (177.22(11) °, **Rh-19c**; 174.6(2) °, **Rh-19o**; 177.24(14) °, **Ir-19c**; 174.9(4) °, **Ir-19o**). These asymmetric configurations are not retained in solution, where time-averaged C_2 symmetry is observed at 298 K (500–600 MHz) consistent with the tetradecamethylene linker being sufficiently large and flexible to accommodate the carbonyl ligand within the annulus of the macrocycle. The more obtuse P2–M1–P3 bite angles and rigid backbone conformations observed in the complexes of **POCOP-14** in the solid state, compared to those of **PCP-14**, are fully in line with expectations for these pincer architectures.[55,74–76] This homologous

Table 3.1. Selected bond lengths (Å) and angles (°) for **M-18o,c** and **M19o,c**.

	Rh-18c	**Rh-18o**	**Rh-19c**	**Rh-19o**	**Ir-18c**	**Ir-18o**	**Ir-19c**	**Ir-19o**
M1-P2	2.2844(6)	2.2704(15)	2.3615(7)	2.3324(12)	2.2817(7)	2.2694(11)	2.3637(9)	2.336(2)
M1-P3	2.2731(6)	2.2856(13)	2.3938(6)	2.3768(11)	2.2760(7)	2.2798(10)	2.3922(8)	2.377(2)
M1-C4	1.865(3)	1.879(6)	2.005(3)	1.996(6)	1.862(3)	1.879(4)	1.940(3)	1.926(9)
M1-C101	2.083(3)	2.037(6)	2.061(3)	2.018(5)	2.085(3)	2.048(4)	2.089(3)	2.034(10)
C4-O6	1.150(3)	1.145(8)	1.106(3)	1.086(7)	1.156(4)	1.146(5)	1.122(4)	1.143(12)
M1-Cl6	-	-	2.3656(5)	2.3616(12)	-	-	2.3828(7)	2.380(2)
M1-Cl7	-	-	2.3591(6)	2.3521(12)	-	-	2.3793(8)	2.371(2)
P2-M1-P3	160.83(2)	155.98(5)	162.17(2)	156.80(5)	161.16(2)	156.21(3)	160.81(3)	156.18(9)
C101-M1-C4	171.38(10)	165.3(3)	177.22(11)	174.6(2)	171.91(12)	165.6(2)	177.24(14)	174.9(4)
Cl6-M1-Cl7	-	-	176.92(2)	176.32(5)	-	-	178.81(3)	177.37(9)
Aryl twist[a]	14.30(6)	6.7(2)	18.52(7)	12.34(13)	13.95(8)	6.49(14)	17.93(9)	11.3(3)

[a] Angle between the least-squares mean planes of the aryl group and the MP_2C(aryl) atoms.

series of complexes showcases the effect of the increased steric crowding on the pincer scaffold, where C_2 symmetric twisting of the central aryl donor is considerably more pronounced in the octahedral M^{III} analogues: presumably steric buttressing between the chlorides and *t*Bu groups is alleviated by twisting of the phosphines about the M-P axis and accompanying twist of the aryl donor. Finally the observed differences in M-P, M-CO, C-O and M-aryl bonds for the M(I) and M(III) congeners correlate with the nature of constituent donors. In particular, longer M–P, M–CO are displayed for M(III) congeners consistently with a lesser extent of available electron density at the metal centre to engage in metal to ligand backdonation and therefore weaker bonds. Conversely, slightly shorter M–aryl bonds are seen for M(III) species, as might be expected from the interaction of an electron-depleted metal centre with an anionic ligand, although a more significant difference in M–aryl bond distance is observed between the POCOP and PCP scaffolds. This is possibly a result of the POCOP scaffold featuring shorter donor arms and thereby maintaining the Rh centre closer to the aryl, but also from a reduced "aryl twist" which positions the aryl π-system more favourably in the coordination plane to welcome π-backdonation.

3.3.4. Carbonyl stretching frequencies

The carbonyl stretching frequencies of our compounds and those of known acyclic pincer complexes [M(pincer)(CO)] (M = Rh, Ir; pincer = *t*Bu$_4$-PCP, *t*Bu$_4$-POCOP) have all been determined by ATR-IR spectroscopy under the same conditions in solution and in the solid state, and are compiled in table 3.2. These data suggest that **PCP-14** and **POCOP-14** are marginally weaker donors than *t*Bu$_4$-PCP and *t*Bu$_4$-POCOP, respectively. Other trends apparent in the IR data associated with the extent of π-backbonding increasing in the order Ir > Rh, M(I) > M(III) and PCP > POCOP are fully in line with expectation and reinforced by similar trends in the X-ray derived C-O bond distances (Table 3.1, line 5). The latter consistently increases with the extent of π-backbonding derived from the IR data. Likewise the observed carbonyl ^{13}C shift in the M(III) series was observed to generally shift upfield with increasing electron richness at the metal centre, most noticeably between the Rh ($\delta(^{13}C) \sim 188$) and Ir ($\delta(^{13}C) \sim 176$) compounds.

Table 3.2. Carbonyl stretching frequencies in toluene and in the solid state (cm^{-1}).

	Macrocyclic		Acyclic	
	Solution	Solid	Solution	Solid
[Rh(PCP)(CO)]	1939	1938	1933	1930
[Rh(POCOP)(CO)]	1958	1953	1954	1945
$[Rh(PCP)Cl_2(CO)]$	2069	2066	-	-
$[Rh(POCOP)Cl_2(CO)]$	2083	2087	-	-
[Ir(PCP)(CO)]	1925	1920	1918	1911
[Ir(POCOP)(CO)]	1943	1940	1939	1929
$[Ir(PCP)Cl_2(CO)]$	2034	2029	-	-
$[Ir(POCOP)Cl_2(CO)]$	2049	2053	-	-

An interesting feature of our macrocyclic complexes may also be seen from the comparison between solution and solid-state measurements. While an expected and consistent difference is clearly observed across the acyclic series (average $\Delta\nu$ = +7.25 cm^{-1}), it is much less pronounced for the compounds bearing the macrocycle (average $\Delta\nu$ = +2.12 cm^{-1}) and is even inverted in the cases of $[Rh(POCOP\text{-}14)Cl_2(CO)]$ and $[Ir(POCOP\text{-}14)Cl_2(CO)]$, which may stem from crystal-packing effects or is perhaps indicative of a time-averaged cavity effect enforced by the macrocycle about the carbonyl ligand that is able to somewhat shield this section of the coordination sphere from the influence of solvation. The trends identified between solid-state and solution data are quite subtle in absolute value and are within the error margin usually associated with the equipment's calibration (± 5 cm-1 commonly observed in our hands, depending on the equipment). However, care was taken to collect the data presented in Table 3.2 on one unique spectrometer, on the same day and in strictly identical experimental conditions. Reproducibility of the measurements was verified on selected samples with absolute errors all within 0.2 cm^{-1}.

3.4. Reactivity of M-15o,c with *tert*-butylethylene

Seeking to apply known pincer chemistry to our complexes, their ability to access the low coordinate M(I) 14VE derivatives was investigated. To that end, toluene solutions of the polyhydride species **M-15o,c** were treated with excess *tert*-butylethylene as a sacrificial hydrogen acceptor.

3.4.1. (POCOP)Rh

Of the four complexes in the series, only **Rh-15o** seemed to yield a species that could be assigned to a low-valent complex, but is likely to be in equilibrium with a complex of TBE (Scheme 3.17). Displacement of H_2 occurred in under 5 min at room temperature in benzene, and was evidenced by the disappearance of the hydride resonance in the ^{1}H NMR spectrum, as well as the presence of a broad signal at 4.71 ppm which we attribute to dynamic binding of TBE. In the ^{31}P{^{1}H} NMR spectrum the signal pertaining to the dihydrogen complex was replaced by one main species shifted upfield to 186.1 ppm, C_2-symmetric and characterised by a broad doublet displaying a large $^1J_{RhP}$ coupling constant (fwhm = 28 Hz, $^1J_{RhP}$ = 175 Hz) that precludes its assignment as a Rh(III) species. Whilst no change could be observed at room temperature over 24h, heating the benzene solution at reflux for 4 h gave rise to three unidentified species, all of which evidence a loss of C_2 symmetry to varying degrees, and Rh(I) $^1J_{RhP}$ coupling constants in the range of 157-170 Hz. The ^{1}H NMR spectrum did not show any hydride signal, however the appearance of several broad signals between 3.5 and 5.3 ppm was noted. Thus it was hypothesized the macrocycle was intramolecularly dehydrogenated in 3 different positions along the alkyl chain. Further heating at reflux in benzene did not yield any changes.

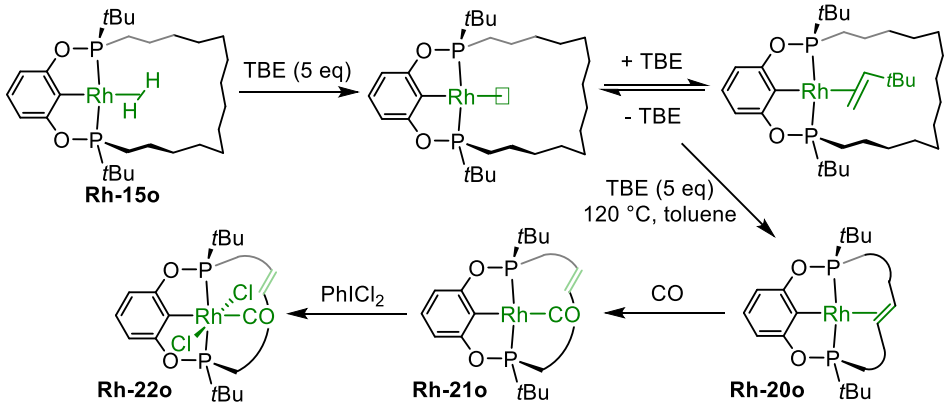

Scheme 3.17. Dehydrogenation of the alkyl tether in **Rh-15o** related reactions.

Switching to toluene allowed higher temperatures to be reached and after heating at 120 °C overnight only one of the products was obtained. Presumably, Rh-catalysed isomerisation provides the most thermodynamically stable π-bound alkene isomer **Rh-20o**.

Further supporting the assignment of **Rh-20o**, placing under a CO atmosphere resulted in the displacement of the bound alkene as evidenced by the appearance of two clear doublets of triplets in the ^{1}H NMR spectrum, with a $^{3}J_{HH}$ = 16.2 Hz characteristic of an *E*-alkene. Unlike its fully aliphatic congener **Rh-18o**, this new species **Rh-21o** is not C_2-symmetric by ^{31}P NMR spectroscopy (δ(^{31}P) 207.0, 203.7), which further indicates the alkyl tether was not dehydrogenated at position C_7-C_8. The lack of purity of all the compounds mentioned in this paragraph unfortunately precluded their isolation and further characterisation in the solid state. In an attempt to facilitate isolation from solution, **Rh-21o** was treated with $PhICl_2$ in toluene and was successfully converted to **Rh-22o**, albeit not cleanly. **Rh-22o** exhibits two ^{31}P resonances at 184.2 and 168.8 ppm highlighting an even more pronounced loss of C_2 symmetry with respect to its saturated congener **Rh-19o**. Complex **Rh-22o** proved fairly unstable on silica and also failed to provide X-ray suitable crystals that would have allowed the unambiguous location of the alkene along the chain, the NMR data (1D and 2D) are insufficient to conclude with certainty.

3.4.2. (PCP)Rh

Treatment of **Rh-15c** with excess TBE in toluene gave a similar outcome to **Rh-15o**, but proceeded to afford **Rh-20c** at room temperature (Scheme 3.18). The absence of other isomers suggests that the backbone conformation and relative flexibility compared to its POCOP analogue favours the activation at a specific position. Further heating of the solution under reflux resulted in the formation of a plethora of unidentified species. Interestingly, it was found that the dehydrogenation reaction occurs at room temperature even in the absence of an external hydrogen acceptor: treatment of a solution of **Rh-14c** with KO*t*Bu at room temperature in toluene yielded an equimolar mixture of **Rh-15c** and **Rh-20c,** presumably *via* the low coordinate pincer acting as a dihydrogen acceptor. As was the case previously for its POCOP congener, the purification of these air-sensitive compounds proved unsuccessful in our hands.

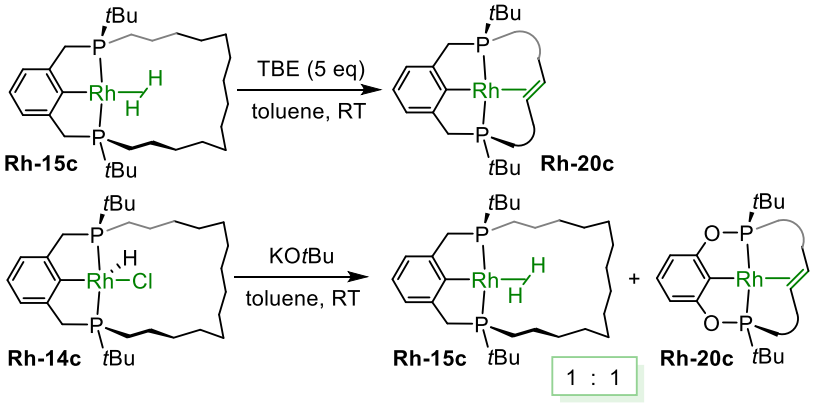

Scheme 3.18. Dehydrogenation of the alkyl tether in **Rh-15c** promoted by TBE (top) and reaction of **Rh-14c** with a base (bottom).

3.4.3. (PXCXP)Ir

The iridium complexes were found to be even more reactive than their rhodium analogues, with the immediate formation of alkene signals in the ^{1}H NMR spectrum upon treatment of **Ir-15o,c** with TBE.

Heating a solution of **Ir-15c** to 80 °C overnight with TBE (5 eq) resulted in the formation of one main species, very asymmetric in nature as evidenced by ^{31}P signals at 34.7 and 86.9 ppm ($^{2}J_{PP}$ = 344 Hz). The ^{1}H NMR spectrum also shows bound alkene-like signals at 4.56 and 3.77 ppm respectively, integrating as 1H each, although significantly less broad than those observed with the rhodium analogues. More surprisingly, a hydride resonance was observed at δ -11.60 (dd, $^{2}J_{PH}$ = 22.3, 10.0 Hz), a shift suggesting the presence of a *trans* ligand. Thus, this new species was formulated as an iridium allyl hydride complex **Ir-23c**, resulting from an alkyl dehydrogenation and subsequent C(sp^{3})–H bond activation to afford this putative 18VE octahedral complex **Ir-23c** (Scheme 3.19). Placing a toluene solution of **Ir-23c** under a CO atmosphere resulted in no reaction, in support of our assignment. Complex **Ir-23c** is air-sensitive, however, and could not be isolated as is. Dissolution in deuterated solvents resulted in extensive deuterium incorporation at the hydride position, the methylene bridges, the *t*Bu substituents and to a lesser extent in the aromatic backbone. This observation may be directly linked to the extensive H/D exchange observed in section 3.2.2 and may suggest that the complexes formulated in this section may intervene as intermediates in the process. In an attempt to stabilise this compound by substituting the hydride

with a halogen, it was treated with excess bromoform which only resulted in an intractable mixture of products.

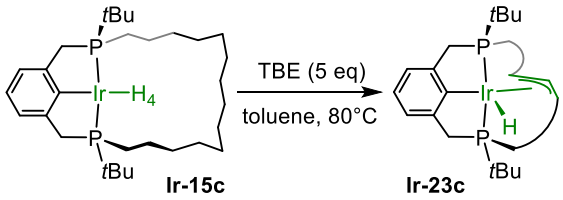

Scheme 3.19. Reaction of **Ir-15c** with TBE.

The POCOP variant on the other hand quickly reached an equilibrium between two asymmetric species in the $^{31}P\{^{1}H\}$ NMR spectrum in a 3:1 ratio. Prolonged heating to 120 °C did not change this ratio as observed by (room temperature) NMR spectroscopy. The major and most asymmetric species is associated with a hydride signal at δ -11.71 (dd, $^{2}J_{PH}$ = 23.4, 13.7 Hz), very similar to the one observed in the (PCP)Ir system. Conversely, at least two sets of alkene-like signals were seen between 3.4 and 4.8 ppm, likely belonging to the two compounds. Therefore it was postulated that the (POCOP)Ir system shows intermediate reactivity compared to the electron rich (PCP)Ir system and the electron deficient rhodium systems; it affords a mixture of the alkene bound compound **Ir-20o** and the allyl hydride isomer **Ir-23o** (Scheme 3.20). In support of this suggestion, placing the mixture of **Ir-20o** and **Ir-23o** under an atmosphere of CO in toluene resulted in the immediate reaction of the minor π-bound alkene complex **Ir-20o** at room temperature, evidenced by appearance of sharp alkene signals, whilst **Ir-23o** remained. This supports our previous assignments and suggests that the barrier for interconversion between the two species is too high for the isomerisation to occur at room temperature. The properties of this complex did not prove conducive to its isolation as a pure compound for full characterization or the determination of its solid-state structure, which would have ideally located the metallation site along the alkyl chain.

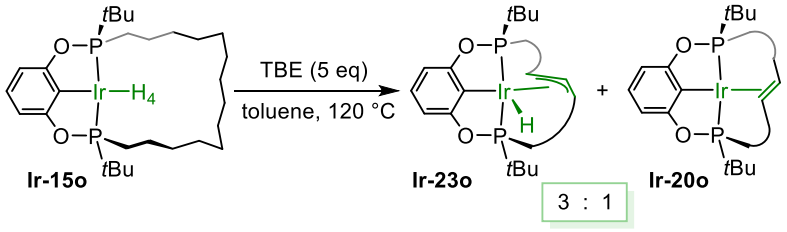

Scheme 3.20. Reaction of **Ir-15o** with TBE.

At the time of writing, recent unpublished work within the group on a cationic (PNP-14)Ir system allowed the isolation and solid-state structure determination of an iridium allyl hydride as initially formulated above with the allyl located on the third, fourth and fifth carbons along the chain (T. M. Hood).

3.5. References

[1] C. J. Moulton, B. L. Shaw, *J. Chem. Soc., Dalton Trans.* **1976**, 1020–1024.
[2] K. Krogh-Jespersen, M. Czerw, K. Zhu, B. Singh, M. Kanzelberger, N. Darji, P. D. Achord, K. B. Renkema, A. S. Goldman, *J. Am. Chem. Soc.* **2002**, *124*, 10797–10809.
[3] H. Salem, L. J. W. Shimon, G. Leitus, L. Weiner, D. Milstein, *Organometallics* **2008**, *27*, 2293–2299.
[4] A. V. Polezhaev, S. A. Kuklin, D. M. Ivanov, P. V. Petrovskii, F. M. Dolgushin, M. G. Ezernitskaya, A. A. Koridze, *Russ. Chem. Bull.* **2009**, *58*, 1847–1854.
[5] S. D. Timpa, C. M. Fafard, D. E. Herbert, O. V. Ozerov, *Dalton Trans.* **2011**, *40*, 5426.
[6] I. Göttker-Schnetmann, P. White, M. Brookhart, *J. Am. Chem. Soc.* **2004**, *126*, 1804–1811.
[7] I. Göttker-Schnetmann, P. S. White, M. Brookhart, *Organometallics* **2004**, *23*, 1766–1776.
[8] D. Morales-Morales, R. Redón, C. Yung, C. M. Jensen, *Inorg Chim Acta* **2004**, *357*, 2953–2956.
[9] Z. Huang, M. Brookhart, A. S. Goldman, S. Kundu, A. Ray, S. L. Scott, B. C. Vicente, *Adv. Synth. Catal.* **2009**, *351*, 188–206.
[10] O. O. Kovalenko, O. F. Wendt, *Dalton Trans.* **2016**, *45*, 15963–15969.
[11] A. Brück, D. Gallego, W. Wang, E. Irran, M. Driess, J. F. Hartwig, *Angew. Chem. Int. Ed.* **2012**, *51*, 11478–11482.
[12] J. M. Goldberg, G. W. Wong, K. E. Brastow, W. Kaminsky, K. I. Goldberg, D. M. Heinekey, *Organometallics* **2015**, *34*, 753–762.
[13] A. Vigalok, O. Uzan, L. J. W. Shimon, Y. Ben-David, J. M. L. Martin, D. Milstein, *J. Am. Chem. Soc.* **1998**, *120*, 12539–12544.
[14] M. E. van der Boom, S.-Y. Liou, Y. Ben-David, M. Gozin, D. Milstein, *J. Am. Chem. Soc.* **1998**, *120*, 13415–13421.
[15] M. E. van der Boom, C. L. Higgitt, D. Milstein, *Organometallics* **1999**, *18*, 2413–2419.
[16] M. E. van der Boom, S.-Y. Liou, Y. Ben-David, L. J. W. Shimon, D. Milstein, *J. Am. Chem. Soc.* **1998**, *120*, 6531–6541.
[17] M. Gupta, C. Hagen, W. C. Kaska, R. E. Cramer, C. M. Jensen, *J. Am. Chem. Soc.* **1997**, *119*, 840–841.
[18] H. A. Y. Mohammad, J. C. Grimm, K. Eichele, H.-G. Mack, B. Speiser, F. Novak, M. G. Quintanilla, W. C. Kaska, H. A. Mayer, *Organometallics* **2002**, *21*, 5775–5784.
[19] M. Rimoldi, A. Mezzetti, *Inorg. Chem.* **2014**, *53*, 11974–11984.
[20] C. M. Frech, Y. Ben-David, L. Weiner, D. Milstein, *J. Am. Chem. Soc.* **2006**, *128*, 7128–7129.
[21] C. J. Pell, O. V. Ozerov, *ACS Catal.* **2014**, *4*, 3470–3480.
[22] M. Findlater, K. M. Schultz, W. H. Bernskoetter, A. Cartwright-Sykes, D. M. Heinekey, M. Brookhart, *Inorg. Chem.* **2012**, *51*, 4672–4678.
[23] T. J. Hebden, K. I. Goldberg, D. M. Heinekey, X. Zhang, T. J. Emge, A. S. Goldman, K. Krogh-Jespersen, *Inorg. Chem.* **2010**, *49*, 1733–1742.
[24] M. Woińska, S. Grabowsky, P. M. Dominiak, K. Woźniak, D. Jayatilaka, *Sci. Adv.* **2016**, *2*, e1600192.
[25] H. Asano, M. Hirabayashi, in *Met. Hydrides* (Ed.: G. Bambakidis), Springer US, Boston, MA, **1981**, pp. 81–103.
[26] T. F. Koetzle, A. J. Schultz, R. Henning, A. Albinati, W. T. Klooster, B. E. Eichler, P. P. Power, *Comptes Rendus Chim.* **2005**, *8*, 1487–1490.
[27] J.-H. Liao, R. S. Dhayal, X. Wang, S. Kahlal, J.-Y. Saillard, C. W. Liu, *Inorg. Chem.* **2014**, *53*, 11140–11145.
[28] G. J. Kubas, R. R. Ryan, B. I. Swanson, P. J. Vergamini, H. J. Wasserman, *J. Am. Chem. Soc.* **1984**, *106*, 451–452.
[29] D. G. Gusev, H. Berke, *Chem. Ber.* **1996**, *129*, 1143–1155.
[30] D. G. Hamilton, R. H. Crabtree, *J. Am. Chem. Soc.* **1988**, *110*, 4126–4133.
[31] P. J. Desrosiers, L. Cai, Z. Lin, R. Richards, J. Halpern, *J. Am. Chem. Soc.* **1991**, *113*, 4173–4184.
[32] K.-W. Huang, J. H. Han, C. B. Musgrave, E. Fujita, *Organometallics* **2007**, *26*, 508–513.
[33] C. A. Tolman, *J. Am. Chem. Soc.* **1970**, *92*, 2953–2956.
[34] C. A. Tolman, *Chem. Rev.* **1977**, *77*, 313–348.
[35] A. R. Chianese, X. Li, M. C. Janzen, J. W. Faller, R. H. Crabtree, *Organometallics* **2003**, *22*, 1663–1667.

[36] S. Leuthäußer, D. Schwarz, H. Plenio, *Chem. - Eur. J.* **2007**, *13*, 7195–7203.
[37] R. A. Kelly III, H. Clavier, S. Giudice, N. M. Scott, E. D. Stevens, J. Bordner, I. Samardjiev, C. D. Hoff, L. Cavallo, S. P. Nolan, *Organometallics* **2008**, *27*, 202–210.
[38] S. Wolf, H. Plenio, *J. Organomet. Chem.* **2009**, *694*, 1487–1492.
[39] T. Dröge, F. Glorius, *Angew. Chem. Int. Ed.* **2010**, *49*, 6940–6952.
[40] D. J. Durand, N. Fey, *Chem. Rev.* **2019**, *119*, 6561–6594.
[41] D. G. Gusev, *Organometallics* **2009**, *28*, 763–770.
[42] D. G. Gusev, *Organometallics* **2009**, *28*, 6458–6461.
[43] J. J. Davidson, J. C. DeMott, C. Douvris, C. M. Fafard, N. Bhuvanesh, C.-H. Chen, D. E. Herbert, C.-I. Lee, B. J. McCulloch, B. M. Foxman, O. V. Ozerov, *Inorg. Chem.* **2015**, *54*, 2916–2935.
[44] Z. Huang, P. S. White, M. Brookhart, *Nature* **2010**, *465*, 598–601.
[45] B. Sheludko, M. T. Cunningham, A. S. Goldman, F. E. Celik, *ACS Catal.* **2018**, *8*, 7828–7841.
[46] D. W. Lee, C. M. Jensen, D. Morales-Morales, *Organometallics* **2003**, *22*, 4744–4749.
[47] S. Kundu, Y. Choliy, G. Zhuo, R. Ahuja, T. J. Emge, R. Warmuth, M. Brookhart, K. Krogh-Jespersen, A. S. Goldman, *Organometallics* **2009**, *28*, 5432–5444.
[48] B. Punji, T. J. Emge, A. S. Goldman, *Organometallics* **2010**, *29*, 2702–2709.
[49] E. Kossoy, M. A. Iron, B. Rybtchinski, Y. Ben-David, L. J. W. Shimon, L. Konstantinovski, J. M. L. Martin, D. Milstein, *Chem. - Eur. J.* **2005**, *11*, 2319–2326.
[50] H. Salem, Y. Ben-David, L. J. W. Shimon, D. Milstein, *Organometallics* **2006**, *25*, 2292–2300.
[51] C. M. Frech, D. Milstein, *J. Am. Chem. Soc.* **2006**, *128*, 12434–12435.
[52] C. M. Frech, L. J. W. Shimon, D. Milstein, *Helv. Chim. Acta* **2006**, *89*, 1730–1739.
[53] J. M. Goldberg, S. D. T. Cherry, L. M. Guard, W. Kaminsky, K. I. Goldberg, D. M. Heinekey, *Organometallics* **2016**, DOI 10.1021/acs.organomet.6b00598.
[54] J. J. Adams, N. Arulsamy, D. M. Roddick, *Organometallics* **2011**, *30*, 697–711.
[55] D. Morales-Morales, R. Redón, Z. Wang, D. W. Lee, C. Yung, K. Magnuson, C. M. Jensen, *Can. J. Chem.* **2001**, *79*, 823–829.
[56] D. B. Lao, A. C. E. Owens, D. M. Heinekey, K. I. Goldberg, *ACS Catal.* **2013**, *3*, 2391–2396.
[57] K. Zhu, P. D. Achord, X. Zhang, K. Krogh-Jespersen, A. S. Goldman, *J. Am. Chem. Soc.* **2004**, *126*, 13044–13053.
[58] R. A. Baber, R. B. Bedford, M. Betham, M. E. Blake, S. J. Coles, M. F. Haddow, M. B. Hursthouse, A. G. Orpen, L. T. Pilarski, P. G. Pringle, R. L. Wingad, *Chem Commun* **2006**, 3880–3882.
[59] *Metal Dihydrogen and σ-Bond Complexes*, Kluwer Academic Publishers, Boston, **2002**.
[60] C. S. Elmore, in *Annu. Rep. Med. Chem.*, Elsevier, **2009**, pp. 515–534.
[61] E. Buncel, *J. Label. Compd. Radiopharm.* **2007**, *50*, 945–946.
[62] J. Zhou, J. F. Hartwig, *Angew. Chem. Int. Ed.* **2008**, *47*, 5783–5787.
[63] V. M. Iluc, A. Fedorov, R. H. Grubbs, *Organometallics* **2012**, *31*, 39–41.
[64] A. V. Polukeev, R. Marcos, M. S. G. Ahlquist, O. F. Wendt, *Organometallics* **2016**, *35*, 2600–2608.
[65] J. D. Smith, G. Durrant, D. H. Ess, B. S. Gelfand, W. E. Piers, *Chem. Sci.* **2020**, DOI 10.1039/D0SC02694H.
[66] L. M. Guard, T. J. Hebden, D. E. Linn, D. M. Heinekey, *Organometallics* **2017**, *36*, 3104–3109.
[67] R. E. Andrew, A. B. Chaplin, *Inorg. Chem.* **2015**, *54*, 312–322.
[68] M. Baranac-Stojanović, *RSC Adv* **2014**, *4*, 308–321.
[69] A. M. Camp, M. R. Kita, J. Grajeda, P. S. White, D. A. Dickie, A. J. M. Miller, *Inorg. Chem.* **2017**, *56*, 11141–11150.
[70] J. D. Hackenberg, S. Kundu, T. J. Emge, K. Krogh-Jespersen, A. S. Goldman, *J. Am. Chem. Soc.* **2014**, *136*, 8891–8894.
[71] A. Kumar, M. Feller, Y. Ben-David, Y. Diskin-Posner, D. Milstein, *Chem. Commun.* **2018**, *54*, 5365–5368.
[72] S. Kundu, J. Choi, D. Y. Wang, Y. Choliy, T. J. Emge, K. Krogh-Jespersen, A. S. Goldman, *J. Am. Chem. Soc.* **2013**, *135*, 5127–5143.
[73] A. V. Polukeev, S. A. Kuklin, P. V. Petrovskii, A. S. Peregudov, F. M. Dolgushin, M. G. Ezernitskaya, A. A. Koridze, *Russ. Chem. Bull.* **2010**, *59*, 745–749.
[74] M. Montag, I. Efremenko, R. Cohen, L. W. Shimon, G. Leitus, Y. Diskin-Posner, Y. Ben-David, H. Salem, J. L. Martin, D. Milstein, *Chem. - Eur. J.* **2010**, *16*, 328–353.

[75] S. A. Kuklin, A. M. Sheloumov, F. M. Dolgushin, M. G. Ezernitskaya, A. S. Peregudov, P. V. Petrovskii, A. A. Koridze, *Organometallics* **2006**, *25*, 5466–5476.
[76] K.-W. Huang, D. C. Grills, J. H. Han, D. J. Szalda, E. Fujita, *Inorg Chim Acta* **2008**, *361*, 3327–3331

Chapter 4

Capturing interlocked hydrocarbon architectures

As a method for capturing interlocked architectures, this chapter details synthetic work focused on C(sp)–C(sp) bond forming reactions through the annulus of complexed PXCXP pincer ligands. Based on the organometallic chemistry of the ligands developed in Chapter 3, and in particular the inability to access reactive 14VE Rh and Ir derivatives, this approach was identified as the most promising for the construction of the target interlocked molecules and makes use of the stable bis(chloride) carbonyl complexes **M-19o,c**. The strategy for the synthesis of [2]rotaxanes involves an initial transmetallation step to install two half axles, followed by decarbonylation and reductive elimination. Conditions for hydrogenation of the resulting aryl terminated diyne axle were also investigated, with a view to obtaining a saturated thread.

During this work, it was discovered that the reductive elimination reaction to form an interlocked diyne complex was reversible: the {(POCOP)Rh} fragment was able to cleanly cleave the central C(sp)–C(sp) bond, with the resulting pentavalent intermediate trapped out with CO. This surprising and interesting result was subsequently studied in detail.

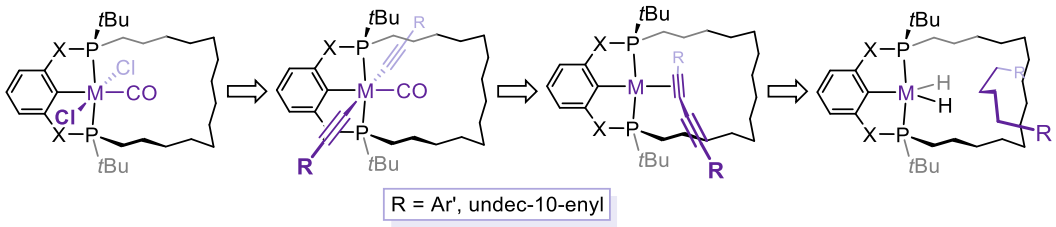

Despite the limitations identified during this work, namely the challenging decarbonylation step and the reversibility of the reductive elimination step, the use of PXCXP ligands for the formation of catenanes was also investigated, with the (POCOP)Rh system showing the most promising results.

4.1. Introduction

4.1.1. C–C bond activation: general considerations

The activation of C–C bonds is strategically important in the synthesis of value added chemicals and complex organic molecules from petrochemical feedstocks.[1–6] The selective activation and cleavage of single C–C bonds by direct insertion of transition metals is a conceptually simple and attractive method but remains challenging nonetheless, despite extensive research.[5,7–9] These processes are usually associated with high activation barriers or are simply thermodynamically unfavourable. Thus the microscopic reverse, reductive elimination, is often the favoured process, with the exception of strained systems such as cyclopropanes,[10,11] and cyclobutane derivatives.[12–14] Alternative strategies involve thermodynamically stabilising the products of C–C bond cleavage, with examples driven by aromatic stabilisation,[1,2,15] or exploiting favourable chelation as was highlighted by the work of Milstein *et. al.* in section 1.2.[16,17]

4.1.2. C(sp)–C(sp) bond activation

Reports pertaining to the activation of C(sp)–C(sp) single bonds are scarce, despite extensive studies on the reverse reductive elimination.[18,19] This may be attributed to its intrinsically high BDE estimated at 160.2 kcal/mol (in buta-1,3-diyne), similar to common Si-F bond strengths (Selected BDE in kcal/mol: Me_3Si-F, 159.9; H_3CCF_2-F, 124.9;).[20] Only a few examples have been reported involving trinuclear Os clusters,[21–23] a tetranuclear Re-Au cluster,[24] or binuclear titanocene and zirconocene complexes.[25–27] Most of these relate to the cleavage of trimethylsilyl substituted diynes, where the central C(sp)-C(sp) bond is substantially weakened by the β-silicon effect.[25] To date, only one example of C(sp)–C(sp) single bond activation by a mononuclear complex, namely $[Ru(CO)_2(PPh_3)_3]$, has been reported by Hill *et. al.*.[28,29] This reaction was discovered in the context of the catalytic demercuration of bis(polycarbyl)mercurials for the synthesis of polyynes by C(sp)–C(sp) bond formation. The complex $[Ru(CO)_2(PPh_3)_3]$ was found to readily react at room temperature with the mercurial bis(alkyne) by oxidative addition of the Hg–C

bond (Scheme 4.1). Over the course of several days, this complex was gradually converted to the η^2-bound diyne complex, accompanied by loss of metallic mercury. This complex could also be obtained directly *via* ligand substitution on $[Ru(CO)_2(PPh_3)_3]$ with the preformed diyne. The π-complex was found capable of reacting further upon heating, cleanly affording the stable bis(alkynyl) octahedral complex by direct C(sp)–C(sp) bond activation.

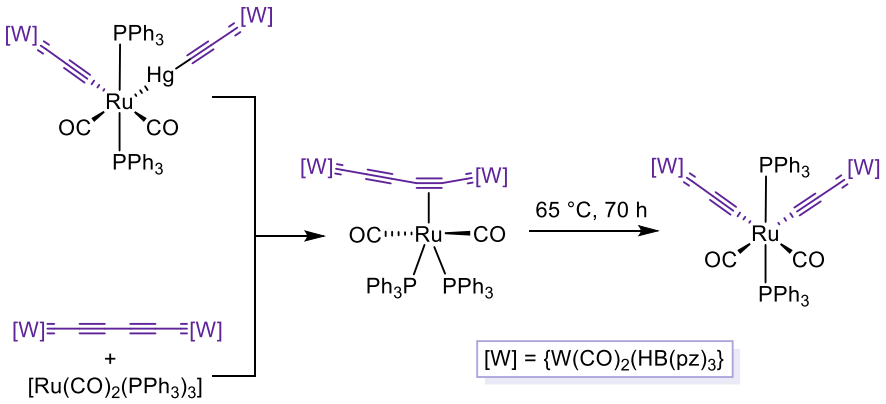

Scheme 4.1. C(sp)–C(sp) bond scission by a $[Ru(CO)_2(PPh_3)_3]$.

In a following publication, the capacity for $[Ru(CO)_2(PPh_3)_3]$ to activate the C(sp)-C(sp) bond in diphenylbutadiyne was investigated.[30] Whilst formation of the η^2-bound diyne complex proceeded easily, contrasting reactivity was observed upon heating. In fact, this complex was found to easily react with a second equivalent of diyne to afford a metallacyclopentadiene motif (Scheme 4.2). Oxidative addition of the central C(sp)–C(sp) bond was never observed. Moreover, the preparation of the *cis*-bis(alkynyl) Ru complex via a different synthetic route showed the reverse, reductive elimination, did not occur even under reflux conditions in toluene. These observations suggest very high barriers associated with both reductive elimination and oxidative addition. Additional investigations involved the reaction of 1,4-bis(trimethylsilyl)butadiyne with $[Ru(CO)_2(PPh_3)_3]$, which also failed to yield any oxidative addition product, despite its electronically weakened central bond.[30]

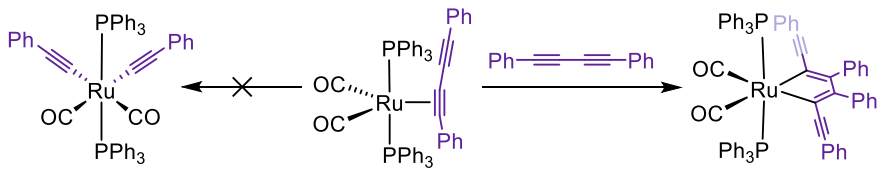

Scheme 4.2. Formation of a metallacyclopentadiene instead of C–C bond scission.

4.1.3. A well defined system demonstrating reversible C(sp)–C(sp²) bond activation

Of particular relevance to the work described in this chapter is the report of a C(sp)-C(sp²) bond cleavage in η^2-bound diphenylacetylene complexes of Pt(0) (Scheme 4.3).[31,32] Simply heating these 3-coordinate compounds did not yield any reaction, hinting that oxidative addition in this case is either thermodynamically unfavourable and/or associated with a prohibitively high activation barrier. Conversely, irradiation with UV-light showed complete conversion to the product of Ph–CCPh bond oxidative addition. This reaction was shown to be reversible: reductive elimination occurred upon heating at 100 °C and was complete after 16 d. This further confirms both the thermodynamically unfavourable character of the oxidative addition reaction as well as the presence of a significant activation barrier.

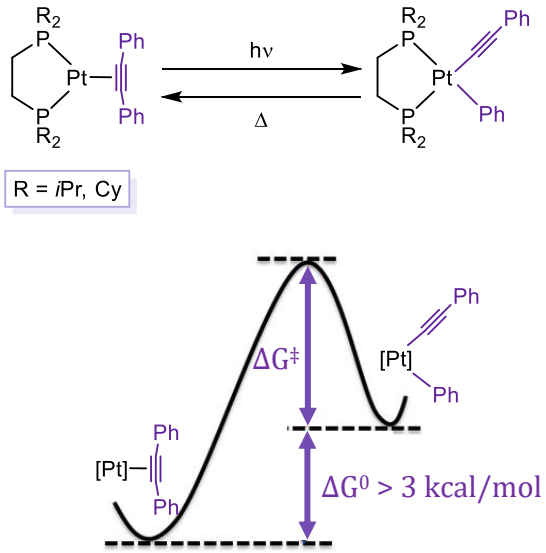

Scheme 4.3. Reversible C(sp²)-C(sp) bond scission in Pt complexes.

As such, these examples of C–C single bond activation are particularly interesting because of their reversible character and the role of the kinetics in enabling the isolation of both compounds. In an additional effort to overturn the thermodynamics and promote the *thermal* activation of C-C bonds, Jones *et. al.* broadened the scope of this reaction by employing diphenylacetylene derivatives that are variously substituted with electron-donating or electron-withdrawing groups, the rationale being the latter would result in the formation of stronger Pt–C bonds.[33] Oxidative addition under thermal conditions (up to 300 °C), however, could not be observed and in all cases, irradiation of the η^2-alkyne

complex was necessary to promote activation. Likewise, heating the activated products resulted in complete reversion to the η^2-alkyne complex. The activation barriers for reductive elimination were measured and were found to be dependent on the substituents. In particular, these kinetic studies confirmed that very electron-withdrawing substituents resulted in more stable high-valent complexes (R = perfluorophenyl, Figure 4.1, entry 4). The very high activation barrier of 47.3 kcal/mol measured in entry 4 effectively demonstrates the stabilisation of the parent complex by strengthening the metal-aryl bond, albeit not sufficiently to render the oxidative addition favourable.

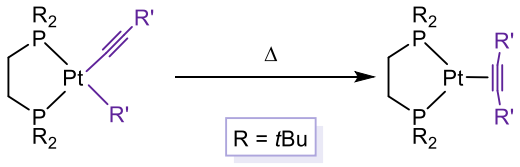

R'	T (°C)	$\Delta G^{\ddagger}$
3,5-dimethylphenyl	80	31.3
Phenyl	80	32.0
p-fluorophenyl	120	32.8
perfluorophenyl	300	47.3

Figure 4.1. Free energies of activation for the reductive elimination reactions of variously substituted aryl alkynyl Pt(II) complexes.

4.2. Transmetallation reactions of M-19o,c

4.2.1. Transmetallation reactions of rhodium complexes

With complexes **Rh-19o,c** in hand, their reactivity with alkynyl Grignard reagents was investigated next. 3,5-di-*tert*-butyl-benzene (Ar') was first chosen as the substituent, as it is sufficiently bulky to enforce entanglement of an alkyne within the macrocycle. Therefore Ar'CCH was treated with a slightly sub-stoichiometric amount of *i*PrMgCl•LiCl in THF (Scheme 4.1) to form Ar'CCMgCl•LiCl. The mixture was heated to 80 °C for 30 minutes to ensure complete consumption of the alkyl Grignard. This is easily evidenced by the disappearance of the characteristic upfield septet resonance in the ^{1}H NMR spectrum. Compounds **Rh-19o,c** were subsequently treated with the resulting Grignard solution (3.5 eq / Rh) which

afforded complete conversion after 18 h at room temperature. The products are characterised by a C_2-symmetric species observed by ^{31}P NMR spectroscopy ($\delta(^{31}P)$ 188.1, $^1J_{RhP}$ = 92 Hz, **Rh-24o**; $\delta(^{31}P)$ 74.1, $^1J_{RhP}$ = 88 Hz, **Rh-24c**), with $^1J_{RhP}$ coupling constants indicative of a +III oxidation state.

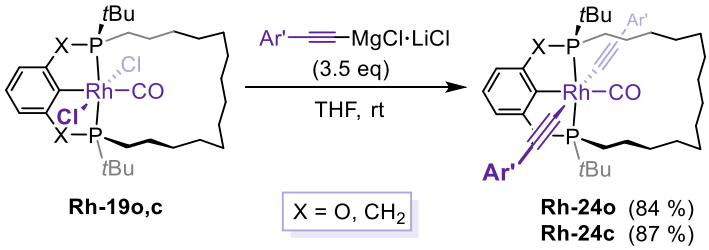

Scheme 4.4. Preparation of **Rh-24o,c**.

Complexes **Rh-24o,c** were assigned as Rh(III) bis-alkynyl carbonyl complexes, a formulation further supported by a significantly downfield PC$\underline{H}_aH_b$ signal (2H, δ 4.05, **Rh-24o**; δ 3.31, **Rh-24c**), arising from diamagnetic anisotropy induced by the proximity of the C≡C triple bonds as observed in **M-19o,c** and the corresponding chloride ligands. The single-crystal X-ray structure of **Rh-24o** was obtained from slow evaporation of an HMDSO solution (Figure 4.2), and demonstrates the adoption of a distorted octahedral geometry, with a slight distortion of the carbonyl out of the plane angle(C101–Rh1–C4, 172.71(8)) enforced by the methylene chain that is skewed to one side, a bite angle of 156.49(3)° (P2–Rh1–P3) and a quasi-linear geometry along the alkyne axes (C6–Rh1–C8, 177.33(7)).

Complexes **Rh-15o,c** were also characterised by ATR-IR spectroscopy in the solid-state with carbonyl stretching frequencies determined to be 2066 cm^{-1} (**Rh-24o**) and 2053 cm^{-1} (**Rh-14c**). These stretching frequencies are slightly red-shifted with respect to the chloride analogues, suggesting a slightly more electron rich Rh centre and consequently a greater extent of π-backdonation. This solid-state measurement is fully consistent with the improved stability of **Rh-24o,c** upon prolonged storage in solution compared to the chloride analogues, as no loss of CO was observed. The ATR-IR spectra of **Rh-24o,c** also display moderately weak C≡C stretching frequencies at 2105 cm^{-1} (**Rh-24o**) and 2107 cm^{-1} (**Rh-24c**).

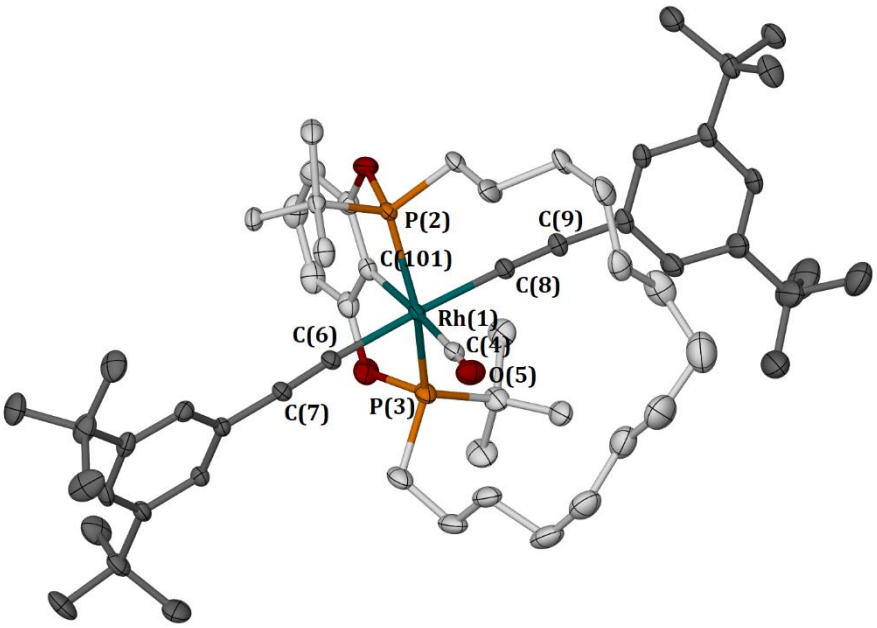

Figure 4.2. Solid-state structure of **Rh-24o**. Thermal ellipsoid drawn at 40% probability; minor disordered components and solvent molecules omitted for clarity. Selected bond lengths (Å) and angles (°): Rh1–P2, 2.3133(4); Rh1–P3, 2.3539(5); P2–Rh1–P3, 156.50(2); Rh1–C101, 2.037(2); Rh1–C4, 1.955(2); C101–Rh1–C4, 172.71(8); Rh1–C6, 2.037(2); Rh1–C8, 2.045(2); C6–Rh1–C8, 177.33(7); C6–C7, 1.204(3); C8–C9, 1.204(3).

4.2.2. Transmetallation reactions of iridium complexes

Likewise, the transmetallation of **Ir-19o,c** was achieved by treatment with a solution of Ar'CCMgCl•LiCl in THF. However, no reaction was observed at room temperature and the solution was thereafter heated at reflux. The appearance of an asymmetric species was observed by ^{31}P NMR spectroscopy along with the simultaneous formation of a new C_2-symmetric species at δ 146.9 (**Ir-24o**) or 38.3 (**Ir-24c**). Gratifyingly, further heating at 120 °C for 2 days in a thick-walled flask afforded complete conversion to the new C_2-symmetric species which were assigned as the iridium bis(alkynyl) carbonyl complexes **Ir-24o,c** (Scheme 4.5).

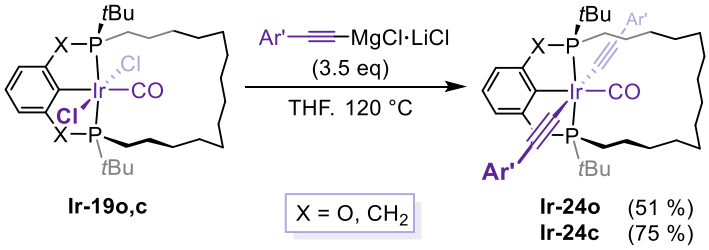

Scheme 4.5. Preparation of **Rh-24o,c**.

The ^{1}H NMR spectra of **Ir-24o,c** share the characteristics of **Rh-24o,c**, with one of the PCH_2 resonances diamagnetically shifted downfield by the alkynyl ligands' proximity (2H, δ 4.09, **Ir-24o**; δ 3.45, **Ir-24c**). Determination of a solid-state structure has proved elusive so far, but further characterisation of **Ir-24o,c** was possible by ATR-IR spectroscopy. In support of their formulation, the spectra of **Ir-24o,c** display intense carbonyl stretching frequencies at 2042 cm^{-1} (**Ir-24o**) and 2029 cm^{-1} (**Ir-24c**), in agreement with the previously observed trends for these compounds in terms of electron density at the metal centre, as well as C≡C stretching frequencies at 2115 cm^{-1} (**Ir-24o**) and 2108 cm^{-1} (**Ir-24c**) that are weaker in intensity.

4.3. Decarbonylation of Rh-24o

4.3.1. Formation of a diyne complex

With **Rh-24o** in hand, conditions to promote loss of CO were trialled to promote reductive elimination. These reactions are usually carried out under photochemical conditions[34,35] or using an oxidant to generate CO_2, typically Me_3NO.[36]

Initial attempts were carried out by dissolving **Rh-24o** in toluene with 10 equivalents of Me_3NO. Unfortunately, no reaction was observed even upon heating at reflux for 24 h. This absence of reactivity can be rationalized by the poor solubility of Me_3NO in non-protic and relatively non-polar solvents. Using fluorobenzene instead allowed this solubility issue to be circumvented, as it is sufficiently polar to fully dissolve the excess Me_3NO (resulting in *ca.* 0.2 M solutions). In this way, heating at 50 °C overnight resulted in a colour change from pale yellow to a light orange, with the appearance of a new species characterised by a single ^{31}P resonance at δ 184.8 that integrated to *ca.* 10 % of the mixture, with 90 % starting material remaining. Encouragingly, the large $^{1}J_{RhP}$ coupling constant of 162 Hz suggests an oxidation state of +I. Further heating at 85 °C for 18 h resulted in clean and quantitative formation to this deep red compound **Rh-25o**, which was subsequently isolated from unreacted Me_3NO by filtration in hexane in excellent yield (Scheme 4.6).

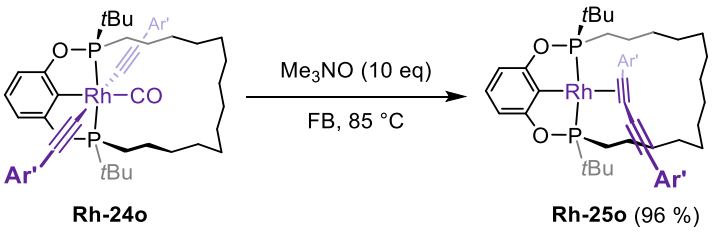

Rh-24o **Rh-25o** (96 %)

Scheme 4.6. Decarbonylation of **Rh-24o**.

Surprisingly, the C_2-symmetry that is evident in the $^{31}P\{^1H\}$ NMR spectrum is not reflected in the ^1H NMR spectrum. On the contrary the latter displays appreciable fluxionality, with the aromatic region the most diagnostic (Figure 4.3). This fluxionality unfortunately impeded collection of ^{13}C NMR data, although the ulterior synthesis of an isotopologue **^{13}C-Rh-25o** (with a Ar'C≡^{13}C–^{13}C≡CAr' axle, see Experimental) allowed the determination of the resonances pertaining to the central C(sp)–C(sp) bond at δ 83.0 and 70.9 with a $^1J_{CC}$ coupling constant of 156 Hz, a large value that is in line with expectation for bonds of this nature.[37]

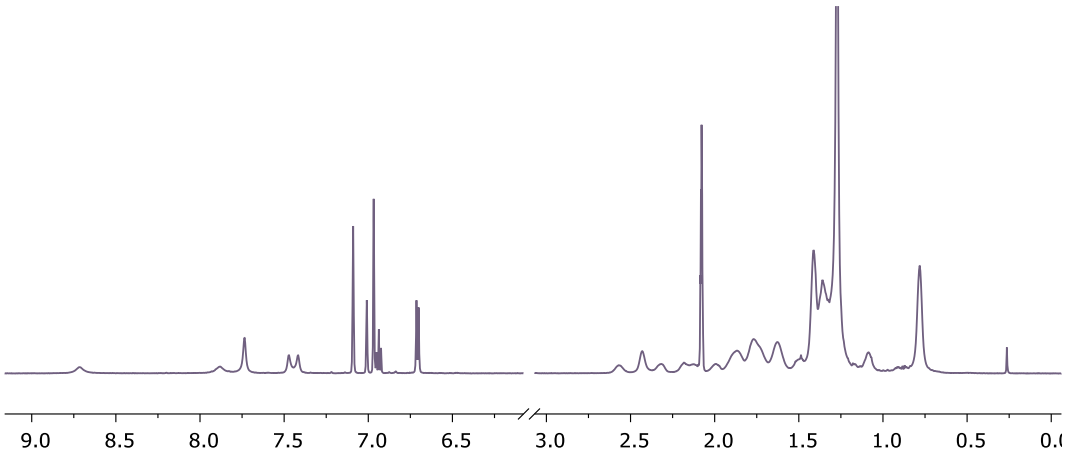

Figure 4.3. ^1H NMR spectrum of **Rh-25o** in toluene-d_8 at 298 K (600 MHz)

Characterization of **Rh-25o** by ATR-IR spectroscopy revealed the presence of two different alkyne stretching frequencies at 2154 cm^{-1} and 1938 cm^{-1}, consistent with η^2 coordination of the diyne.[38] The solid-state structure of **Rh-25o** was obtained from slow evaporation of a TMS solution and enabled the unambiguous assignment of **Rh-25o** as an asymmetrically bound diyne complex (Figure 4.4).

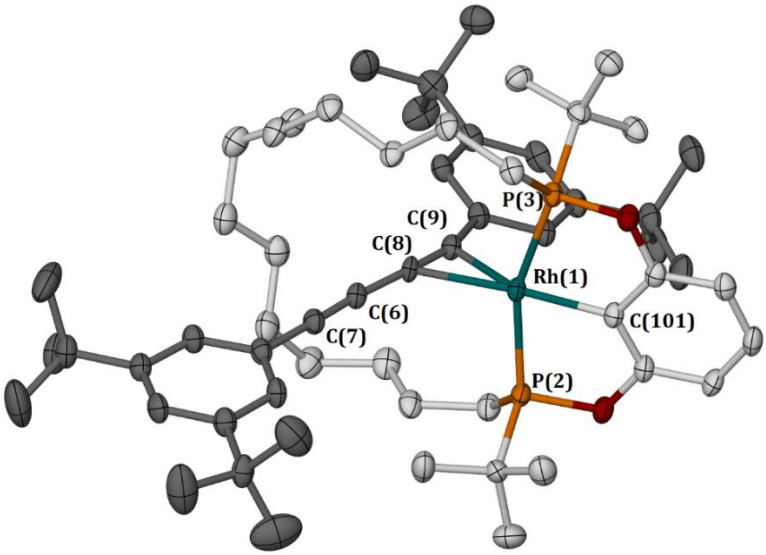

Figure 4.4. Solid-state structure of **Rh-25o** (not unique, *Z'*=2). Thermal ellipsoids drawn at 40% probability; minor disordered components and solvent molecules omitted. Selected bond lengths (Å) and angles (°): 1, Rh1–P2, 2.2579(11); Rh1–P3, 2.3041(11); P2–Rh1–P3, 158.55(4); Rh1–C101, 2.006(4); Rh1–Cnt(C8,C9), 2.072(4); C101–Rh1–Cnt(C8,C9), 160.12(13); C6–C7, 1.202(6); C6–C8, 1.379(6); C8–C9, 1.243(6); C6–C8–C9, 169.3(4); Rh11–P12, 2.2522(11); Rh11–P13, 2.3082(11); P12–Rh11–P13, 157.94(4); Rh11–C201, 2.005(4); Rh11–Cnt(C48,C49), 2.071(3); C201–Rh1–Cnt(C48,C49), 161.7(2); C46–C47, 1.203(6); C46–C48, 1.384(6); C48–C49, 1.244(6); C46–C48–C49, 168.3(4).

The structure shows a η^2-coordinated diyne, appreciably skewed with respect to ideal square planar geometry (C–Rh–Cnt(C≡C) = 160.12(13); 161.7(2) °). In agreement with expectations from metal to ligand π-backbonding interactions, the diyne chain is significantly deviated from linearity (C6–C8–C9, 169.3(4)) and is accompanied by a C≡C bond elongation (C6–C7, 1.202(6), free; C8–C9, 1.243(6), bound). The acyclic congener [(*t*Bu$_4$-POCOP)Rh(Ar'C$_4$Ar')], ***t*Bu-Rh-25o**, was prepared by reacting the corresponding hydrido chloride with KO*t*Bu in the presence of the free diyne and its solid-state structure was also determined (Figure 4.5, right). In contrast to macrocyclic **Rh-25o**, the acyclic shows a static ^{1}H NMR spectrum and its structure does not display any significant distortion from square planar geometry (C–Rh–Cnt(C≡C) = 178.68(8)). This distortion in the manner the diyne is coordinated to the metal in **Rh-25o** is therefore caused by the presence of the macrocycle, possibly through steric buttressing with the bulky Ar' group attached to the bound alkyne, thereby pushing this moiety back towards the aromatic pincer backbone (Figure 4.5). The larger C≡C bond elongation in the acyclic complex (C8–C9, 1.257(3)) as well as diyne distortion from linearity (C6–

C8–C9, 158.1(2)) are in agreement with our ligand being a marginally weaker donor than its acyclic *t*Bu$_4$-POCOP counterpart as noted in section 3.3.4.

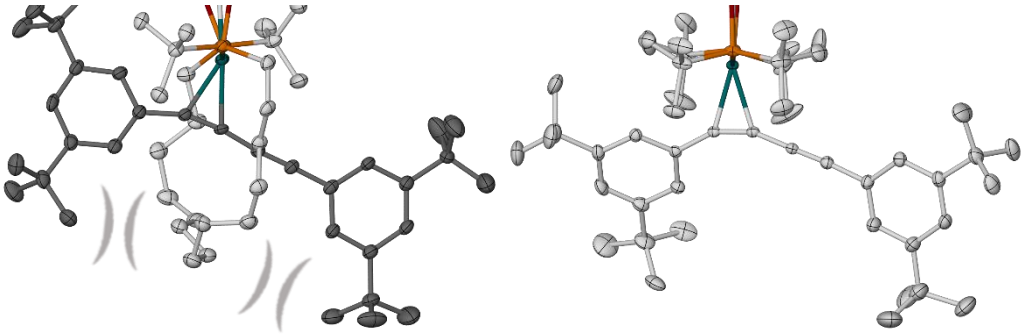

Figure 4.5. Solid-state structure of **Rh-25o** (left) and its acyclic analogue ***t*Bu-Rh-25o** (right).

*4.3.2. Dynamics of **Rh-25o***

The pronounced fluxionality of **Rh-25o** observed by NMR spectroscopy at 298 K led us to further investigate this process across a wider temperature range.

On cooling down to 183 K, the ^{31}P resonance broadened significantly but full decoalescence was not achieved. The structural dynamics of **Rh-25o** and its ^{13}C isotopologue are instead more readily interrogated using variable temperature ^{1}H NMR spectroscopy (183 – 373 K), where the slow exchange regime could be observed at temperatures below 243 K. The spectra were modelled using GNMR and two distinct processes identified: (i) a shuttling motion from one alkyne to the other and (ii) a restricted Ar' group rotation when the corresponding alkyne moiety is bound to the Rh centre. The associated model converged readily in the temperature range 243 – 318 K and was able to accurately fit the experimentally determined spectra (Figure 4.6).

Eyring analysis of the obtained rate constants (Figure 4.7) allowed the determination of the activation barriers for both processes, namely the shuttling ($\Delta H^{\ddagger}$ = 75.2 ± 0.6 kJ/mol, $\Delta S^{\ddagger}$ = 40 ± 2 J/mol/K, $\Delta G^{\ddagger}$(298 K) = 63 ± 1 kJ/mol) and the restricted rotation ($\Delta H^{\ddagger}$ = 50.1 ± 0.5 kJ/mol, $\Delta S^{\ddagger}$ = -39 ± 2 J/mol/K, $\Delta G^{\ddagger}$(298 K) = 62 ± 1 kJ/mol).

The values for the shuttling process show a relatively high enthalpic barrier that is to an extent offset by a positive activation entropy term. The latter suggests dissociation of the diyne occurs and is rate-determining. The same analysis was

carried out for the isotopologue **^{13}C-Rh-25o** which yielded identical values within error and therefore did not allow any significant KIE to be determined for these processes.

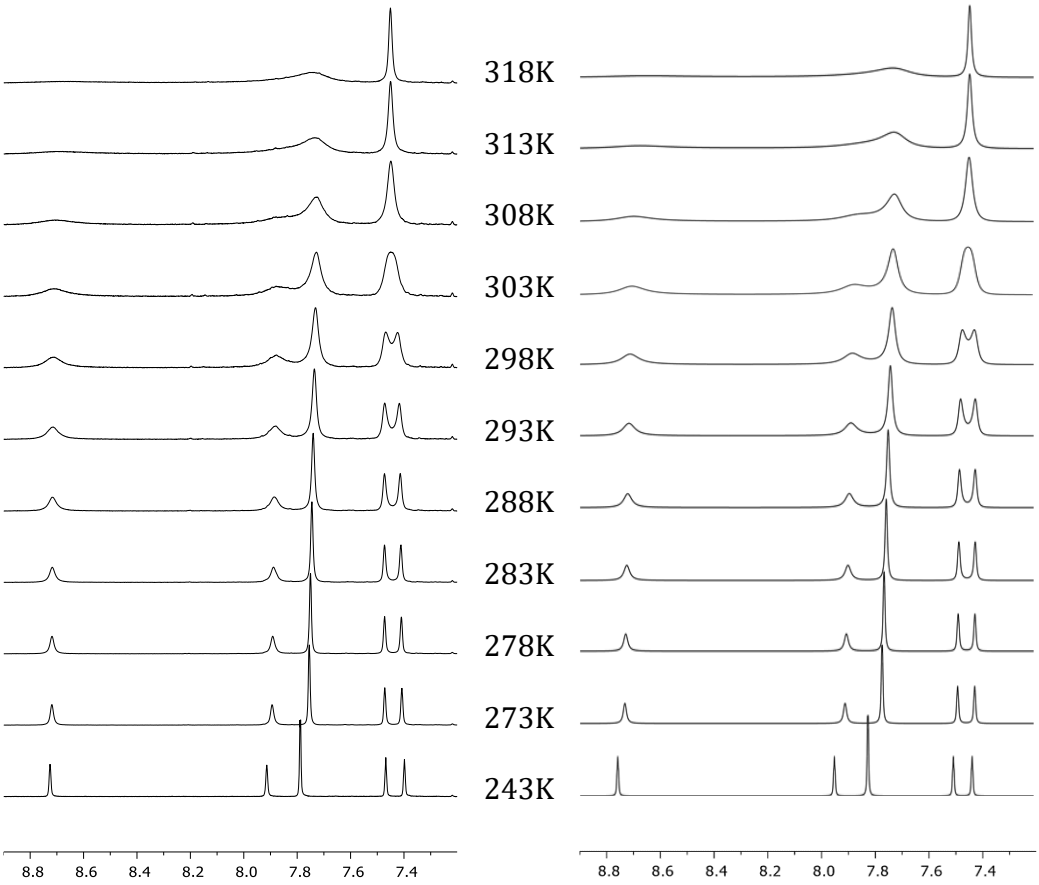

Figure 4.6. Experimental (left) and simulated (right) variable-temperature ^{1}H NMR spectra of **Rh-25o** (toluene-d_8, 600 MHz).

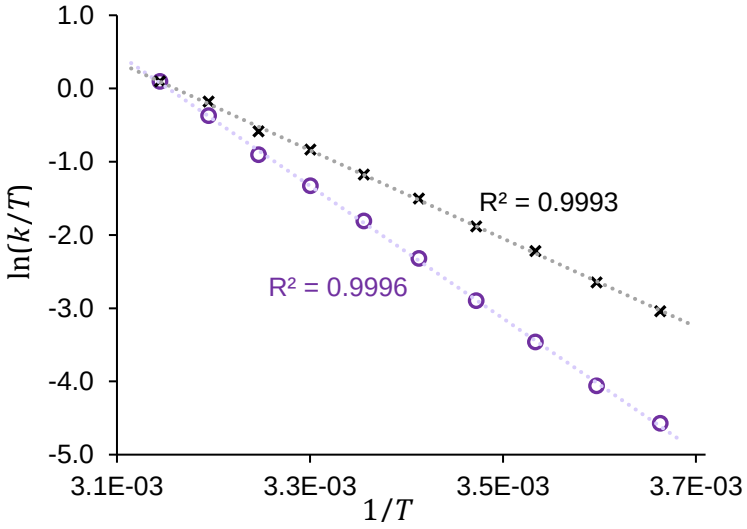

Figure 4.7. Eyring analysis of the shuttling (purple circles) and restricted rotation (black crosses) processes for **Rh-25o**.

*4.3.3. Reactions of **Rh-25o** with H_2 and CO*

With an interlocked diyne complex in hand, attention turned naturally to the development of reaction conditions for its hydrogenation to a saturated alkane. A toluene solution of **Rh-25o** was placed under an atmosphere of H_2 and the reaction monitored by NMR spectroscopy. Surprisingly, after heating at 50 °C overnight, the appearance of ca. 10% **Rh-15o** was observed by ^{31}P NMR spectroscopy. Subsequent heating to 85 °C for 24 h afforded **Rh-15o** in quantitative spectroscopic yield as well as two equivalents of 1,3-di-*tert*-butyl-5-ethylbenzene (Scheme 4.7). Formation of the latter was confirmed by comparison to a sample prepared independently by hydrogenation of the parent alkyne using Pd/C (see Experimental). The outcome of this reaction strongly suggests the diyne was hydrogenated following C–C bond activation. This constitutes a most unusual transformation, the mechanism of which could involve either direct C(sp)–C(sp) oxidative addition and subsequent hydrogenation or the reverse, i.e. hydrogenation of the diyne to the enyne or further and subsequent cleavage of the C–C bond.

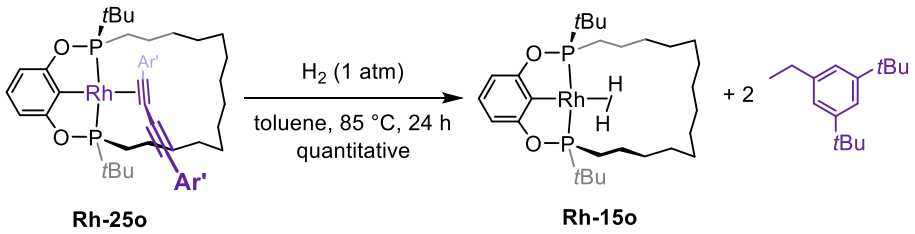

Scheme 4.7. Hydrogenolysis of **Rh-25o** in toluene.

In order to rule out the possibility of diyne dethreading, a toluene solution of **Rh-25o** was placed under an atmosphere of CO (Figure 4.8, top). This was followed by an immediate reaction as was apparent by a marked colour change from deep red to near colourless. Analysis by ^{31}P NMR spectroscopy revealed the quantitative formation of **Rh-26o**, a distinctly asymmetric species as indicated by two ^{31}P resonances at δ 195.3 (dd, $^{2}J_{PP}$ = 420 Hz, $^{1}J_{RhP}$ = 115 Hz) and δ 182.5 (dd, $^{2}J_{PP}$ = 420, $^{1}J_{RhP}$ = 109) and by the aromatic region of the ^{1}H NMR spectrum. This data rules out formation of carbonyl complex **Rh-18o** and confirms the diyne is robustly retained within the macrocyclic ligand. The significant decrease in the $^{1}J_{RhP}$ coupling constant was at first surprising as such changes typically indicate

formation of a complex with an oxidation state of +III. Upon repeating the reaction in TMS, crystals of that species were obtained in minutes following freeze-pump-thaw degassing and placing under a CO atmosphere.

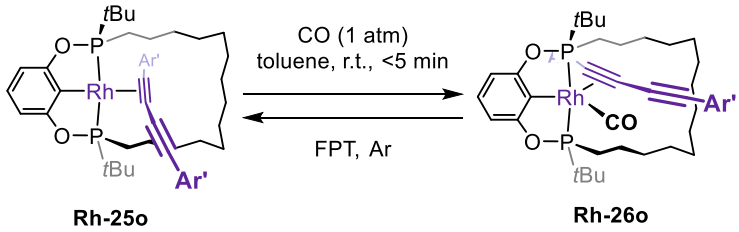

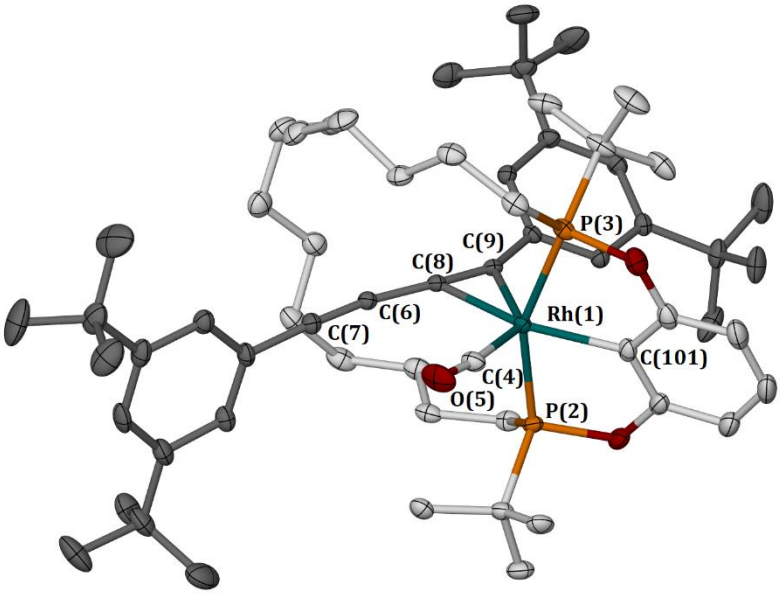

Figure 4.8. Preparation of **Rh-26o** in toluene (top); Solid-state structure of **Rh-26o** (bottom). Thermal ellipsoids drawn at 40% probability; minor disordered components and solvent molecules omitted. Selected bond lengths (Å) and angles (°):Rh1–P2, 2.2935(5); Rh1–P3, 2.3273(5); P2–Rh1–P3, 155.32(2); Rh1–C101, 2.066(2); Rh1–C4, 1.942(2); C101–Rh1–C4, 106.01(8); Rh1–Cnt(C8,C9), 2.0482(12); C101–Rh1–Cnt(C8,C9), 135.41(7); C6–C7, 1.205(3); C6–C8, 1.384(2); C8–C9, 1.270(3); C6–C8–C9, 163.3(2).

The solid-state structure of **Rh-26o** was determined by X-ray crystallography and revealed a five coordinate η^2-diyne carbonyl complex with a distorted trigonal bipyramidal coordination geometry (Figure 4.8, bottom). The metrics associated with the structure of **Rh-26o** indicate stronger π-complexation than in **Rh-25o** as shown by a shorter Rh···alkyne bond length (Rh–Cnt(C≡C) = 2.0482(12) Å) and a markedly elongated bound alkyne bond (C≡C = 1.205(3) (free), 1.270(3) (bound) Å). These trends were confirmed by ATR-IR spectroscopy with a significant red-shift for the bound alkyne resonance down from 1938 cm^{-1} to 1863 cm^{-1}. Contrasting with **Rh-25o**, all shuttling motion was frozen (298 K, 600 MHz) in

Rh-26o upon carbonyl coordination. Accordingly, the only fluxional behaviour observable in the ^{1}H NMR spectrum involves solely the two aromatic protons in the bound Ar' group whose rotation is restricted by the steric buttressing with the ligand backbone. The shift from a square planar (sp^2d hybridization) to a trigonal bipyramidal (sp^3d hybridization) geometry about the rhodium centre results in a decrease in %s-character involved in the binding to the phosphorus atoms and thereby accounts for the marked reduction in the $^{1}J_{RhP}$ coupling constant. Coordination of CO was found to be reversible, as repeated freeze-pump-thaw degassing (ca. 4 – 5 FPT cycles) a sample of **Rh-26o** in toluene resulted in the quantitative regeneration of **Rh-25o**.

Heating a solution of **Rh-26o** in toluene at 50 °C under a CO atmosphere overnight resulted in the formation of ca. 10% of the bis alkynyl complex **Rh-24o** by ^{31}P NMR spectroscopy. Further heating at 85 °C for 24 h afforded **Rh-24o** smoothly and in quantitative spectroscopic yield (Scheme 4.8).

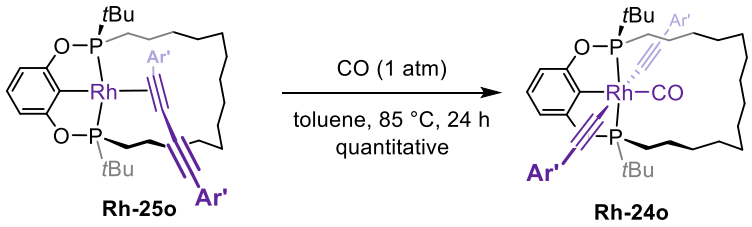

Scheme 4.8. Thermolysis of **Rh-26o** under CO atmosphere.

This result is fully consistent with the previous reactivity observed under H_2. Both reactions seem to proceed on a very similar timescale which may point to a common mechanism which ultimately results in the cleavage of the central C(sp)–C(sp) bond in the diyne axle. This result is particularly remarkable as direct insertion of a transition metal into a C–C bond is usually associated with unfavourable thermodynamics and high activation energy barriers, all the more so with a very strong C(sp)-C(sp) bond.

Further emphasizing the importance of the macrocycle in these processes, reactions of ***t*Bu-Rh-25o** in toluene with H_2 and CO resulted in complete hydrogenation to the linear alkyne or simple ligand displacement, respectively (Scheme 4.9).

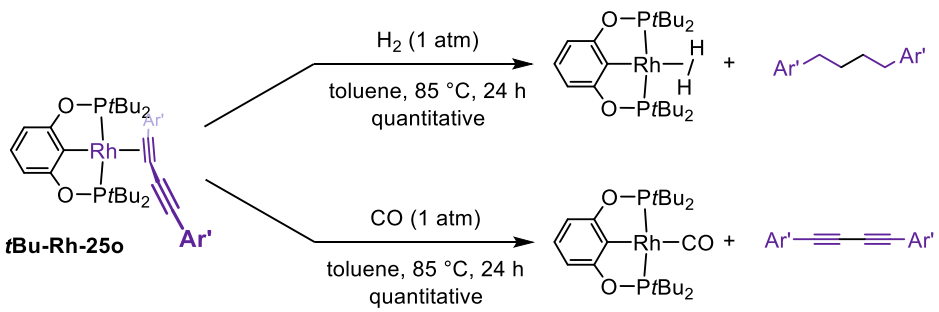

Scheme 4.9. Control reactions with ***t*Bu-Rh-25o** under H_2 (top) and CO atmosphere (bottom).

The reversible character of the carbonyl binding as well as this unusual reactivity towards the central C(sp)–C(sp) single bond prompted us to carry out further mechanistic investigations.

*4.3.4. UV-vis spectroscopy study of the equilibrium between **Rh-25o** and **Rh-26o***

As a prelude to studying the formation of **Rh-24o** in detail, the reversible binding of CO to **Rh-25o** was first investigated. Taking advantage of the markedly different colours of the two complexes and therefore their very different UV-vis spectra, the thermodynamics associated with this equilibrium were studied with UV-vis spectroscopy. Specifically, **Rh-25o** shows absorption bands in the 400 – 550 nm region of the spectrum with molar extinction coefficient values comprised between 4500 $L.mol^{-1}.cm^{-1}$ and 10000 $L.mol^{-1}.cm^{-1}$, thereby indicating the likely presence of Metal-to-Ligand Charge Transfer (MLCT) transitions responsible for **Rh-25o**'s characteristic deep red colour.

To this end, a 0.2 mM standard solution of **Rh-25o** was prepared and placed in a T-shaped quartz cuvette equipped with a J. Young's tap. Following acquisition of standard spectra for **Rh-25o** at each temperature in the chosen range (*vide infra*), that sample was rigorously degassed and place under a CO atmosphere (1 atm) which resulted in immediate conversion to **Rh-26o**. A standard spectra of **Rh-26o** was obtained after cooling the sample to -10 °C so as to preclude the presence of any free **Rh-25o** in solution. Spectra were then acquired in the temperature range 35 – 85 °C, each subsequently deconvoluted as a linear combination of the two reference spectra (Figure 4.9).

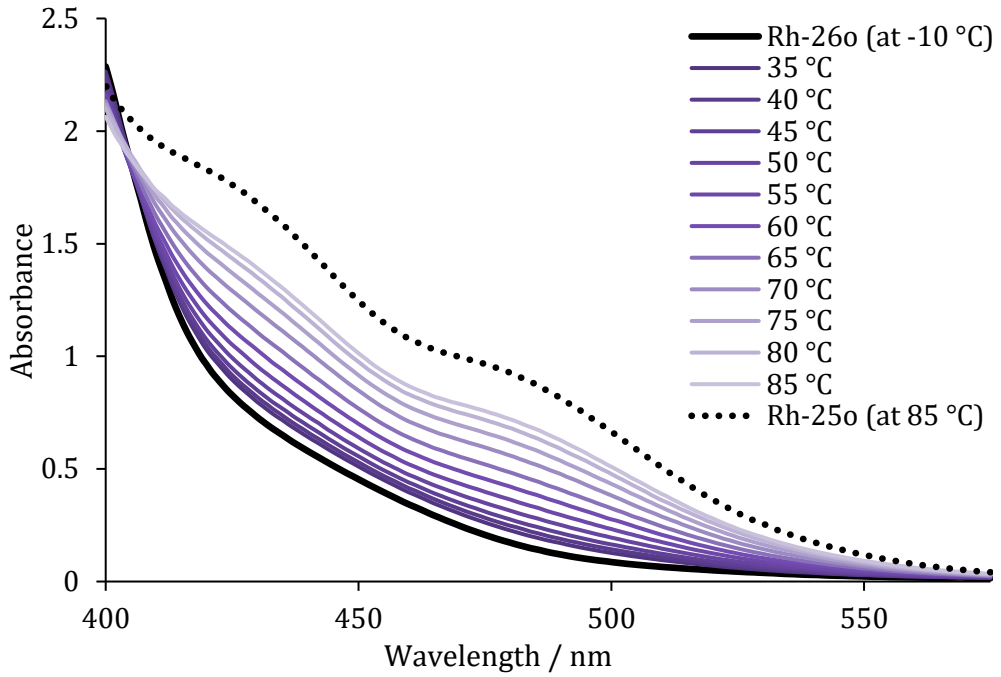

Figure 4.9. Overlaid UV-vis spectra of a solution of **Rh-25o** in toluene under an atmosphere of CO (1 atm).

The solubility of CO in toluene at the various acquisition temperatures was estimated from literature data (see Experimental). The results were used to estimate the equilibrium constant defined as:

$$K = \frac{[\mathbf{Rh\ 25o}][\mathrm{CO}]}{[\mathbf{Rh\ 26o}]}$$

Van't Hoff analysis was conducted based on the calculated equilibrium constants (Figure 4.10) allowing the thermodynamic parameters for the equilibrium to be determined: ΔH = 71 ± 1 kJ/mol and ΔS = 226 ± 3 J/mol/K. These values show that coordination of CO to **Rh-25o** is enthalpically very favourable albeit at a very high entropic cost, which cannot be explained solely by the usual entropic penalty associated with the reactivity of bimolecular systems (60 – 90 J/mol/K too high).

An important additional contribution to the entropic term may stem from a significant loss of conformational freedom upon CO coordination for both the axle (no shuttling motion) and the macrocyclic ligand. The latter is particularly noticeable in the ^{1}H NMR spectrum of **Rh-26o**, whereby the signals belonging to the alkyl tether are markedly spread out and resolved, with each proton in a different and unique magnetic environment as a result of a locked conformation of the macrocycle. Ultimately, this results in a calculated ΔG = 0 kJ/mol at a

temperature of *ca.* 43 °C, with the reaction exergonic above. More practically, in the conditions described for the sample above and hereafter, **Rh-25o** is the major component of the mixture above 70 °C.

T / °C	*K*
35	0.529076
40	0.786822
45	1.150949
50	1.718844
55	2.536923
60	3.697728
65	5.442869
70	8.224702
75	12.03832
80	17.53894
85	26.05725

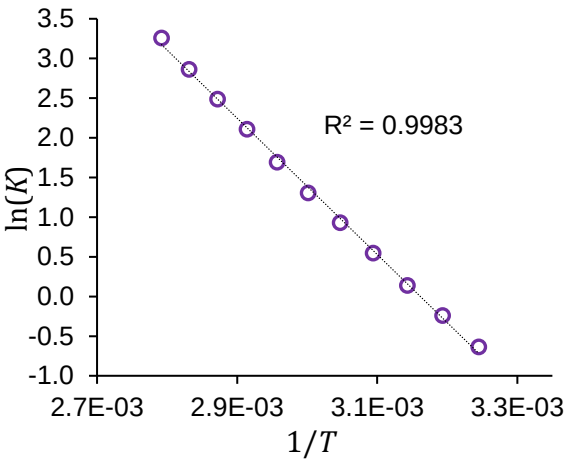

Figure 4.10. Van't Hoff analysis of the equilibrium **Rh-26o** ⇌ **Rh-25o** + CO.

*4.3.5. UV-vis spectroscopy kinetic study of the reaction of **Rh-25o** with CO*

Complementary kinetic studies by UV-vis spectroscopy were carried out with a view to fully determining the thermodynamic parameters associated with the C(sp)-C(sp) bond activation process.

The working mechanism comprises (Figure 4.11): (i) carbonyl coordination to **Rh-25o**, in rapid pre-equilibrium with the parent complex **Rh-26o**, (ii) C–C bond scission of Rh-25o to form pentavalent intermediate **Rh-25o'**, (iii) C–C bond formation by reductive elimination from Rh-25o' to re-form **Rh-25o**, (iv) trapping of **Rh-25o'** with CO to form **Rh-24o**.

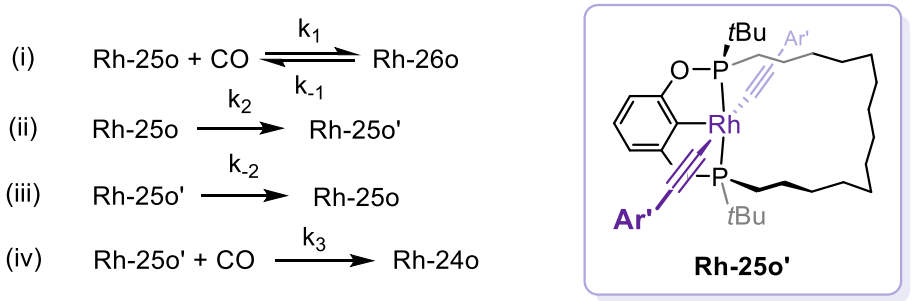

Figure 4.11. Mechanism for the C(sp)–C(sp) bond cleavage and associated rate constants observed in Rh(POCOP) complexes.

As **Rh-25o'** was never observed by NMR spectroscopy during the reactions of **Rh-25o** with CO or during the decarbonylation of **Rh-24o**, the steady-state approximation can be applied. Given the rapid equilibrium between **Rh-25o** and **Rh-26o**, the rate law can be written as:

$$\frac{d[\mathbf{Rh\ 25o}]}{dt} = -\frac{k_2 k_3 [CO]}{k_{-2} + k_3 [CO]} [\mathbf{Rh\ 25o}]$$

with an apparent rate constant dependent on the concentration of CO in solution. As the reaction was found to be independent of CO pressure (1.0 – 1.3 atm), thereby justifying the hypothesis $k_3 >>> k_2 > k_{-2}$, the rate law can be simplified to:

$$\frac{d[\mathbf{Rh\ 25o}]}{dt} = -k_2 [\mathbf{Rh\ 25o}]$$

Samples were prepared from a 0.2 mM solution of **Rh-25o** in toluene and placed under CO in the same fashion as described in section 4.3.4. Kinetic runs were carried out in 5 °C intervals in the temperature range 80 – 100 °C. Such temperatures allow sufficiently fast reactions for the practical determination of the associated kinetic parameters, but also take advantage of there being a majority of deep red **Rh-25o** even under one atmosphere of CO so as to provide readily measurable absorbance values in the range 400-600 nm where absorption by **Rh-24o** is very weak (see Experimental).

Thus, plotting the consumption of **Rh-25o** against time indicated first order dependence in the latter which could be reliably modelled by a decreasing exponential function of the form $A \times \exp(-k_2 \times t) + B$, which consistently resulted in correlation coefficients >0.9999 across the 10 wavelengths chosen for the fitting, *i.e.* [400, 410, 420, 430, 440, 450, 460, 470, 480, 490] nm. With that methodology established, the kinetic parameters associated with the reaction were determined for **Rh-25o** and its isotopomer **^{13}C-Rh-25o** (Figure 4.12).

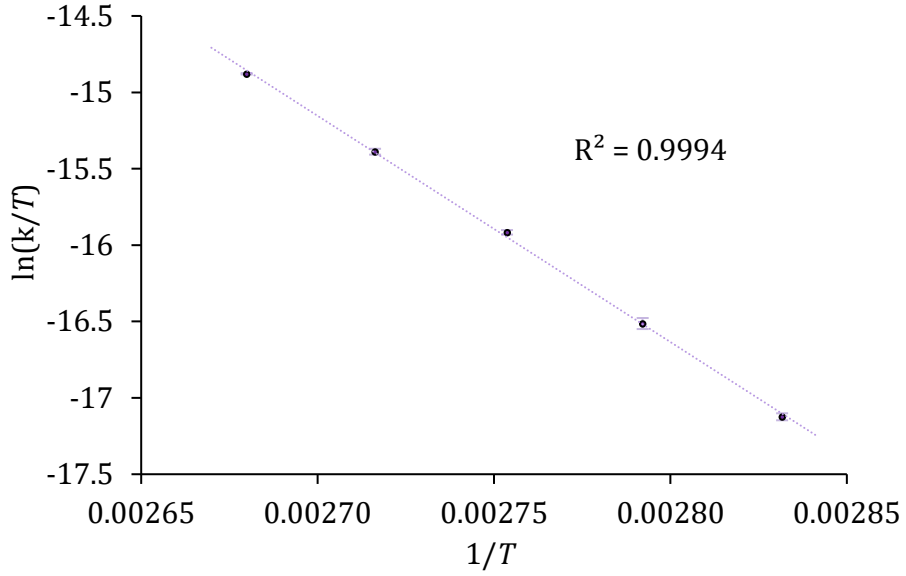

Compound	T / °C	k_2 / 10^{-5} s^{-1}	$t_{1/2}$ / h
Rh-25o	80[a]	2.31 ± 0.02	8.4
Rh-25o	85 [a]	4.3 ± 0.6	4.5
Rh-25o	90 [a]	7.8 ± 0.4	2.5
Rh-25o	95 [a]	13.4 ± 0.8	1.4
Rh-25o	100 [b]	22.3 ± 0.1	0.86
^{13}C- Rh-25o	100 [b]	20.8 ± 0.3	0.93

[a]kinetic run carried out twice; [b]kinetic run carried three times

Figure 4.12. Eyring analysis for the thermolysis of **Rh-25o** under CO.

Eyring analysis for **Rh-25o** allowed the determination of activation parameters: $\Delta H^{\ddagger}$ = 123 ± 2 kJ/mol, $\Delta S^{\ddagger}$ = +8 ± 5 J/mol/K, $\Delta G^{\ddagger}$(298 K) = 120 ± 3 kJ/mol. In further support to the C–C bond activation step being rate-determining is the observation of a measurable kinetic isotope effect of 1.08 ± 0.02 measured for **Rh-25o**/**^{13}C-Rh-25o**, slightly higher than a theoretical KIE of $\sqrt{26/24}$ = 1.041 expected for a ^{13}C-^{13}C bond cleavage with respect to a ^{12}C-^{12}C bond cleavage.

4.3.6. Computational studies

With a view to further substantiating the dynamics observed for **Rh-25o** as well as the mechanism proposed for the C(sp)–C(sp) bond scission, theoretical calculations were also undertaken.

In order to fully capture the dynamics of the entire system, a complete, untruncated model of **Rh-25o** was optimised using the GFN2-xTB method developed by the Grimme group as implemented in the xTB package.[39] The optimized structure of **Rh-25o** was found able to accurately describe the geometry of the system at hand and was comparable to the structure optimized at the DFT level (*vide infra*). That structure was subsequently subjected to several molecular dynamics runs for a duration of 1 ns, and thermostatted at various temperatures (293 – 573 K). Hydrogen mass repartitioning ($H_{mass} \times 4$) allowed the use of a longer time step, chosen as 2 fs.

Gratifyingly, all runs displayed dynamic behaviour in agreement with the VT-NMR spectroscopy measurements and simulations in section 4.3.2, namely the shuttling motion of the diyne from coordination of one alkyne to the other *via* a dissociative mechanism and the restricted rotation of the Ar' group attached to the bound alkyne. Figure 4.13 shows the time evolution of the C(sp)-C(sp)-Rh angle, stacked with a dihedral angle chosen relevant to the rotation of the Ar' group about its axis.

Interestingly, all molecular dynamics runs mentioned above showed the presence of a σ-bound C(sp)-C(sp) complex, observable at nearly every shuttling event. These runs were subsequently used as a basis for further optimization at the DFT level. Early DFT-level optimizations using the solid-state structure as a basis for the starting geometry did not allow the optimisation of such a complex. We attribute this to the difficulty to sample the conformational space with static methods in order to provide an optimal macrocycle conformation for this intermediate.

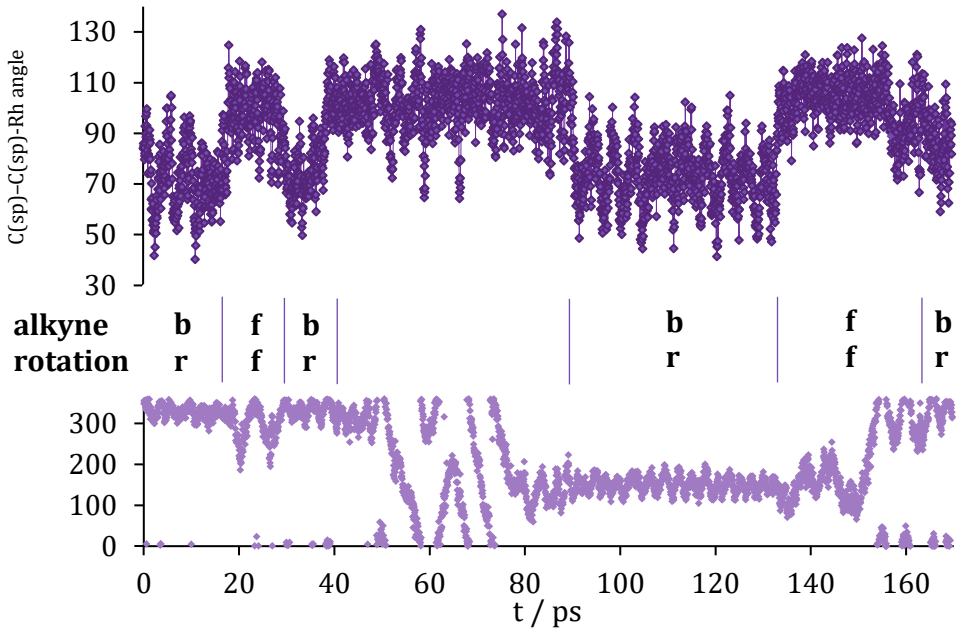

Figure 4.13. Time-plot of the C(sp)–C(sp)-Rh angle, denoting the bound (b) or free (f) character of the alkyne of interest (top); Time-plot of a Rh-C(sp)-C(sp^2)-C(sp^2) dihedral angle denoting the rotation of the Ar' group attached to the alkyne of interest, the rotation of which is either restricted (r) or free (f) (bottom).

Interestingly, all molecular dynamics runs mentioned above showed the presence of a σ-bound C(sp)-C(sp) complex, observable at nearly every shuttling event. These runs were subsequently used as a basis for further optimization at the DFT level. Early DFT-level optimizations using the solid-state structure as a basis for the starting geometry did not allow the optimisation of such a complex. We attribute this to the difficulty to sample the conformational space with static methods in order to provide an optimal macrocycle conformation for this intermediate.

Thus, using the geometry provided by the MD runs as input allowed the optimization of the σ-bound C(sp)-C(sp) complex intermediate **INT1** which was verified as a local minima by vibrational analysis, all at the ωB97x-D3/def2-TZVP//ωB97x-D3/def2-SV(P) level.[40–43] This intermediate was calculated to be ΔH = +72.5 kJ/mol above **Rh-25o** (Figure 4.14). The transition state **TS1** was located using the Nudged-Elastic-Band method and calculated at $\Delta H^{\ddagger}$ = +73.9 kJ/mol above **Rh-25o**, merely 1.4 kJ/mol above the σ-intermediate. A result that is in excellent agreement with the experimentally measured enthalpy of activation of 75.2 ± 0.6 kJ/mol. Replacing the two central atoms in the axle by their ^{13}C isotope in the vibrational analysis predicted a $\Delta H^{\ddagger}(^{13}C)$= +74.0 kJ/mol,

with a calculated KIE of only 1.017, a value that was indeed not realistically measurable experimentally.

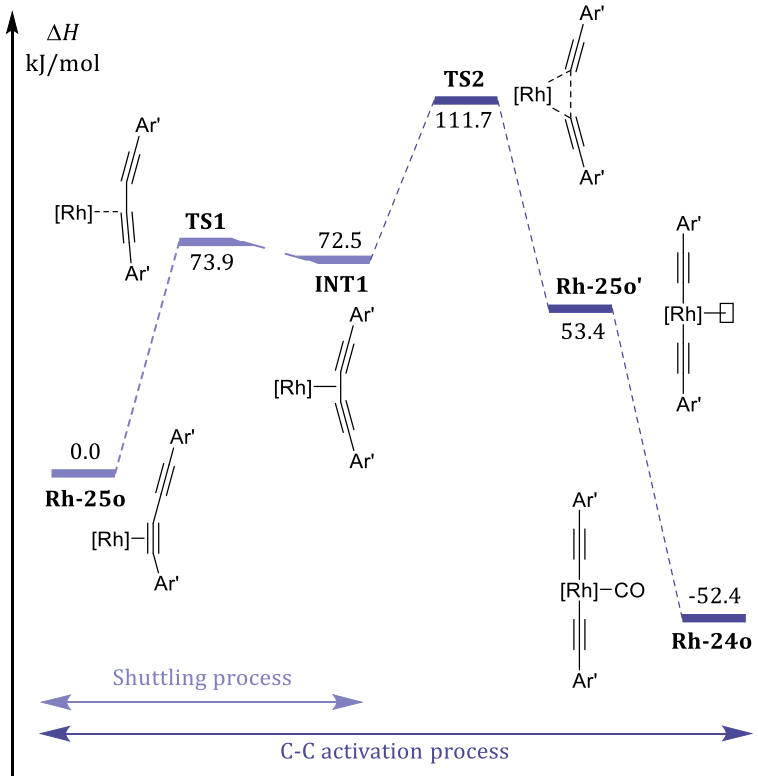

Figure 4.14. Computed energy profile for the shuttling and C(sp)-C(cp) activation processes observed in **Rh-25o**.

With intermediate **INT1** in hand, a relaxed surface scan along the C(sp)–C(sp) bond distance allowed the subsequent geometry optimisation of transition state **TS2**, pertaining to the C–C bond cleavage. The latter was located at $\Delta H^{\ddagger}$ = +111.7 kJ/mol, in fairly good agreement with the experimentally determined value of 123 ± 2 kJ/mol. Satisfyingly, the theoretical KIE associated with this process was calculated at 100 °C to be 1.073, in excellent agreement with the experimental value of 1.075 (rounded to 1.08). Finally, pentavalent complex **Rh-25o'** was calculated to be 53.4 kJ/mol above **Rh-25o**, but gets stabilised upon CO coordination to **Rh-24o**, at ΔH = -52.4 kJ/mol.

The results presented here do not include the DFT-calculated entropy corrections, as these were found to be unusually largely underestimated by the method. Particularly in the case of the diyne shuttling process, the predicted $\Delta S^{\ddagger}$ = +14.1 J/mol/K falls short of the experimentally determined $\Delta S^{\ddagger}$ = +40 ± 2 J/mol/K, thereby resulting in a predicted $\Delta G^{\ddagger}$ that is overestimated by nearly 10 kJ/mol at

298 K. This discrepancy is likely attributable to the "static" nature of these calculations, which can intrinsically not capture the dynamic processes associated with the conformational freedom of our ligand system. It was therefore suspected that in this system, significant steric hindrance drastically reduces the alkyl chain's conformational freedom, as a result of the close proximity of a bulky Ar' stopper group when one alkyne is bound to the Rh centre. Conversely, this steric hindrance is expected to be alleviated around the transition state geometry as a result of the increased average distance with the Ar' bulky groups, thus conferring the system a greater conformational flexibility and in turn a greater entropy gain at the transition state. Complementary studies based on molecular dynamics approaches are currently ongoing with the aim to verify these hypotheses.

*4.3.7. Stepwise hydrogenation of **Rh-25o**.*

The unexpected reactivity of **Rh-25o** with H_2 precludes any access to an interlocked alkyl chain analogue *via* direct hydrogenation reaction. With a view to preventing C–C bond hydrogenation, a new strategy was envisioned involving protonation at the Rh centre, promoting the formation of a metal alkenyl, and subsequent addition of hydride, to enable reductive elimination of an enyne: thereby forming a central C(sp^2)–C(sp) bond that may prove less reactive.

To this end, a solution of **Rh-25o** was treated with a stoichiometric amount of $[H(OEt_2)_2][BAr^F{}_4]$ in 1,2-difluorobenzene (Scheme 4.10). This resulted in the immediate formation of a new species by ^{31}P NMR spectroscopy, characterised by asymmetric ^{31}P resonances at δ 179.2 (dd, $^2J_{PP}$ = 364 Hz, $^1J_{RhP}$ = 124 Hz) and δ 171.0 (dd, $^2J_{PP}$ = 364 Hz, $^1J_{RhP}$ = 116 Hz) with $^1J_{RhP}$ coupling constants suggesting an oxidation state of +III. The absence of hydride resonances in the ^1H NMR spectrum suggests that subsequent alkyne insertion into a Rh-H bond occurred immediately following protonation. Acquisition of the $^{13}C\{^1H\}$-APT NMR data for the ^{13}C isotopologue supports this assignment; the spectrum shows the presence of two doublets with a $^1J_{CC}$ coupling constant of 88 Hz, a sharp resonance at δ 64.2 consistent with the free alkyne and a broader doublet of multiplets at δ 94.1 with an opposite indicating the presence of a proton. The combined spectroscopic data

point to the formulation of **Rh-27o** as a cationic alkenyl rhodium complex, with the Rh–C bond α to a Ar' group.

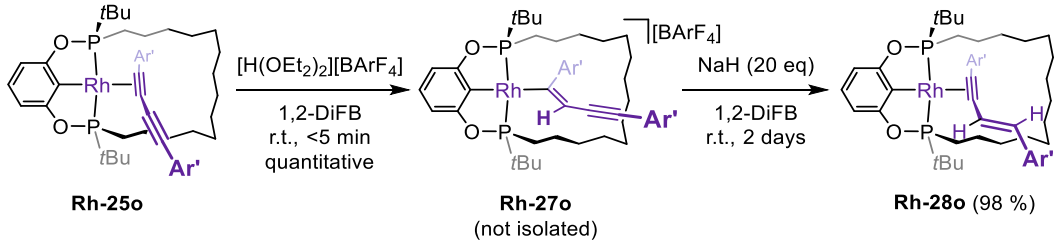

Scheme 4.10. Stepwise hydrogenation of **Rh-25o**.

Treatment of **Rh-27o** with sodium hydride (20 eq) as a suspension in 1,2-difluorobenzene for 2 days with vigorous stirring resulted in the quantitative conversion to the *E*-enyne complex **Rh-28o**. The presence of a coordinated enyne was confirmed by the presence of two doublets in the ^{1}H NMR spectrum at δ 8.25 and δ 7.17 with a $^{3}J_{HH}$ coupling constant of 15.4 Hz, and ^{13}C signals at δ 117.7 and δ 88.0. The $^{1}J_{CC}$ coupling constant across this C(sp^2)-C(sp) bond was determined using **^{13}C-Rh28o** to be 89 Hz, down from the 156 Hz coupling constant observed in the diyne complex **Rh-25o**. The near identical $^{1}J_{CC}$ coupling constants observed for **Rh-27o** and **Rh-28o** supports the presence of a C(sp^2)-C(sp) bond in the former.

Treatment of **Rh-28o** with H_2 and heating at reflux for 24 h yielded no reaction (Scheme 4.11), indicating the absence of dynamic C(sp)-C(sp^2) cleavage but frustrating the overall objective of obtaining a saturated axle. It is possible that with the non-linear enyne axle, the Rh centre in **Rh-28o** is effectively sterically shielded on either side of the coordination plane by the Ar' group, thereby disfavouring the coordination of an additional weak ligand such as H_2. Thus, hydrogenolysis of **Rh-25o** did not proceed *via* initial hydrogenation of the axle to the enyne but rather through direct C(sp)–C(sp) oxidative addition.

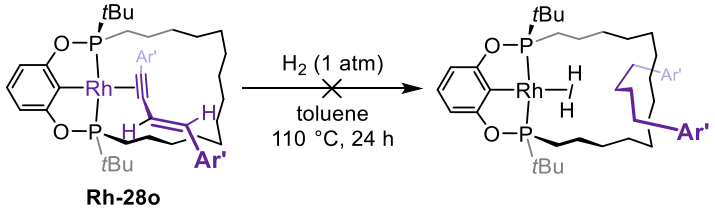

Scheme 4.11. Attempted hydrogenation of **Rh-28o**.

To probe the steric profile of **Rh-28o**, a sample in toluene was degassed and placed under an atmosphere of CO (Scheme 4.12). Conversely, an immediate reaction was observed, evidenced by a colour change from dark orange to light orange. The analysis by ^{31}P NMR spectroscopy revealed the presence of three species. One is characterized by a broadened doublet of doublets at δ 181.9 ($^{2}J_{PP}$ = 420 Hz, $^{1}J_{RhP}$ = 118 Hz) and an extremely broadened signal centre at δ 197 of equivalent integration. These coupling constants are reminiscent of the pentavalent diyne carbonyl complex **Rh-26o**, which led to the assignment of this new compound as the pentavalent enyne carbonyl complex **Rh-29o**. Its ^{31}P signals are significantly broader however, which we attribute to more dynamic CO coordination, which is presumably impeded by the added steric buttressing imposed by the non-linear enyne axle. In fact, **Rh-29o** is unstable at room temperature, with >50% of the reaction mixture consisting of two additional compounds by ^{31}P NMR spectroscopy after 18 h. More surprisingly, these two new compounds share an identical coupling pattern, with one phosphine resonance coupling to a Rh centre (δ(^{31}P) 199.7, $^{1}J_{RhP}$ = 158 Hz, δ(^{31}P) 194, $^{1}J_{RhP}$ = 159 Hz) in oxidation state +I, whilst the other phosphine resonance is shifted considerably upfield and displays no coupling to Rh (δ(^{31}P) 141.1 and 151.3, respectively), consistent with a free phosphine donor. This outcome is tentatively explained by CO-induced κ^3 to κ^2 coordination of the pincer as a result of steric buttressing with the enyne axle. Such stress is subsequently relieved upon dissociation of one phosphine arm: such species would be C_1-symmetric and therefore diastereomers are expected reconciling the formation of the two compounds. Isomerisation and coordination of an additional CO ligand would result in a square-based pyramidal 18VE complex with a vacant site across a carbonyl with a high *trans* effect. Remarkably, no dethreading was observed and removing CO by repeated freeze pump-thaw degassing completely regenerated **Rh-28o**.

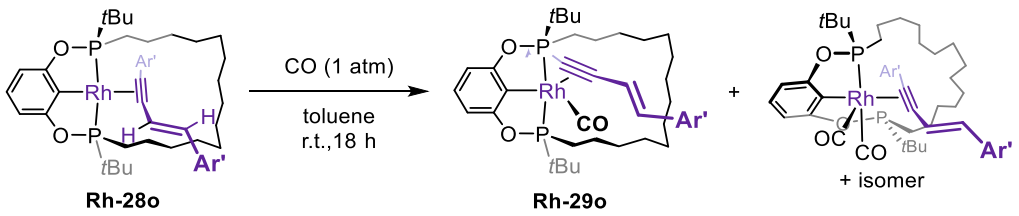

Scheme 4.12. Reaction of **Rh-28o** with CO.

Given the lack of reactivity of **Rh-28o** with H_2, our attention turned to continuing the hydrogenation of the axle in a stepwise fashion. To this end, a solution of **Rh-28o** in 1,2-difluorobenzene was treated with stoichiometric $[H(OEt_2)_2][BAr^F{}_4]$ which afforded immediate conversion to a new species. Analysis by ^{31}P NMR spectroscopy revealed an asymmetric species ($\delta(^{31}P)$ 187.8, $^2J_{PP}$ = 347 Hz, $^1J_{RhP}$ = 118 Hz; $\delta(^{31}P)$ 175.2, $^2J_{PP}$ = 347 Hz, $^1J_{RhP}$ = 115 Hz) with $^1J_{RhP}$ coupling constants suggesting an oxidation state of +III. Likewise the absence of hydridic resonances suggests the rapid insertion of the enyne into a Rh–H bond. This compound was therefore formulated as **Rh-30o** (Scheme 4.12). Compound **Rh-30o** was subsequently treated with NaH (20 eq) which afforded mainly one compound **Rh-31o** by ^1H NMR spectroscopy although the broadness observed in the $^{31}P\{^1H\}$ NMR spectrum did not allow confirmation. Surprisingly, the ^1H NMR spectrum was also very broad, suggesting significant dynamics. Only one broad alkene-like proton resonance could be located with certainty at δ 6.10, observed as a doublet with a $^1J_{CH}$ of 154.6 Hz in **^{13}C-Rh-31o**. In the $^{13}C\{^1H\}$ NMR spectrum of the isotopomer **^{13}C-Rh-31o**, a sharp singlet was observed at δ 129.2 ppm which indicates that the two central ^{13}C atoms in the axle are equivalent and points to a time-averaged C_2-symmetric species. On this basis, **Rh-31o** was tentatively assigned as a diene complex, which is reconcilable with the observation of central equivalent alkene signals, the observed ^{13}C shift and the dynamic behaviour which could arise from a rapid shuttling process.

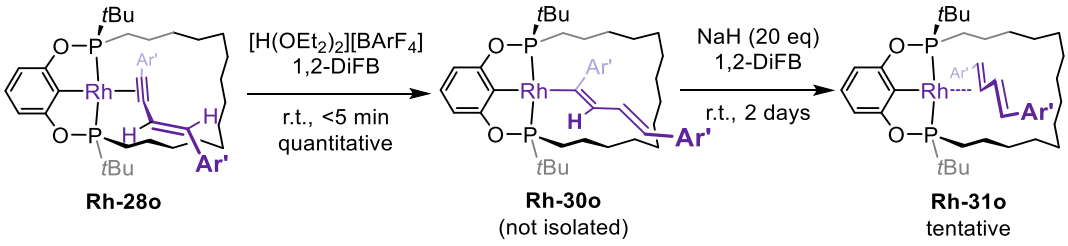

Scheme 4.13. Stepwise hydrogenation of **Rh-28o**.

Gratifyingly, **Rh-31o**/**^{13}C-Rh-31o** reacted with H_2 at room temperature over the course of two days in toluene solution. The reaction afforded one main species, observable by ^{31}P and ^1H NMR spectroscopy ($\delta(^{31}P)$ 185.4, $^2J_{PP}$ = 343 Hz, $^1J_{RhP}$ = 170 Hz; $\delta(^{31}P)$ 182.6, $^2J_{PP}$ = 343 Hz, $^1J_{RhP}$ = 166 Hz), which was assigned as the monoalkene axle species **Rh-32o** (Scheme 4.14).

Signals belonging to the axle in the ^{1}H NMR spectrum could be readily pinpointed in **Rh-32o** by comparison to the corresponding spectrum of **^{13}C-Rh-32o**, where splitting was observed for the central alkene signal ($^{1}J_{CH}$ = 149.2 Hz) and central alkyl signal ($^{1}J_{CH}$ = 113.2 Hz) (Figure 4.1). In addition, the ^{13}C{^{1}H} NMR spectrum

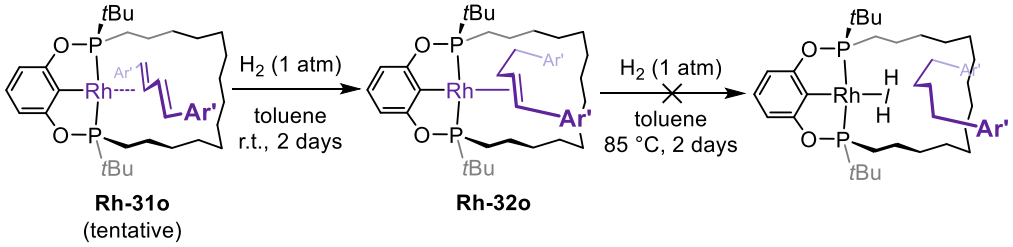

Scheme 4.14. Formation of **Rh-32o** and attempted hydrogenation thereof.

of **^{13}C-Rh-32o** shows two intense resonances congruent with a bound alkene (δ(^{13}C) 66.5, $^{1}J_{CC}$ = 40 Hz, $^{1}J_{RhC}$ = 9 Hz) and an adjacent alkyl (δ(^{13}C) 39.7, $^{1}J_{CC}$ = 40 Hz). Further heating under an atmosphere of H_2 up to 85 °C for 2 days did not result in further hydrogenation of the axle. As the (POCOP)Rh has previously been shown to promote rapid alkyl dehydrogenation (of the methylene chain, section 3.4), it is likely that if hydrogenation of the alkene did occur, it would be reversible and could not be detected.

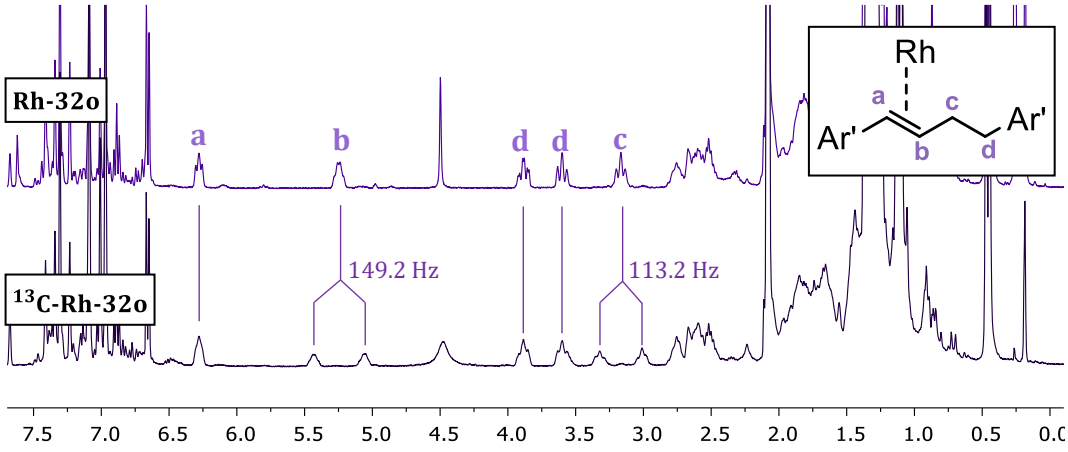

Figure 4.15. Stacked ^{1}H NMR spectra of **Rh-32o** (top) and **^{13}C-Rh-32o** (bottom) (400 MHz).

4.4. Decarbonylation of Ir-24o,c and Rh-24c

Following the detailed investigation of **Rh-25o**, attention turned to the application of the bis(alkynyl)carbonyl complex templating strategy to the three other systems in the series.

A solution of **Ir-24o** in fluorobenzene was treated with Me_3NO (10 eq). Heating the solution up to 120 °C for several hours did not show any sign of decarbonylation, leaving **Ir-24o** untouched (Scheme 4.15). However, in the ^1H NMR spectrum, thermal decomposition of Me_3NO was apparent by the slow formation of Me_3N. Alternatively, **Ir-24o** was placed under dynamic vacuum (2.10^{-3} mbar) and heated at temperatures up to 160 °C in attempt to promote the thermal dissociation of CO. Unfortunately, this resulted only in the formation of an intractable brown residue. Likewise, prolonged photolysis of **Ir-24o** in cyclohexane under UV only resulted in decomposition to unidentified products, as an off-white insoluble precipitate: the NMR spectra only showed a gradual decrease in intensity for the resonances of **Ir-24o**.

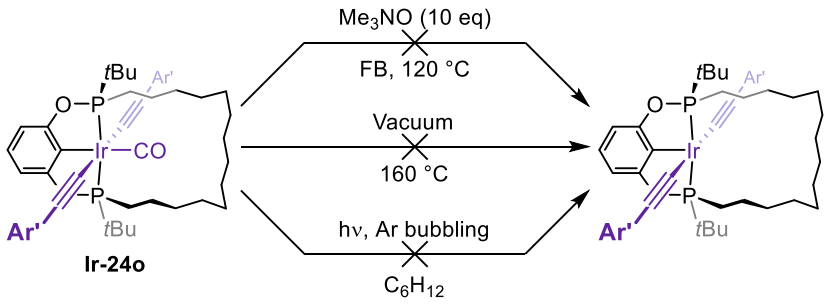

Scheme 4.15. Attempts to decarbonylate **Ir-24o**.

When applying the same methods to **Ir-24c**, similar outcomes resulted. Treatment with excess Me_3NO in fluorobenzene left **Ir-24c** untouched, as did prolonged photolysis under UV. These results can be rationalized by stronger CO binding in **Ir-24o,c**, compared to **Rh-24o** (*viz.* ν(CO) = 2040 cm^{-1}, **Ir-24o**; 2028 cm^{-1}, **Ir-24c**). More forcing conditions were applied to **Ir-24c**, namely by placing a sample under dynamic vacuum and heating at 200 °C for 3 h (Scheme 4.16). Surprisingly, an intensely purple product was observed to sublime up the flask walls. Analysis by ^{31}P NMR spectroscopy revealed a mixture composed of 93% starting material and 7% of a new C_2-symmetric species at δ 46.4. The C_2 symmetry of this product is

mirrored in the ^{1}H NMR spectrum, which also displays a new PC$\underline{H}_aH_b$ signal at δ 4.30 consistent with the alkynyl groups remaining in a similar position after the reaction, and was therefore assigned as **Ir-24c'**; a pentavalent bis(alkynyl) iridium complex.

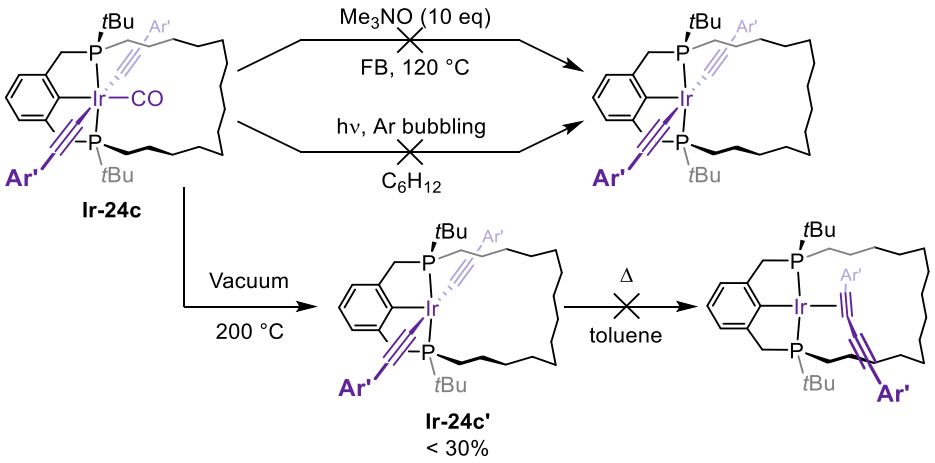

Scheme 4.16. Attempts at the decarbonylation of **Ir-24c**.

Additional heating for 18 h allowed for a *ca.* 30% yield of **Ir-24c'**, but higher conversion could not be achieved upon further heating. This observation is rationalized by the reaction of sublimed **Ir-24c'** with CO liberated from the bulk of the sample.

Time-dependent DFT calculations on a truncated model of **Ir-24c'** further supports its formulation: the theoretical UV spectrum exhibits a strong absorption band at 516 nm (unscaled) that is congruent with the very intense purple colour observed for experimentally (Figure 4.16). This absorption arises from a transition between a filled d_{xz} to a vacant d_{z2}, consistent with the splitting pattern expected for a square pyramidal coordination geometry.

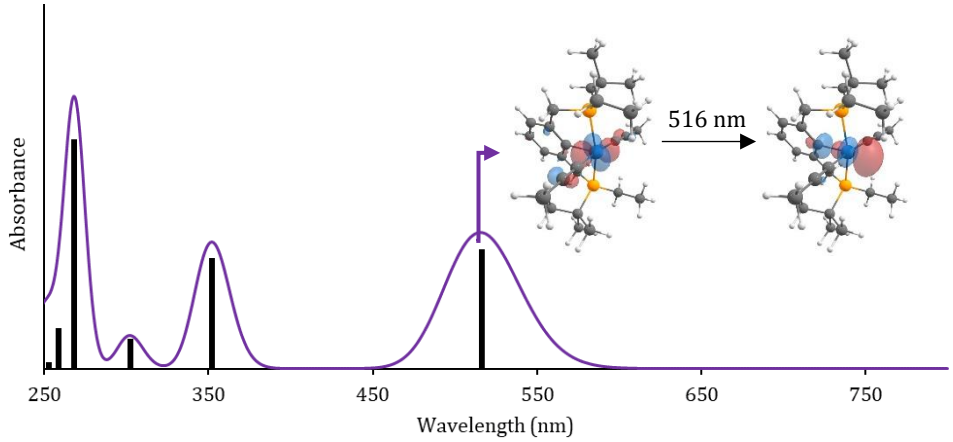

Figure 4.16. TD-DFT calculated spectrum of a truncated model of **Ir-24c'**.

Nonetheless, with a view to generating the diyne derivative, a mixture containing **Ir-24c'** in toluene was heated at reflux in attempt to induce reductive elimination. However, no reaction was observed on prolonged (24 h) heating. This result may be explained in reference to the work of Goldman *et. al*. in 2008,[19] which highlighted the importance of steric bulk in promoting reductive elimination reaction of bis(alkynyl) iridium complexes. As **PCP-14** is considerably less sterically imposing than the *t*Bu$_4$-PCP used in this study, the steric driving force for the reductive elimination is reduced. Moreover, DFT-based energy calculations were carried out at the ωB97x-D3/def2-TZVP// ωB97x-D3/def2-SV(P) level and showed the reductive elimination process to be slightly thermodynamically disfavoured for **Ir-24c'** (ΔH = +15.8 kJ/mol) and only marginally favoured for a hypothetical **Ir-24o'** (ΔH = -1.8 kJ/mol), with respect to the accuracy of the method.

Thus, attention turned to **Rh-24c**, a system more likely to manifest favourable thermodynamics for the reductive elimination to generate a diyne complex. A solution of **Rh-24c** in fluorobenzene was treated with the decarbonylating agent Me$_3$NO (20 eq) and heated at 85 °C. After 18 h, analysis by ^{31}P NMR spectroscopy revealed the presence of ca. 55% of starting material, 25% of a C_2-symmetric species (δ(^{31}P) 64.9, $^1J_{RhP}$ = 100 Hz) and 20% of an asymmetric species (δ(^{31}P) 78.5, $^2J_{PP}$ = 224 Hz, $^1J_{RhP}$ = 171 Hz; δ(^{31}P) 71.4, $^2J_{PP}$ = 224 Hz, $^1J_{RhP}$ = 171 Hz) with $^1J_{RhP}$ coupling constant congruent with an oxidation state of +I. The latter species were assigned as pentavalent **Rh-24c'** and diyne complex **Rh-25c**, respectively (Scheme 4.17). Further heating at 85 °C for 4 d was necessary to achieve complete conversion to **Rh-25c**.

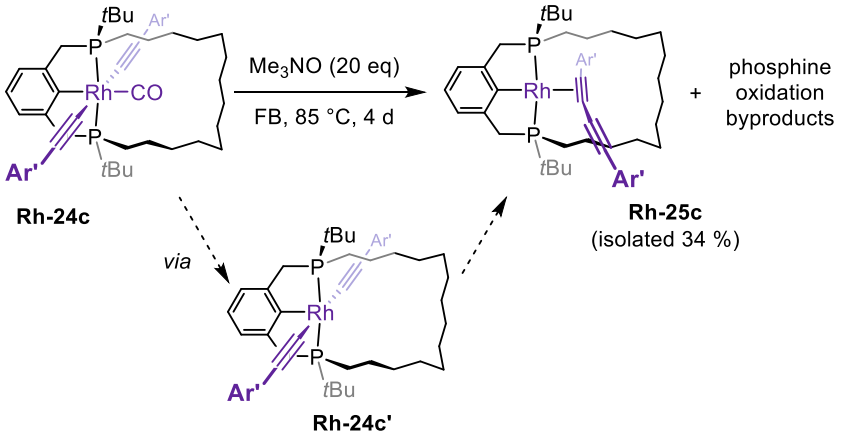

Scheme 4.17. Decarbonylation of **Rh-24c**.

This longer timescale suggests a higher activation barrier associated with decarbonylation, compared to its POCOP congener **Rh-24o**, in agreement with carbonyl stretching bands determined by ATR-IR spectroscopy (2053 cm^{-1}, **Rh-24c**; 2066 cm^{-1}, **Rh-24o**). Unfortunately, the conversion to **Rh-25c** was accompanied by the formation of byproducts, with several singlet ^{31}P resonances at δ 50-55, suggesting decomposition to phosphine oxide products. The prolonged heating and the large excess of Me_3NO are indeed likely to promote the oxidation of the phosphine donors upon decoordination, even more so with the phosphines in PCP scaffolds than with the electron deficient phosphinite moieties of the POCOP pincer. A short silica plug allowed the isolation of a >85% pure sample of **Rh-25c**, albeit with *ca.* 50% loss of material in the process. In stark contrast to the dynamic behaviour observed for **Rh-25o** in section 4.3.2, no evidence of shuttling motion was apparent by NMR spectroscopy (400 MHz) for **Rh-25c**, with two very distinct sets of Ar' groups are observed in the ^{1}H NMR spectrum (Figure 4.17); an asymmetry also reflected in the alkyl region of the spectrum with two singlets integrating to 18H each.

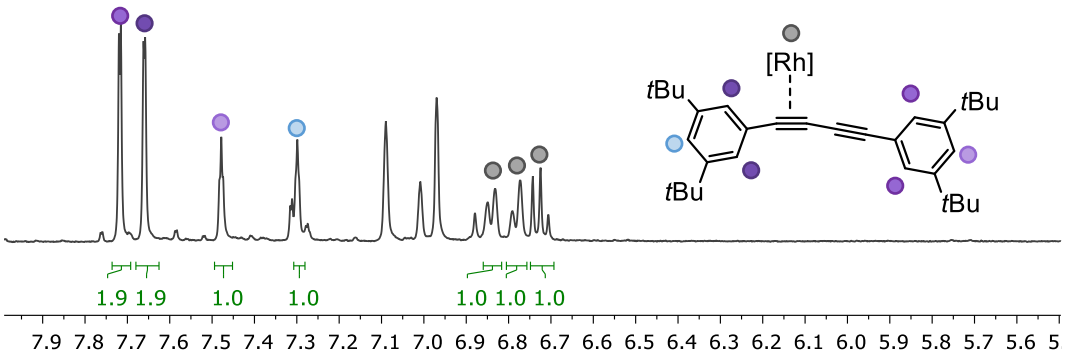

Figure 4.17. Aromatic region of the ^{1}H NMR spectrum of **Rh-25c** (toluene-d_8, 400 MHz).

As the (PCP)Rh system is more electron rich than its (POCOP)Rh counterpart, the absence of fluxionality could be rationalized by a stronger binding of the diyne to the Rh, by virtue of more pronounced π-backdonation. The ^{1}H NMR data points to free rotation of the Ar' substituents, suggesting significant differences in the steric characteristics of the coordination sphere of **Rh-25c** also compared to its POCOP analogue **Rh-25o**. Steric differences may be reconciled by the greater flexibility of the PCP backbone allowing the P*t*Bu groups to be twisted away from the diyne substituent.

In an effort to minimize the formation of phosphine oxide byproducts, the reaction was repeated and monitored by ^{31}P NMR spectroscopy until complete disappearance of **Rh-24c**, affording a mixture of only **Rh-24c'** and **Rh-25c** after ca. 36 h at 85 °C, in a 1:2 ratio. The mixture was subsequently extracted in hexane to remove Me_3NO, redissolved in fluorobenzene and heated at 85 °C. Unexpectedly, the 1:2 ratio observed before extraction was unchanged even after 48 h. This suggests that the reductive elimination from **Rh-24c'** has a high barrier and is promoted by Me_3NO in some manner. In agreement with its formulation, placing a sample containing **Rh-24c'** under an atmosphere CO resulted in its immediate conversion back to **Rh-24c**.

The reactivity of **Rh-25c** towards CO was investigated next. An immediate reaction was observed upon placing a solution of **Rh-25c** in toluene under an atmosphere of CO, as evidenced by a colour change from dark orange to yellow (Scheme 4.18). Analysis by ^{31}P NMR spectroscopy revealed the presence of two very broad signals centred at δ 78 and 0, with the latter resonance most consistent with free phosphine. By comparison to the chemistry of **Rh-28o**, this species was assigned to a diyne bis(carbonyl) rhodium complex, with the pincer bound in a κ^2 fashion. Freeze-pump-thaw degassing this sample allowed the regeneration of **Rh-25c**, albeit with weaker ^{1}H and ^{31}P signals which suggests partial decomposition. Heating a solution of **Rh-25c** under CO yielded an identical outcome, only with a more pronounced loss of starting material.

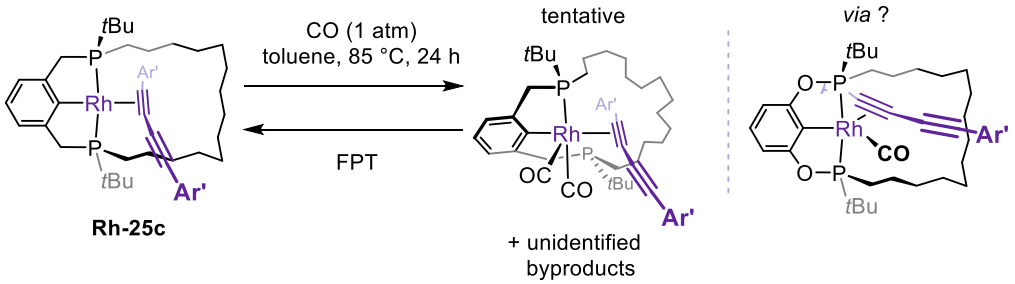

Scheme 4.18. Reaction of **Rh-25c** with CO.

Placing a toluene solution of **Rh-25c** under an atmosphere of H_2 did not yield any reaction at up to 50 °C. However, heating at 80 °C overnight resulted in dramatic decrease of the intensity of the ^{31}P resonances pertaining to **Rh-25c**, but no new signals were observed. The absence of 1,3-di-*tert*-butyl-5-ethylbenzene and hydridic resonances in the ^{1}H NMR spectrum strongly discredits the possibility of

C(sp)–C(sp) bond cleavage and subsequent hydrogenation. The intensity of the ^{1}H NMR signals also decreased, suggesting decomposition to insoluble species. It thus appears the C(sp)-C(sp) bond cleavage is unique to the Rh(POCOP) system and enabled by a unique combination of steric and electronic factors.

4.5. Towards a metallo-catenane

4.5.1. Transmetallation and RCM

Despite the limitations apparent from the work described above, extension of the transmetallation strategy to the preparation of catenanes was assessed.

Tridec-1-ene-12-yne was prepared using a literature procedure starting from 11-bromoundecene and lithium alkynyl in 75% yield (Scheme 4.19).[44] The transmetallation reaction was subsequently carried out on **Rh-19o**, and **Ir-19o,c,** under the conditions developed previously. Gratifyingly, the bis(alkynyl) carbonyl complexes **Rh-33o** and **Ir-33o,c** were all readily obtained in moderate to excellent yields, as evidenced by ^{31}P shifts similar to their Ar' analogues (δ(^{31}P) 188.4, $^{1}J_{RhP}$ = 94 Hz, **Rh-33o**; δ(^{31}P) 147.0, **Ir-33o**; δ(^{31}P) 37.3, **Ir-33c**) and the presence of terminal alkene resonances in the ^{1}H NMR spectra.

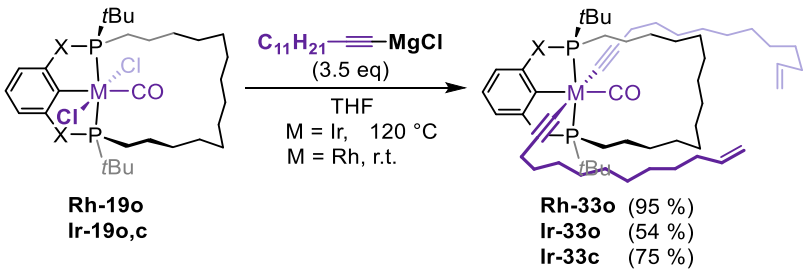

Scheme 4.19. Transmetallation reaction of **Rh-19o** and **Ir-19o,c** with a long alkenyl chain Grignard reagent.

Attention thereafter turned to identifying suitable reaction conditions for achieving the ring closing metathesis of the terminal alkenyl moieties. A step that was expected to be challenging, given the length of the alkyl chains, the absence of templation and the potential steric bulk imposed by the PXCXP scaffold, which may favour the formation of polymers rather than intramolecular RCM.[45] To minimize the risk for polymerisation, high dilution conditions were chosen (1 mM). With a view to obtaining a sufficient catalytic activity under these dilute conditions, Grubbs' second generation catalyst (5 mol%) was employed for its improved activity over the first generation variant.[46] In addition, DCM was swapped for fluorobenzene in order to further improve catalytic efficiency.[47] Gratifyingly, these conditions enabled complete conversion of **Rh-33o** and **Ir-**

33o,c to the pre-catenates **Rh-34o** and **Ir-34o,c**, in moderate to good yields after 24 h with periodic Ar bubbling (Scheme 4.20).

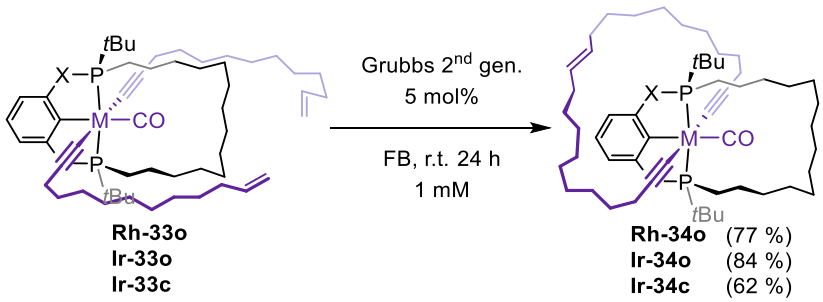

Scheme 4.20. Ring closing metathesis of **Rh-33o** and **Ir-33o,c**.

This outcome was evidenced by the complete disappearance of the terminal alkene peaks in the ^{1}H NMR spectra that are replaced by a single alkene resonance, and was corroborated by TLC monitoring, with the cyclised products markedly less polar than their corresponding starting material. Analysis by ^{31}P NMR spectroscopy showed near identical resonances to the starting materials **33**, thus confirming minimal changes in the first coordination sphere. Ultimately, the monomeric nature of these complexes was unambiguously verified by the determination of the solid-state structures for **Ir-34o,c** by X-ray diffraction (Figure 4.18).

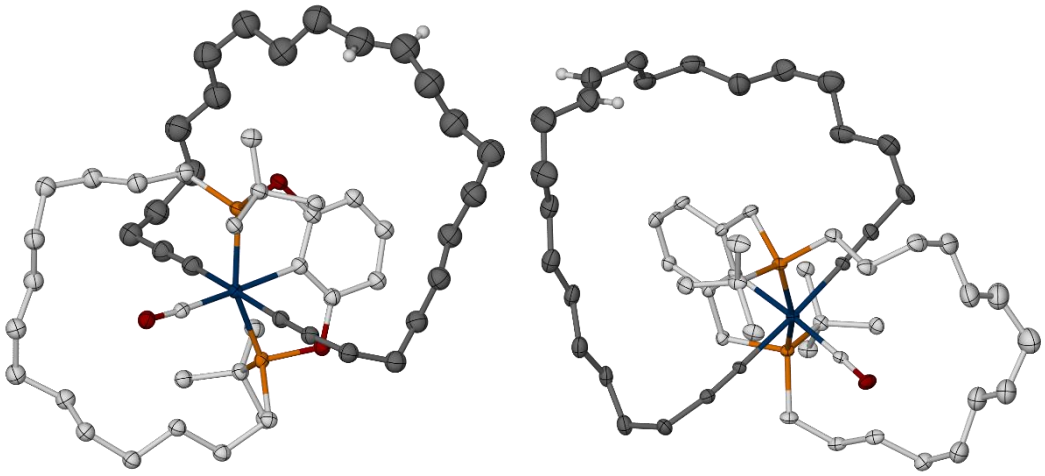

Figure 4.18. Solid-state structures for **Ir-34o** (not unique, *Z*'=2, left) and **Ir-34c** (right). Preliminary refinements. Thermal ellipsoids drawn at 30% probability; minor disordered components and hydrogen atoms omitted for clarity.

The structures of **Ir-34o,c** show the adoption of a distorted octahedral geometry, sharing the characteristics exhibited by the structure of their acyclic axle congener **M-24o,c**. Notably, the newly formed macrocycles are located at the back of the pincer scaffold, suggesting a lesser extent of steric buttressing than would be imposed by the alkyl tether. Whilst the solid-state structures show C_1-symmetry, the 2nd macrocycle is not locked in this position in solution as evidenced by time-averaged C_2-symmetry observed in the ^{31}P and ^{1}H NMR spectra, notably with equivalent 3,5-aromatic protons. This implies a high degree of conformational fluxionality, at the very least on the aromatic side of the pincer scaffold.

*4.5.2. Decarbonylation of **Ir-34o,c** and **Rh-34o***

The conditions for decarbonylation trialled in sections 4.3.1 and 4.4 were next trialled on complexes **Ir-34o,c** and **Rh-34o**.

Unsurprisingly, treatment of either Ir complexes with excess Me_3NO in fluorobenzene yielded no reaction, as was observed for their non macrocyclic counterparts. Likewise, attempts at decarbonylation by photolysis in alkanes (n-heptane, cyclohexane), with or without Ar bubbling, all failed to provide any product, only resulting in the slow decomposition of either substrates and the formation of an off-white precipitate. Thermolysis at elevated temperatures (180 – 200 °C) under dynamic vacuum only promoted decomposition to a brown residue in the case of **Ir-34o**. Thermolysis of its PCP analogue **Ir-34c** did display some reactivity, as evidenced by the formation of a distinctly intense pink compound, in low yield, tentatively assigned as **Ir-34c'** (Scheme 4.21). Both reactions were marred by a pronounced tendency for both **Ir-34c** and **Ir-34c'** to sublime at high temperature.

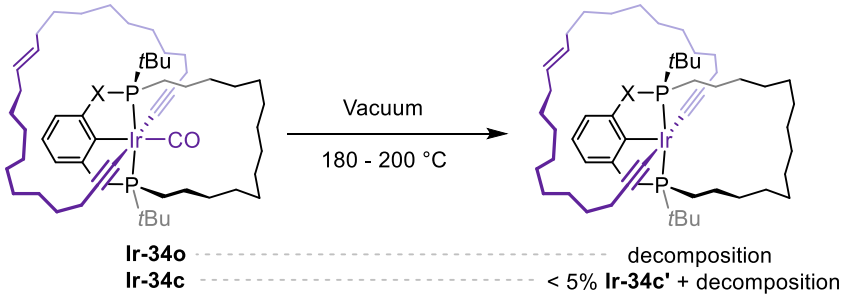

Scheme 4.21. Attempts to decarbonylate **Ir-34o,c**.

Complex **Rh-34o** was treated with Me_3NO in fluorobenzene at 85 °C, which appeared to promote the desired decarbonylation. The reaction proceeded on a longer timescale than its non-macrocyclic analogue, however, and it was found to benefit from a greater excess of Me_3NO (up to 20 eq) to achieve complete consumption of the starting material after 3 days. This observation suggests a greater extent of shielding of the carbonyl moiety by the second coordination sphere, even compared to the bulky Ar' groups. As a result of the forcing conditions, the formation of phosphine oxide byproducts could not be avoided as evidenced by the appearance a resonance at δ 63.0 in the $^{31}P\{^1H\}$ NMR spectrum. Surprisingly, formation of carbonyl complex **Rh-18o** was detected during the decarbonylation, alongside a very broad signal at δ 188–182. The latter signal was attributed to a reductive elimination product **Rh-35o**, featuring a coordinated allene, based on work by Findlater's group which shows the isomerisation of internal alkynes to allenes for (tBu$_4$-POCOP)Ir systems.[48] This hypothesis is supported by the presence of several alkene resonances in the ^1H NMR spectrum, although their exact assignment remains challenging.

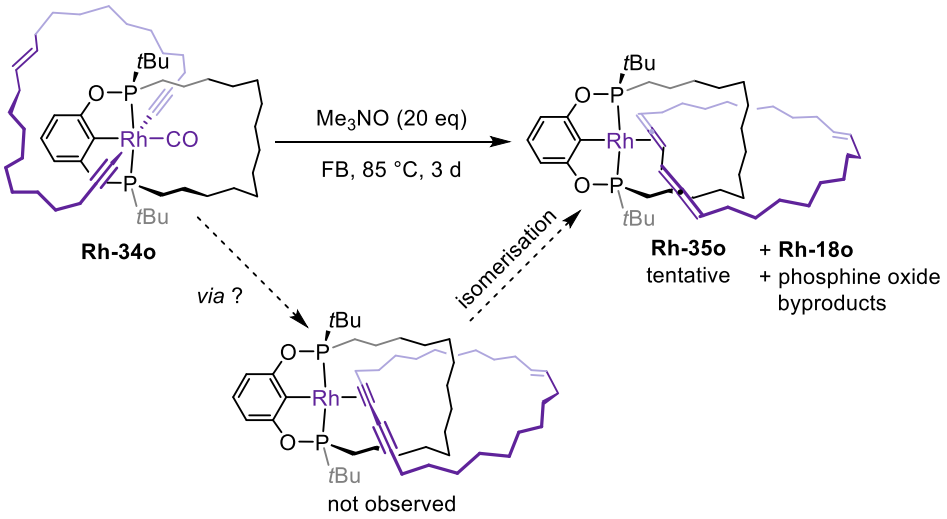

Scheme 4.22. Decarbonylation of **Rh-34o**.

The toluene-d_8 mixture containing **Rh-35o** was freeze-pump-thaw degassed and placed under an atmosphere of H_2. No reaction was apparent at room temperature overnight. Heating the mixture at 85 °C for 3 days resulted in the formation of a small amount of dihydrogen complex **Rh-15o** and a new C_2-symmetric species in the $^{31}P\{^1H\}$ NMR spectrum at δ 184.5 ($^1J_{RhP}$ = 169 Hz) accompanied by a collapse of the alkene signals to a single resonance at δ 4.63 (fwhm = 13 Hz) (Scheme 4.23).

These characteristics are consistent with the formation of a monoalkene complex likely incorporated in the ring, and this final compound was assigned as the (*E*)-cyclotetracosene complex **Rh-36o**, but only represented *ca.* 25 % of the reaction mixture. Further work would, however, be required to verify this result and unequivocally determine its structure. Its C_2-symmetry, ^{31}P shift, $^1J_{RhP}$ coupling constant and reactivity towards H_2 are highly reminiscent of the alkene complex **Rh-32o**. Within the timeframe of this project, this was unfortunately not possible. Any future work would require extensive optimisation of the reaction conditions and possibly purification by chromatography to obtain suitably pure samples of **Rh-32o**. Nevertheless, this result suggests it is in principle possible to form an interlocked hydrocarbon ring.

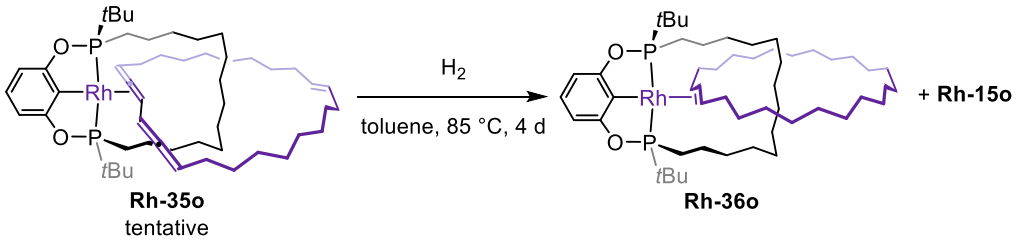

Scheme 4.23. Hydrogenation of **Rh-35o**.

4.6. References

[1] P. Eilbracht, P. Dahler, *J. Organomet. Chem.* **1977**, *135*, C23–C25.
[2] R. H. Crabtree, *Chem. Rev.* **1985**, *85*, 245–269.
[3] W. D. Jones, *Nature* **1993**, *364*, 676–677.
[4] B. Rybtchinski, D. Milstein, *Angew. Chem. Int. Ed.* **1999**, *38*, 870–883.
[5] L. Souillart, N. Cramer, *Chem. Rev.* **2015**, *115*, 9410–9464.
[6] F. Song, T. Gou, B.-Q. Wang, Z.-J. Shi, *Chem. Soc. Rev.* **2018**, *47*, 7078–7115.
[7] F. Chen, T. Wang, N. Jiao, *Chem. Rev.* **2014**, *114*, 8613–8661.
[8] K. Ruhland, *Eur. J. Org. Chem.* **2012**, *2012*, 2683–2706.
[9] B. G. Harvey, R. D. Ernst, *Eur. J. Inorg. Chem.* **2017**, *2017*, 1205–1226.
[10] S. C. Bart, P. J. Chirik, *J. Am. Chem. Soc.* **2003**, *125*, 886–887.
[11] T. Matsuda, T. Tsuboi, M. Murakami, *J. Am. Chem. Soc.* **2007**, *129*, 12596–12597.
[12] M. Murakami, H. Amii, Y. Ito, *Nature* **1994**, *370*, 540–541.
[13] D. A. Laviska, C. Guan, T. J. Emge, M. Wilklow-Marnell, W. W. Brennessel, W. D. Jones, K. Krogh-Jespersen, A. S. Goldman, *Dalton Trans* **2014**, *43*, 16354–16365.
[14] M. Wilklow-Marnell, W. W. Brennessel, W. D. Jones, *Polyhedron* **2016**, *116*, 38–46.
[15] M. A. Halcrow, F. Urbanos, B. Chaudret, *Organometallics* **1993**, *12*, 955–957.
[16] J. William Suggs, S. D. Cox, *J. Organomet. Chem.* **1981**, *221*, 199–201.
[17] M. Gozin, A. Weisman, Y. Ben-David, D. Milstein, *Nature* **1993**, *364*, 699–701.
[18] R. Ghosh, X. Zhang, P. Achord, T. J. Emge, K. Krogh-Jespersen, A. S. Goldman, *J. Am. Chem. Soc.* **2007**, *129*, 853–866.
[19] R. Ghosh, T. J. Emge, K. Krogh-Jespersen, A. S. Goldman, *J. Am. Chem. Soc.* **2008**, *130*, 11317–11327.
[20] "BDEs of C–C bonds | Comprehensive Handbook of Chemical Bond Energies | Taylor & Francis Group," can be found under https://www.taylorfrancis.com/, **n.d.**
[21] A. J. Deeming, M. S. B. Felix, P. A. Bates, M. B. Hursthouse, *J. Chem. Soc. Chem. Commun.* **1987**, *0*, 461–463.
[22] A. J. Deeming, M. S. B. Felix, D. Nuel, *Inorg Chim Acta* **1993**, *213*, 3–10.
[23] R. D. Adams, B. Qu, M. D. Smith, T. A. Albright, *Organometallics* **2002**, *21*, 2970–2978.
[24] R. V. Chedia, F. M. Dolgushin, A. F. Smol'yakov, O. I. Lekashvili, T. V. Kakulia, L. K. Janiashvili, A. M. Sheloumov, M. G. Ezernitskaya, S. M. Peregudova, P. V. Petrovskii, A. A. Koridze, *Inorg Chim Acta* **2011**, *378*, 264–268.
[25] U. Rosenthal, H. Görls, *J. Organomet. Chem.* **1992**, *439*, C36–C41.
[26] V. V. Burlakov, A. Ohff, C. Lefeber, A. Tillack, W. Baumann, R. Kempe, U. Rosenthal, *Chem. Ber.* **1995**, *128*, 967–971.
[27] P.-M. Pellny, V. V. Burlakov, W. Baumann, A. Spannenberg, R. Kempe, U. Rosenthal, *Organometallics* **1999**, *18*, 2906–2909.
[28] R. D. Dewhurst, A. F. Hill, A. D. Rae, A. C. Willis, *Organometallics* **2005**, *24*, 4703–4706.
[29] P. J. Low, M. I. Bruce, in *Adv. Organomet. Chem.*, Elsevier, **2001**, pp. 71–288.
[30] A. F. Hill, A. D. Rae, M. Schultz, A. C. Willis, *Organometallics* **2007**, *26*, 1325–1338.
[31] C. Müller, C. N. Iverson, R. J. Lachicotte, W. D. Jones, *J. Am. Chem. Soc.* **2001**, *123*, 9718–9719.
[32] A. Gunay, C. Müller, R. J. Lachicotte, W. W. Brennessel, W. D. Jones, *Organometallics* **2009**, *28*, 6524–6530.
[33] A. Gunay, W. D. Jones, *J. Am. Chem. Soc.* **2007**, *129*, 8729–8735.
[34] *Coord. Chem. Rev.* **1984**, *53*, 227–259.
[35] S. A. Hauser, J. Emerson-King, S. Habershon, A. B. Chaplin, *Chem. Commun.* **2017**, *53*, 3634–3636.
[36] *Coord. Chem. Rev.* **1984**, *60*, 255–276.
[37] K. Kamieńska-Trela, J. Wójcik, in *Sci. Technol. At. Mol. Condens. Matter Biol. Syst.*, Elsevier, **2013**, pp. 347–424.
[38] H. L. M. van Gaal, M. W. M. Graef, A. van der Ent, *J. Organomet. Chem.* **1977**, *131*, 453–465.
[39] C. Bannwarth, S. Ehlert, S. Grimme, *J. Chem. Theory Comput.* **2019**, *15*, 1652–1671.
[40] S. Grimme, J. Antony, S. Ehrlich, H. Krieg, *J. Chem. Phys.* **2010**, *132*, 154104.
[41] F. Weigend, R. Ahlrichs, *Phys. Chem. Chem. Phys.* **2005**, *7*, 3297–3305.
[42] F. Weigend, *Phys. Chem. Chem. Phys.* **2006**, *8*, 1057–1065.
[43] Y.-S. Lin, G.-D. Li, S.-P. Mao, J.-D. Chai, *J. Chem. Theory Comput.* **2013**, *9*, 263–272.

[44] S.-Y. Chen, M. M. Joullié, *Synth. Commun.* **1984**, *14*, 591–597.
[45] S. Monfette, D. E. Fogg, in *Green Metathesis Chem.* (Eds.: V. Dragutan, A. Demonceau, I. Dragutan, E.Sh. Finkelshtein), Springer Netherlands, Dordrecht, **2010**, pp. 129–156.
[46] M. Scholl, S. Ding, C. W. Lee, R. H. Grubbs, *Org. Lett.* **1999**, *1*, 953–956.
[47] C. Samojłowicz, M. Bieniek, A. Pazio, A. Makal, K. Woźniak, A. Poater, L. Cavallo, J. Wójcik, K. Zdanowski, K. Grela, *Chem. - Eur. J.* **2011**, *17*, 12981–12993.
[48] N. Phadke, M. Findlater, *Organometallics* **2014**, *33*, 16–18.

Chapter 5

Experimental procedures

General considerations

All manipulations were performed under an atmosphere of argon using Schlenk and glove box techniques unless otherwise stated. Hydrogen was dried by passage through a stainless-steel column of activated 3 Å molecular sieves. Carbon monoxide was used as received. Glassware was oven dried at 150 °C overnight and flame-dried under vacuum prior to use. Molecular sieves were activated by heating at 300 °C *in vacuo* overnight. CD_2Cl_2 was freeze-pump-thaw degassed and dried over 3 Å molecular sieves. Toluene-d_8 and C_6D_6 were dried over sodium overnight, distilled, freeze-pump-thaw degassed and stored over 3 Å molecular sieves. CD_2Cl_2 was freeze-pump-thaw degassed and dried over 3 Å molecular sieves. THF was distilled from sodium and benzophenone and stored over 3 Å molecular sieves. Et_2NH was distilled from CaH_2. Fluorobenzene and 1,2-DiFB were pre-dried over Al_2O_3, distilled from calcium hydride and dried twice over 3 Å molecular sieves. *Tert*-butylethylene was freeze-pump-thaw degassed and stored over 3 Å molecular sieves. $SiMe_4$ and HMDSO were distilled from liquid Na/K alloy and stored over a potassium mirror. Neohexane (2,2-dimethylbutane) was distilled from liquid Na/K alloy and stored over 3 Å molecular sieves. EtOH was sparged with argon for 2 hours before drying over two successive batches of molecular sieves and stored under an argon atmosphere. Other anhydrous solvents were purchased from Acros Organics or Sigma-Aldrich, freeze-pump-thaw degassed and stored over 3 Å molecular sieves. The concentration of *n*BuLi was titrated by ^{1}H NMR spectroscopy before use.[1] Oxazaphospholidine **7**,[2–4] $MgBr(C_8H_{15})$,[5] **1** and **2**,[6] $PhICl_2$,[7] $[Rh(PPh_3)_3Cl]$,[8] $[Rh(COE)_2Cl]_2$,[9] $[Ir(COD)Cl]_2$,[10] $[Ir(COE)_2Cl]_2$,[10] [M(pincer)(CO)] (M = Rh, Ir; pincer = *t*Bu$_4$-PCP, *t*Bu$_4$-POCOP),[11–15] $[H(OEt_2)_2][BAr^F{}_4]$,[16] 3,5-bis(tert-butyl)phenylacetylene,[17] 1,4-bis(3,5-di-tert-butylphenyl)buta-1,3-diyne,[18] Ar'C^{13}CH[19] were synthesised according to published procedures. NMR spectra were recorded on Bruker spectrometers under argon at 298 K unless otherwise stated. Chemical shifts are quoted in ppm and coupling constants in Hz.[20] NMR spectra in toluene-d_0 were recorded using an internal capillary of C_6D_6. HR ESI-MS were recorded on a Bruker

MaXis mass spectrometer and LR ESI-MS were collected using an Agilent 6130B single Quad mass spectrometer. IR spectra were recorded on a Bruker Alpha Platinum ATR FT-IR spectrometer at RT (for full details see ESI). Microanalyses were performed at the London Metropolitan University by Stephen Boyer in all cases, except for samples of **M-18o,c** and which were analysed by Elemental Microanalysis Ltd. In particular, microanalyses were carried out to complete existing data for published compounds or soon-to-be published, when NMR purity upon isolation was deemed satisfactory.

5.1. Chapter 2

*5.1.1. Racemic synthesis of **POCOP-14'***

Preparation of **3**

A solution of resorcinol (3.53 g, 32.1 mmol) in THF (10 mL) was added to a suspension of NaH (1.62 g, 67.3 mmol) in THF (10 mL). The resulting suspension was heated at reflux for 1 h, allowed to cool to RT and a solution of **8** (16.6 g, 70.5 mmol) in THF (10 mL) added. The reaction mixture was then heated at reflux for a further 1 h. Volatiles were removed *in vacuo* and the residue extracted with hexane (3 x 10 mL) to afford **9** (1:1 mixture of diastereoisomers) as a colourless oil on drying. Yield: 16.1 g (95%).

^{1}H NMR (300 MHz, C_6D_6): δ 7.43 (s, 1H, Ar{2-CH}), 7.04 (t, $^{3}J_{HH}$ = 8.0, 1H, Ar), 6.95 (d, $^{3}J_{HH}$ = 8.4, 2H, Ar), 5.76 (ddt, $^{3}J_{HH}$ = 16.8, 11.8, 6.7, 2H, C<u>H</u>=CH_2), 4.95 – 5.10 (m, 4H, CH=C<u>H</u>$_2$), 1.95 (app q, $^{3}J_{HH}$ = 7, 4H, C<u>H</u>$_2$CH=CH_2), 1.75 – 1.90 (m, 2H, CH_2), 1.61 (app sex, J = 8, 4H, CH_2), 1.15 – 1.40 (m, 14H, CH_2), 1.04 (d, $^{3}J_{PH}$ = 12.0, 18H, *t*Bu).

^{13}C{^{1}H} NMR (75 MHz, C_6D_6): δ 161.0 (d, $^{2}J_{PH}$ = 9.0, Ar{C}), 139.2 (s, <u>C</u>H=CH_2), 130.2 (s, Ar), 114.6 (s, CH=<u>C</u>H$_2$), 112.4 (d, $^{3}J_{PH}$ = 11, Ar), 109.6 (t, $^{3}J_{PH}$ = 12, Ar{2-CH}), 34.2 (s, <u>C</u>H$_2$CH=CH), 32.7 (d, $^{1}J_{PH}$ =16, *t*Bu{C}), 31.5 (d, $^{2}J_{PH}$ = 12, CH_2), 29.3 (s, CH_2), 29.2 (s, CH_2), 29.2 (d, $^{1}J_{PH}$ = 24, PCH_2), 25.9 (d, $^{3}J_{PH}$ = 16, CH_2), 25.4 (d, $^{2}J_{PH}$ = 16, *t*Bu{CH_3}).

^{31}P{^{1}H} NMR (121 MHz, C_6D_6): δ 142.40 (s, 1P), 142.36 (s, 1P).

HR ESI-MS (positive ion, 4 kV): 561.3231, [M+2O+Na]$^{+}$ (calcd 561.3233) *m/z*.

Preparation of **3•S$_2$**

A solution of **3** (955 mg, 1.88 mmol) in THF (5 mL) was added to a suspension of S_8 (133 mg, 4.15 mmol) in THF (2 mL). The reaction mixture was stirred overnight at room temperature and volatiles were removed *in vacuo* to afford the crude material as a brown oil. Purification by flash column chromatography in air (silica, 2% EtOAc in hexane, R_f = 0.15) afforded **3•S$_2$** as a colourless oil. Yield 711 mg (66%).

^{1}H NMR (300 MHz, $CDCl_3$): δ 7.22 (t, $^3J_{HH}$ = 7.9, 1H, Ar), 7.11 (s, 1H, Ar), 6.97 (t, $^3J_{HH}$ = 7.9, 2H, Ar), 5.78 (m, 2H, C$\underline{H}$=CH$_2$), 4.99 (m, 4H, CH=C$\underline{H_2}$), 2.25 – 2.07 (m, 2H, C$\underline{H_2}$CH=CH$_2$), 2.07 – 1.89 (m, 6H, CH$_2$), 1.89 – 1.69 (m, 2H, CH$_2$), 1.69 – 1.48 (m, 2H, CH$_2$), 1.48 – 1.25 (m, 12H, CH$_2$), 1.33 (d, $^3J_{PH}$ = 17.1, 18H, *t*Bu).

^{31}P{^{1}H} NMR (121 MHz, $CDCl_3$): δ 118.83 (s, diastereomer 1) 118.77 (s, diastereomer 2).

Preparation of **4**

BH_3·SMe_2 (4.63 g, 5.78 mL, 61.0 mmol) was added dropwise to a stirred solution of **3** (15.4 g, 30.5 mmol) in THF (50 mL) at -78 °C. The reaction mixture was warmed to RT overnight and volatiles removed *in vacuo* to afford the crude material as an opaque colourless oil. Purification by flash column chromatography in air (silica, 8% EtOAc in hexane, R_f = 0.41) afforded **4** (1:1 mixture of diastereoisomers) as a colourless oil. Yield: 12.9 g (79%).

^{1}H NMR (600 MHz, $CDCl_3$): δ 7.19 (t, $^3J_{HH}$ = 8.2, 1H, Ar), 6.99 (app q, J = 2, 1H, Ar{2-CH}), 6.90 (app dt, $^3J_{HH}$ = 8.4, J = 2, 2H, Ar), 5.79 (app ddt, $^3J_{HH}$ = 16.9, 10.1, 6.7, 2H, C$\underline{H}$=CH$_2$), 4.99 (app dq, $^3J_{HH}$ = 17.0, J_{HH} = 2, 2H, CH=C$\underline{H_2}$), 4.93 (app dq, $^3J_{HH}$ = 10.2, J_{HH} = 2, 2H, CH=C$\underline{H_2}$), 2.04 (app q, $^3J_{HH}$ = 7, 4H, C$\underline{H_2}$CH=CH$_2$), 1.92 – 2.01 (m, 2H, PCH$_2$), 1.68 – 1.79 (m, 4H, CH$_2$), 1.55 – 1.65 (m, 2H, CH$_2$), 1.28 – 1.44 (m, 12H, CH$_2$), 1.26 (d, $^3J_{PH}$ = 14.0, 18H, *t*Bu), 0.53 (partially collapsed quartet, fwhm = 300 Hz, 6H, BH_3).

^{13}C{^{1}H} NMR (151 MHz, $CDCl_3$): δ 154.2 (d, $^2J_{PC}$ = 6, Ar{C}), 139.1 (s, $\underline{C}$H=CH$_2$), 129.6 (s, Ar), 117.0 (d, $^3J_{PC}$ = 3, Ar), 114.5 (s, CH=$\underline{C}$H$_2$), 114.1 (t, $^3J_{PC}$ = 3.0, Ar{2-CH}), 33.8 (s, $\underline{C}$H$_2$CH=CH$_2$), 32.9 (d, $^1J_{PC}$ = 37, *t*Bu{C}), 31.4 (d, $^2J_{PC}$ = 13.0, CH$_2$), 28.9

(d, $^4J_{PC}$ = 3, CH_2), 28.7 (s, CH_2), 25.4 (d, $^1J_{PC}$ = 33, PCH_2), 24.9 (d, $^2J_{PC}$ = 3, *t*Bu{CH_3}), 22.8 (s, CH_2).

$^{31}P\{^1H\}$ NMR (121 MHz, $CDCl_3$): δ 143.7 (partially collapsed quartet, fwhm = 165 Hz).

HR ESI-MS (positive ion, 4 kV): 557.4000, [*M*+Na]$^+$ (calcd 557.4001) *m/z*.

Preparation of **5**

A solution of [$Ru(PCy_3)_2Cl_2(CHPh)$] (36.0 mg, 43.7 μmol, 2.5 mol%) in CH_2Cl_2 (3 mL) was added at RT to a solution of **4** (930 mg, 1.74 mmol) in CH_2Cl_2 (350 mL, 5 mmol L^{-1}). The solution was stirred at RT with periodic (every 12 h) argon sparging (ca. 10 min) for 2 days. Volatiles were removed *in vacuo* and the crude mixture was purified by flash column chromatography in air (silica, 10% EtOAc in hexane, R_f = 0.40) to afford **5** (1:1 mixture of diastereoisomers) as a colourless oil. Yield: 832 mg (94%).

^1H NMR (500 MHz, $CDCl_3$): δ 7.20 (t, $^3J_{HH}$ = 8.3, 0.5H, Ar syn), 7.19 (t, $^3J_{HH}$ = 8.3, 0.5H, Ar anti), 7.03 (dd, $^3J_{HH}$ = 8.3, $^4J_{HH}$ = 2.4, 1H, Ar syn), 6.97 (t, $^4J_{HH}$ = 2.3, 0.5H, Ar{2-CH} anti), 6.89 (dd, $^3J_{HH}$ = 8.3, $^4J_{HH}$ = 2.3, 1H, Ar anti), 6.74 (t, $^4J_{HH}$ = 2.4, 0.5H, Ar{2-CH} syn), 5.26 – 5.36 (m, 2H, CH=CH), 1.93 – 2.10 (m, 6H, CH_2), 1.61 – 1.81 (m, 4H, CH_2), 1.24 – 1.60 (m, 14H, CH_2), 1.27 (d, $^3J_{PH}$ = 14.0, 18H, *t*Bu), 0.55 (partially collapsed quartet, fwhm = 300 Hz, 6H, BH_3).

$^{13}C\{^1H\}$ NMR (126 MHz, $CDCl_3$): δ 154.4 (d, $^2J_{PC}$ = 6, Ar{C} syn), 154.1 (d, $^2J_{PC}$ = 6, Ar{C} anti), 130.9 (s, CH=CH anti), 130.8 (s, CH=CH syn), 129.7 (s, Ar syn), 129.5 (s, Ar anti), 117.0 (d, $^3J_{PC}$ = 4, Ar anti), 116.4 (d, $^3J_{PC}$ = 3, Ar syn), 114.4 (t, $^3J_{PC}$ = 3, Ar{2-CH} anti), 113.3 (t, $^3J_{PC}$ = 4, Ar{2-CH} syn), 32.8 (d, $^1J_{PC}$ = 37, *t*Bu{C} syn), 32.7 (d, $^1J_{PC}$ = 38, *t*Bu{C} anti), 32.10 (s, $\underline{C}H_2CH$=CH anti), 32.06 (s, $\underline{C}H_2CH$=CH syn), 31.6 (d, $^2J_{PC}$ = 13, CH_2 anti), 31.2 (d, $^2J_{PC}$ = 13, CH_2 syn), 28.8 (s, CH_2 anti), 28.7 (s, CH_2 syn), 28.1 (s, CH_2 anti), 27.9 (s, CH_2 syn), 25.5 (d, $^1J_{PC}$ = 33, PCH_2 syn), 25.4 (d, $^1J_{PC}$ = 33, PCH_2 anti), 24.9 (d, $^2J_{PC}$ = 3, *t*Bu{CH_3} syn), 24.8 (d, $^2J_{PC}$ = 3, *t*Bu{CH_3} anti), 23.0 (d, $^3J_{PC}$ = 2, CH_2 anti), 22.7 (d, $^3J_{PC}$ = 2, CH_2 syn). Data for major alkene isomer only.

$^{31}P\{^1H\}$ NMR (162 MHz, $CDCl_3$): δ 142.0 – 144.6 (br m).

HR ESI-MS (positive ion, 4 kV): 529.3689, [*M*+Na]$^+$ (calcd 529.3687) *m/z*.

Preparation of **6**

A suspension of [Rh(PPh$_3$)$_3$Cl] (201 mg, 220 μmol, 5 mol%) in benzene (20 mL) was added to a stirred solution of **5** (2.20 g, 4.34 mmol) in benzene. The suspension was freeze-pump-thaw degassed and placed under a hydrogen atmosphere and the resulting solution stirred at 50 °C for 2 days. Volatiles were removed under reduced pressure and the crude mixture was eluted through a short silica plug in air (5% EtOAc in hexane) to afford **6** as a mixture of diastereomers (2.02 g, 3.97 mmol, 92%). Subsequent purification by repeated flash column chromatography in air (silica, 5% EtOAc in hexane) enabled separation of the *syn*- and *anti*-diastereomers.

POCOP-14'·2BH$_3$ (***anti*-6**, R_f = 0.45). Yield: 951 mg (43%, colourless oil which slowly crystallised upon standing).

^{1}H NMR (600 MHz, $CDCl_3$): δ 7.19 (t, $^3J_{HH}$ = 8.2, 1H, Ar), 7.03 (t, $^4J_{HH}$ = 2.5, 1H, Ar{2-CH}), 6.93 (dd, $^3J_{HH}$ = 8.2, $^4J_{HH}$ = 2.5, 2H, Ar), 1.94 – 2.04 (m, 2H, PCH_2), 1.67 – 1.76 (m, 4H, CH_2), 1.50 – 1.61 (m, 2H, CH_2), 1.36 – 1.44 (m, 4H, CH_2), 1.22 – 1.34 (m, 16H, CH_2), 1.26 (d, $^3J_{PH}$ = 13.8, 18H, *t*Bu), 0.58 (partially collapsed quartet, fwhm = 300 Hz, 6H, BH_3).

^{13}C{^{1}H} NMR (151 MHz, $CDCl_3$): δ 154.2 (d, $^2J_{PC}$ = 6, Ar{C}), 129.6 (s, Ar), 116.9 (d, $^3J_{PC}$ = 3, Ar), 114.1 (t, $^3J_{PC}$ = 3, Ar{2-CH}), 32.8 (d, $^1J_{PC}$ = 37, *t*Bu{C}), 30.7 (d, $^2J_{PC}$ = 12, CH_2), 28.1 (s, CH_2), 28.0 (s, CH_2), 27.6 (s, CH_2), 27.5 (s, CH_2), 25.1 (d, $^1J_{PC}$ = 33, PCH_2), 24.8 (d, $^3J_{PC}$ = 3, *t*Bu{CH_3}), 22.3 (s, CH_2).

^{31}P{^{1}H} NMR (243 MHz, $CDCl_3$): δ 143.8 (partially collapsed quartet, fwhm = 165 Hz).

HR ESI-MS (positive ion, 4 kV): 531.3840, $[M+Na]^+$ (calcd 531.3844) *m/z*.

Anal. Calcd for $C_{28}H_{56}B_2O_2P_2$ (508.32 g.mol^{-1}): C, 66.16; H, 11.10; Found: C, 66.09; H, 11.26.

***syn*-6** (R_f = 0.42). Yield: 984 mg (45%, white crystalline solid).

^{1}H NMR (500 MHz, $CDCl_3$): δ 7.20 (t, $^3J_{HH}$ = 8.3, 1H, Ar), 7.03 (dd, $^3J_{HH}$ = 8.3, $^4J_{HH}$ = 2.3, 2H, Ar), 6.82 (t, $^4J_{HH}$ = 2.5, 1H, Ar{2-CH}), 1.90 – 2.06 (m, 2H, PCH_2), 1.67 – 1.81 (m, 4H, CH_2), 1.53 – 1.66 (m, 2H, CH_2), 1.20 – 1.50 (m, 20H, CH_2), 1.26 (d, $^3J_{PH}$ = 14.0, 18H, *t*Bu), 0.61 (partially collapsed quartet, fwhm = 285 Hz, 6H, BH_3).

^{13}C{^{1}H} NMR (126 MHz, $CDCl_3$): δ 154.4 (d, $^{2}J_{PC}$ = 6, Ar{C}), 129.7 (s, Ar), 116.6 (d, $^{3}J_{PC}$ = 3, Ar), 113.4 (t, $^{3}J_{PC}$ = 4, Ar{2-CH}), 32.9 (d, $^{1}J_{PC}$ = 37, *t*Bu{C}), 30.5 (d, $^{2}J_{PC}$ = 12, CH_2), 28.2 (s, CH_2), 27.9 (s, CH_2), 27.8 (s, CH_2), 27.6 (s, CH_2), 25.2 (d, $^{1}J_{PC}$ = 33, PCH_2), 24.9 (d, $^{3}J_{PC}$ = 3, *t*Bu{CH_3}), 22.0 (d, $^{3}J_{PC}$ = 2, CH_2).

^{31}P{^{1}H} NMR (162 MHz, $CDCl_3$): δ 143.7 (br, fwhm = 175 Hz).

HR ESI-MS (positive ion, 4 kV): 531.3840, $[M+Na]^+$ (calcd 557.3844) *m/z*.

Anal. Calcd for $C_{28}H_{56}B_2O_2P_2$ (508.32 g.mol^{-1}): C, 66.16; H, 11.10; Found: C, 66.09; H, 11.26.

Preparation of **POCOP-14'**

A solution of ***anti*-6** (231 mg, 455 µmol) in Et_2NH (7 mL) was heated at 60 °C for 2 days. Volatiles were removed *in vacuo* to afford **POCOP-14'** as a colourless oil. Yield: 217 mg (>99%).

^{1}H NMR (500 MHz, toluene-d_8): δ 7.30 (app p, J = 2, 1H, Ar{2-CH}), 6.97 (t, $^{3}J_{HH}$ = 8.1, 1H, Ar), 6.87 (app dt, $^{3}J_{HH}$ = 8.2, J = 2, 2H, Ar), 1.84 (dtd, $^{2}J_{HH}$ = 14.4, $^{3}J_{HH}$ = 7.3, $^{2}J_{PH}$ = 3.2, 2H, PCH_2), 1.54 – 1.67 (m, 4H, CH_2), 1.15 – 1.50 (m, 22H, CH_2), 1.00 (d, $^{3}J_{PH}$ = 12.1, 18H, *t*Bu).

^{13}C{^{1}H} NMR (126 MHz, toluene-d_8): δ 160.9 (d, $^{2}J_{PC}$ = 9, Ar{C}), 129.9 (s, Ar), 112.2 (d, $^{3}J_{PC}$ = 11, Ar), 109.2 (t, $^{3}J_{PC}$ = 12, Ar{2-CH}), 32.5 (d, $^{1}J_{PC}$ = 16, *t*Bu{C}), 31.1 (d, $^{2}J_{PC}$ = 11, CH_2), 29.0 (d, $^{1}J_{PC}$ = 24, PCH_2), 28.9 (s, CH_2), 28.5 (s, CH_2), 28.2 (s, CH_2), 28.0 (s, CH_2), 25.5 (d, $^{3}J_{PC}$ = 15, CH_2), 25.3 (d, $^{2}J_{PC}$ = 15, *t*Bu{CH_3}).

^{31}P{^{1}H} NMR (162 MHz, toluene-d_8): δ 141.6 (s).

Preparation of the *syn*- diastereomer of **POCOP-14'**

A solution of *cis*-**6** (10.0 mg, 19.7 µmol) in Et_2NH (0.5 mL) was heated at 80 °C for 2 days. Volatiles were removed *in vacuo* to afford the *cis*-diastereoisomer of POCOP-14' as a colourless oil. Yield: 9.4 mg (>99%).

^{1}H NMR (500 MHz, toluene-d_8): δ 7.21 (app p, J = 2, 1H, Ar{2-CH}), 6.97 (t, $^{3}J_{HH}$ = 7.9, 1H, Ar), 6.91 (app dt, $^{3}J_{HH}$ = 7.9, J = 2, 2H, Ar), 1.85 (dtd, $^{2}J_{HH}$ = 14.2,

$^3J_{HH}$ = 7.4, $^2J_{PH}$ = 3.1, 1H, PCH_2), 1.58 – 1.68 (m, 4H, CH_2), 1.41 – 1.52 (m, 2H, CH_2), 1.16 – 1.40 (m, 20H, CH_2), 1.01 (d, $^3J_{PH}$ = 12.0, 18H, *t*Bu).

$^{13}C\{^1H\}$ NMR (126 MHz, toluene-d_8): δ 160.8 (d, $^2J_{PC}$ = 9, Ar{C}), 129.9 (s, Ar), 111.7 (d, $^3J_{PC}$ = 13, Ar), 109.4 (t, $^3J_{PC}$ = 11, Ar{2-CH}), 32.5 (d, $^1J_{PC}$ = 16, *t*Bu{C}), 30.9 (d, $^2J_{PC}$ = 11, CH_2), 29.1 (d, $^1J_{PC}$ = 24, PCH_2), 28.9 (s, CH_2), 28.5 (s, CH_2), 28.2 (s, CH_2), 28.1 (s, CH_2), 25.4 (d, $^3J_{PC}$ = 15, CH_2), 25.3 (d, $^3J_{PC}$ = 15, *t*Bu{CH_3}).

$^{31}P\{^1H\}$ NMR (162 MHz, C_6D_6): δ 140.5 (s).

*5.1.2. Asymmetric synthesis of **PCP-14'***

Preparation of **8**

A solution of $MgBr(C_8H_{15})$ in THF (0.37 M, 45 mL, 17 mmol) was added dropwise in three equal portions separated by 30 minutes to a solution of **7** (1.39 g, 5.57 mmol) in toluene at 80 °C. The solution was concentrated under reduced pressure and the residue re-dissolved in a minimal amount of toluene (20 mL) and heated at reflux for 3 days. The reaction mixture was cooled to 0 °C, exposed to air and quenched with saturated aqueous NH_4Cl (10 mL). The aqueous phase was extracted with EtOAc (3 × 20 mL) and the combined organic fractions dried ($MgSO_4$), filtered, and concentrated under reduced pressure to give a pale-yellow oil. Purification by flash column chromatography (silica, 8% EtOAc in hexane, R_f = 0.15) afforded **8** as a colourless oil. Yield: 1.92 g (95%).

^1H NMR (500 MHz, $CDCl_3$): δ 7.35 – 7.42 (m, 1H, Ar), 7.23 – 7.28 (m, 3H, Ar), 5.81 (ddt, $^3J_{HH}$ = 16.9, 10.1, 6.5, 1H, C<u>H</u>=CH_2), 5.01 (app dq, $^3J_{HH}$ = 16.9, J_{HH} = 2, 1H, CH=C<u>H</u>$_2$), 4.95 (ddt, $^3J_{HH}$ = 10.1, $^2J_{HH}$ = 2.2, $^4J_{HH}$ = 1.2, 1H, CH=C<u>H</u>$_2$), 4.77 (app td, J = 10, $^3J_{HH}$ = 4.5, 1H, NC<u>H</u>), 4.51 (app q, $^3J_{HH}$ = 5, 1H, OC<u>H</u>), 3.10 (dd, $^2J_{HH}$ = 16.6, $^3J_{HH}$ = 4.7, 1H, OCHC<u>H</u>$_2$), 2.90 (d, $^2J_{HH}$ = 16.6, 1H, OCHC<u>H</u>$_2$), 2.11 (d, $^3J_{HH}$ = 10.0, NH), 2.05 (app q, $^3J_{HH}$ = 7, 2H, C<u>H</u>$_2$CH=CH_2), 1.81 (d, $^3J_{HH}$ = 4.4, 1H, OH), 1.56 – 1.83 (m, 4H, CH_2), 1.30 – 1.49 (m, 6H, CH_2), 1.26 (d, $^3J_{PH}$ = 13.6, 9H, *t*Bu), 0.55 (partially collapsed quartet, fwhm = 310 Hz, 3H, BH_3).

$^{13}C\{^1H\}$ NMR (126 MHz, $CDCl_3$): δ 142.9 (d, $^3J_{PC}$ = 7, Ar{C}), 139.9 (s, Ar{C}), 139.1 (s, <u>C</u>H=CH_2), 128.1 (s, Ar), 127.1 (s, Ar), 125.6 (s, Ar), 124.3 (s, Ar), 114.5 (s, CH=<u>C</u>H_2), 74.8 (s, OCH), 62.3 (d, $^2J_{PC}$ = 3, NCH), 39.4 (s, OCH<u>C</u>H_2), 33.8 (s,

$\underline{C}H_2CH=CH_2$), 31.9 (d, $^1J_{PC}$ = 39, *t*Bu{C}), 31.5 (d, $^2J_{PC}$ = 13, CH_2), 28.9 (s, CH_2), 28.8 (s, CH_2), 25.1 (d, $^2J_{PC}$ = 2, *t*Bu{CH_3}), 24.1 (d, $^1J_{PC}$ = 36, PCH_2), 23.0 (s, CH_2).

$^{31}P\{^1H\}$ NMR (121 MHz, $CDCl_3$): δ 76.5 (partially collapsed quartet, fwhm = 200 Hz).

HR ESI-MS (positive ion, 4 kV): 384.2603, [*M*+Na]$^+$ (calcd 384.2602) *m/z*.

Preparation of **9**

H_2SO_4 (98%, 5.4 mL, 99 mmol) was added dropwise to a solution of **8** (4.52 g, 12.5 mmol) in a MeOH-water mixture (140 mL:45 mL). The reaction mixture was heated at 70 °C for 4 days, with periodic monitoring by TLC. The mixture was allowed to cool to RT, exposed to air, and CH_2Cl_2 (40 mL) and saturated aqueous NaCl (20 mL) added. The aqueous phase was extracted with CH_2Cl_2 (3 × 15 mL) and the combined organic extracts dried ($MgSO_4$), filtered, and concentrated under reduced pressure to give a colourless opaque oil. The crude material was dissolved in a minimal amount of CH_2Cl_2 and run through a short silica plug, eluting with CH_2Cl_2 (R_f = 0.6). The volatiles were removed under reduced pressure to afford **9** as a colourless oil. Yield: 2.51g (87%).

^1H NMR (500 MHz, toluene-d_8): δ 5.75 (ddt, $^3J_{HH}$ = 17.0, 10.2, 6.7, 1H, C$\underline{H}$=CH_2), 5.02 (br d, $^3J_{HH}$ = 17.1, 1H, CH=C$\underline{H}_2$), 4.97 (br d, $^3J_{HH}$ = 10.1, 1H, CH=C$\underline{H}_2$), 3.14 (br, 1H, OH), 1.95 (app q, $^3J_{HH}$ = 7, 2H, C$\underline{H}_2$CH=CH_2), 1.60 – 1.75 (m, 1H, CH_2), 1.39 – 1.56 (m, 2H, CH_2), 1.03 – 1.38 (m, 7H, CH_2), 0.95 (d, $^3J_{PH}$ = 13.7, 9H, *t*Bu), 0.63 – 1.30 (obscured, 3H, BH_3).

$^{13}C\{^1H\}$ NMR (126 MHz, toluene-d_8): δ 139.1 (s, $\underline{C}$H=CH_2), 114.6 (s, CH=$\underline{C}H_2$), 34.2 (s, $\underline{C}H_2$CH=CH_2), 31.5 (d, $^2J_{PC}$ = 12, CH_2), 31.0 (d, $^1J_{PC}$ = 38, *t*Bu{C}), 29.24 (s, CH_2), 29.15 (s, CH_2), 24.5 (d, $^1J_{PC}$ = 35, PCH_2), 24.0 (d, $^2J_{PC}$ = 3, *t*Bu{CH_3}), 22.8 (s, CH_2).

$^{31}P\{^1H\}$ NMR (121 MHz, toluene-d_8): δ 125.6 (partially collapsed quartet, fwhm = 200 Hz).

Preparation of **10**

Triethylamine (3.79 mL, 27.2 mmol) was added dropwise to a solution of **9** (2.51 g, 10.9 mmol) and methanesulfonic anhydride (2.84 g, 16.3 mmol) in dichloromethane (15 mL) at -20 °C and the resulting solution stirred at this

temperature for 1 h. A solution of tetrabutylammonium borohydride (2.81 g, 10.9 mmol) in CH_2Cl_2 (10 mL) was added at -20 °C and the reaction mixture stirred for a further 16 h at -20 °C. The mixture was allowed to warm to 0 °C and HCl (0.5 M, 20 mL) added slowly. The mixture was exposed to air, diluted with distilled water, and the aqueous phase extracted with CH_2Cl_2 (3 × 15 mL). The combined organic extracts were dried ($MgSO_4$), filtered and concentrated under reduced pressure to give a colourless oil. Purification by flash column chromatography (silica, 5% EtOAc in hexane, R_f = 0.42) afforded **10** as a colourless oil. Yield: 1.83 g (79%).

^{1}H NMR (500 MHz, $CDCl_3$): δ 5.80 (ddt, $^3J_{HH}$ = 17.0, 10.0, 6.5, 1H, C<u>H</u>=CH_2), 4.99 (app dq, $^3J_{HH}$ = 17.0, J_{HH} = 2, 1H, CH=C<u>H</u>$_2$), 4.94 (ddt, $^3J_{HH}$ = 10.0, $^2J_{HH}$ = 2.3, $^4J_{HH}$ = 1.2, 1H, CH=C<u>H</u>$_2$), 4.23 (dm, $^1J_{PH}$ = 350.6, 1H, PH), 2.04 (app q, $^3J_{HH}$ = 7, 2H, C<u>H</u>$_2$CH=CH_2), 1.65 – 1.90 (m, 2H, CH_2), 1.45 – 1.60 (m, 2H, CH_2), 1.24 – 1.40 (m, 6H, CH_2), 1.21 (d, $^3J_{PH}$ = 14.2, 9H, *t*Bu), 0.46 (partially collapsed quartet, fwhm = 330, 3H, BH_3).

^{13}C{^{1}H} NMR (126 MHz $CDCl_3$): δ 139.0 (s, <u>C</u>H=CH_2), 114.5 (s, CH=<u>C</u>H_2), 33.8 (s, CH_2), 30.9 (d, $^2J_{PC}$ = 11, CH_2), 28.8 (s, CH_2), 28.7 (s, CH_2), 26.9 (d, $^2J_{PC}$ = 2, *t*Bu{CH_3}), 26.8 (d, $^1J_{PC}$ = 35, *t*Bu{C}), 25.0 (d, $^3J_{PC}$ = 2, CH_2), 17.6 (d, $^1J_{PC}$ = 32, PCH_2).

^{31}P NMR (202 MHz, $CDCl_3$): δ 22.2 (br d, $^1J_{PH}$ = 352).

^{31}P{^{1}H} NMR (202 MHz, $CDCl_3$): δ 22.2 (partially collapsed quartet, fwhm = 165 Hz).

<u>Preparation of **11**</u>

*n*BuLi (1.60 M, 4.11 mL, 6.59 mmol) was added dropwise to a solution of **10** (1.41 g, 6.59 mmol) in THF (15 mL) at -78 °C. The reaction mixture was stirred for 30 min at this temperature and a solution of 1,3-bis(bromomethyl)benzene (870 mg, 3.30 mmol) in THF (3 mL) was added at -78 °C. The reaction mixture was stirred at -78 °C for 1 h, allowed to warm to RT over 3 h, then quenched by slow addition of water (10 mL) at 0 °C in air. THF was removed under reduced pressure and aqueous mixture extracted with CH_2Cl_2 (3 × 20 mL). The combined organic extracts were dried ($MgSO_4$), filtered and concentrated under reduced pressure to give a colourless oil. Purification by flash column chromatography (silica, 5% EtOAc in hexane, R_f = 0.33) afforded **5** as a colourless oil, which was carried forward directly. Yield: 1.60 g (91%).

^{1}H NMR (300 MHz, $CDCl_3$): δ 7.12 – 7.24 (m, 4H, Ar), 5.78 (ddt, $^3J_{HH}$ = 16.9, 10.2, 6.8, 2H, C<u>H</u>=CH_2), 4.88 – 5.03 (m, 4H, CH=C<u>H</u>$_2$), 2.85 – 3.10 (m, 4H, PCH_2), 2.01 (app q, $^3J_{HH}$ = 7.0, 4H, C<u>H</u>$_2$CH=CH_2), 1.10 – 1.65 (m, 24H, CH_2), 1.17 (d, $^3J_{PH}$ = 13.1, 18H, *t*Bu), 0.44 (partially collapsed quartet, fwhm = 270 Hz, 6H, BH_3).

^{13}C{^{1}H} NMR (126 MHz, $CDCl_3$): δ 139.1 (s, CH{alkene}), 133.9 (dd, $^2J_{PC}$ = 5, $^4J_{PC}$ = 2, Ar), 132.1 (t, $^3J_{PC}$ = 4, Ar), 128.7 (app t, J_{PC} = 3, Ar), 128.5 (s, ArCH), 114.4 (s, CH_2{alkene}), 33.8 (s, CH_2), 31.6 (d, $^2J_{PC}$ = 13, CH_2), 28.8 (d, $^1J_{PC}$ = 31, *t*Bu{C}), 28.7 (d, $^1J_{PC}$ = 27, PCH_2), 28.94 (d, $^1J_{PC}$ = 22, CH_2), 28.88 (d, $^1J_{PC}$ = 25, Ar-<u>C</u>H_2-P), 28.86 (s, CH_2), 28.7 (s, CH_2), 25.9 (d, $^2J_{PC}$ = 2, *t*Bu{CH_3}), 23.8 (s, CH_2), 20.3 (d, $^2J_{PC}$ = 30, CH_2).

^{31}P{^{1}H} NMR (162 MHz, $CDCl_3$): δ 32.3 (partially collapsed quartet, fwhm = 140 Hz).

HR ESI-MS (positive ion, 4 kV): 553.4469, $[M+Na]^+$ (calcd 553.4416) *m/z*.

<u>Preparation of **12**</u>

A solution of **11** (1.60 g, 3.01 mmol) in CH_2Cl_2 (5 mmol L^{-1}, 600 mL) was treated with a solution of [$Ru(PCy_3)_2Cl_2$(CHPh)] (248 mg, 301 μmol, 10 mol%) in CH_2Cl_2 (2 mL) in 4 equal portions – every 12 h – over 2 days with periodic argon sparging (ca. 10 min). Volatiles were removed *in vacuo* and the crude mixture was purified by flash column chromatography in air (silica, 8% EtOAc in hexane, R_f = 0.26) to afford **12** (mixture of alkene isomers) as a colourless oil, which was carried forward directly. Yield: 1.37 g (91%).

^{1}H NMR (500 MHz, $CDCl_3$): δ 7.14 – 7.25 (m, 4H, Ar), 5.21 – 5.29 (m, 0.6H, CH=CH minor), 5.21 – 5.29 (m, 1.4H, CH=CH major), 3.02 (dd, $^2J_{HH}$ = 13.8, $^2J_{PH}$ = 9.0, 2H, ArC<u>H</u>$_2$), 2.92 (app t, ^2J = 14, 1.4H, ArC<u>H</u>$_2$ major), 2.92 (app t, ^2J = 14, 1.4H, ArC<u>H</u>$_2$ major), 2.91 (app t, ^2J = 14, 0.6H, ArC<u>H</u>$_2$ minor), 1.88 – 2.05 (m, 4H, CH_2), 0.93 – 1.70 (m, 20H, CH_2), 1.21 (d, $^3J_{PH}$ = 13.0, 5.4H, *t*Bu minor), 1.20 (d, $^3J_{PH}$ = 13.0, 12.6H, *t*Bu major), 0.45 (partially collapsed quartet, fwhm = 270 Hz, 6H, BH_3).

^{13}C{^{1}H} NMR (126 MHz, $CDCl_3$): δ 133.8 (s, Ar), 132.3 (s, Ar), 131.0 (s, CH{alkene}, major), 130.2 (s, CH{alkene}, minor), 128.7 (s, 2 × ArCH), 128.4 (s, Ar), 31.9 (s, CH_2, major), 26.5 (s, CH_2, minor), 31.3 (d, $^2J_{PC}$ = 12, CH_2, major), 31.1 (d, $^2J_{PC}$ = 12, CH_2, minor), 28.9 (d, $^1J_{PC}$ = 28, *t*Bu, minor), 28.83 (d, $^1J_{PC}$ = 30, *t*Bu{C}, major) 28.81

(d, $^{1}J_{PC}$ = 31, PCH_2), 28.49 (s, CH_2, major), 28.47 (s, CH_2, minor), 28.2 (s, CH_2, minor), 27.6 (s, CH_2, major), 25.8 (d, $^{2}J_{PC}$ = 1, *t*Bu{CH_3}, minor), 25.7 (d, $^{2}J_{PC}$ = 1, *t*Bu{CH_3}, major), 24.03 (s, CH_2, minor), 24.01 (s, CH_2, major), 20.2 (d, $^{1}J_{PC}$ = 30, CH_2, minor), 19.6 (d, $^{1}J_{PC}$ = 30, CH_2, major).

$^{31}P\{^{1}H\}$ NMR (162 MHz, $CDCl_3$): δ 31.3 – 33.4 (br m).

HR ESI-MS (positive ion, 4 kV): 525.4105, [*M*+Na]$^{+}$ (calcd 525.4102) *m/z*.

Preparation of **13**

A suspension of [$Rh(PPh_3)_3Cl$] (126 mg, 136 μmol, 5 mol%) in benzene (5 mL) was added to a stirred solution of **12** (1.37 g, 2.73 mmol) in benzene (20 mL). The suspension was freeze-pump-thaw degassed, placed under dihydrogen and the resulting solution stirred at 50 °C for 2 days. Volatiles were removed under reduced pressure and the crude product purified by flash column chromatography in air (silica, 5% EtOAc in hexane, R_f = 0.25) to afford **13** as a colourless oil. Yield: 1.21 g (88%).

^{1}H NMR (600 MHz, $CDCl_3$): δ 7.25 (s, 1H, Ar{2-CH}), 7.22 (t, $^{3}J_{HH}$ = 7.6, 1H, Ar), 7.17 (d, $^{3}J_{HH}$ = 7.6, 2H, Ar), 3.03 (dd, $^{2}J_{HH}$ = 14.0, $^{2}J_{PH}$ = 9.9, 2H, $ArC\underline{H}_2$), 3.03 (app t, ^{2}J = 14, 2H, $ArC\underline{H}_2$), 1.50 – 1.61 (m, 4H, PCH_2), 1.40 – 1.50 (m, 2H, CH_2), 1.13 – 1.35 (m, 22H, CH_2), 1.17 (d, $^{3}J_{PH}$ = 13.1, 18H, *t*Bu), 0.46 (partially collapsed quartet, fwhm = 270 Hz, 6H, BH_3).

$^{13}C\{^{1}H\}$ NMR (151 MHz, $CDCl_3$): δ 133.9 (dd, $^{2}J_{PC}$ = 5, $^{4}J_{PC}$ = 2, Ar{C}), 132.0 (t, $^{3}J_{PC}$ = 4, Ar{2-CH}), 128.7 (dd , $^{3}J_{PC}$ = 4, $^{5}J_{PC}$ = 3, Ar), 128.5 (t, $^{4}J_{PC}$ = 2, Ar), 30.8 (d, $^{2}J_{PC}$ = 12, CH_2), 28.8 (d, $^{1}J_{PC}$ = 31, *t*Bu{C}), 28.7 (d, $^{1}J_{PC}$ = 27, $Ar\underline{C}H_2$), 27.8 (s, CH_2), 27.6 (s, 2 × CH_2), 27.4 (s, CH_2), 25.8 (d, $^{2}J_{PC}$ = 1, *t*Bu{CH_3}), 23.3 (s, CH_2), 20.2 (d, $^{1}J_{PC}$ = 31, PCH_2).

$^{31}P\{^{1}H\}$ NMR (243 MHz, $CDCl_3$): δ 32.5 (partially collapsed quartet, fwhm = 155 Hz).

HR ESI-MS (positive ion, 4 kV): 527.4250, [*M*+Na]$^{+}$ (calcd 527.4259) *m/z*.

Anal. Calcd for $C_{30}H_{60}B_2P_2$ (508.32 g.mol^{-1}): C, 71.44; H, 11.99; Found: C, 71.37; H, 12.10.

5.1.3. Attempted asymmetric synthesis of the POCOP scaffold

Attempted reaction of mesylate of **9** with disodium resorcinolate

Triethylamine (19 µL, 0.14 mmol) was added dropwise to a solution of **9** (20.0 mg, 92.5 µmol) and methanesulfonic anhydride (16.1 mg, 92.5 µmol) in dichloromethane (1 mL) at -20 °C and the resulting solution stirred at this temperature for 1 h. A suspension of resorcinol (3.4 mg, 31 µmol) and sodium hydride (1.6 mg, 67 µmol) in dichloromethane (1 mL), which had been stirred at RT for 30 minutes, was added and the solution stirred at -20 °C for 2 days. Analysis of an aliquot by ESI-MS and ^{1}H and ^{31}P NMR spectroscopy was consistent with no reaction having taken place.

Attempted reaction of the conjugate base of **9** with 1,3-difluorobenzene

A solution of **9** (30.0 mg, 139 µmol) and KHMDS (27.7 mg, 139 µmol) in anhydrous DMF (2 mL) was stirred at RT for 1 h. To this solution 1,3-difluorobenzene (7 µL, 71 µmol) was added, the flask sealed, and heated at 150 °C overnight. Analysis of the reaction mixture by ^{31}P NMR spectroscopy was consistent with no reaction having taken place.

Attempted acidolysis of **8** with HCl

A solution of HCl (1M in Et_2O, 0.06 mL, 0.06 mmol) was added to a solution of **2** (10.4 mg, 28.8 µmol) in C_6D_6 (0.5 mL) within J Young's valve NMR tube. Storage at RT followed by heating at 60 °C gave ^{1}H and $^{31}P\{^{1}H\}$ NMR spectra consistent with a mixture of the two reactants.

*5.1.4. Attempted synthesis of **2•BH$_3$***

Preparation of **8-Me**

A suspension of **8** (226 mg, 625 µmol) and NaH (56 mg, 2.3 mmol) in THF (ca. 5 mL) was stirred at RT for 1 h. MeI (0.39 mL, 6.3 mmol) was added and the suspension stirred at RT overnight. The reaction was exposed to air, quenched with saturated aqueous NH_4Cl (20 mL), and the aqueous phase extracted with EtOAc (3 x 15 mL). The combined organic fractions were dried ($MgSO_4$), filtered and volatiles removed under reduced pressure to afford **8-Me** as a colourless oil, which was dried *in vacuo* and used without further purification. Yield: 235 mg (97%).

^{1}H NMR (500 MHz, $CDCl_3$): δ 7.26 – 7.31 (m, 1H, Ar), 7.20 – 7.26 (m, 3H, Ar), 5.81 (ddt, $^3J_{HH}$ = 16.9, 10.2, 6.7, 1H, C<u>H</u>=CH_2), 5.10 (dd, $^3J_{PH}$ = 9.9, $^3J_{HH}$ = 5.7, 1H, NC<u>H</u>), 4.99 (app dq, $^3J_{HH}$ = 17, J_{HH} = 2, 1H, CH=C<u>H</u>$_2$), 4.93 (br d, $^3J_{HH}$ = 10.1, 1H, CH=C<u>H</u>$_2$), 4.27 (app td, $^3J_{HH}$ = 5, $^3J_{HH}$ = 1.5, 1H, OCH),

3.33 (s, 3H, OCH_3), 2.97 (dd, $^2J_{HH}$ = 16.5, $^3J_{HH}$ = 1.5, 1H, OCHC<u>H</u>$_2$), 2.88 (dd, $^2J_{HH}$ = 16.5, $^3J_{HH}$ = 5.2, 1H, OCHC<u>H</u>$_2$), 2.64 (d, $^3J_{PH}$ = 6.1, 3H, NCH_3), 2.11 – 2.18 (m, 1H, PCH_2), 2.08 (app q, $^3J_{HH}$ = 7, 2H, C<u>H</u>$_2$CH=CH_2), 1.75 – 1.91 (m, 1H, CH_2), 1.52 – 1.72 (m, 2H, CH_2), 1.34 – 1.52 (m, 6H, CH_2), 1.26 (d, $^3J_{PH}$ = 13.3, 9H, *t*Bu), 0.61 (partially collapsed quartet, fwhm = 310 Hz, 3H, BH_3).

^{13}C{^{1}H} NMR (126 MHz, $CDCl_3$): δ 140.68 (d, $^3J_{PC}$ = 6, Ar{C}), 140.65 (s, Ar{C}), 139.1 (s, <u>C</u>H=CH_2), 127.7 (s, Ar), 126.6 (s, Ar), 125.9 (s, Ar), 124.7 (s, Ar), 114.5 (s, CH=<u>C</u>H_2), 86.4 (s, OCH), 67.2 (d, $^2J_{PC}$ = 10, NCH), 56.9 (s, OCH_3), 35.7 (s, OCH<u>C</u>H_2), 34.4 (d, $^1J_{PC}$ = 35, *t*Bu{C}), 33.93 (d, $^2J_{PC}$ = 4, NCH_3), 33.87 (s, <u>C</u>H_2CH=CH_2), 31.6 (d, $^2J_{PC}$ = 14, CH_2), 29.0 (s, CH_2), 28.9 (s, CH_2), 26.6 (d, $^2J_{PC}$ = 2, *t*Bu{CH_3}), 22.4 (s, CH_2), 20.6. (d, $^1J_{PC}$ = 39, PCH_2).

^{31}P{^{1}H} NMR (121 MHz, $CDCl_3$): δ 86.0 (partially collapsed quartet, fwhm = 215 Hz).

HR ESI-MS (positive ion, 4 kV): 412.2923, [*M*+Na]$^+$ (calcd 412.2915); 801.5956, [2*M*+Na]$^+$ (calcd 801.5945) *m/z*.

<u>Attempted acidolysis of **8-Me** with HCl</u>

A solution of HCl (1M in Et_2O, 0.2 mL, 0.2 μmol) was added to a solution of **8-Me** (40.3 mg, 104 μmol) in C_6D_6 (0.5 mL) within a J Young's valve NMR tube. Storage at room temperature followed by heating at 75 °C gave ^{1}H and ^{31}P{^{1}H} NMR spectra consistent with a mixture of the two reactants.

*5.1.5. Preparation of phosphine oxides **POCOP-14'•O$_2$** and **PCP-14'•O$_2$***

<u>Preparation of **POCOP-14'•O$_2$**</u>

Following an adapted literature procedure.[21] To a stirred solution of **POCOP-14'** (25.1 mg, 52.2 μmol) in EtOH (2 mL) cooled to -78 °C was added H_2O_2 (30% w/w

in H_2O, 16 μL, 0.16 mmol). The mixture was allowed to warm to RT overnight before the volatiles were removed *in vacuo*. Toluene (1 mL) was added and the solution was stirred over 3 Å molecular sieves (45.2 mg) overnight. The solution was filtered, extracting the sieves with additional toluene (3 × 1 mL), and reduced to dryness to afford **POCOP-14'·O_2** as a colourless oil, which crystallised upon standing. Yield: 26.2 mg (95%).

^{1}H NMR (500 MHz, CD_2Cl_2): δ 7.23 (t, $^3J_{HH}$ = 8.3, 1H, Ar), 7.19 (t, $^4J_{HH}$ = 2.4, 1H, Ar{2-CH}), 7.04 (dd, $^3J_{HH}$ = 8.3, $^4J_{HH}$ = 7.1, 2H, Ar), 1.75 – 1.91 (m, 4H, CH_2), 1.16 – 1.73 (m, 24H, CH_2), 1.22 (d, $^3J_{PH}$ = 15.5, 18H, *t*Bu).

^{13}C{^{1}H} NMR (126 MHz, CD_2Cl_2): δ 153.6 (d, $^2J_{PC}$ = 10, Ar{C}), 130.2 (s, Ar), 116.4 (d, $^3J_{PC}$ = 4, Ar), 113.3 (t, $^3J_{PC}$ = 4, Ar{2-CH}), 33.9 (d, $^1J_{PC}$ = 91, *t*Bu{C}), 30.9 (d, $^2J_{PC}$ = 14, CH_2), 28.5 (s, CH_2), 28.3 (s, CH_2), 28.0 (s, CH_2), 27.7 (s, CH_2), 24.6 (s, *t*Bu{CH_3}), 24.4 (d, $^1J_{PC}$ = 83, PCH_2), 21.9 (d, $^3J_{PC}$ = 6, CH_2).

^{31}P{^{1}H} NMR (162 MHz, CD_2Cl_2): δ 64.1 (s).

HR ESI-MS (positive ion, 4 kV): 535.3078, $[M+Na]^+$ (calcd 535.3077) *m/z*.

Preparation of **PCP-14'•O_2**

Following an adapted literature procedure.[21] To a stirred solution of PCP-14' (24.8 mg, 52.0 μmol) in EtOH (1 mL) cooled to -78 °C was added H_2O_2 (30% w/w in H_2O, 16 μL, 0.16 mmol). The mixture was allowed to warm to RT overnight before the volatiles were removed *in vacuo*. Toluene (0.5 mL) was added and the solution was stirred over 3 Å molecular sieves (15 mg) overnight. The solution was filtered, extracting the sieves with additional toluene (3 × 1 mL), and reduced to dryness to afford PCP-14'·O_2 as a colourless oil, which crystallised upon standing. Yield: 22.3 mg (84%).

^{1}H NMR (500 MHz, CD_2Cl_2): δ 7.37 (s, 1H, Ar), 7.23 – 7.28 (m, 1H, Ar), 7.21 (d, $^3J_{HH}$ = 7.6, 2H, Ar), 3.12 (app t, ^2J = 14, 2H, Ar$C\underline{H}_2$), 3.02 (dd, $^2J_{HH}$ = 14.5, $^2J_{PH}$ = 10.1,

2H, ArC$\underline{H}_2$), 1.61 – 1.76 (m, 2H, PCH_2), 1.50 – 1.61 (m, 2H, PCH_2), 1.39 – 1.50 (m, 2H, CH_2), 1.10 – 1.50 (m, 22H, CH_2), 0.98 (d, $^3J_{PH}$ = 10.9, 18H, *t*Bu).

$^{13}C\{^1H\}$ NMR (126 MHz, CD_2Cl_2): δ 134.2 (dd, $^2J_{PC}$ = 8, $^4J_{PC}$ = 2, Ar{C}), 131.9 (t, $^3J_{PC}$ = 5, Ar{2-CH}), 128.8 (t, $^4J_{PC}$ = 2, Ar), 128.6 (app t, J_{PC} = 3, Ar), 33.2 (d, $^1J_{PC}$ = 65, *t*Bu{C}), 32.9 (d, $^1J_{PC}$ = 55, Ar$\underline{C}H_2$), 30.9 (d, $^2J_{PC}$ = 12, CH_2), 28.3 (s, CH_2), 28.2 (s, CH_2), 28.14 (s, CH_2), 28.08 (s, CH_2), 24.9 (s, *t*Bu{CH_3}), 24.4 (d, $1J_{PC}$ = 62, PCH_2), 22.0 (d, $^3J_{PC}$ = 5, CH_2).

$^{31}P\{^1H\}$ NMR (162 MHz, CD_2Cl_2): δ 52.2 (s)

HR ESI-MS (positive ion, 4 kV): 531.3490, $[M+Na]^+$ (calcd 531.3491) *m/z*.

5.1.6. Enantiomeric excess determination

To a solution of **POCOP-14'** or **PCP-14'** (5 μmol) in CD_2Cl_2 in a J. Young's NMR tube under Ar was added (−)-3,5-dinitro-N-(1-phenylethyl)benzamide (1, 2 and 5 eq).

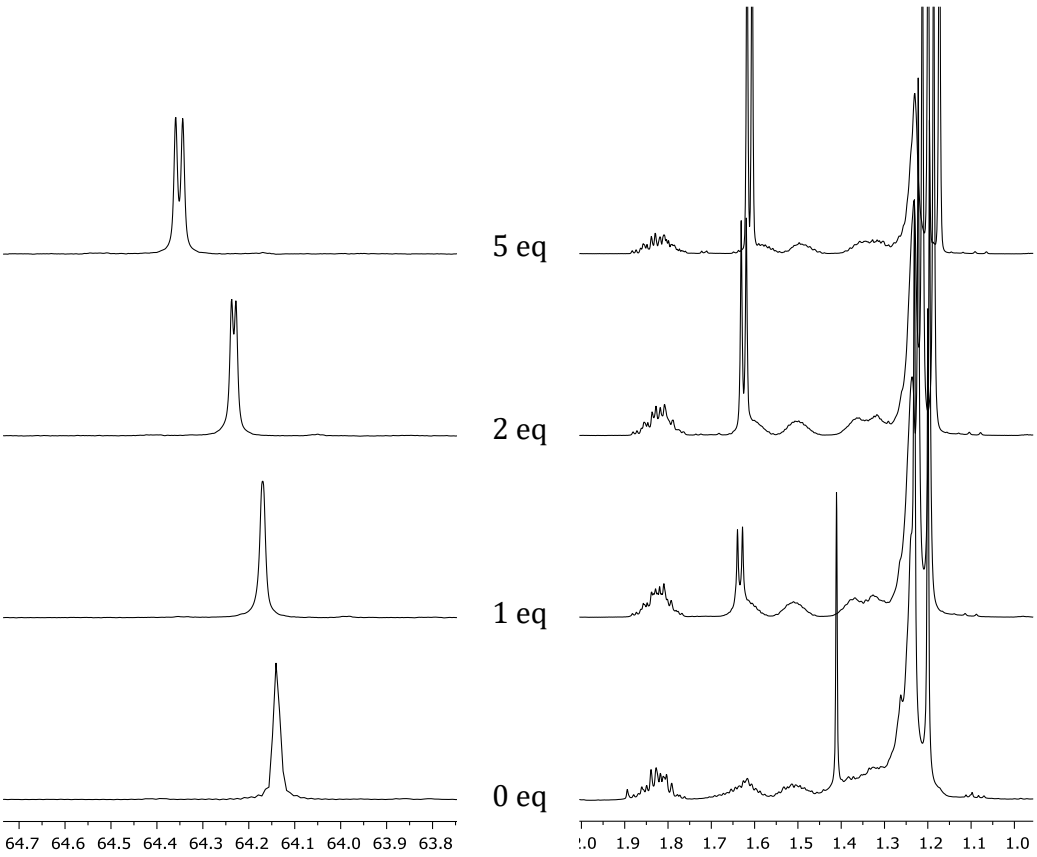

Figure 5.1. $^{31}P\{^1H\}$ (left) and ^1H (right) NMR spectra of **POCOP-14'·O_2** with 0, 1, 2 and 5 equiv. of chiral shift agent (CD_2Cl_2; 0 equiv.,162/500 MHz; 1, 2 and 5 equiv., 243/600 MHz).

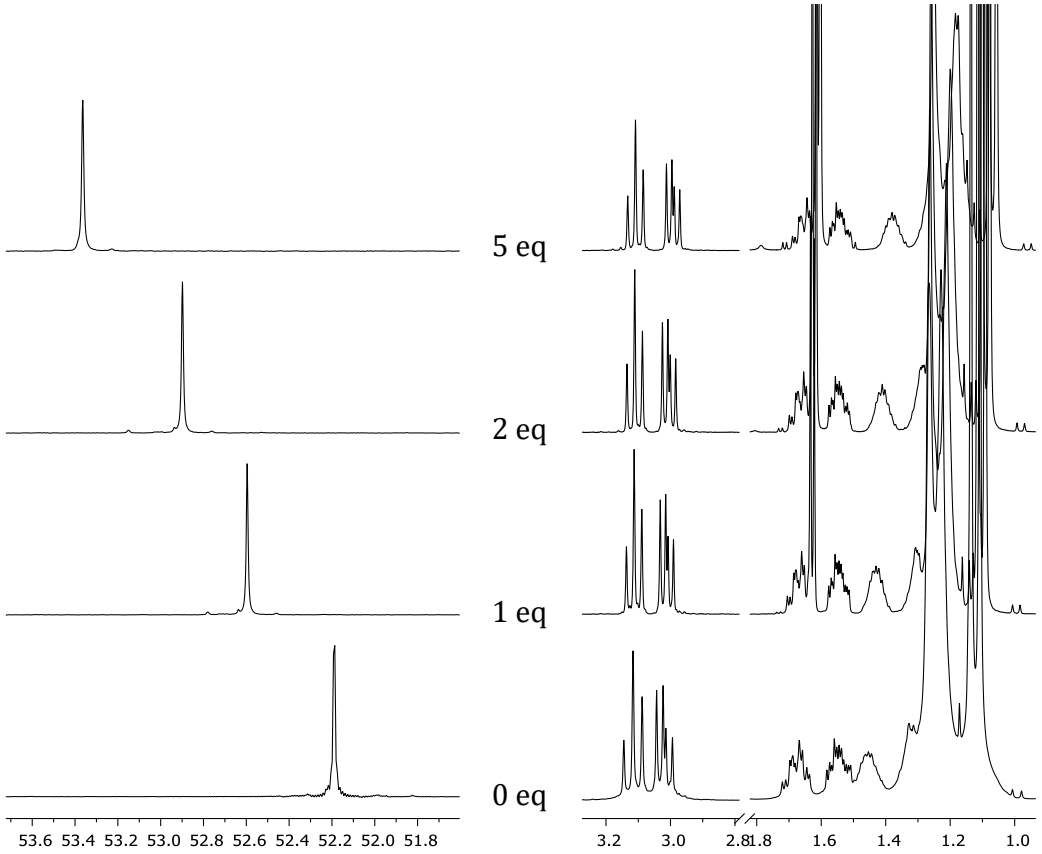

Figure 5.2. $^{31}P\{^{1}H\}$ (left) and ^{1}H (right) NMR spectra of **PCP-14'·O₂** with 0, 1, 2 and 5 equiv. of chiral shift agent (CD_2Cl_2; 0 equiv.,162/500 MHz; 1, 2 and 5 equiv., 243/600 MHz).

5.2. Chapter 3

*5.2.1. Synthesis of iridium complexes of **POCOP-14***

<u>One-pot preparation of **Ir-19o**</u>

A solution of **POCOP-14'** (69.1 mg, 144 μmol) and $[Ir(COD)Cl]_2$ (53.1 mg, 79.1 μmol) in toluene (5 mL) within a reaction flask fitted with a J Young's value was freeze-pump-thaw-degassed and placed under dihydrogen (1 atm), sealed, and heated at 100 °C for 3 days. The solution was cooled to RT and cannula transferred under dihydrogen into a reaction flask fitted with a J Young's value and charged with KO*t*Bu (19.4 mg, 173 μmol). The flask was then sealed and heated at 120 °C for 2 h to generate **Ir-15o**, which was characterised *in situ*. The solution was freeze-pump-thaw degassed and placed under carbon monoxide (1 atm) resulting in immediate formation of ***cis*-Ir-16o**, which was characterised *in situ*. To this

solution *tert*-butylethylene (93 µL, 0.72 mmol) was added and the reaction mixture heated under carbon monoxide (1 atm, sealed flask) at 120 °C for 18 h, resulting in partial conversion to ***trans*-Ir-16o** but ultimately affording **Ir-17o**. The solution was freeze-pump-thaw degassed and placed under argon to afford **Ir-18o**, filtered, and slowly added to a suspension of $PhICl_2$ (39.5 mg, 144 µmol) in toluene (2 mL) at -78 °C. The reaction mixture was allowed to warm to RT overnight, the volatiles removed *in vacuo*, and the resulting residue extracted with hexane to afford the crude product, which was purified by silica chromatography in air (20 % CH_2Cl_2 in hexane, R_f = 0.28) to afford analytically pure **Ir-19o.** Yield: 107.9 mg (73%).

^{1}H NMR (500 MHz, toluene-d_8): δ 6.80 (t, $^3J_{HH}$ = 8.0, 1H, Ar), 6.64 (d, $^3J_{HH}$ = 8.0, 2H, Ar), 3.57 (app dp, $^2J_{HH}$ = 14.3, $^3J_{HH}$ = 7.3, $^2J_{PH}$ = 7.3, 2H, PC$\underline{H}_a$H$_b$), 1.85 – 1.99 (m, 2H, PCH$_2$C$\underline{H}_c$H$_d$), 1.72 – 1.83 (m, 2H, PCH$_a$$\underline{H}_b$), 1.61 – 1.71 (m, 2H, PCH$_2$CH$_2$C$\underline{H}_e$H$_f$), 1.32 – 1.61 (m, 16H, CH$_2$), 1.26 (vt, $^3J_{PH}$ = 7.7, 18H, 2 × tBu), 1.11 – 1.36 (m, 4H, CH$_2$).

^{13}C{^{1}H} NMR (126 MHz, toluene-d_8): δ 175.6 (t, $^2J_{PC}$ = 3, CO), 164.4 (vt, $^2J_{PC}$ = 6, ArC-O), ~129 (obsc), 128.9 (s, ArCH), 106.8 (vt, $^3J_{PC}$ = 6, 2 × ArCH), 41.0 (vt, $^1J_{PC}$ = 15, 2 × *t*Bu{C}), 30.3 (vt, $^2J_{PC}$ = 6, PCH$_2$$\underline{C}H_2$), 29.5 (s, CH$_2$), 29.4 (s, CH$_2$), 29.1 (s, CH$_2$), 28.3 (s, CH$_2$), 26.5 (s, 2 × *t*Bu{CH$_3$}), 24.2 (vt, $^3J_{PC}$ = 2, PCH$_2$CH$_2$$\underline{C}H_2$), 22.0 (vt, $^1J_{PC}$ = 16, PCH$_2$).

^{31}P{^{1}H} NMR (121 MHz, toluene-d_8): δ 144.4 (s).

IR (toluene): ν(CO) 2049 cm^{-1}.

Anal. Calcd for $C_{29}H_{49}Cl_2IrO_3P_2$ (770.77 g.mol^{-1}): C, 45.19; H, 6.41; Found: C, 44.95; H, 6.30.

In situ characterisation of **Ir-15o**

This complex is unstable to vacuum, ultimately resulting in irreversible decomposition. Attempts to prepare samples in toluene-d_8 resulted in extensive H/D exchange of hydride ligands, pincer backbone and some positions of the tetramethylene linker. T_1 values were determined following rapid freeze-pump-thaw-degassing and placing under argon.

^{1}H NMR (500 MHz, toluene-d_0, H_2, 298K, selected data): δ 6.67 (d, $^{3}J_{HH}$ = 7.9, 2H, ArCH), 1.09 (vt, $^{3}J_{PH}$ = 7.5, 18H, tBu), -8.24 (t, $^{2}J_{PH}$ = 9.9, 4H, 4 × Ir-H).

^{13}C{^{1}H} NMR (126 MHz, toluene-d_0): 162.7 (t, $^{2}J_{PC}$ = 6, Ar<u>C</u>-Ir), 148.1 (vt, $^{2}J_{PC}$ = 8, Ar<u>C</u>-CH_2), 123.7 (s, ArCH), 120.5 (vt, $^{3}J_{PC}$ = 8, 2 × ArCH), 35.4 (vt, $^{1}J_{PC}$ = 17, *t*Bu{C}), 33.6 (vt, $^{1}J_{PC}$ = 16, P<u>C</u>H_2CH_2), 29.9 (s, CH_2), 29.6 (vt, $^{3}J_{PC}$ = 3, $PCH_2CH_2CH_2$), 29.5 (s, CH_2), 29.3 (s, CH_2), 28.6 (s, CH_2), 27.8 (br s, PCH_2CH_2<u>C</u>H_2), 25.6 (vt, $^{2}J_{PC}$ = 3, PCH_2<u>C</u>H_2), 24.9 (vt, $^{2}J_{PC}$ = 3, 2 × *t*Bu{CH_3}).

^{31}P{^{1}H} NMR (162 MHz, toluene-d_0): δ 165.0 (s)

^{1}H NMR (600 MHz, toluene-d_0, Ar, 298K, selected data): δ -8.26 (t, $^{2}J_{PH}$ = 10.0, 4H, 4 × Ir-H, T_1 = 194 ± 4 ms).

^{1}H NMR (600 MHz, toluene-d_0, Ar, 200K, selected data): δ -8.10 (br s, 4H, 4 × Ir-H, T_1 = 242 ± 15 ms).

<u>*In situ* characterisation of *cis*-**Ir-16o**</u>

This complex is most conveniently characterised *in situ* by placing a toluene-d_8 (0.5 mL) solution of analytically pure **Ir-18o** (6.0 mg, 8.6 μmol) under dihydrogen (1 atm) in a J Young's valve NMR tube.

^{1}H NMR (500 MHz, toluene-d_8): 6.86 (t, $^{3}J_{HH}$ = 7.8, 1H, ArH), 6.70 (dd, $^{3}J_{HH}$ = 7.9, $^{4}J_{PH}$ = 1.9, 2H, ArH), 2.68 – 2.79 (m, 1H, CH_2), 2.30 – 2.46 (m, 3H, CH_2), 1.85 – 1.97 (m, 1H, CH_2), 1.50 – 1.70 (m, 6H, CH_2), 1.25 – 1.50 (m, 14H, CH_2), 1.12 – 1.24 (m, 3H, CH_2), 1.08 (d, $^{2}J_{PH}$ = 14.8, 9H, *t*Bu), 1.04 (d, $^{2}J_{PH}$ = 15.0, 9H, *t*Bu), -9.82 (t, $^{2}J_{PH}$ = 9.1, 1H, hydride), -10.75 (dd, $^{2}J_{PH}$ = 21.8, $^{2}J_{PH}$ = 14.7, 1H, hydride).

^{13}C{^{1}H} NMR (126 MHz, toluene-d_8): 180.6 (app q, $^{2}J_{PC}$ = 16, 8, CO), 163.2 (dd, $^{2}J_{PC}$ = 6, $^{4}J_{PC}$ = 4, Ar<u>C</u>-O), 162.8 (dd, $^{2}J_{PC}$ = 7, $^{4}J_{PC}$ = 4, Ar<u>C</u>-O), 126.2 (s, ArCH), 123.0 (t, $^{2}J_{PC}$ = 6, ArC-Ir), 104.8 (d, $^{3}J_{PC}$ = 12, ArCH), 104.7 (d, $^{3}J_{PC}$ = 16, ArCH), 37.1 (dd, $^{1}J_{PC}$ = 28, $^{3}J_{PC}$ = 7, <u>C</u>$(CH_3)_3$), 37.0 (dd, $^{1}J_{PC}$ = 27, $^{3}J_{PC}$ = 6, *t*Bu{C}), 34.6 (dd, $^{1}J_{PC}$ = 30, $^{3}J_{PC}$ = 5, P<u>C</u>H_2CH_2), 33.0 (dd, $^{1}J_{PC}$ = 27, $^{3}J_{PC}$ = 5, P<u>C</u>H_2CH_2), 30.3 (s, CH_2), 29.8 (s, CH_2), 29.7 (d, $^{2}J_{PC}$ = 6, PCH_2<u>C</u>H_2), 29.5 (s, CH_2), 29.16 (s, CH_2), 29.15 (s, CH_2), 28.9 (s, CH_2), 28.6 (s, CH_2), 28.5 (s, CH_2), 27.7 (d, $^{2}J_{PC}$ = 6, PCH_2<u>C</u>H_2), 25.7 (d, $^{3}J_{PC}$ = 5, PCH_2CH_2<u>C</u>H_2), 25.2 (vt, $^{2}J_{PC}$ = 5, 2 × *t*Bu{CH_3}), 25.1 (d, $^{3}J_{PC}$ = 6, PCH_2CH_2<u>C</u>H_2).

$^{31}P\{^{1}H\}$ NMR (162 MHz, toluene-d_8): δ 160.4 (d, $^{2}J_{PP}$ = 305), 154.6 (d, $^{2}J_{PP}$ = 305).

In situ characterisation of ***trans*-Ir-16o**

^{1}H NMR (400 MHz, toluene, selected data): 1.10 (vt, $^{2}J_{PH}$ = 7.6, 18H, *t*Bu), -9.76 (t, $^{2}J_{PH}$ = 16.5, 2H, hydride).

$^{31}P\{^{1}H\}$ NMR (162 MHz, toluene): δ 167.3 (s).

Preparation of **Ir-18o**

A solution of **Ir-19o** (12.3 mg, 16.0 μmol) in pentane (2 mL) was added to a flask charged with KC_8 (21.6 mg, 160 μmol), and stirred at RT for 2 days. The solution was filtered, reduced to dryness *in vacuo*, and **Ir-18o** obtained following recrystallisation by slow evaporation of TMS. Yield 8.8 mg (79%).

^{1}H NMR (500 MHz, toluene-d_8): δ 6.87 (t, $^{3}J_{HH}$ = 7.9, 1H, Ar), 6.74 (d, $^{3}J_{HH}$ = 7.9, 2H, Ar), 2.03 – 2.19 (m, 4H, CH_2), 1.73 – 1.87 (m, 4H, CH_2), 1.23 – 1.66 (m, 20H, CH_2), 1.15 (vt, $^{3}J_{PH}$ = 7.4, 18H, 2 × tBu).

$^{13}C\{^{1}H\}$ NMR (126 MHz, toluene-d_8): δ 200.5 (t, $^{2}J_{PC}$ = 5, CO), 168.3 (vt, $^{2}J_{PC}$ = 8, ArC-O), 148.7 (t, $^{2}J_{PC}$ = 9, Ar<u>C</u>-Ir), 129.5 (s, ArCH), 104.4 (vt, $^{3}J_{PC}$ = 6, 2 × ArCH), 39.5 (vt, $^{1}J_{PC}$ = 16, 2 × *t*Bu{C}), 30.7 (vt, $^{2}J_{PC}$ = 2, $PCH_2\underline{C}H_2$), 29.6 (vt, $^{1}J_{PC}$ = 14, PCH_2), 29.4 (s, CH_2), 29.3 (s, CH_2), 29.2 (s, CH_2), 28.9 (s, CH_2), 26.7 (vt, $^{2}J_{PC}$ = 3, 2 × *t*Bu{CH_3}), 26.0 (vt, $^{3}J_{PC}$ = 3, $PCH_2CH_2\underline{C}H_2$).

$^{31}P\{^{1}H\}$ NMR (162 MHz, toluene-d_8): δ 186.7 (s).

IR (toluene): ν(CO) 1943 cm^{-1}.

Anal. Calcd for $C_{29}H_{49}IrO_3P_2$ (699.87 $g.mol^{-1}$): C, 49.77; H, 7.06; Found: C, 49.85; H 7.01.

*5.2.2. Synthesis of iridium complexes of **PCP-14***

One-pot preparation of **Ir-19c**

A solution of **PCP-14'** (57.6 mg, 121 μmol) and $[Ir(COE)_2Cl]_2$ (54.1 mg, 60.4 μmol) in toluene (5 mL) within a reaction flask fitted with a J Young's value was freeze-pump-thaw-degassed and placed under dihydrogen (1 atm), sealed, and heated at 70 °C for 18 h. The solution was cooled to RT and cannula transferred under dihydrogen into a reaction flask fitted with a J Young's value and charged with KO*t*Bu (16.3 mg, 145 μmol). The flask was then sealed and heated at 120 °C for 18 h to generate **Ir-15c**, which was characterised *in situ*. The solution was freeze-pump-thaw degassed and placed under carbon monoxide (1 atm) resulting in immediate formation of ***cis*-Ir-16c**, which was characterised *in situ*. To this solution *tert*-butylethylene (78 μL, 0.60 mmol) was added and the reaction mixture heated under carbon monoxide (1 atm, sealed flask) at 120 °C for 18 h, resulting in partial conversion to ***trans*-Ir-16c** but ultimately affording **Ir-17c**. The solution was freeze-pump-thaw degassed and placed under argon to afford **Ir-18c**, filtered, and slowly added to a suspension of $PhICl_2$ (33.3 mg, 121 μmol) in toluene (1 mL) at -78 °C. The reaction mixture was allowed to warm to RT overnight, the volatiles removed *in vacuo*, and the resulting residue extracted with hexane to afford the crude product, which was purified by silica chromatography in air (40 % CH_2Cl_2 in hexane, R_f = 0.43) to afford analytically pure **Ir-19c.** Yield: 76.9 mg (51%).

^{1}H NMR (500 MHz, toluene-d_8): δ 6.94 – 7.00 (m, 3H, Ar), 3.64 (dt, $^2J_{HH}$ = 15.8, $^2J_{PH}$ = 5.0, 2H, Ar-C$\underline{H_2}$-P), 3.05 (dt, $^2J_{HH}$ = 15.8, $^2J_{PH}$ = 3.8, 2H, Ar-C$\underline{H_2}$-P), 2.96 (app ddq, $^2J_{HH}$ = 14.3, $^3J_{HH}$ = 9.7, 5.1, $^2J_{PH}$ = 5.1, 2H, PC$\underline{H_a}$H$_b$CH$_2$), 1.81 – 1.97 (m, 2H, PCH$_2$C$\underline{H_c}$H$_d$), 1.68 – 1.81 (m, 2H, PCH$_2$CH$_2$C$\underline{H_e}$H$_f$), 1.67 – 0.8 (m, 22H, CH$_2$), 1.13 (br s, 18H, 2 × tBu).

^{13}C{^{1}H} NMR (126 MHz, toluene-d_8): δ 175.7 (t, $^2J_{PC}$ = 5, CO), 155.3 (s, Ar$\underline{C}$-Ir), 148.5 (vt, $^2J_{PC}$ = 8, Ar$\underline{C}$-CH$_2$), 126.0 (s, ArCH), 121.6 (vt, $^3J_{PC}$ = 8, 2 × ArCH), 38.9 (vt, $^1J_{PC}$ = 17, 2 × Ar-$\underline{C}$H$_2$-P), 34.3 (vt, $^1J_{PC}$ = 13, 2 × *t*Bu{C}), 30.8 (vt, $^2J_{PC}$ = 5, PCH$_2\underline{C}$H$_2$), 29.2 (s, CH$_2$), 29.1 (s, CH$_2$), 29.0 (s, CH$_2$), 28.6 (s, CH$_2$), 27.5 (s, 2 × *t*Bu{CH$_3$}), 26.4 (s, PCH$_2$CH$_2\underline{C}$H$_2$), 20.6 (vt, $^1J_{PC}$ = 13, P$\underline{C}$H$_2$CH$_2$).

^{31}P{^{1}H} NMR (162 MHz, toluene-d_8): δ 33.8 (s).

IR (toluene): ν(CO) 2034 cm^{-1}.

Anal. Calcd for $C_{31}H_{53}Cl_2IrOP_2$ (766.83 $g.mol^{-1}$): C, 48.56; H, 6.97; Found: C, 48.66; H, 6.92.

In situ characterisation of **Ir-15c**

This complex is unstable to vacuum but was characterised *in situ* using a sample (ca. 10 μmol) prepared in a similar manner within a J Young's valve NMR tube following concentration *in vacuo*, placing under dihydrogen (1 atm), concentration to dryness *in vacuo*, addition of toluene-d_8 (0.5 mL) under argon, freeze-pump-thaw-degassing, and placing under dihydrogen (1 atm). NB: Long term storage in toluene-d_8 resulted in extensive H/D exchange of the hydride ligands, pincer backbone and some positions of the tetramethylene linker. T_1 values were subsequently determined following rapid freeze-pump-thaw-degassing and placing under argon.

^{1}H NMR (600 MHz, toluene-d_8, H_2, 298K, selected data): δ 6.99 – 7.03 (m, 3H, ArH), 3.50 (dt, $^2J_{HH}$ = 16.1, $^2J_{PH}$ = 3.6, 2H, Ar-C$\underline{H_2}$-P), 2.89 (dt, $^2J_{HH}$ = 16.6, $^2J_{PH}$ = 4.6, 2H, Ar-C$\underline{H_2}$-P), 1.78 – 1.88 (m, 2H, CH_2), 1.67 – 1.77 (m, 2H, CH_2), 1.53 – 1.63 (m, 2H, CH_2), 1.27 – 1.53 (m, 22H, CH_2), 0.94 (vt, $^3J_{PH}$ = 6.8, 18H, 2 × tBu), -8.99 (t, $^2J_{PH}$ = 9.8, 4H, 4 × Ir-H).

^{13}C{^{1}H} NMR (151 MHz, toluene-d_8): 151.7 (s, Ar$\underline{C}$-Ir), 147.7 (vt, $^2J_{PC}$ = 8, Ar$\underline{C}$-CH_2), 123.3 (s, ArCH), 120.2 (vt, $^3J_{PC}$ = 8, 2 × ArCH), 46.1 (vt, $^1J_{PC}$ = 17, 2 × Ar-$\underline{C}H_2$-P), 30.0 (vt, $^2J_{PC}$ = 4, $PCH_2\underline{C}H_2$), 29.7 (s, CH_2), 29.3 (vt, $^1J_{PC}$ = 15, 2 × *t*Bu{C}), 29.1 (s, CH_2), 28.9 (s, CH_2), 28.2 (s, CH_2), 27.4 (br s, $PCH_2CH_2\underline{C}H_2$), 27.2 (vt, $^1J_{PC}$ = 15, PCH_2), 25.7 (vt, $^2J_{PC}$ = 3, 2 × *t*Bu{CH_3}).

^{31}P{^{1}H} NMR (243 MHz, toluene-d_8): δ 49.9 (s).

^{1}H NMR (600 MHz, toluene-d_8, Ar, 298K, selected data): δ -8.99 (t, $^2J_{PH}$ = 9.8, 4H, 4 × Ir-H, T_1 = 300 ± 10 ms).

^{1}H NMR (600 MHz, toluene-d_8, Ar, 200K, selected data): δ -8.95 (br s, 4H, 4 × Ir-H, T_1 = 626 ± 15 ms).

In situ characterisation of ***cis*-Ir-16c**

This complex is most conveniently characterised *in situ* by placing a toluene-d_8 (0.5 mL) solution of analytically pure **Ir-18c** (6.0 mg, 8.6 μmol) under dihydrogen (1 atm) in a J Young's valve NMR tube.

^{1}H NMR (500 MHz, toluene-d_8): 6.99 – 7.04 (m, 3H, ArH), 3.50 – 3.65 (m, 2H, Ar-C$\underline{H_2}$-P), 2.98 (dd, $^2J_{HH}$ = 16.0, $^2J_{PH}$ = 7.3, 1H, Ar-C$\underline{H_2}$-P), 2.86 (dd, $^2J_{HH}$ = 16.8, $^2J_{PH}$ = 8.8, 1H, Ar-C$\underline{H_2}$-P), 2.06 – 2.16 9 (m, 1H, CH_2), 1.92 – 2.04 (m, 2H, CH_2), 1.14 – 1.91 (m, 25H, CH_2), 0.96 (d, $^2J_{PH}$ = 13.3, 9H, *t*Bu), 0.89 (d, $^2J_{PH}$ = 13.6, 9H, *t*Bu), -10.66 (ddd, $^2J_{PH}$ = 23.4, $^2J_{PH}$ = 10.5, $^2J_{HH}$ = 3.0, 1H, hydride), -11.59 (td, $^2J_{PH}$ = 11.8, $^2J_{HH}$ = 3.0, 1H, hydride).

^{13}C{^{1}H} NMR (126 MHz, toluene-d_8): 183.3 (s, CO), 155.1 (s, ArC-Ir), 148.8 (dd, $^2J_{PC}$ = 10, $^4J_{PC}$ = 4, Ar$\underline{C}$-CH_2-P), 148.1 (dd, $^2J_{PC}$ = 9, $^4J_{PC}$ = 4, Ar$\underline{C}$-CH_2-P), 123.5 (s, ArCH), 120.0 (d, $^3J_{PC}$ = 14, ArCH), 119.8 (d, $^3J_{PC}$ = 16, ArCH), 48.4 (d, $^1J_{PC}$ = 35, ArC-$\underline{C}H_2$-P), 46.2 (d, $^1J_{PC}$ = 35, ArC-$\underline{C}H_2$-P), 31.2 (dd, $^1J_{PC}$ = 24, $^3J_{PC}$ = 3, *t*Bu{C), 30.5 (dd, $^1J_{PC}$ = 27, $^3J_{PC}$ = 5, *t*Bu{C}), 30.2 (d, $^2J_{PC}$ = 10, $PCH_2\underline{C}H_2$), 29.9 (s, CH_2), 29.7 (d, $^2J_{PC}$ = 9, $PCH_2\underline{C}H_2$), 29.4 (s, CH_2), 29.3 (s, CH_2), 29.1 (s, CH_2), 28.8 (s, CH_2), 28.5 (s, CH_2), 28.3 (s, CH_2), 28.2 (s, CH_2), 27.9 (dd, $^1J_{PC}$ = 29, $^3J_{PC}$ = 4, P$\underline{C}H_2CH_2$), 27.7 (s, $PCH_2CH_2\underline{C}H_2$), 27.3 (dd, $^1J_{PC}$ = 24, $^3J_{PC}$ = 3, P$\underline{C}H_2CH_2$), 27.2 (s, $PCH_2CH_2\underline{C}H_2$), 26.2 (s, CH_2), (d, $^2J_{PC}$ = 4, *t*Bu{CH_3}), 26.1 (d, $^2J_{PC}$ = 4, *t*Bu{CH_3}).

^{31}P{^{1}H} NMR (162 MHz, toluene-d_8): δ 51.0 (d, $^2J_{PP}$ = 286), 45.8 (d, $^2J_{PP}$ = 286).

In situ characterisation of ***trans*-Ir-16c**

^{1}H NMR (400 MHz, toluene, selected data): 0.98 (vt, $^2J_{PH}$ = 7.1, 18H, *t*Bu), -9.65 (t, $^2J_{PH}$ = 14.4, 2H, hydride)**.**

^{31}P{^{1}H} NMR (162 MHz, toluene): δ 54.2 (s).

Preparation of **Ir-18c**

A solution of **Ir-19c** (17.2 mg, 22.4 μmol) in pentane (2 mL) was added to a flask charged with KC_8 (30.4 mg, 225 μmol), and stirred at RT for 2 days. The solution

was filtered, reduced to dryness *in vacuo*, and **Ir-18c** obtained following recrystallisation by slow evaporation of TMS. Yield 13.1 mg (84%).

^{1}H NMR (500 MHz, toluene-d_8): δ 7.14 (d, $^{3}J_{HH}$ = 7.5, 2H, Ar), 7.02 (t, $^{3}J_{HH}$ = 7.5, 1H, Ar), 3.35 (dt, $^{2}J_{HH}$ = 16.4, $^{2}J_{PH}$ = 4.0, 2H, Ar-C$\underline{H_2}$-P), 3.09 (dt, $^{2}J_{HH}$ = 16.4, $^{2}J_{PH}$ = 3.8, 2H, Ar-C$\underline{H_2}$-P), 2.03 – 2.19 (m, 2H, CH_2), 1.90 – 1.78 (m, 2H, CH_2), 1.76 – 1.34 (m, 24H, CH_2), 1.01 (vt, $^{3}J_{PH}$ = 6.7, 18H, 2 × tBu)

^{13}C{^{1}H} NMR (126 MHz, toluene-d_8): δ 198.7 (t, $^{2}J_{PC}$ = 7, CO), 181.4 (t, $^{2}J_{PC}$ = 4, Ar$\underline{C}$-Ir), 153.8 (vt, $^{2}J_{PC}$ = 11, Ar$\underline{C}$-CH_2), 126.1 (s, ArCH), 120.2 (vt, $^{3}J_{PC}$ = 8, 2 × ArCH), 41.7 (vt, $^{1}J_{PC}$ = 15, 2 × Ar-$\underline{C}H_2$-P), 33.5 (vt, $^{1}J_{PC}$ = 14, 2 × *t*Bu{C}), 30.5 (vt, $^{2}J_{PC}$ = 5, $PCH_2\underline{C}H_2$), 29.5 (s, CH_2), 29.3 (s, CH_2), 28.9 (s, CH_2), 28.2 (s, CH_2), 28.2 (vt, $^{2}J_{PC}$ = 3, 2 × *t*Bu{CH_3}), 26.3 (vt, $^{3}J_{PC}$ = 3, $PCH_2CH_2\underline{C}H_2$), 24.2 (vt, $^{1}J_{PC}$ = 13, PCH_2).

^{31}P{^{1}H} NMR (162 MHz, toluene-d_8): δ 68.1 (s).

IR (toluene): ν(CO) 1925 cm^{-1}.

Anal. Calcd for $C_{31}H_{53}IrOP_2$ (695.93 g.mol^{-1}): C, 53.50; H, 7.68; Found: C, 53.24; H, 7.76.

*5.2.3. Synthesis of rhodium complexes of **POCOP-14***

<u>One-pot preparation of **Rh-19o**</u>

A solution of POCOP-14' (217 mg, 452 μmol) and $[Rh(COE)_2Cl]_2$ (163 mg, 227 μmol) in toluene (5 mL) within a reaction flask fitted with a J Young's value was freeze-pump-thaw-degassed and placed under dihydrogen (1 atm), sealed, and heated at 120 °C for 3 days. The solution was cooled to RT and cannula transferred under dihydrogen into a reaction flask fitted with a J Young's value and charged with KO*t*Bu (61.1 mg, 545 μmol). The flask was then sealed and heated at 120 °C for 1 h to generate **Rh-15o**, which was characterised *in situ*. The solution was freeze-pump-thaw degassed and placed under carbon monoxide (1 atm) resulting in immediate formation of **Rh-18o**, which was isolated by removal of the volatiles *in vacuo* and extraction of the residue with hexane. Crude **Rh-18o** obtained in this way was dissolved in toluene (5 mL) and then slowly added to a suspension of $PhICl_2$ (125 mg, 455 μmol) in toluene (2 mL) at -78 °C. The reaction mixture was allowed to warm to RT overnight, the volatiles removed *in vacuo*, and the resulting

residue extracted with hexane to afford the crude product, which was purified by alumina chromatography in air (20 % CH_2Cl_2 in hexane, R_f = 0.45) to afford analytically pure **Rh-19o.** Yield: 149.3 mg (48%). Complex **Rh-19o** is stable in the solid state, but partial loss of CO was observed in solution over time.

^{1}H NMR (500 MHz, toluene-d_8): δ 6.80 (t, $^3J_{HH}$ = 7.9, 1H, Ar), 6.61 (d, $^3J_{HH}$ = 7.9, 2H, Ar), 3.63 (app dp, $^2J_{HH}$ = 14.1, $^3J_{HH}$ = 7.2, $^2J_{PH}$ = 7.2, 2H, PC$\underline{H_a}H_b$), 1.87 – 1.94 (m, 2H, $PCH_2C\underline{H_c}H_d$), 1.78 – 1.87 (m, 2H, $PCH_a\underline{H_b}$), 1.61 – 1.72 (m, 2H, $PCH_2CH_2C\underline{H_e}H_f$), 1.32 – 1.61 (m, 16H, CH_2), 1.29 (vt, $^3J_{PH}$ = 7.6, 18H, 2 × tBu), 1.11 – 1.25 (m, 4H, CH_2).

^{13}C{^{1}H} NMR (126 MHz, toluene-d_8): δ 187.2 (dt, $^1J_{RhC}$ = 41, $^2J_{PC}$ = 5, CO), 163.6 (vt, $^2J_{PC}$ = 6, ArC-O), 136.1 (dt, $^1J_{RhC}$ = 22, $^3J_{PC}$ = 6, ArC-Rh), 128.4 (s, ArCH), 107.6 (vt, $^3J_{PC}$ = 6, 2 × ArCH), 41.5 (vt, $^1J_{PC}$ = 11, 2 × *t*Bu{C}), 30.7 (vt, $^2J_{PC}$ = 6), 29.5 (s, CH_2), 29.4 (s, CH_2), 29.2 (s, CH_2), 28.2 (s, CH_2), 26.5 (s, 2 × *t*Bu{CH_3}), 24.1 (vt, $^3J_{PC}$ = 3, $PCH_2CH_2\underline{C}H_2$), 23.8 (vt, $^1J_{PC}$ = 13, PCH_2).

^{31}P{^{1}H} NMR (162 MHz, toluene-d_8): δ 181.0 (d, $^1J_{RhP}$ = 92).

IR (toluene): ν(CO) 2083 cm^{-1}.

Anal. Calcd for $C_{29}H_{49}Cl_2O_3P_2Rh$ (681.46 g.mol^{-1}): C, 51.11; H, 7.25; Found: C, 51.09; H, 7.31.

In situ characterisation of **Rh-15o**

This complex is unstable to vacuum but was characterised *in situ* using a sample (ca. 10 μmol) prepared in a similar manner within a J Young's valve NMR tube following removal of volatiles, addition of toluene-d_8 (0.5 mL) under argon, freeze-pump-thaw-degassing, and placing under dihydrogen (1 atm). T_1 values were subsequently determined following rapid freeze-pump-thaw-degassing and placing under argon.

^{1}H NMR (500 MHz, toluene-d_8, H_2): δ 6.94 (t, $^3J_{HH}$ = 8.0, 1H, ArH), 6.76 (d, $^3J_{HH}$ = 7.9, 2H, ArH), 1.93 – 2.04 (m, 4H, CH_2), 1.83 – 1.92 (m, 2H, CH_2), 1.17 – 1.67 (m, 22H, CH_2), 1.15 (vt, $^3J_{PH}$ = 7.1, 18H, 2 × tBu), -2.87 (br d, $^1J_{RhH}$ = 18.8, 2H, Rh-H_2).

^{13}C{^{1}H} NMR (126 MHz, toluene-d_8): 167.3 (vt, $^2J_{PC}$ = 10, Ar$\underline{C}$-O), 143.1 (dt, $^1J_{RhC}$ = 35, $^2J_{PC}$ = 10, Ar$\underline{C}$-Rh), 126.7 (s, ArCH), 104.8 (vt, $^3J_{PC}$ = 7, 2 × ArCH), 36.7 (vtd, $^1J_{PC}$

= 12, $^{2}J_{RhC}$ = 2, 2 × *t*Bu{C}), 29.0 (vt, $^{2}J_{PC}$ = 2, $PCH_2CH_2\underline{C}H_2$), 28.9 (s, CH_2), 28.7 (s, CH_2), 28.6 (s, CH_2), 28.1 (vtd, $^{1}J_{PC}$ = 9, $^{2}J_{RhC}$ = 2, PCH_2), 27.7 (s, CH_2), 26.8 (vt, $^{2}J_{PC}$ = 4, 2 × *t*Bu{CH_3}), 25.0 (vt, $^{2}J_{PC}$ = 4, $PCH_2\underline{C}H_2$).

$^{31}P\{^{1}H\}$ NMR (162 MHz, toluene-d_8): δ 198.4 (d, $^{1}J_{RhP}$ = 165).

^{1}H NMR (600 MHz, toluene, Ar, 298K, selected data): δ -2.87 (br d, $^{1}J_{RhH}$ = 18.9, 2H, Rh-H_2, T_1 = 42 ± 2 ms).

^{1}H NMR (600 MHz, toluene, Ar, 200K, selected data): δ -2.72 (br s, 2H, Rh-H_2, T_1 = 89 ± 11 ms).

Preparation of **Rh-18o**

To a solution of **Rh-19o** (20.0 mg, 29.3 μmol) in THF (2 mL) at RT was added *i*PrMgCl·LiCl (1.3 M in THF, 68 μL, 89 μmol). The resulting solution was stirred at RT for 1 h, excess MeOH added and then reduced to dryness *in vacuo*. The residue was extracted with pentane to afford the crude product on removal of volatiles, which was subsequently recrystallised by slow evaporation of $SiMe_4$ to afford **Rh-18o** as an orange crystalline solid. Yield: 16.8 mg (94%).

^{1}H NMR (600 MHz, toluene-d_8): δ 6.91 (t, $^{3}J_{HH}$ = 7.9, 1H, Ar), 6.70 (d, $^{3}J_{HH}$ = 7.9, 2H, Ar), 2.00 – 2.06 (m, 4H, CH_2), 1.73 – 1.85 (m, 4H, CH_2), 1.51 – 1.60 (m, 4H, CH_2), 1.26 – 1.51 (m, 16H, CH_2), 1.15 (vt, $^{3}J_{PH}$ = 7.2, 18H, 2 × tBu).

$^{13}C\{^{1}H\}$ NMR (151 MHz, toluene-d_8): δ 201.2 (dt, $^{1}J_{RhC}$ = 60, $^{2}J_{PC}$ = 10, CO), 168.7 (vt, $^{2}J_{PC}$ = 9, Ar$\underline{C}$-O), 145.5 (dt, $^{1}J_{RhC}$ = 26, $^{3}J_{PC}$ = 10, ArC-Rh), 128.8 (obsc, ArCH), 104.8 (vt, $^{3}J_{PC}$ = 7, 2 × ArCH), 38.1 (vt, $^{1}J_{PC}$ = 12, 2 × *t*Bu{C}), 30.6 (br s, $PCH_2\underline{C}H_2$), 29.4 (s, CH_2), 29.3 (s, CH_2), 29.24 (vt, $^{1}J_{PC}$ = 9, PCH_2), 29.16 (s, CH_2), 28.8 (s, CH_2), 26.8 (vt, $^{2}J_{PC}$ = 4, 2 × *t*Bu{CH_3}), 25.8 (vt, $^{3}J_{PC}$ = 4, $PCH_2CH_2\underline{C}H_2$).

$^{31}P\{^{1}H\}$ NMR (243 MHz, toluene-d_8): δ 201.6 (d, $^{1}J_{RhP}$ = 156).

IR (toluene): ν(CO) 1958 cm^{-1}.

Anal. Calcd for $C_{29}H_{49}O_3P_2Rh$ (610.56 $g.mol^{-1}$): C, 57.05; H, 8.09; Found: C, 57.14; H, 8.07.

*5.2.4. Synthesis of rhodium complexes of **PCP-14***

One-pot preparation of **Rh-19c**

A solution of **PCP-14'** (118.2 mg, 248 μmol) and $[Rh(COE)_2Cl]_2$ (88.9 mg, 124 μmol) in toluene (5 mL) within a reaction flask fitted with a J Young's value was freeze-pump-thaw-degassed and placed under dihydrogen (1 atm), sealed, and heated at 100 °C for 18 h. The solution was cooled to RT and cannula transferred under dihydrogen into a reaction flask fitted with a J Young's value and charged with KO*t*Bu (34.0 mg, 303 μmol). The flask was then sealed and heated at 120 °C for 2 h to generate **Rh-15c**, which was characterised *in situ*. The solution was freeze-pump-thaw degassed and placed under carbon monoxide (1 atm) resulting in immediate formation of **Rh-18c**, which was isolated by removal of the volatiles *in vacuo* and extraction of the residue with hexane. Crude **Rh-18c** obtained in this way was dissolved in toluene (5 mL) and then slowly added to a suspension of $PhICl_2$ (68.7 mg, 250 μmol) in toluene (2 mL) at -78 °C. The reaction mixture was allowed to warm to RT overnight, the volatiles removed *in vacuo*, and the resulting residue extracted with hexane to afford the crude product, which was purified by alumina chromatography in air (20% CH_2Cl_2 in hexane, R_f = 0.55) to afford analytically pure **Rh-19c.** Yield: 136.4 mg (80%). Complex **Rh-19c** is stable in the solid state, but partial loss of CO was observed in solution over time.

^{1}H NMR (600 MHz, toluene-d_8): δ 6.95 (dd, $^3J_{HH}$ = 8.5, $^3J_{HH}$ = 6.2, 1H, Ar), 6.90 (d, $^3J_{HH}$ = 7.4, 2H, Ar) 3.71 (dt, $^2J_{HH}$ = 15.6, $^2J_{PH}$ = 4.8, 2H, Ar-C$\underline{H_2}$-P), 3.00 (app ddq, $^2J_{HH}$ = 14.1, $^3J_{HH}$ = 9.2, 4.6, $^2J_{PH}$ = 4.6, 2H, PC$\underline{H_a}$H$_b$CH$_2$), 2.91 (dt, $^2J_{HH}$ = 15.6, $^2J_{PH}$ = 4.1, 2H, Ar-C$\underline{H_2}$-P), 1.84 – 1.95 (m, 2H, PCH$_2$C$\underline{H_c}$H$_d$), 1.69 – 1.78 (m, 2H, PCH$_2$CH$_2$C$\underline{H_e}$H$_f$), 1.60 – 1.68 (m, 2H, PCH$_2$CH$_c$$\underline{H_d}$), 1.25 – 1.60 (m, 22H, CH$_2$), 1.16 (br s, 18H, 2 × tBu).

^{13}C{^{1}H} NMR (151 MHz, toluene-d_8): δ 189.1 (t, $^1J_{RhC}$ = 39, $^2J_{PC}$ = 7, CO), 163.7 (d, $^1J_{RhC}$ = 21, Ar$\underline{C}$-Rh), 147.4 (vt, $^2J_{PC}$ = 8, Ar$\underline{C}$-CH$_2$), 125.6 (s, ArCH), 122.6 (vt, $^3J_{PC}$ = 9, 2 × ArCH), 38.1 (vt, $^1J_{PC}$ = 14, 2 × Ar-$\underline{C}$H$_2$-P), 34.9 (vt, $^1J_{PC}$ = 10, 2 × *t*Bu{C}), 30.9 (vt, $^2J_{PC}$ = 5, PCH$_2$$\underline{C}H_2$), 29.22 (s, CH$_2$), 29.15 (s, CH$_2$), 28.9 (s, CH$_2$), 28.6 (s, CH$_2$), 27.6 (s, 2 × *t*Bu{CH$_3$}), 26.4 (s, PCH$_2CH_2$$\underline{C}H_2$), 22.3 (vt, $^1J_{PC}$ = 11, P$\underline{C}$H$_2$CH$_2$).

^{31}P{^{1}H} NMR (243 MHz, toluene-d_8): δ 87.0 (d, $^1J_{RhP}$ = 87).

IR (toluene): ν(CO) 2069 cm^{-1}.

Anal. Calcd for $C_{31}H_{53}Cl_2OP_2Rh$ (677.52 g.mol^{-1}): C, 54.96; H, 7.89; Found: C, 54.99; H, 8.06.

In situ characterisation of **Rh-15c**

This complex is unstable to vacuum but was characterised *in situ* using a sample (ca. 10 μmol) prepared in a similar manner within a J Young's valve NMR tube following removal of volatiles, addition of toluene-d_8 (0.5 mL) under argon, freeze-pump-thaw-degassing, and placing under dihydrogen (1 atm). T_1 values were subsequently determined following rapid freeze-pump-thaw-degassing and placing under argon.

^{1}H NMR (500 MHz, toluene-d_8, H_2): δ 7.12 (d, $^3J_{HH}$ = 7.4, 2H, ArH), 7.05 (t, $^3J_{HH}$ = 7.4, 1H, ArH), 3.08 (t, $^2J_{PH}$ = 3.9, 4H, Ar-C$\underline{H_2}$-P), 1.87 – 2.00 (m, 2H, CH_2), 1.74 – 1.84 (m, 2H, CH_2), 1.17 – 1.67 (m, 24H, CH_2), 1.01 (vt, $^3J_{PH}$ = 6.5, 18H, 2 × tBu), -4.36 (br s, 2H, Rh-H_2).

^{13}C{^{1}H} NMR (126 MHz, toluene-d_8): δ 176.3 (dt, $^1J_{RhC}$ = 40, $^2J_{PC}$ = 6, Ar$\underline{C}$-Rh), 151.6 (vtd, $^2J_{PC}$ = 12, $^2J_{RhC}$ = 3, , Ar$\underline{C}$-CH_2), 124.1 (s, ArCH), 120.7 (vt, $^3J_{PC}$ = 10, 2 × ArCH), 39.9 (vt, $^1J_{PC}$ = 10, $^2J_{RhC}$ = 4, 2 × Ar-$\underline{C}H_2$-P), 31.9 (vt, $^1J_{PC}$ = 11, 2 × *t*Bu{C}), 29.5 (vt, $^2J_{PC}$ = 4, $PCH_2\underline{C}H_2$), 29.2 (s, CH_2), 29.0 (s, CH_2), 28.6 (s, CH_2), 28.4 (vt, $^2J_{PC}$ = 3, 2 × *t*Bu{CH_3}), 27.7 (s, CH_2), 25.6 (vt, $^2J_{PC}$ = 4, $PCH_2CH_2\underline{C}H_2$), 22.9 (vt, $^1J_{PC}$ = 8, PCH_2).

^{31}P{^{1}H} NMR (162 MHz, toluene-d_8): δ 70.4 (d, $^1J_{RhP}$ = 153).

^{1}H NMR (600 MHz, toluene-d_8, Ar, 298K, selected data): δ -4.36 (br d, $^1J_{RhH}$ = 17.9, 2H, Rh-H_2, T_1 = 74 ± 5 ms).

^{1}H NMR (600 MHz, toluene-d_8, Ar, 200K, selected data): δ -4.26 (br m, 2H, Rh-H_2, T_1 = 117 ± 15 ms).

Preparation of **Rh-18c**

To a solution of **Rh-19c** (20.0 mg, 29.5 μmol) in THF (2 mL) at RT was added *i*PrMgCl·LiCl (1.3 M in THF, 68 μL, 89 μmol). The resulting solution was stirred at RT for 1 h, excess MeOH added and then reduced to dryness *in vacuo*. The residue was extracted with pentane to afford the crude product on removal of volatiles,

which was subsequently recrystallised by slow evaporation of $SiMe_4$ to afford **Rh-18c** as an orange crystalline solid. Yield: 15.2 mg (85%).

^{1}H NMR (600 MHz, toluene-d_8): δ 7.06 (d, $^3J_{HH}$ = 7.3, 2H, Ar), 7.02 (dd, $^3J_{HH}$ = 8.6, $^3J_{HH}$ = 8.2, 1H, Ar) 3.19 (dt, $^2J_{HH}$ = 16.3, $^2J_{PH}$ = 3.4, 2H, Ar-C$\underline{H_2}$-P), 3.15 (dt, $^2J_{HH}$ = 16.5, $^2J_{PH}$ = 4.2, 2H, Ar-C$\underline{H_2}$-P), 2.10 – 2.01 (m, 2H, CH_2), 1.77 – 1.36 (m, 26H, CH_2), 1.00 (vt, , $^3J_{PH}$ = 6.6, 18H, 2 × tBu).

^{13}C{^{1}H} NMR (151 MHz, toluene-d_8): δ 201.5 (t, $^1J_{RhC}$ = 41, $^2J_{PC}$ = 12, CO), 179.4 (d, $^1J_{PC}$ = 29, Ar$\underline{C}$-Rh), 152.2 (vt, $^2J_{PC}$ = 12, Ar$\underline{C}$-CH_2), 125.7 (s, ArCH), 120.5 (vt, $^3J_{PC}$ = 9, 2 × ArCH), 41.3 (vt, $^1J_{PC}$ = 12, 2 × Ar-$\underline{C}H_2$-P), 32.7 (vt, $^1J_{PC}$ = 11, 2 × *t*Bu{C}), 30.5 (vt, $^2J_{PC}$ = 4, $PCH_2\underline{C}H_2$), 29.4 (s, CH_2), 29.2 (s, CH_2), 29.0 (s, CH_2), 28.52 (vt, $^2J_{PC}$ = 4, 2 × *t*Bu{CH_3}), 28.47 (s, CH_2), 26.4 (vt, $^2J_{PC}$ = 4, $PCH_2CH_2\underline{C}H_2$), 24.2 (vt, $^1J_{PC}$ = 9, P$\underline{C}H_2CH_2$).

^{31}P{^{1}H} NMR (243 MHz, toluene-d_8): δ 75.0 (d, $^1J_{RhP}$ = 146).

IR (toluene): ν(CO) 1939 cm^{-1}.

Anal. Calcd for $C_{31}H_{53}OP_2Rh$ (606.62 g mol^{-1}): C, 61.38; H, 8.81; Found: C, 61.34; H, 8.74.

*5.2.5. Selected data for reactions of **M-15o,c** with TBE*

In situ characterisation of **Rh-20o**

To a solution of **Rh-15o** (*ca.* 10 μmol) in toluene-d_8 (0.5 mL) in a J Young NMR tube was added TBE (7 μL, 0.05 mmol). The solution was heated at reflux at 120 °C overnight to give *ca.* 90% of **Rh-20o** by ^{31}P NMR spectroscopy.

^{1}H NMR (300 MHz, toluene-d_8, selected data): δ 6.94 (t, $^3J_{HH}$ = 7.8, 1H, Ar), 6.79 (br d, $^3J_{HH}$ = 7.8, 2H, Ar), 4.19 – 4.06 (m, 1H, CH{alkene}), 3.53 (br q, $^3J_{HH}$ = 10.7, 1H, CH{alkene}), 1.22 – 1.18 (m, 9H, P*t*Bu), 1.17 – 1.13 (m, 9H, P*t*Bu).

^{13}C{^{1}H} NMR (75 MHz, toluene-d_8, selected data): δ 67.2 (d, $^1J_{RhC}$ = 6, CH{alkene}), 64.4 (vt, $^2J_{PC}$ = 7, CH{alkene}), 27.1 (d, $^2J_{PC}$ = 5, C{*t*Bu}), 26.7 (d, $^2J_{PC}$ = 6, C{*t*Bu}).

^{31}P{^{1}H} NMR (121 MHz, toluene-d_8): δ 200.1 (dd, $^2J_{PP}$ = 256, $^1J_{RhP}$ = 158), 197.0 (dd, $^2J_{PP}$ = 256, $^1J_{RhP}$ = 159).

In situ characterisation of **Rh-21o**

A solution of **Rh-20o** (*ca.* 10 μmol) in toluene-d_8 (0.5 mL) in a J Young NMR tube was freeze-pump-thaw degassed and placed under an atmosphere of CO (1 atm), which resulted in immediate (<5 min) conversion to **Rh-21o** by ^{31}P NMR spectroscopy.

^{1}H NMR (300 MHz, toluene-d_8, selected data): δ 6.95 (t, $^{3}J_{HH}$ = 7.9, 1H, Ar), 6.72 – 6.66 (m, 2H, Ar), 5.70 (dt, $^{3}J_{HH}$ = 15.0, 6.9, 1H, CH{alkene}), 5.50 (dt, $^{3}J_{HH}$ = 15.0, 6.3, 1H, CH{alkene}), 1.22 – 1.18 (br vt, $^{3}J_{PH}$ = 7.8, 18H, 2 × P*t*Bu overlapping).

^{31}P{^{1}H} NMR (121 MHz, toluene-d_8): δ 206.9 (dd, $^{2}J_{PP}$ = 302, $^{1}J_{RhP}$ = 156), 203.9 (dd, $^{2}J_{PP}$ = 302, $^{1}J_{RhP}$ = 157).

In situ characterisation of **Rh-22o**

A solution of **Rh-21o** (*ca.* 10 μmol) in toluene (2 mL) was added to a suspension of $PhICl_2$ (3.0 mg, 11 μmol) in toluene at -78 °C. The reaction was allowed to warm to room temperature and the volatiles were removes *in vacuo*. The crude was purified by flash column chromatography (50% DCM/hexane, R_f = 0.55) to afford **Rh-22o** as a light yellow oil. Yield 4.4 mg (*ca.* 64%, *ca.* 80% purity by ^{31}P NMR spectroscopy).

^{1}H NMR (300 MHz, toluene-d_8, selected data): δ 6.85 (t, $^{3}J_{HH}$ = 8.1, 1H, Ar), 6.75 – 6.60 (m, 2H, Ar), 5.42 – 5.32 (m, 1H, CH{alkene}), 5.08 (br t, $^{3}J_{HH}$ = 13.0, 1H, CH{alkene}), 3.49 – 3.38 (m, 1H, PC$\underline{H}_a$H$_b$), 3.34 – 3.19 (m, 1H, PC$\underline{H}_c$H$_d$), 1.44 (d, $^{3}J_{PH}$ = 14.1, 9H, P*t*Bu), 1.34 (d, $^{3}J_{PH}$ = 14.1, 9H, P*t*Bu).

^{31}P{^{1}H} NMR (121 MHz, toluene-d_8): δ 206.9 (dd, $^{2}J_{PP}$ = 302, $^{1}J_{RhP}$ = 156), 203.9 (dd, $^{2}J_{PP}$ = 302, $^{1}J_{RhP}$ = 157).

In situ characterisation of **Rh-20c**

To a solution of **Rh-15c** (*ca.* 10 μmol) in toluene (0.5 mL) in a J Young NMR tube equipped with a C_6D_6 capillary was added TBE (7 μL, 0.05 mmol). The solution was heated at reflux at 120 °C overnight to give *ca.* 90% of **Rh-20o** by ^{31}P NMR spectroscopy.

^{1}H NMR (400 MHz, toluene-d_0, selected data): δ 5.15 – 4.95 (m, 1H, CH{alkene}), 4.65 (br q, $^{3}J_{HH}$ = 9.6, 1H, CH{alkene}), 0.95 (d, $^{3}J_{PH}$ = 13.0, 9H, P*t*Bu), 0.86 (d, $^{3}J_{PH}$ = 12.0, 9H, P*t*Bu).

^{31}P{^{1}H} NMR (162 MHz, toluene-d_0): δ 97.5 (dd, $^{2}J_{PP}$ = 305, $^{1}J_{RhP}$ = 155), 54.5 (dd, $^{2}J_{PP}$ = 305, $^{1}J_{RhP}$ = 146).

In situ characterisation of **Ir-23c**

A solution of **Ir-15c** (*ca.* 10 μmol) in toluene (0.5 mL) was placed in a J. Young NMR tube equipped with a C_6D_6 capillary under an atmosphere of H_2 (1 atm). The solution was degassed and TBE (6 μL, 0.05 mmol) was immediately added. The reaction mixture was heated at 120 °C overnight, affording a 3:1 mixture of **Ir-23o** and **Ir-20o**.

^{1}H NMR (300 MHz, toluene-d_0, selected data): δ 4.57 (q, $^{3}J_{HH}$ = 8.6, 1H , allyl), 3.77 (t, $^{3}J_{HH}$ = 7.0, 1H, allyl), 0.96 (d, $^{3}J_{HH}$ = 12.8, 9H, P*t*Bu), 0.82 (d, $^{3}J_{PH}$ = 11.0, 9H, P*t*Bu), -11.60 (dd, $^{2}J_{PH}$ = 22.4, 10.0, 1H, IrH).

^{31}P{^{1}H} NMR (162 MHz, toluene-d_0): δ 86.9 (d, $^{2}J_{PP}$ = 344), 34.7 (d, $^{2}J_{PP}$ = 344).

In situ characterisation of **Ir-20o** and **Ir-23o**

A solution of **Ir-15o** (*ca.* 9 μmol) in toluene (0.5 mL) was placed in a J. Young NMR tube equipped with a C_6D_6 capillary under an atmosphere of H_2 (1 atm). The solution was degassed and TBE (6 μL, 0.05 mmol) was immediately added. The reaction mixture was heated at 120 °C overnight, affording a 3:1 mixture of **Ir-23o** and **Ir-20o**.

Ir-20o

^{31}P{^{1}H} NMR (121 MHz, toluene-d_0): δ 179.9 (d, $^{2}J_{PP}$ = 265), 172.0 (d, $^{2}J_{PP}$ = 265).

Ir-23o

^{1}H NMR (300 MHz, toluene-d_0, selected data): δ 4.72 (q, $^{3}J_{HH}$ = 9.0, 1H, allyl), 4.05 (t, $^{3}J_{HH}$ = 6.7, 1H, allyl), 3.73 – 3.54 (m, 1H, allyl), -11.71 (dd, $^{2}J_{PH}$ = 23.4, 13.7, 1H, IrH).

^{31}P{^{1}H} NMR (121 MHz, toluene-d_0): δ 191.2 (d, $^{2}J_{PP}$ = 362), 147.8 (d, $^{2}J_{PP}$ = 362).

5.2.6. Method for the measurement of IR data

All IR spectra were recorded using a Bruker Alpha Platinum ATR FT-IR spectrometer at RT. All measurements in the solid state were recorded in air. The high valent carbonyl complexes [M(pincer)Cl_2(CO)] (M = Rh, Ir; pincer = PCP-14, POCOP-14) are sufficiently stable in solution to be analysed in air; the low valent carbonyl complexes [M(pincer)(CO)] (M = Rh, Ir; pincer = PCP-14, POCOP-14, PCP-*t*Bu, POCOP-*t*Bu) are not and data were collected under an argon atmosphere using the experimental setup outlined in the figure below, using a right angle Rotaflo stopcock adapter which was attached to the IR spectrometer over the ATR crystal using adhesive tack and connected to a Schlenk line. Solution-phase data were collected in toluene using the "drop method", whereby a drop of the desired solution (either prepared or generated by addition of a drop of solvent to the solid analyte on the ATR crystal) is placed directly onto the ATR crystal and the reflective anvil is not employed; reflection of the incident radiation from the inner surface of the droplet instead enables collection of high-quality data.

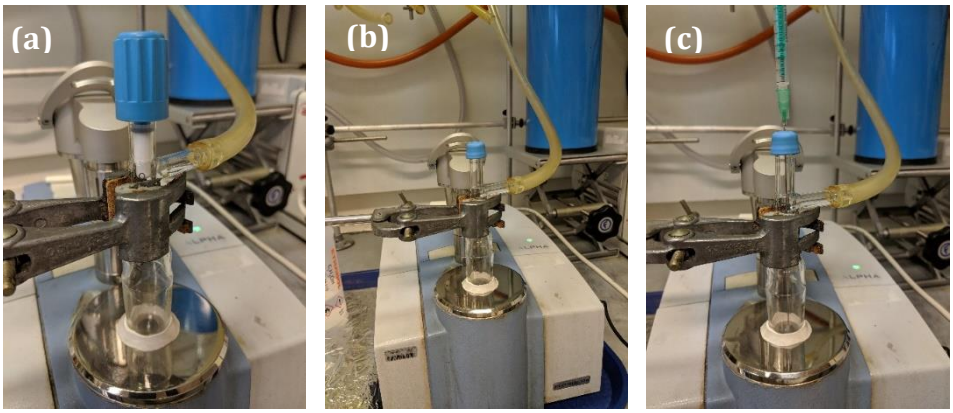

ATR-IR setup under argon atmosphere: (a) The atmosphere within can subjected to vacuum and cycled to the desired gas, but care was taken to adapt the overpressure in the Schlenk line to a minimum above atmospheric pressure so as to not put unnecessary strain on the seal; (b) The Rotaflo adapter can be fitted with a rubber septum and; (c) the background or sample solution to be measured can be transferred anaerobically onto the ATR crystal.

5.3. Chapter 4

5.3.1. Transmetallation reactions on rhodium complexes

Preparation of **Rh-24o**

A solution of Ar'CCH (188 mg, 876 μmol, 4.5 eq) in THF (2 mL) was treated with *i*PrMgCl·LiCl (0.59 mL, 1.3 M, 0.77 mmol, 4 eq) and heated at 80 °C for 30 minutes. The solution was allowed to cool to room temperature and was added to a solution of **Rh-19o** (149 mg, 219 μmol, 1 eq) in THF (1 mL). The reaction mixture was left to stir at room temperature for 18 h. In air, the excess Grignard was quenched with water (0.2 mL) and the volatiles were removed in vacuo. The crude was extracted with hexane (3 × 3 mL) and dried. Purification by silica chromatography afforded the title compound as a colourless oil. Yield 191.4 mg (84%).

^{1}H NMR (600 MHz, toluene-d_8): δ 7.32 (d, $^{4}J_{HH}$ = 1.8, 4H, 3,5-*t*Bu$_2$C$_6$H$_3$), 7.28 (t, $^{4}J_{HH}$ = 1.8, 2H, 3,5-*t*Bu$_2$C$_6$H$_3$), 6.72 (t, $^{3}J_{HH}$ = 8.0, 1H, RhC$_6$H$_3$), 6.57 (d, $^{3}J_{HH}$ = 8.0, 2H, RhC$_6$H$_3$), 4.05 (app dp, $^{2}J_{HH}$ = 13.4, J = 7, 2H, PCH$_2$), 2.31 – 2.21 (m, 2H, PCH$_2$), 1.98 – 1.88 (m, 2H, CH$_2$), 1.87 – 1.77 (m, 2H, CH$_2$), 1.70 – 1.52 (m, 8H, CH$_2$), 1.46 (vt, J_{PH} = 7.6, 18H, P*t*Bu), 1.52 – 1.39 (m, 8H, CH$_2$), 1.35 – 1.28 (m, 2H, CH$_2$), 1.26 (s, 36H, 3,5-*t*Bu$_2$C$_6$H$_3$), 1.24 – 1.17 (m, 2H, CH$_2$).

^{13}C{^{1}H} NMR (151 MHz, toluene-d_8): δ 188.9 (dt, $^{1}J_{RhC}$ = 42, $^{2}J_{PC}$ = 5, CO),162.8 (vt, J_{PC} = 5, RhC$_6$H$_3${C}), 150.2 (s, 3,5-*t*Bu$_2$C$_6$H$_3${C}), 135.3 (dt, $^{1}J_{RhC}$ = 22, $^{2}J_{PC}$ = 5, RhC$_6$H$_3${CRh}), 128.3 (s, 3,5-*t*Bu$_2$C$_6$H$_3${CC$_2$}), 127.1 (s, RhC$_6$H$_3$), 125.5 (s, 3,5-*t*Bu$_2$C$_6$H$_3$), 119.9 (s, 3,5-*t*Bu$_2$C$_6$H$_3$), 111.6 (d, $^{2}J_{RhC}$ = 7, RhC≡C), 107.0 (vt, J_{PC} = 6, RhC$_6$H$_3$), 95.4 (dt, $^{1}J_{RhC}$ = 35, $^{2}J_{PC}$ = 15, RhC≡C), 40.2 (vt, J_{PC} = 12, P*t*Bu{C}), 34.8 (s, 3,5-*t*Bu$_2$C$_6$H$_3${C}), 31.6 (s, 3,5-*t*Bu$_2$C$_6$H$_3${CH$_3$}), 30.8 (vt, $^{2}J_{PC}$ = 5, CH$_2$), 29.64 (s, CH$_2$), 29.62 (s, CH$_2$), 29.2 (s, CH$_2$), 28.6 (s, CH$_2$), 28.0 (vt, J_{PC} = 14, PCH$_2$), 26.0 (s, P*t*Bu{CH$_3$}), 24.8 (br, CH$_2$).

^{31}P{^{1}H} NMR (243 MHz, toluene-d_8): δ 188.1 (d, $^{1}J_{RhP}$ = 92).

Anal. Calcd for C$_{61}$H$_{91}$O$_3$P$_2$Rh (1037.25 g·mol^{-1}): C, 70.64; H, 8.84; Found: C, 70.87; H, 9.15.

IR (ATR): ν(C≡C) 2105 cm^{-1}, ν(C≡O) 2066 cm^{-1}.

Preparation of **Rh-24c**

A solution of Ar'CCH (14.2 mg, 66.4 μmol, 4.5 eq) in THF (1 mL) was treated with *i*PrMgCl·LiCl (45 μL, 1.3 M, 59 μmol, 4 eq) and heated at 50 °C for 30 minutes. The solution was allowed to cool to room temperature and was added to a solution of **Rh-19c** (10.0 mg, 14.8 μmol, 1 eq) in THF (1 mL). The reaction mixture was left to stir at room temperature for 18 h. In air, the excess Grignard was quenched with excess water and the volatiles were removed in vacuo. The crude was extracted with hexane (3 × 1 mL) and dried. Purification by silica chromatography afforded the title compound as a colourless oil. Yield 14.0 mg (91%).

^{1}H NMR (400 MHz, $CDCl_3$): δ 7.14 (t, $^4J_{HH}$ = 1.8, 2H, 3,5-*t*Bu$_2$C$_6$H$_3$), 7.03 (d, $^4J_{HH}$ = 1.8, 4H, 3,5-*t*Bu$_2$C$_6$H$_3$), 6.88 (d, $^3J_{HH}$ = 7.4, 2H, RhC$_6$H$_3$), 6.80 (t, $^3J_{HH}$ = 7.4, 1H, RhC$_6$H$_3$), 3.96 (d vt, $^2J_{HH}$ = 15.5, $^2J_{PH}$ = 4.9, 2H, ArCH$_2$P), 3.37 – 3.25 (m, 2H, PCH$_a$H$_b$), 3.27 (d vt, $^2J_{HH}$ = 15.5, $^2J_{PH}$ = 6.0, 2H, ArCH$_2$P), 2.18 – 2.07 (m, 2H, PCH$_a$H$_b$), 2.06 – 1.91 (m, 2H, CH$_2$), 1.89 – 1.78 (m, 2H, CH$_2$), 1.78 – 1.67 (m, 2H, CH$_2$), 1.67 – 1.50 (m, 4H, CH$_2$), 1.38 (vt, J_{PH} = 7.0, 18H, P*t*Bu), 1.42 – 1.19 (m, 14H, CH$_2$), 1.26 (s, 36H, 3,5-*t*Bu$_2$C$_6$H$_3$).

^{31}P{^{1}H} NMR (162 MHz, $CDCl_3$): δ 74.1 (d, $^1J_{RhP}$ = 88).

IR (ATR): ν(C≡C) 2053 cm^{-1}, ν(C≡O) 2066 cm^{-1}.

5.3.2. Transmetallation reactions on iridium complexes

Preparation of **Ir-24o**

A solution of Ar'CCH (37.0 mg, 173 μmol, 4.5 eq) in THF (1 mL) was treated with *i*PrMgCl·LiCl (0.12 mL, 1.3 M, 0.16 mmol, 4 eq) and heated at 80 °C for 30 minutes. The solution was allowed to cool to room temperature and was added to a solution of **Ir-19o** (29.6 mg, 38.4 μmol, 1 eq) in THF (1 mL). The reaction mixture was stirred at 120 °C for 2 days. In air, the excess Grignard was quenched with water (0.2 mL) and the volatiles were removed in vacuo. The crude was extracted with hexane (3 × 3 mL) and dried. Purification by silica chromatography afforded the title compound as a colourless oil. Yield 22.0 mg (51%).

^{1}H NMR (600 MHz, toluene-d_8): δ 7.29 (d, $^4J_{HH}$ = 1.9, 4H, 3,5-*t*Bu$_2$C$_6$H$_3$), 7.27 (t, $^4J_{HH}$ = 1.9, 2H, 3,5-*t*Bu$_2$C$_6$H$_3$), 6.74 (t, $^3J_{HH}$ = 8.0, 1H, IrC$_6$H$_3$), 6.59 (d, $^3J_{HH}$ = 8.0, 2H,

IrC_6H_3), 4.09 (app dp, $^2J_{HH}$ = 14.1, J = 7, 2H, PCH_2), 2.33 – 2.25 (m, 2H, PCH_2), 2.03 – 1.94 (m, 2H, CH_2), 1.85 – 1.74 (m, 2H, CH_2), 1.71 – 1.38 (m, 16H, CH_2), 1.42 (vt, J_{PH} = 7.6, 18H, P*t*Bu), 1.38 – 1.29 (m, 2H, CH_2), 1.25 (s, 36H, 3,5-$\underline{t}Bu_2C_6H_3$), 1.24 – 1.17 (m, 2H, CH_2).

$^{13}C\{^1H\}$ NMR (151 MHz, toluene-d_8): δ 173.6 (t, $^2J_{PC}$ = 3, CO), 163.4 (vt, J_{PC} = 5, $IrC_6H_3\{C\}$), 150.1 (s, 3,5-*t*$Bu_2\underline{C}_6H_3\{C\}$), 128.4 (s, 3,5-*t*$Bu_2\underline{C}_6H_3\{\underline{C}C_2\}$), 127.5 (s, IrC_6H_3), 125.8 (s, 3,5-*t*$Bu_2\underline{C}_6H_3$), 125 (obscured, $IrC_6H_3\{CIr\}$), 119.9 (s, 3,5-*t*$Bu_2\underline{C}_6H_3$), 109.2 (s, Ir$C\equiv\underline{C}$), 106.5 (vt, J_{PC} = 5, IrC_6H_3), 75.4 (t, $^2J_{PC}$ = 12, $Ir\underline{C}\equiv C$), 39.7 (vt, $^1J_{PC}$ = 15, P*t*Bu{C}), 34.8 (s, 3,5-$\underline{t}Bu_2C_6H_3\{C\}$), 31.6 (s, 3,5-$\underline{t}Bu_2C_6H_3\{CH_3\}$), 30.5 (vt, J_{PC} = 5, CH_2), 29.7 (s, CH_2), 29.6 (s, CH_2), 29.1 (s, CH_2), 28.6 (s, CH_2), 26.5 (vt, J_{PC} = 17, PCH_2), 25.9 (s, P*t*Bu{CH_3}), 24.8 (br, CH_2).

$^{31}P\{^1H\}$ NMR (162 MHz, toluene-d_8): δ 146.9 (s).

IR (ATR): ν(C≡C) 2115 cm^{-1}, ν(C≡O) 2042 cm^{-1}.

Preparation of **Ir-24c**

A solution of Ar'CCH (8.8 mg, 41 μmol, 4.5 eq) in THF (1 mL) was treated with *i*PrMgCl (18 μL, 2 M, 0.37 mmol, 4 eq) and heated at 80 °C for 30 minutes. The solution was allowed to cool to room temperature and was added to a solution of **Ir-19c** (7.0 mg, 9.1 μmol, 1 eq) in THF (1 mL). The reaction mixture was stirred at 120 °C for 2 days. In air, the excess Grignard was quenched with water (0.2 mL) and the volatiles were removed in vacuo. The crude was extracted with hexane (3 × 1 mL) and dried. Purification by silica chromatography (DCM-hexane) afforded the title compound as a colourless oil. Yield 7.7 mg (75%).

^1H NMR (400 MHz, C6D6): δ 7.38 (d, $^4J_{HH}$ = 2.0, 4H, 3,5-*t*$Bu_2C_6\underline{H}_3$), 7.33 (t, $^4J_{HH}$ = 2.0, 2H, 3,5-*t*$Bu_2C_6\underline{H}_3$), 7.05 – 6.97 (m, 3H, IrC_6H_3), 3.96 (d vt, $^2J_{HH}$ = 15.9, $^2J_{PH}$ = 5.1, 2H, $ArCH_2P$), 3.53 – 3.37 (m, 2H, $PC\underline{H}_aH_b$), 3.30 (d vt, $^2J_{HH}$ = 15.5, $^2J_{PH}$ = 3.7, 2H, $ArCH_2P$), 2.08 – 1.89 (m, 4H, alkyl), 1.89 – 1.78 (m, 2H, CH_2), 1.77 – 1.36 (m, 20H, alkyl), 1.25 (s, 54H, P*t*Bu and 3,5-$\underline{t}Bu_2C_6H_3$ overlapping).

$^{31}P\{^1H\}$ NMR (162 MHz, toluene-d_8): δ 38.5 (s).

IR (ATR): ν(C≡C) 2108 cm^{-1}, ν(C≡O) 2029 cm^{-1}.

*5.3.3. Decarbonylation of **Rh-24o** with Me_3NO*

Preparation of **Rh-25o**

A solution of **Rh-24o** (135.1 mg, 130.2 μmol) and trimethylamine *N*-oxide (97.8 mg, 1.30 mmol, 10 eq) in fluorobenzene (5 mL) was heated at 85 °C for 18 h. The mixture was allowed to cool to room temperature and the volatiles were removed *in vacuo*. The crude was extracted with hexane (3 × 5 mL) and the resulting solution reduced to dryness *in vacuo* to afford **Rh-25o** as a dark red solid. Yield 125.8 mg (96%).

^{1}H NMR (600 MHz, toluene-d_8): δ 8.71 (br, 1H, 3,5-*t*Bu$_2$C$_6$H$_3$), 7.88 (br, 1H, 3,5-*t*Bu$_2$C$_6$H$_3$), 7.73 (br, 2H, 3,5-*t*Bu$_2$C$_6$H$_3$), 7.47 (br, 1H, 3,5-*t*Bu$_2$C$_6$H$_3$), 7.43 (br, 1H, 3,5-*t*Bu$_2$C$_6$H$_3$), 6.93 (t, $^{3}J_{HH}$ = 7.9, 1H, RhC$_6$H$_3$), 6.70 (d, $^{3}J_{HH}$ = 7.9, 2H, RhC$_6$H$_3$), 2.63 – 1.00 (br m, 46H, CH$_2$ + 3,5-*t*Bu$_2$C$_6$H$_3$), 1.41 (br, 9H, P*t*Bu), 1.28 (br, 18H, 3,5-*t*Bu$_2$C$_6$H$_3$), 0.79 (br, 9H, P*t*Bu).

^{13}C{^{1}H} NMR (126 MHz, toluene-d_8): δ broad.

^{31}P{^{1}H} NMR (243 MHz, toluene-d_8): δ 184.8 (d, $^{1}J_{RhP}$ = 162).

Anal. Calcd for $C_{60}H_{91}O_2P_2Rh$ (1009.24 g·mol^{-1}): C, 71.41; H, 9.09; Found: C, 71.39; H, 8.80.

IR (ATR): ν(C≡C) 2154 cm^{-1}, ν((Rh)C≡C) 1938 cm^{-1}.

The ^{13}C labelled analogue was prepared following the above procedure and using **[(POCOP)Rh(CO)(CCAr)$_2$]** (20.6 mg, 19.8 μmol) and trimethylamine *N*-oxide (14.9 mg, 198 μmol, 10 eq). Yield 19.2 mg (96%).

^{13}C{^{1}H} NMR (151 MHz, toluene-d_8, 298 K, selected data): δ 83.0 (br d, $^{1}J_{CC}$ = 156, (Rh)C≡C–C≡C), 70.9 (br d, $^{1}J_{CC}$ = 156, (Rh)C≡C–C≡C).

^{13}C{^{1}H} NMR (151 MHz, toluene-d_8, 233 K, selected data): δ 82.9 (d, $^{1}J_{CC}$ = 152, (Rh)C≡C–C≡C), 71.1 (dd, $^{1}J_{CC}$ = 152, $^{1}J_{RhC}$ = 4, (Rh)C≡C–C≡C).

^{31}P{^{1}H} NMR (243 MHz, toluene-d_8): δ 184.8 (d, $^{1}J_{RhP}$ = 162).

^{31}P{^{1}H} NMR (243 MHz, toluene-d_8, 233 K): δ 185.5 (d, $^{1}J_{RhP}$ = 161, $^{2}J_{PC}$ = 11).

IR (ATR): ν(C≡C) 2115 cm^{-1}, ν((Rh)C≡C) 1902 cm^{-1}.

Preparation of ***t*Bu-Rh-25o**

A solution of [(*t*Bu-POCOP)Rh(H)(Cl)] (40.0 mg, 74.5 µmol), KO*t*Bu (10.0 mg, 89.4 µmol) and diyne (31.8 mg, 74.5 µmol) in toluene was stirred for 2 h at room temperature. The volatiles were removed in vacuo and the crude was extracted with hexane (3 × 5 mL). The resulting solution was reduced to dryness in vacuo to afford the title compound as a dark red crystalline solid. Yield 63.9 mg (93%).

^{1}H NMR (500 MHz, toluene-d_8): δ 7.93 (d, $^{4}J_{HH}$ = 1.9, 2H, 3,5-*t*Bu$_2$C$_6$H$_3$), 7.61 (d, $^{4}J_{HH}$ = 1.9, 2H, 3,5-*t*Bu$_2$C$_6$H$_3$), 7.45 (t, $^{4}J_{HH}$ = 1.9, 1H, 3,5-*t*Bu$_2$C$_6$H$_3$), 7.44 (t, $^{4}J_{HH}$ = 1.9, 1H, 3,5-*t*Bu$_2$C$_6$H$_3$), 6.98 (t, $^{3}J_{HH}$ = 7.9, 1H, RhC$_6$H$_3$), 6.77 (d, $^{3}J_{HH}$ = 7.9, 2H, RhC$_6$H$_3$), 1.53 (vt, J_{PC} = 6.6, 9H, P*t*Bu), 1.29 (s, 18H, 3,5-*t*Bu$_2$C$_6$H$_3$), 1.27 (vt, J_{PC} = 6.7, 9H, P*t*Bu), 1.23 (s, 18H, 3,5-*t*Bu$_2$C$_6$H$_3$).

^{13}C{^{1}H} NMR (126 MHz, toluene-d_8): δ 169.5 (vt, J_{PC} = 7, RhC$_6$H$_3${C}), 151.3 (s, 3,5-*t*Bu$_2$C$_6$H$_3${C}), 150.8 (s, 3,5-*t*Bu$_2$C$_6$H$_3${C}), 144.1 (dt, $^{1}J_{RhC}$ = 33, $^{2}J_{PC}$ = 7, RhC$_6$H$_3${CRh}), 130.1 (s, RhC$_6$H$_3$), 128.4 (s, 3,5-*t*Bu$_2$C$_6$H$_3${CC$_2$}), 127.7 (s, 3,5-*t*Bu$_2$C$_6$H$_3$), 125.7 (s, 3,5-*t*Bu$_2$C$_6$H$_3$), 124.5 (s, 3,5-*t*Bu$_2$C$_6$H$_3${CC$_2$}), 122.7 (s, 3,5-*t*Bu$_2$C$_6$H$_3$), 122.0 (s, 3,5-*t*Bu$_2$C$_6$H$_3$), 104.2 (vt, J_{PC} = 6, RhC$_6$H$_3$), 97.1 (s, (Rh)C≡C–C≡C), 92.6 (d, $^{1}J_{RhC}$ = 10, (Rh)C≡C–C≡C), 81.6 (d, $^{2}J_{RhC}$ = 2, (Rh)C≡C–C≡C), 70.6 (d, $^{1}J_{RhC}$ =7, (Rh)C≡C–C≡C), 39.8 (vtd, J_{PC} = 6, $^{2}J_{RhC}$ = 2, P*t*Bu{C}), 39.4 (vtd, J_{PC} = 6, $^{2}J_{RhC}$ = 2, P*t*Bu{C}), 35.1 (s, 3,5-*t*Bu$_2$C$_6$H$_3${C}), 34.9 (s, 3,5-*t*Bu$_2$C$_6$H$_3${C}), 31.6 (s, 3,5-*t*Bu$_2$C$_6$H$_3${CH$_3$}), 31.4 (s, 3,5-*t*Bu$_2$C$_6$H$_3${CH$_3$}), 28.70 (vt, J_{PC} = 4, P*t*Bu{CH$_3$}), 28.65 (vt, J_{PC} = 4, P*t*Bu{CH$_3$}).

^{31}P{^{1}H} NMR (162 MHz, toluene-d_8): δ 186.5 (d, $^{1}J_{RhP}$ = 160).

Anal. Calcd for $C_{54}H_{81}O_2P_2Rh$ (927.09 g·mol^{-1}): C, 69.96; H, 8.81; Found: C, 70.04; H, 8.88.

IR (ATR): ν(C≡C) 2161 cm^{-1}, ν((Rh)C≡C) 1924 cm^{-1}.

Preparation of 1,4-bis(3,5-di-tert-butylphenyl)buta-1,3-diyne

A solution of 1,3-di-*tert*-butyl-5-ethynylbenzene (150 mg. 700 µmol), CuCl (1.4 mg, 14 µmol, 2 mol%) and piperidine (7 µL, 0.07 mmol, 10 mol%) in toluene (1 mL) was stirred at 60 °C for 18 h, in air. The volatiles were removed *in vacuo* and the crude was eluted through a short silica plug (cyclohexane). The resulting

solution was reduced to dryness *in vacuo* to afford the title compound as a white solid. Yield 138.7 mg (93%).

^{1}H NMR (500 MHz, $CDCl_3$): δ 7.43 (t, $^{4}J_{HH}$ = 1.9, 2H, C_6H_3), 7.39 (d, $^{4}J_{HH}$ = 1.9, 4H, C_6H_3), 1.32 (s, *t*Bu).

^{13}C{^{1}H} NMR (126 MHz, $CDCl_3$): δ 151.1 (s, C_6H_3{C}), 126.9 (s, C_6H_3), 123.9 (s, C_6H_3), 121.0 (s, $C_6H_3\{\underline{C}C_2\}$), 82.6 (s, Ar'$\underline{C}$), 73.0 (s, Ar'C≡$\underline{C}$), 35.0 (s, *t*Bu{C}), 31.4 (s, *t*Bu{CH_3}).

Preparation of 1,4-bis(3,5-di-tert-butylphenyl)butane

A suspension of 1,4-bis(3,5-di-tert-butylphenyl)buta-1,3-diyne (30.0 mg, 70.3 μmol) and Pd/C (15.0 mg, 14.1 μmol) in THF (2 mL) was freeze-pump-thaw degassed and placed under an atmosphere of H_2 and heated at 50 °C for 2 days. The suspension was allowed to cool to room temperature and the supernatant was collected by filtration and further extraction with THF (3 × 2 mL). The resulting solution was reduced to dryness *in vacuo* to afford the title compound as a white waxy solid. Yield 27.7 mg (91%).

^{1}H NMR (400 MHz, toluene-d_8): δ 7.36 (t, $^{4}J_{HH}$ = 1.9, 2H, C_6H_3), 7.10 (d, $^{4}J_{HH}$ = 1.9, 4H, C_6H_3), 2.64 – 2.56 (m, 4H, Ar'C$\underline{H}_2$), 1.75 – 1.65 (m, 4H, Ar'$CH_2C\underline{H}_2$), 1.32 (s, 36H, *t*Bu).

^{13}C{^{1}H} NMR (101 MHz, toluene-d_8): δ 150.7 (s, C_6H_3{C}), 142.2 (s, $C_6H_3\{\underline{C}CH_2\}$), 123.0 (s, C_6H_3), 119.8 (s, C_6H_3), 36.9 (s, 2 × Ar'$\underline{C}H_2$), 34.9 (s, *t*Bu{C}), 32.2 (s, Ar'$CH_2\underline{C}H_2$), 31.8 (s, *t*Bu{CH_3}).

*5.3.4. VT-NMR spectroscopy study of **Rh-25o** and **^{13}C-Rh-25o***

Analysis was performed using 20 mM solutions of **Rh-25o** or **^{13}C-Rh-25o** in toluene-d_8 prepared in J. Young's valve NMR tubes. Samples were equilibrated at the required temperature for a period of 10 min before spectra were acquired (^{1}H, 600 MHz; ^{31}P, 243 MHz; ^{13}C, 151 MHz).

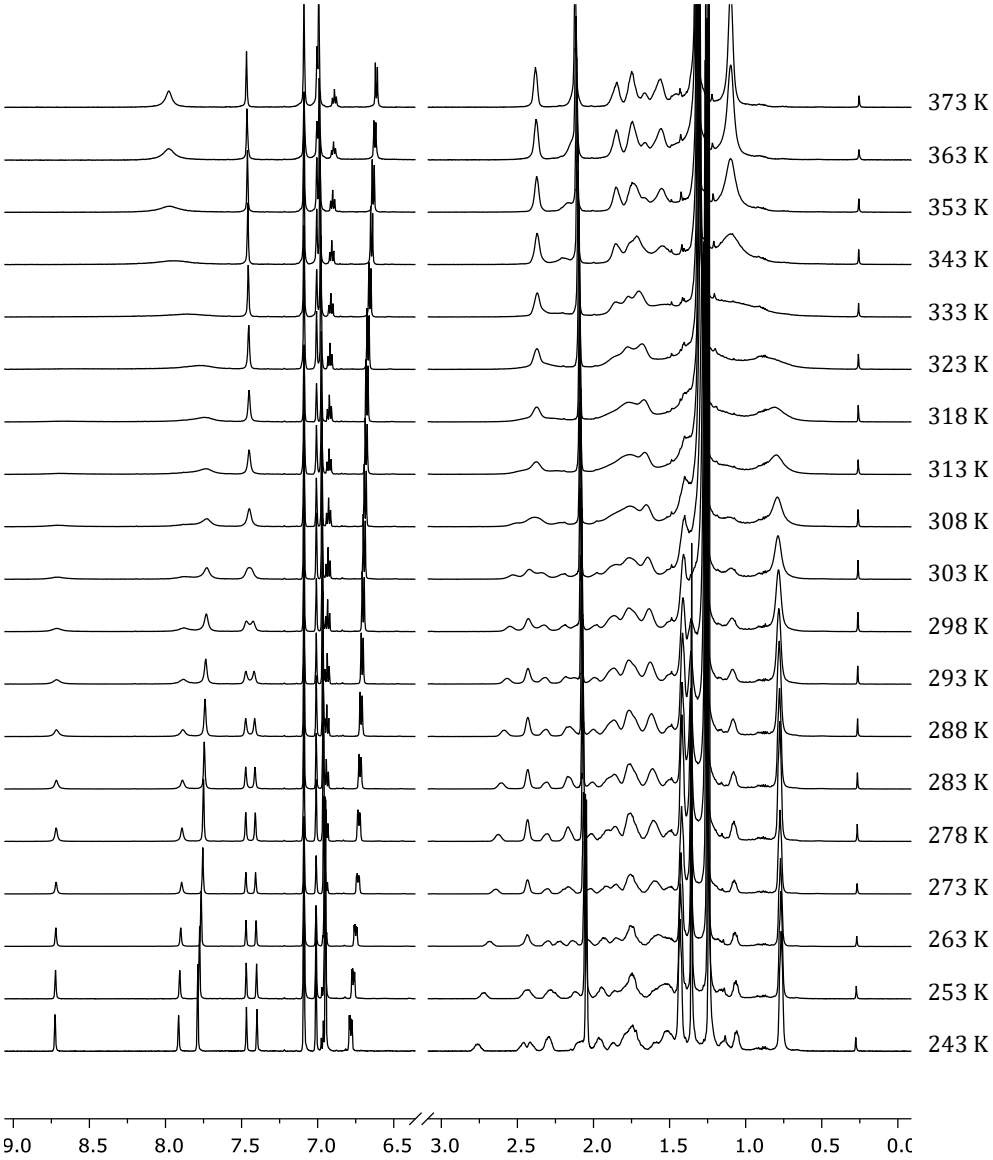

Figure 5.3. Variable-temperature ^{1}H NMR spectra of **Rh-25o** (toluene-d_8, 600 MHz).

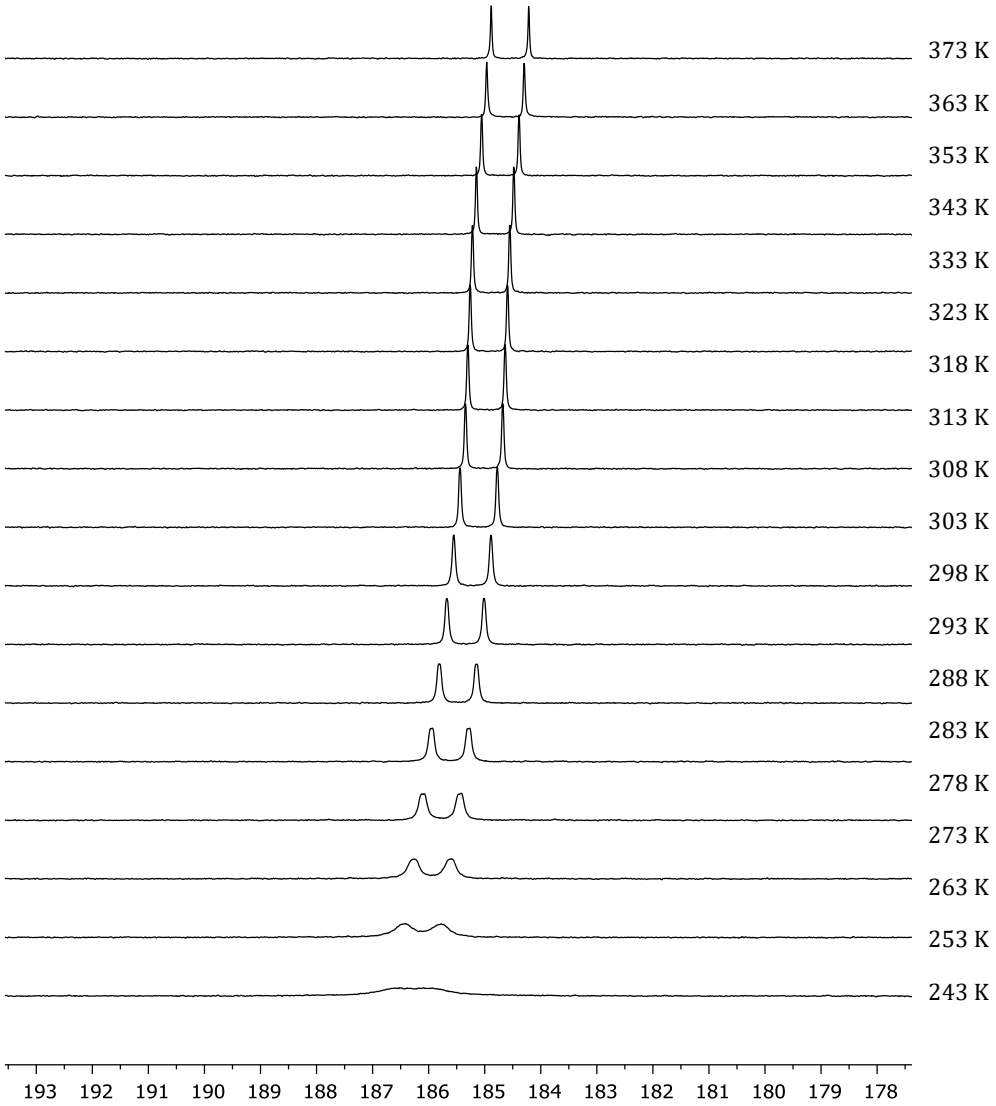

Figure 5.4. Variable-temperature $^{31}P\{^{1}H\}$ NMR spectra of **Rh-25o** (toluene-d_8, 243 MHz).

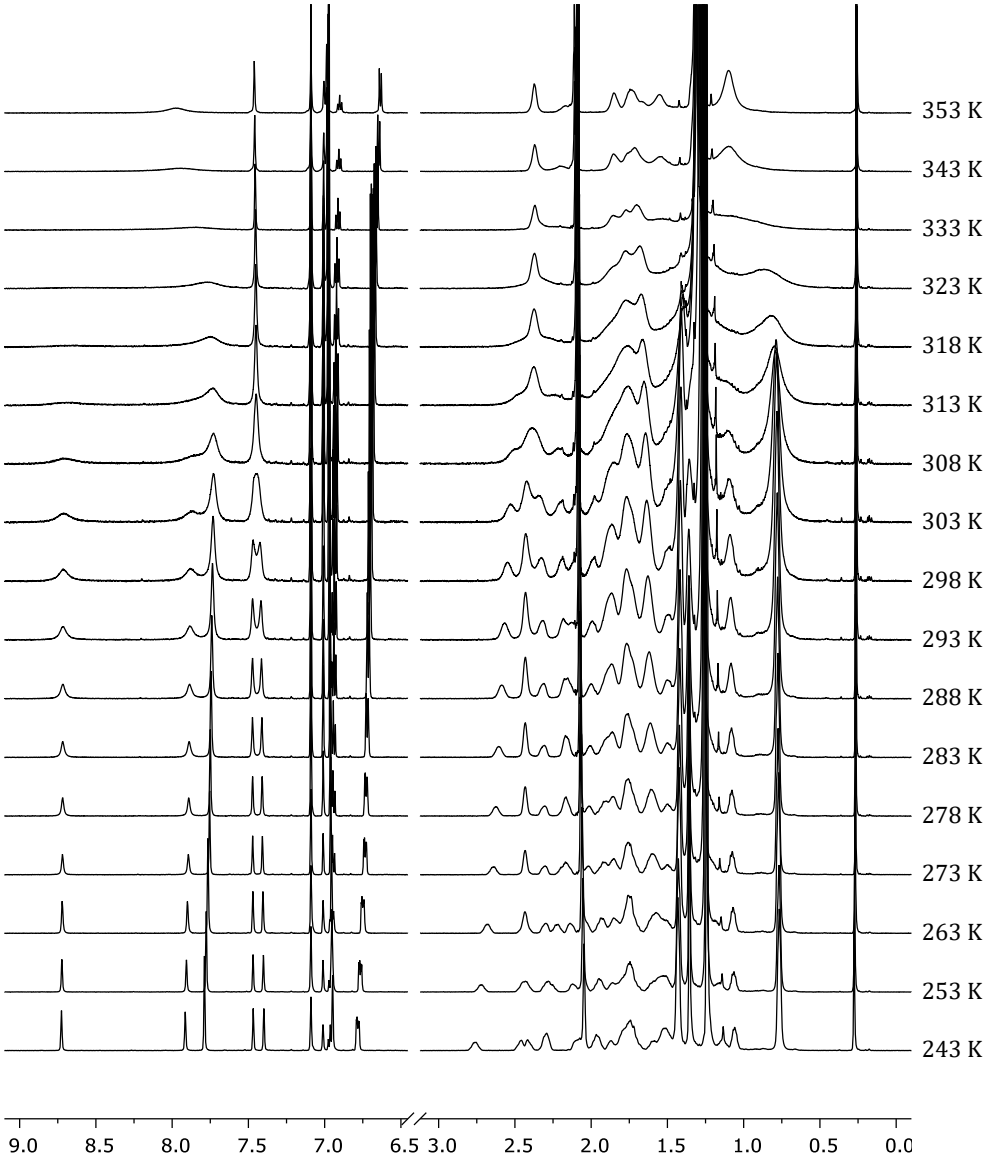

Figure 5.5. Variable-temperature ^{1}H NMR spectra of **^{13}C-Rh-25o** (toluene-d_8, 600 MHz).

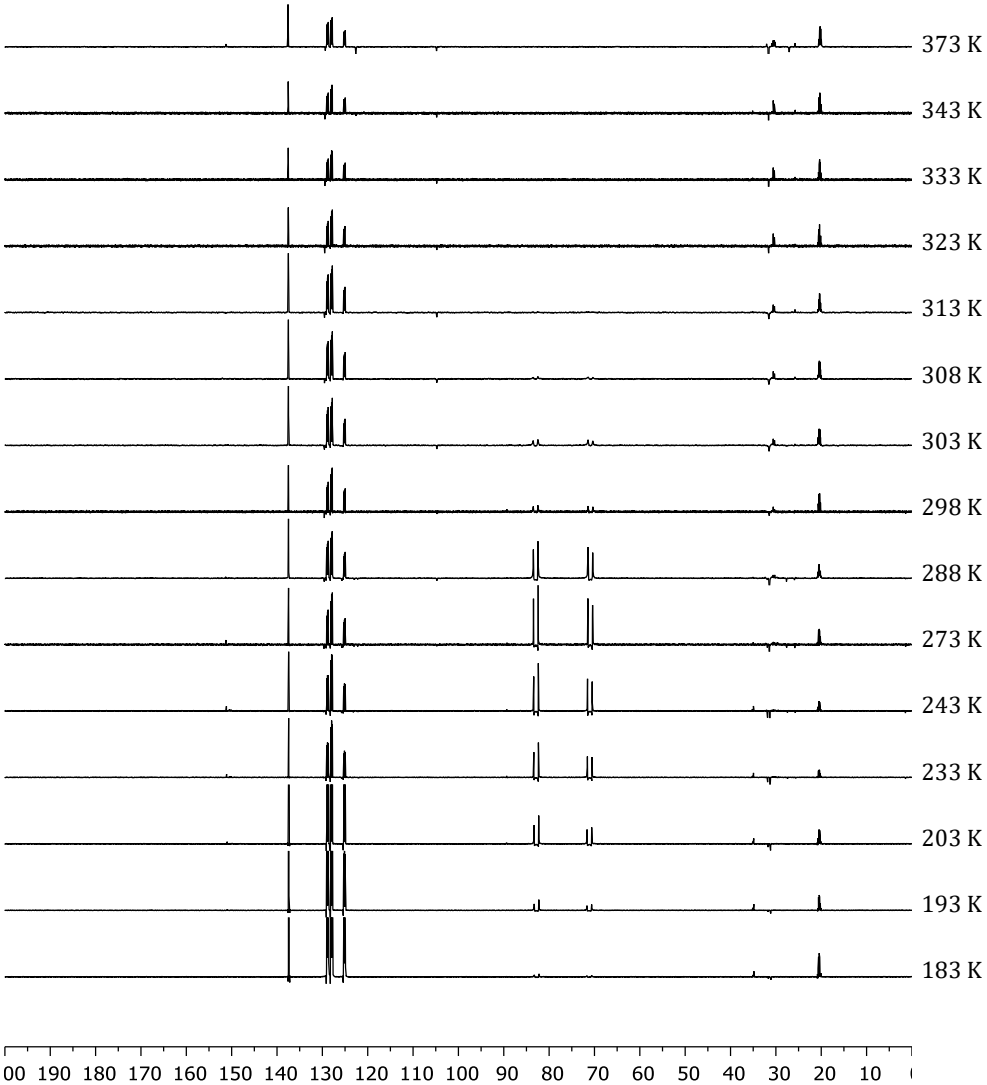

Figure 5.6. Variable temperature $^{13}C\{^{1}H\}$ APT NMR spectrum of **^{13}C-Rh-25o** (toluene-d_8, 151 MHz).

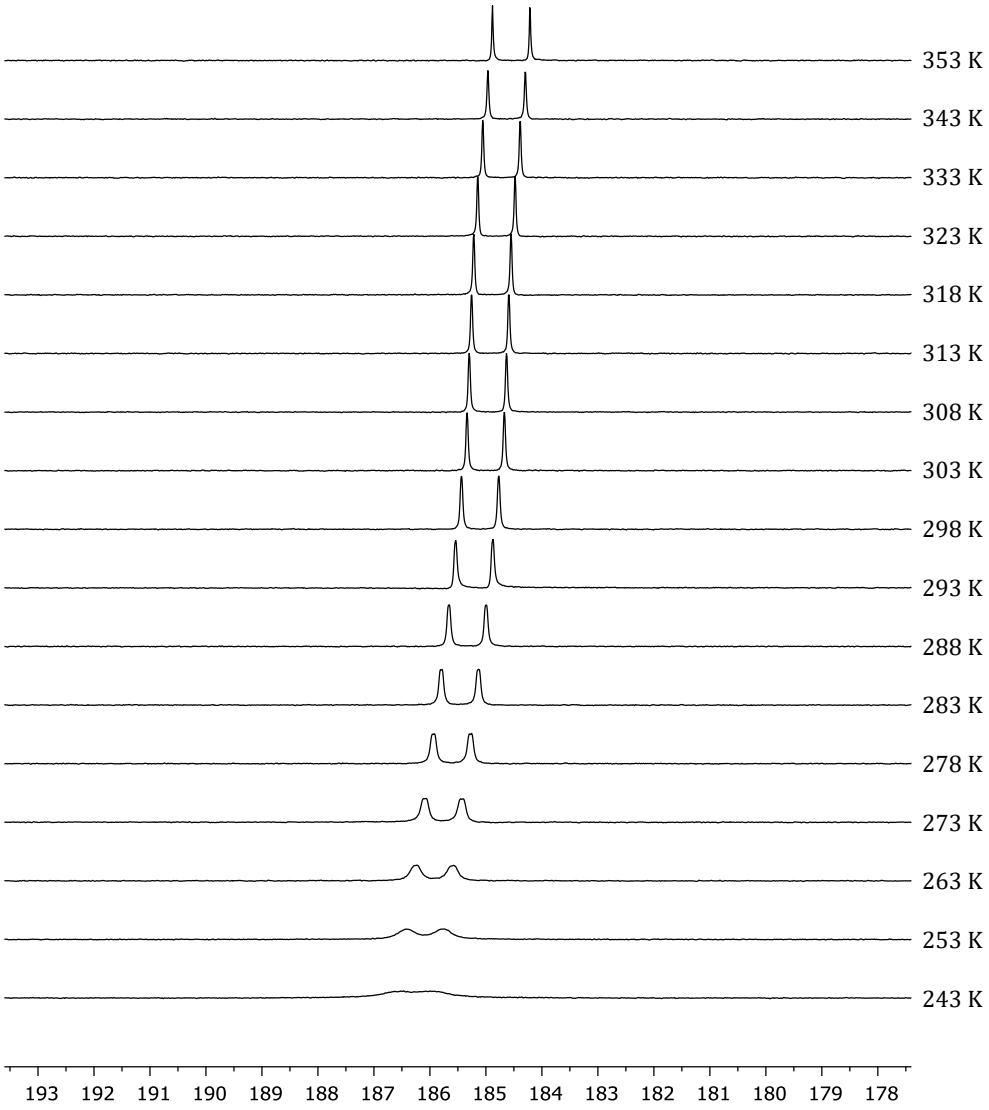

Figure 5.7. Variable-temperature $^{31}P\{^{1}H\}$ NMR spectra of **^{13}C-Rh-25o** (toluene-d_8, 243 MHz).

Exchange processes observed by ^{1}H NMR were simulated using gNMR,[1] with reference line widths estimated with MNOVA based on the pincer backbone aryl signals and coupling constants fixed following analysis of low temperature data. Activation parameters were determined using the equation $\Delta G^{\ddagger} = RT\,[\ln(k_B/h) + \ln(T/k_{exchange})]$; reported values and errors are based on a statistical analysis of the linear regression of $\ln(k_{exchange}/T) = f(1/T)$. For both **Rh-25o** and **^{13}C-Rh-25o**, the axle's aromatic region was modelled with 6 protons and 2 dynamic exchange processes for the shuttling motion and the sterically hindered rotation of Ar, with associated rate constants $k_{shuttling}$ and $k_{slowrotation}$, respectively.

[1] gNMR, v. 4.1.2; Adept Scientific: Herts, U.K.

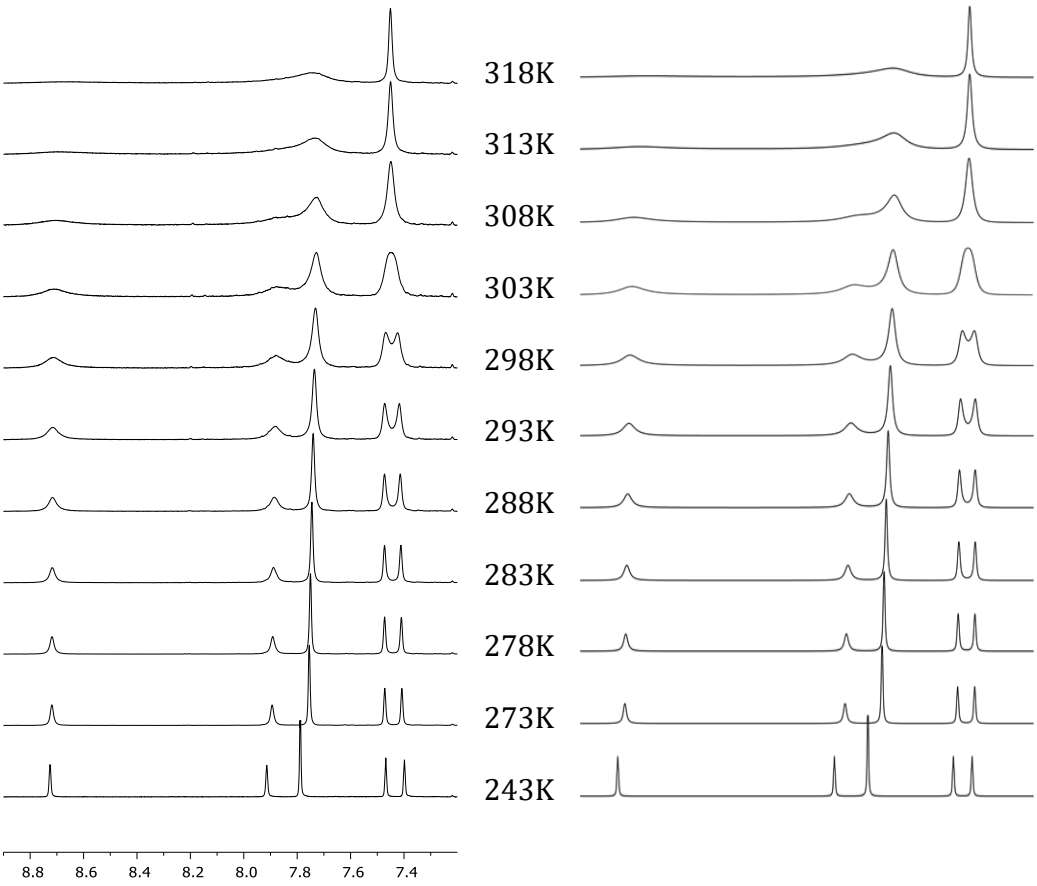

Figure 5.8. Experimental (left) and simulated (right) variable-temperature ^{1}H NMR spectra of **Rh-25o** (toluene-d_8, 600 MHz).

Table 5.1. Variable-Temperature ^{1}H NMR fitted data for **Rh-25o**.

T (K)	$\log(k_{shuttling})$	$\log(k_{slowrotation})$	$k_{shuttling}$ (s^{-1})	$k_{slowrotation}$ (s^{-1})	$\ln(k_{shuttling}/T)$	$\ln(k_{slowrotation}/T)$
273	0.4505	1.1146	2.82	13.02	-4.572	-3.043
278	0.6800	1.2936	4.79	19.66	-4.062	-2.649
283	0.9496	1.4880	8.90	30.76	-3.459	-2.219
288	1.2021	1.6423	15.93	43.88	-2.895	-1.881
293	1.4584	1.8143	28.73	65.21	-2.322	-1.503
298	1.6891	1.9638	48.88	92.00	-1.808	-1.175
303	1.9056	2.1190	80.46	131.52	-1.326	-0.835
308	2.0955	2.2339	124.59	171.36	-0.905	-0.586
313	2.3351	2.4174	216.32	261.46	-0.369	-0.180
318	2.5441	2.5439	350.03	349.86	0.096	0.095

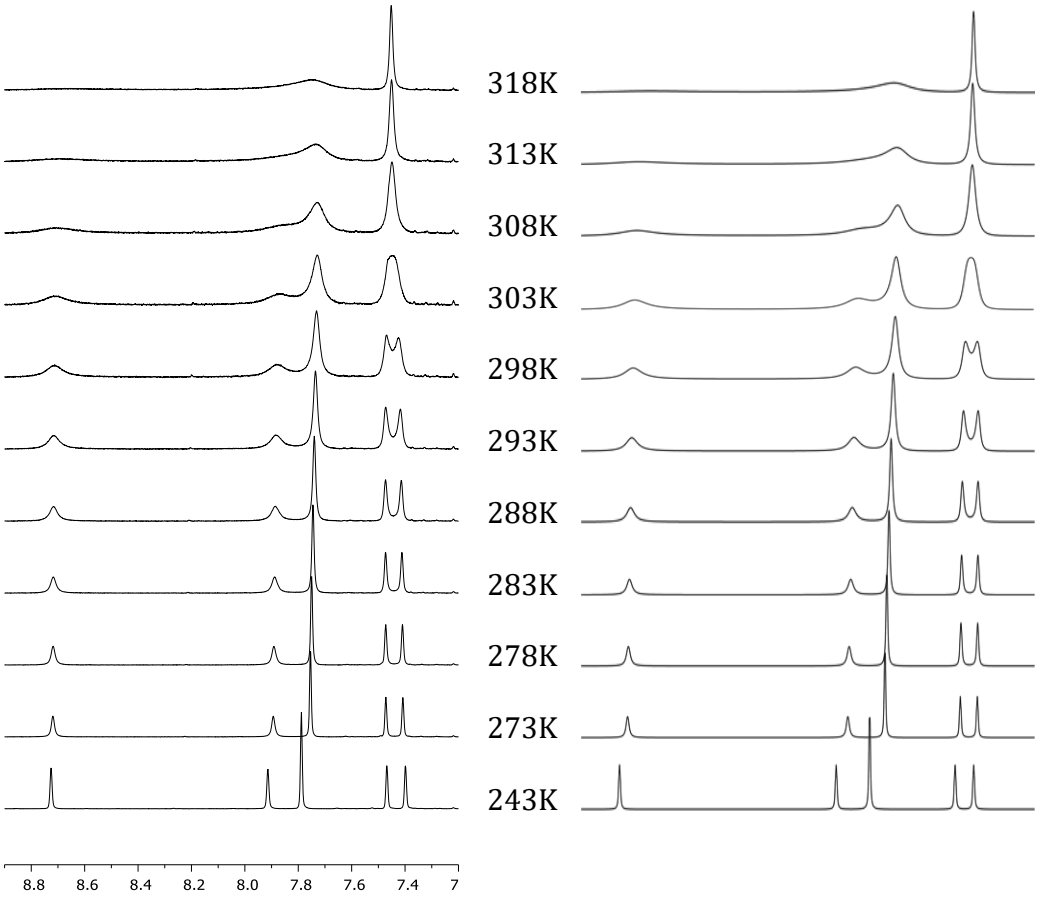

Figure 5.9. Experimental and simulated variable-temperature ^{1}H NMR spectra of **^{13}C-Rh-25o** (toluene-d_8, 600 MHz).

Table 5.2. Variable-Temperature ^{1}H NMR fitted data for **^{13}C-Rh-25o**.

T (K)	$\log(k_{shuttling})$	$\log(k_{slowrotation})$	$k_{shuttling}$ (s^{-1})	$k_{slowrotation}$ (s^{-1})	$\ln(k_{shuttling}/T)$	$\ln(k_{slowrotation}/T)$
273	0.4270	1.1189	2.67	13.15	-4.626	-3.033
278	0.6580	1.2803	4.55	19.07	-4.113	-2.680
283	0.9226	1.4576	8.37	28.68	-3.521	-2.289
288	1.1821	1.6347	15.21	43.12	-2.941	-1.899
293	1.4381	1.8014	27.42	63.30	-2.369	-1.532
298	1.6566	1.9690	45.35	93.11	-1.883	-1.163
303	1.8587	2.1104	72.23	128.94	-1.434	-0.854
308	2.0710	2.2582	117.76	181.22	-0.961	-0.530
313	2.2925	2.4098	196.11	256.92	-0.468	-0.197
318	2.5224	2.5498	332.97	354.65	0.046	0.109

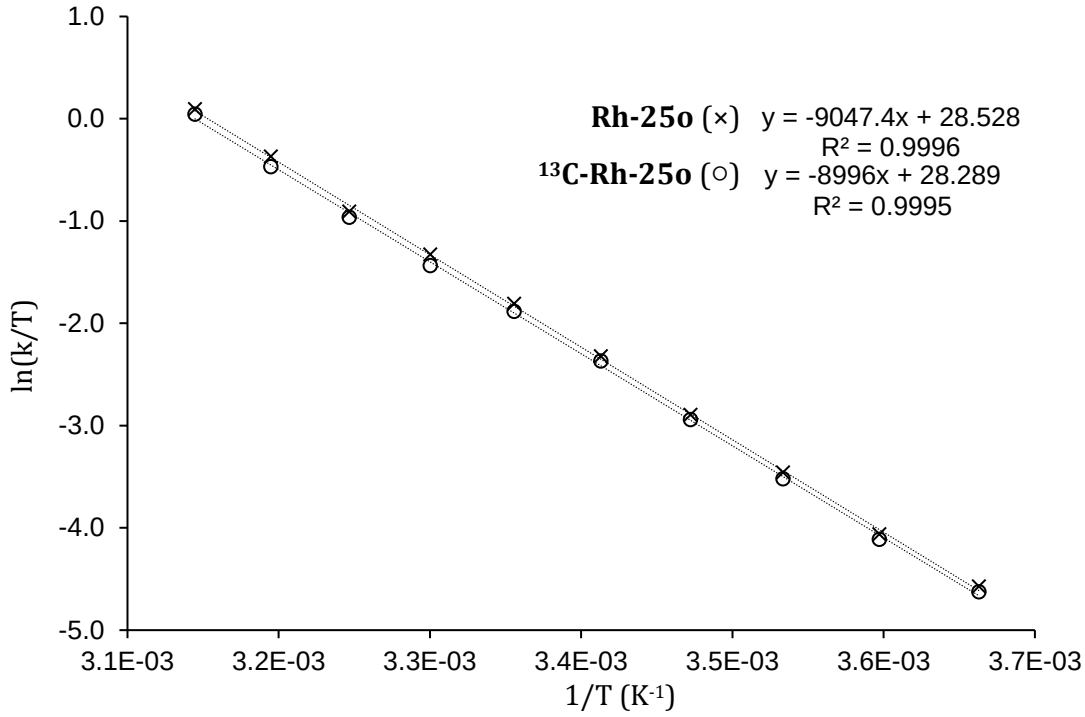

Figure 5.10. Eyring plots of the fitted rate constants for the shuttling process in **Rh-25o** and **^{13}C-Rh-25o**.

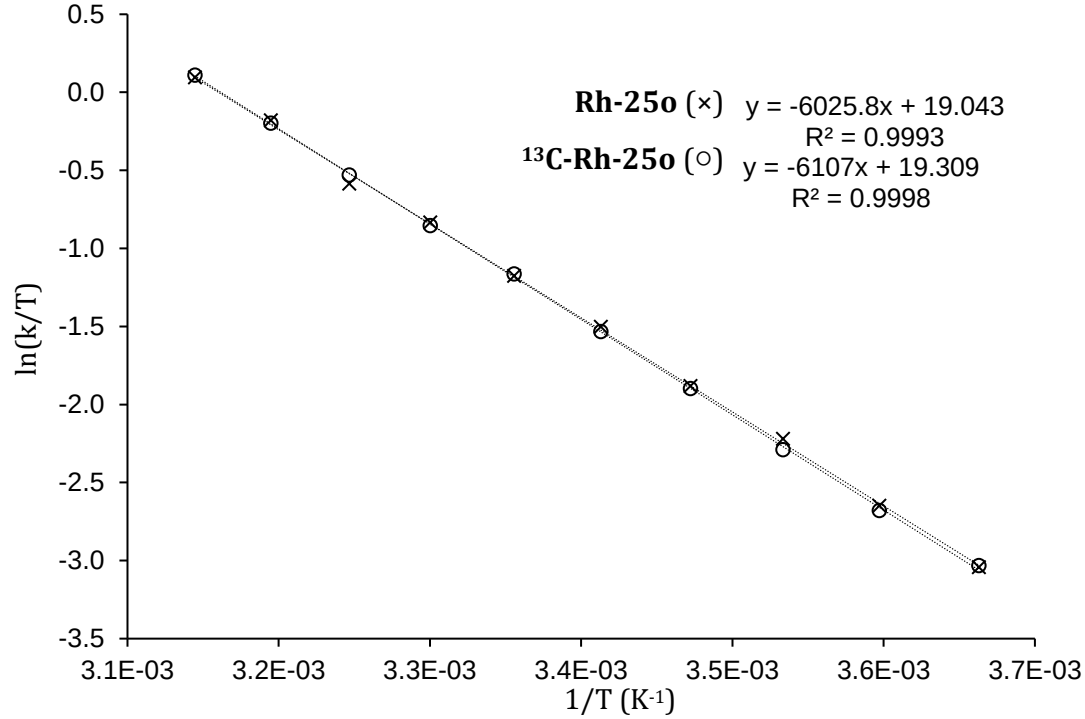

Figure 5.11. Eyring plots of the fitted rate constants for the slow rotation process in **Rh-25o** and **^{13}C-Rh-25o**.

Table 5.3. Calculated thermodynamic data for **Rh-25o** and **^{13}C-Rh-25o**.

	Shuttling			Slow rotation		
	$\Delta H^{\ddagger}$ (kJ/mol)	$\Delta S^{\ddagger}$ (J/mol/K)	$\Delta G^{\ddagger}_{298K}$ (kJ/mol)	ΔH (kJ/mol)	ΔS (J/mol/K)	$\Delta G^{\ddagger}_{298K}$ (kJ/mol)
Rh-25o	75.2 ± 0.6	40 ± 2	63 ± 1	50.1 ± 0.5	-39 ± 2	62 ± 1
^{13}C-Rh-25o	74.8 ± 0.6	38 ± 2	64 ± 1	50.8 ± 0.3	-37 ± 1	62 ± 1

*5.3.5. **Rh-26o** and equilibrium with **Rh-25o***

Preparation of **Rh-26o**

In a sealed J Young flask, a solution of **Rh-25o** (25.0 mg, 24.8 μmol) in TMS (1 mL) was freeze-pump-thaw degassed and placed under carbon monoxide. The solution was left to stand at room temperature for 30 minutes during which **Rh-26o** precipitated as a pale orange crystalline solid, then filtered. The product was dried briefly *in vacuo*. Yield 23.1 mg (90%).

For NMR characterisation, a sample was prepared similarly by dissolving an aliquot of **Rh-25o** in toluene-d_8 in a J Young NMR tube. The solution was freeze-pump-thaw degassed and placed under CO atmosphere (1atm) to afford the title compound in < 5 min.

^{1}H NMR (600 MHz, toluene-d_8, CO atm): δ 7.84 (br, 1H, 3,5-*t*Bu$_2$C$_6$H$_3$), 7.82 (d, $^{4}J_{HH}$ = 1.8, 2H, 3,5-*t*Bu$_2$C$_6$H$_3$), 7.79 (br, 1H, 3,5-*t*Bu$_2$C$_6$H$_3$), 7.44 (t, $^{4}J_{HH}$ = 1.8, 1H, 3,5-*t*Bu$_2$C$_6$H$_3$), 7.30 (t, $^{4}J_{HH}$ = 1.7, 1H, 3,5-*t*Bu$_2$C$_6$H$_3$), 6.87 (app t, $^{3}J_{HH}$ = 8, 1H, RhC$_6$H$_3$), 6.82 (d, $^{3}J_{HH}$ = 7.9, 1H, RhC$_6$H$_3$), 6.64 (d, $^{3}J_{HH}$ = 7.9, 1H, RhC$_6$H$_3$), 2.45 – 2.82 (m, 4H, CH$_2$), 1.15 – 2.35 (m, 21H, CH$_2$), 1.38 (br, 9H, 3,5-*t*Bu$_2$C$_6$H$_3$), 1.32 (br, 18H, 3,5-*t*Bu$_2$C$_6$H$_3$), 1.24 (br, 9H, 3,5-*t*Bu$_2$C$_6$H$_3$), 1.12 (d, $^{3}J_{PH}$ = 14.0, 9H, P*t*Bu), 1.07 – 0.89 (m, 3H, CH$_2$), 0.73 (d, $^{3}J_{PH}$ = 12.8, 9H, P*t*Bu).

^{13}C{^{1}H} NMR (151 MHz, toluene-d_8, CO atm): δ 164.7 (d, $^{2}J_{PC}$ = 4, RhC$_6$H$_3${C}), 164.2 (d, $^{2}J_{PC}$ = 6, RhC$_6$H$_3${C}), 151.1 (s, 3,5-*t*Bu$_2$C$_6$H$_3${C}), 150.3 (s, 3,5-*t*Bu$_2$C$_6$H$_3${C}), 137 (obscured, RhC$_6$H$_3${CRh}), 133.7 (br, 3,5-*t*Bu$_2$C$_6$H$_3$), 132.4 (s, 3,5-*t*Bu$_2$C$_6$H$_3${CC$_2$}), 126.1 (br, 3,5-*t*Bu$_2$C$_6$H$_3$), 125.9 (s, 3,5-*t*Bu$_2$C$_6$H$_3$), 125.7 (s, RhC$_6$H$_3$), 122.4 (s, 3,5-*t*Bu$_2$C$_6$H$_3$), 120.7 (s, 3,5-*t*Bu$_2$C$_6$H$_3$), 106.3 (s, (Rh)C≡C–C≡C), 105.5 (d, $^{3}J_{PC}$ = 14,

RhC_6H_3), 105.3 (d, $^3J_{PC}$ = 12, RhC_6H_3), 87.2 (d, $^1J_{RhC}$ = 14, (Rh)C≡C–C≡C), 87.1 (s, (Rh)C≡C–C≡C), 77.6 (d, $^1J_{RhC}$ = 5, (Rh)C≡C–C≡C), 40.7 (vt, J_{PC} = 6, P*t*Bu{C}), 37.6 (dd, $^1J_{PC}$ = 14, $^3J_{PC}$ = 10, P*t*Bu{C}), 35.10 (br, 3,5-*t*Bu$_2$$C_6H_3${C}), 35.05 (s, 3,5-*t*Bu$_2$$C_6H_3${C}), 34.7 (dd, $^1J_{PC}$ = 15, $^3J_{PC}$ = 7, PCH_2), 32.3 (s, CH_2), 31.9 (br, 3,5-*t*Bu$_2$$C_6H_3${$CH_3$}), 31.5 (s, 3,5-*t*Bu$_2$$C_6H_3${$CH_3$}), 31.4 (br, 3,5-*t*Bu$_2$$C_6H_3${$CH_3$}), 30.8 (s, CH_2), 30.4 (s, CH_2), 30.2 (s, CH_2), 29.6 – 29.8 (m, 2×CH_2), 29.4 (s, CH_2), 29.3 (d, $^1J_{PC}$ = 12, PCH_2), 28.4 (s, CH_2), 27.8 (s, CH_2), 27.6 (s, CH_2), 26.7 (s, CH_2), 25.9 (br, P*t*Bu{CH_3}), 25.0 (d, $^2J_{PC}$ = 6, P*t*Bu{CH_3}), 22.0 (d, J_{PC} = 4, CH_2). The carbonyl resonance could not be located, presumably due to extensive line broadening. One of the 3,5-*t*Bu$_2$$C_6H_3${$C_2$} appears to be obscured by the solvent peaks.

^{31}P{^{1}H} NMR (243 MHz, toluene-d_8, CO atm): δ 195.2 (dd, $^2J_{PP}$ = 420, $^1J_{RhP}$ = 115), 182.5 (dd, $^2J_{PP}$ = 420, $^1J_{RhP}$ = 109).

Satisfactory microanalysis could not be obtained due to partial loss of CO in the solid state.

IR (ATR): ν(C≡C) 2159 cm^{-1}, ν(C≡O) 1975 cm^{-1}, ν((Rh)C≡C) 1863 cm^{-1}.

Characterisation of **^{13}C-Rh-26o**

The ^{13}C analogue was prepared for similarly by dissolving an aliquot of **^{13}C-Rh-25o** in toluene-d_8 in a J Young NMR tube. The solution was freeze-pump-thaw degassed and placed under CO atmosphere (1atm) to afford the title compound in < 5 min.

^{13}C{^{1}H} NMR (101 MHz, toluene-d_8, selected data, CO atm): δ 87.1 (dd, $^1J_{CC}$ = 141, $^1J_{RhC}$ = 2, (Rh)C≡C–C≡C), 77.6 (dd, $^1J_{CC}$ = 141, $^1J_{RhC}$ = 5, (Rh)C≡C–C≡C).

^{31}P{^{1}H} NMR (161 MHz, toluene-d_8, CO atm): δ 195.3 (dd, $^2J_{PP}$ = 420, $^1J_{RhP}$ = 115), 182.4 (dd, $^2J_{PP}$ = 420, $^1J_{RhP}$ = 109).

Acquisition of UV-Vis spectroscopic data

A 0.2 mM standard solution of 1 in toluene was prepared and 3 mL were transferred in a T-shaped quartz cuvette equipped with a J. Young's tap (Figure 5.12). The solution was rigorously freeze-pump-thaw degassed in the thick-walled part of the glassware and placed under a carbon monoxide atmosphere (1 atm). The solution was decanted in the cuvette which was placed in the UV-Vis spectrometer's heating block. Care was taken to rigorously insulate the heating block with a 4 cm layer of cotton wool, whilst the top part of the flask was maintained at room temperature with a constant flow of air in order to maintain the inner pressure close to 1 atm. The sample was equilibrated at the desired temperatures for a period of 5 minutes before the spectra were acquired.

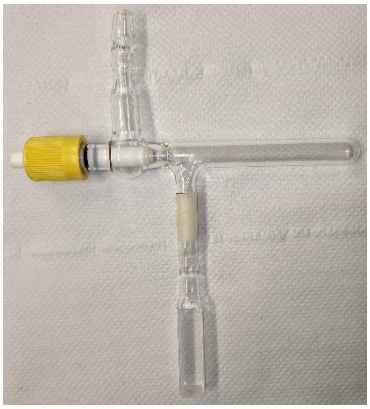

Figure 5.12. T-shaped quartz cuvette with graded seal adapted with a J Young teflon stopcock and thick walled receptacle.

Reference spectra were acquired likewise for a sample of 1 under Ar at each temperature. The reference for compound 3 was taken from the above sample cooled to 10 °C. For each temperature the resulting spectrum was deconvoluted as a linear combination of the two reference spectra *via* the least squares method and with the aid of a solver. The results were used to estimate the equilibrium constant as:

$$K = \frac{[\mathbf{Rh\ 25o}].[\mathrm{CO}]}{[\mathbf{Rh\ 26o}]}$$

Various literature values[22,23] were used to estimate the solubility of CO in toluene at the given temperatures and modelled with a linear regression. Thereafter, the following equation was used:

$$[\mathrm{CO}]^{1\ \mathrm{atm}} = 0.0166*\mathrm{T(K)} + 2.655$$

Table 5.4. Calculated equilibrium constants in the temperature range 35 – 85 °C

T / °C	K	1/T	ln(K)
35	0.529075837	0.003245	-0.63662
40	0.786821903	0.003193	-0.23975
45	1.15094864	0.003143	0.140587
50	1.718844079	0.003095	0.541652
55	2.536923434	0.003047	0.930952
60	3.697727938	0.003002	1.307719
65	5.442869383	0.002957	1.694306
70	8.224701891	0.002914	2.107142
75	12.03831767	0.002872	2.488095
80	17.53893741	0.002832	2.864423
85	26.05724983	0.002792	3.260296

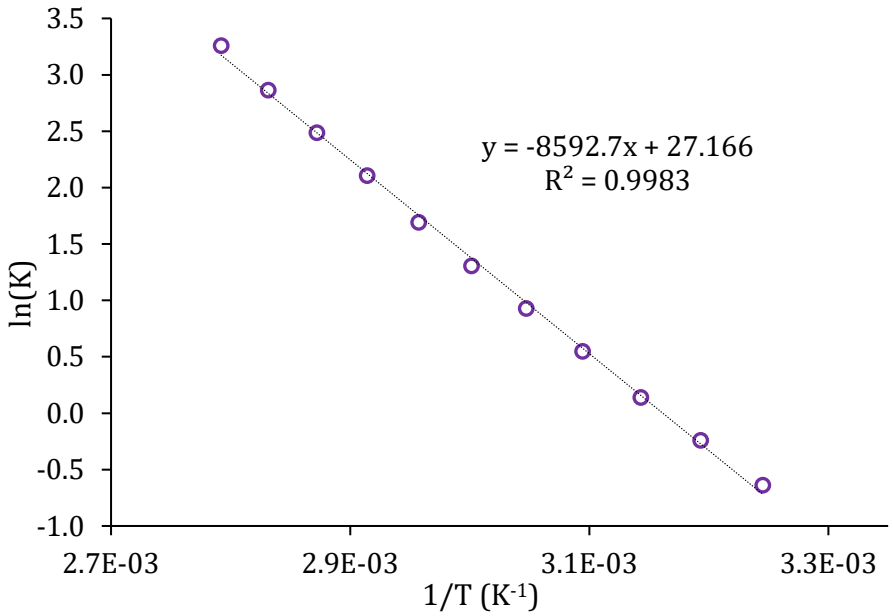

Figure 5.13. Van't Hoff plot for the equilibrium between **Rh-25o** and **Rh-26o**.

Van't Hoff analysis was conducted based on the calculated equilibrium constants allowing the thermodynamic parameters for the equilibrium to be determined: $\Delta H = 71 \pm 1$ kJ/mol and $\Delta S = 226 \pm 3$ J/mol/K

*5.3.6. Kinetic studies of the reaction of **Rh-25o** with CO*

A 0.2 mM standard solution of **Rh-25o**/**^{13}C-Rh-25o** in toluene was prepared and 3 mL were transferred in a T-shaped quartz cuvette equipped with a J. Young's tap. The solution was rigorously freeze-pump-thaw degassed in the thick-walled part of the glassware and placed under a carbon monoxide atmosphere (1 atm). The solution was decanted in the cuvette which was placed in the spectrometer's heating block. Care was taken to rigorously insulate the heating block with a 4 cm layer of cotton wool, whilst the top part of the flask was maintained at room temperature with a constant flow of air in order to maintain the inner pressure close to 1 atm. The sample was equilibrated at the desired temperatures for a period of exactly 5 minutes and the kinetic run was started. Spectra were recorded between 400 nm and 600 nm every 5 minutes for the runs at 80 °C, 85 °C, 90 °C and 95 °C, and every 2.5 minutes for the runs at 100 °C.

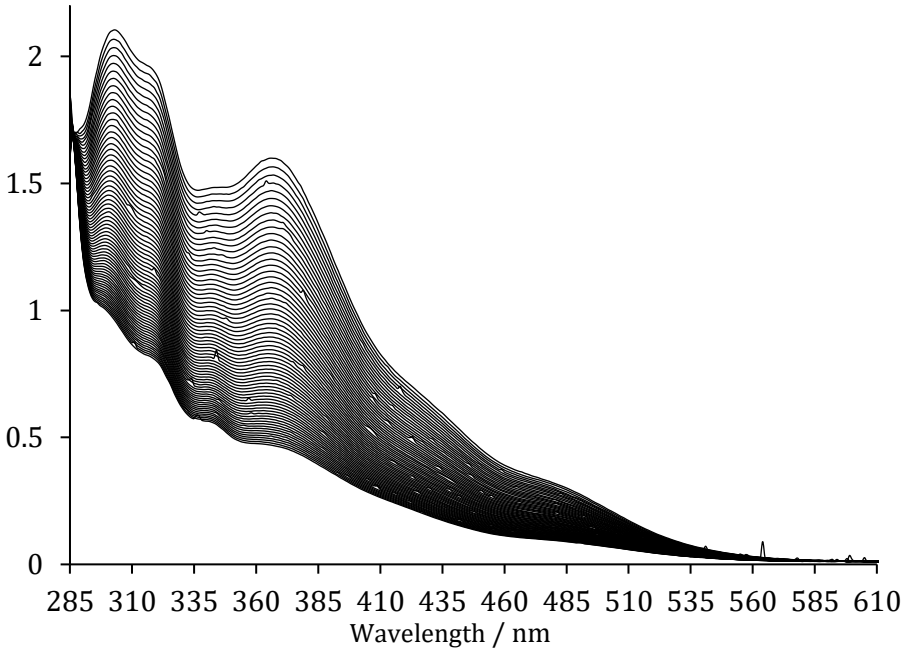

Figure 5.14. Typical time evolution of the spectra during a kinetic run at 80 °C over the course of 16 h.

Time course graphs were extracted from the obtained data at [400, 410, 420, 430, 440, 450, 460, 470, 480, 490] nm. Analysis of the resulting data indicated a first order in substrate which could be accurately modelled by a decreasing exponential of the type A*exp(-*k*t)+B, where k is the rate constant at the temperature T. For each run, *k* was calculated *via* the least squares fitting method

over the 10 chosen wavelengths and consistently resulted in correlation coefficients > 0.9999.

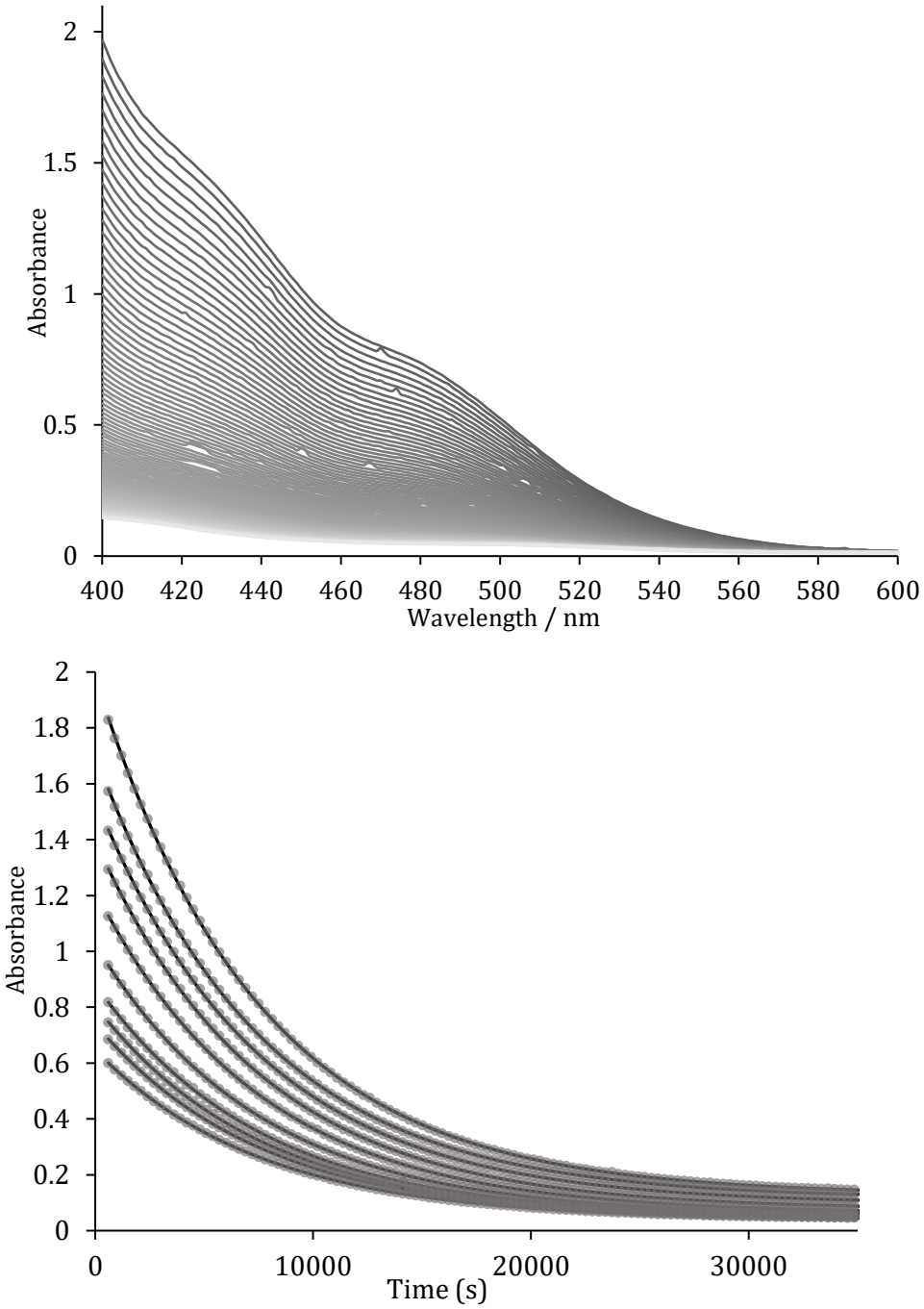

Figure 5.15. Time evolution of the spectra during a kinetic run at 95 °C over a course of 16 h (top); time course graphs extracted at the 10 specified wavelengths (●) overlaid with least squares fitting curves (–) for a time-scale of *ca.* 10 h (bottom).

Standard errors for the averaged rate constants were calculated for a confidence interval of 95% with the formula:

$$\text{st. error} = \text{st. dev.} \times \frac{t}{\sqrt{n}}$$

where t = 12.71 for a population n = 2, t = 4.303 for a population n = 3.

Table 5.5. Kinetic parameters for the reaction of **Rh-25o** under CO (1 atm).

Compound	T(°C)	k_2 (run 1)	k_2 (run 2)	k_2 (run 3)	**k_2 (average)**	**st. error**
Rh-25o	80	2.307E-05	2.303E-05	-	**2.305E-05**	**2.0E-07**
Rh-25o	85	4.338E-05	4.198E-05	-	**4.268E-05**	**6.3E-06**
Rh-25o	90	7.850E-05	7.760E-05	-	**7.805E-05**	**4.0E-06**
Rh-25o	95	1.327E-04	1.344E-04	-	**1.335E-04**	**7.6E-06**
Rh-25o	100	2.232E-04	2.237E-04	2.227E-04	**2.232E-04**	**9.8E-07**
^{13}C-Rh25o	100	2.086E-04	2.080E-04	2.061E-04	**2.075E-04**	**2.7E-06**

*5.3.7. Stepwise hydrogenation of **Rh-25o***

Preparation of **Rh-28o**

A solution of **Rh-25o** (30.0 mg, 29.7 μmol) and $[H(OEt_2)_2][BAr^F{}_4]$ (30.7 mg, 30.3 μmol) in 1,2-difluorobenzene (2 mL) was stirred at room temperature for 30 minutes to give **Rh-27o** characterised *in situ*. Sodium hydride (14.3 mg, 596 μmol) was added and the suspension was vigorously stirred at room temperature for 2 days. Volatiles were removed *in vacuo* and the crude was extracted with hexane (3 × 3 mL). The resulting solution was reduced to dryness *in vacuo* to afford **Rh-28o** as a dark red solid. Yield 29.4 mg (98%).

^{1}H NMR (600 MHz, toluene-d_8): δ 8.88 (br, 1H, 3,5-*t*Bu$_2$C$_6$H$_3$), 8.25 (d, $^3J_{HH}$ = 15.4, 1H, C≡CCHCH), 7.77 (br, 1H, 3,5-*t*Bu$_2$C$_6$H$_3$), 7.62 (d, $^4J_{HH}$ = 1.8, 1H, 3,5-*t*Bu$_2$C$_6$H$_3$), 7.44 (t, $^3J_{HH}$ = 1.8, 1H, 3,5-*t*Bu$_2$C$_6$H$_3$), 7.39 (t, $^3J_{HH}$ = 1.8, 1H, 3,5-*t*Bu$_2$C$_6$H$_3$), 7.17 (d, $^3J_{HH}$ = 15.4, 1H, C≡CCHCH), 6.95 (t, $^3J_{HH}$ = 7.9, 1H, RhC$_6$H$_3$), 6.74 (d, $^3J_{HH}$ = 7.9, 1H, RhC$_6$H$_3$), 6.69 (d, $^3J_{HH}$ = 7.9, 1H, RhC$_6$H$_3$), 2.59 – 2.26 (m, 6H, CH$_2$), 2.11 – 1.98 (m, 1H, CH$_2$), 1.88 – 0.94 (m, 21H, CH$_2$), 1.38 (br, 9H, 3,5-*t*Bu$_2$C$_6$H$_3$), 1.299 (br, 9H, 3,5-

*t*Bu$_2$C$_6$H$_3$), 1.300 (s, 18H, 3,5-*t*Bu$_2$C$_6$H$_3$), 1.22 (d, $^3J_{PH}$ = 11.4, 9H, P*t*Bu), 0.77 (d, $^3J_{PH}$ = 11.6, 9H, P*t*Bu).

^{13}C{^{1}H} NMR (151 MHz, toluene-d_8): δ 167.8 (dd, $^2J_{PC}$ = 10, J_{PC} = 4, RhC$_6$H$_3${C}), 167.6 (dd, $^2J_{PC}$ = 9, J_{PC} = 4, RhC$_6$H$_3${C}), 151.6 (s, 3,5-*t*Bu$_2$C$_6$H$_3${C}), 150.5 (br, 3,5-*t*Bu$_2$C$_6$H$_3${C}), 150.2 (br, 3,5-*t*Bu$_2$C$_6$H$_3${C}), 144.4 (s, C≡CCHCH), 144.2 (dt, $^2J_{RhC}$ = 30, $^2J_{PC}$ = 7, RhC$_6$H$_3${CRh}), 137.4 (s, 3,5-*t*Bu$_2$C$_6$H$_3${CCHCH}), 131.4 (s, 3,5-*t*Bu$_2$C$_6$H$_3${CC$_2$}), 130.5 (br, 3,5-*t*Bu$_2$C$_6$H$_3$), 129.2 (s, RhC$_6$H$_3$), 124.5 (br, 3,5-*t*Bu$_2$C$_6$H$_3$), 122.7 (s, 3,5-*t*Bu$_2$C$_6$H$_3$), 121.8 (s, 3,5-*t*Bu$_2$C$_6$H$_3$), 121.5 (s, 3,5-*t*Bu$_2$C$_6$H$_3$), 117.7 (s, C≡CCHCH), 105.0 (d, $^3J_{PC}$ = 11, RhC$_6$H$_3$), 104.8 (d, $^3J_{PC}$ = 10, RhC$_6$H$_3$), 93.5 (d, $^1J_{RhC}$ = 7, C≡CCHCH), 88.0 (d, $^1J_{RhC}$ = 7, C≡CCHCH), 39.2 (vt, J_{PC} = 7, P*t*Bu{C}), 38.0 (vt, J_{PC} = 7, P*t*Bu{C}), 35.3 (br, 3,5-*t*Bu$_2$C$_6$H$_3${C}), 35.1 (br, 3,5-*t*Bu$_2$C$_6$H$_3${C}), 35.0 (s, 3,5-*t*Bu$_2$C$_6$H$_3${C}), 32.5 (br, CH$_2$), 32.1 (br, 3,5-*t*Bu$_2$C$_6$H$_3${CH$_3$}), 31.9 (d, J_{PC} = 5, CH$_2$), 31.63 (s, 3,5-*t*Bu$_2$C$_6$H$_3${CH$_3$}), 31.59 (br, 3,5-*t*Bu$_2$C$_6$H$_3${CH$_3$}), 31.41 (s, CH$_2$), 31.38 (br, CH$_2$), 30.8 (s, CH$_2$), 30.7 (s, CH$_2$), 30.30 (br, CH$_2$), 30.28 (s, CH$_2$), 30.25 (s, CH$_2$), 30.0 (s, CH$_2$), 29.8 (s, CH$_2$), 27.1 (d, $^2J_{PC}$ = 6, P*t*Bu{CH$_3$}), 26.1 (d, $^2J_{PC}$ = 6, P*t*Bu{CH$_3$}), 26.0 (d, J_{PC} = 4, CH$_2$), 25.1 (d, J_{PC} = 4, CH$_2$).

^{31}P{^{1}H} NMR (162 MHz, toluene-d_8): δ 185.1 (dd, $^1J_{PP}$ = 401, $^1J_{RhP}$ = 160), 182.5 (dd, $^1J_{PP}$ = 420, $^1J_{RhP}$ = 165).

Anal. Calcd for $C_{60}H_{93}O_2P_2Rh$ (1011.26 g·mol^{-1}): C, 71.26; H, 9.27; Found: C, 71.12; H, 9.28.

IR (ATR): ν((Rh)C≡C) 1943 cm^{-1}

Preparation of **^{13}C-Rh-28o**

The ^{13}C labelled analogue was prepared following the above procedure and using **^{13}C-Rh-25o**(7.5 mg, 7.4 μmol), [H(OEt$_2$)$_2$][BAr$^F_4$] (7.5 mg, 7.4 μmol) and sodium hydride (3.5 mg, 0.15 mmol). Yield 7.5 mg (quantitative).

^{13}C{^{1}H} NMR (101 MHz, toluene-d_8, selected data): δ 117.7 (d, $^1J_{CC}$ = 89, ArC-CH=CH), 88.0 (dd, $^1J_{CC}$ = 89, $^1J_{RhC}$ = 8, alkyne).

^{31}P{^{1}H} NMR (162 MHz, toluene-d_8): δ 185.1 (dd, $^1J_{PP}$ = 401, $^1J_{RhP}$ = 160), 182.5 (dd, $^1J_{PP}$ = 420, $^1J_{RhP}$ = 165).

Preparation of **Rh-32o**

A solution of **Rh-28o** (10.4 mg, 10.0 μmol) and $[H(OEt_2)_2][BAr^F{}_4]$ (10.1 mg, 10.0 μmol) in 1,2-difluorobenzene in a J Young NMR tube was agitated at room temperature, resulting in and spectroscopically quantitative conversion to **Rh-29o** by ^{31}P NMR spectroscopy. Sodium hydride (4.8 mg, 0.20 mmol, 20 eq) was added and the solution was well agitated for 2 days at room temperature to afford **Rh-31o**. The volatiles were removed *in vacuo* and the crude was extracted with hexane (3 × 1 mL), dried and redissolved in toluene-d_8. The resulting solution was freeze-pump-thaw degassed, place under an atmosphere of H_2 (1 atm), and stored at room temperature for 2 days with constant agitation to give **Rh-32o**, which was characterised *in situ* by NMR spectroscopy.

^{1}H NMR (400 MHz, toluene-d_8, selected data): δ 8.22 (s, 1H, 3,5-*t*Bu$_2$C$_6$H$_3$), 7.41 (s, 1H, 3,5-*t*Bu$_2$C$_6$H$_3$), 7.34 (s, 1H, 3,5-*t*Bu$_2$C$_6$H$_3$), 7.31 (s, 2H, 3,5-*t*Bu$_2$C$_6$H$_3$), 7.23 (s, 1H, 3,5-*t*Bu$_2$C$_6$H$_3$), 6.89 (t, $^3J_{HH}$ = 7.9, 1H, RhC$_6$H$_3$), 6.66 (d, $^3J_{HH}$ = 7.9, 1H, RhC$_6$H$_3$), 6.28 (t, $^3J_{HH}$ = 9.5, 1H, Ar'-CH=CH), 5.25 (app q, $^3J_{HH}$ = 10.2, 9.7, 1H, Ar'-CH=CH), 3.88 (td, $^2J_{HH}$ = 13.8, $^3J_{HH}$ = 5.0, 1H, Ar'-CH$_a$H$_b$-CH$_2$), 3.60 (t, $^2J_{HH}$ = 13.2, 1H, Ar'-CH$_a$H$_b$-CH$_2$), 3.17 (t, $^2J_{HH}$ = 13.5, 1H, Ar'-CH$_2$-CH$_c$H$_d$), 1.33 (s, 9H, 3,5-*t*Bu$_2$C$_6$H$_3$), 1.32 (s, 18H, 3,5-*t*Bu$_2$C$_6$H$_3$), 1.28 (s, 9H, 3,5-*t*Bu$_2$C$_6$H$_3$), 1.11 (d, $^3J_{PH}$ = 10.3, 9H, P*t*Bu), 0.46 (d, $^3J_{PH}$ = 10.6, 9H, P*t*Bu).

^{31}P{^{1}H} NMR (162 MHz, toluene-d_8): δ 185.4 (d, $^2J_{PP}$ = 343, $^1J_{RhP}$ = 170), 182.6, $^2J_{PP}$ = 343, $^1J_{RhP}$ = 166).

Preparation of **^{13}C-Rh-32o**

The ^{13}C labelled analogue was prepared following the above procedure and using **^{13}C-Rh-28o**(7.5 mg, 7.4 μmol), $[H(OEt_2)_2][BAr^F{}_4]$ (7.5 mg, 7.4 μmol) and sodium hydride (3.5 mg, 0.15 mmol) and was also characterized in situ by NMR spectroscopy

^{1}H NMR (400 MHz, toluene-d_8, selected data): δ 6.28 (t, $^3J_{HH}$ = 9.5, 1H, Ar'-CH=^{13}CH), 5.25 (app dq, $^1J_{CH}$ = 149.2, $^3J_{HH}$ = 10.2, 9.7, 1H, Ar'-CH=^{13}CH), 3.88 (td, $^2J_{HH}$ = 13.8, $^3J_{HH}$ = 5.0, 1H, Ar'-CH$_a$H$_b$-^{13}CH$_2$), 3.60 (t, $^2J_{HH}$ = 13.2, 1H, Ar'-CH$_a$H$_b$-^{13}CH$_2$), 3.17 (dt, $^1J_{CH}$ = 113.2, $^2J_{HH}$ = 13.5, 1H, Ar'-CH$_2$-^{13}CH$_c$H$_d$).

$^{13}C\{^{1}H\}$ NMR (151 MHz, toluene-d_8, selected data): δ 66.5 (dd, $^{1}J_{CC}$ = 40, $^{1}J_{RhC}$ = 9, alkene{CH}, bound), 39.7 (d, $^{1}J_{CC}$ = 40, alkyl{CH_2}).

*5.3.8. Decarbonylation of **Ir-24o,c** and **Rh-24c***

Attempts to decarbonylate **Ir-24o,c** – Representative procedures

Decarbonylating agent:

A solution of **Ir-24o,c** (*ca.* 10 μmol) and trimethylamine *N*-oxide (7.5 mg, 0.10 mmol, 10 eq) in fluorobenzene (0.5 mL) in a J Young NMR tube was heated at 120 °C for 2 h. Analysis by NMR spectroscopy was consistent with a mixture of the starting materials with trimethylamine.

Photolysis:

A solution of **Ir-24o,c** (*ca.* 10 μmol) in heptane/cyclohexane/acetonitrile (0.5 mL) in a quartz J Young flask was irradiated using a 100 W Hg arc lamp equipped with a water IR filter for intervals of 2 h with/without Ar bubbling through a cannula, after which the volatiles were removed *in vacuo*. Analysis by NMR spectroscopy was consistent with the presence of only the starting material in solution.

*Thermolysis of **Ir-24o***:

A J Young's flask was charged with **Ir-24o** (8.6 mg, 7.6 μL) and placed under dynamic vacuum (2.10^{-3} mbar). The flask was heated at 160 °C in a sand bath for 3 h, affording an insoluble brown residue. Analysis by NMR spectroscopy was consistent with the presence of only the starting material in solution.

Thermolysis of **Ir-24c –** *In situ* characterisation of **Ir-24c'**

A J Young's flask was charged with **Ir-24c** (7.7 mg, 6.9 μmol) and placed under dynamic vacuum (2.10^{-3} mbar). The flask was heated at 200 °C in a sand bath for 18 h, affording a mixture containing *ca.* 30% of **Ir-24c'** and 70% of starting material by ^{31}P NMR spectroscopy.

^{1}H resonances for **Ir-24c'** obtained by subtraction of the spectrum for **Ir-24c** from the spectrum for the obtained mixture.

^{1}H NMR (400 MHz, toluene-d_8): δ 7.48 (s, 4H, 3,5-*t*Bu$_2$C$_6$H$_3$), 7.35 (s, 2H, 3,5-*t*Bu$_2$C$_6$H$_3$), 6.69 (t, $^3J_{HH}$ = 7.3, 1H, IrC$_6$H$_3$), 6.56 (d, $^3J_{HH}$ = 7.3, 1H, IrC$_6$H$_3$), 3.65 – 3.54 (m, 2H, PCH$_a$H$_b$), 3.43 (d, $^2J_{HH}$ = 15.4, 2H, ArCH$_2$P), 3.02 (d, $^2J_{HH}$ = 15.5, 2H, ArCH$_2$P), 2.46 – 2.33 (m, 2H, alkyl), 2.09 – 1.93 (m, 2H, alkyl), 1.39 (vt, $^3J_{PH}$ = 6.5, 18H, P*t*Bu), 1.33 (s, 36H, 3,5-*t*Bu$_2$C$_6$H$_3$), 1.62 – 1.14 (m, 16H, alkyl).

^{31}P{^{1}H} NMR (162 MHz, toluene-d_8): δ 46.5 (s).

Preparation of **Rh-25c**

A solution of **Rh-24c** (14.0 mg, 13.5 μmol) and trimethylamine *N*-oxide (20.4 mg, 0.135 mmol, 20 eq) in fluorobenzene (1 mL) was heated at 85 °C for 4 days. The mixture was allowed to cool to room temperature and the volatiles were removed *in vacuo*. The crude was extracted with hexane (3 × 2 mL) and the resulting solution reduced to dryness *in vacuo*. Purification by flash column chromatography (neutralized SiO_2, 5% DCM-hexane) afforded **Rh-25c** as a dark orange gum. Yield 6.5 mg (48%).

^{1}H NMR (400 MHz, toluene-d_8): δ 7.72 (d, $^3J_{HH}$ =1.8, 2H, 3,5-*t*Bu$_2$C$_6$H$_3$), 7.66 (d, $^3J_{HH}$ =1.8, 2H, 3,5-*t*Bu$_2$C$_6$H$_3$), 7.48 (t, $^3J_{HH}$ =1.8, 2H, 3,5-*t*Bu$_2$C$_6$H$_3$), 7.30 (t, $^3J_{HH}$ =1.8, 1H, 3,5-*t*Bu$_2$C$_6$H$_3$), 6.84 (d, $^3J_{HH}$ = 7.3, 1H, RhC$_6$H$_3$), 6.78 (d, $^3J_{HH}$ = 7.4, 1H, RhC$_6$H$_3$), 6.72 (t, $^3J_{HH}$ = 7.4, 1H, RhC$_6$H$_3$), 3.04 (dd, $^2J_{HH}$ = 13.5, $^2J_{PH}$ = 5.8, 1H, ArCH$_2$P), 2.60 – 2.46 (m 3H, 3 × ArCH$_2$P), 2.44 – 2.29 (m, 2H alkyl), 2.02 – 1.68 (m, 6H alkyl), 1.67 – 1.18 (m, 20H, alkyl), 1.44 (br, 9H, P*t*Bu), 1.41 (br, 9H, P*t*Bu), 1.37 (s, 18H, 3,5-*t*Bu$_2$C$_6$H$_3$), 1.29 (s, 18H, 3,5-*t*Bu$_2$C$_6$H$_3$).

^{31}P{^{1}H} NMR (162 MHz, toluene-d_8): δ 78.5 (dd, $^1J_{PP}$ = 224, $^1J_{RhP}$ = 171), 71.4 (dd, $^1J_{PP}$ = 224, $^1J_{RhP}$ = 171).

5.3.9. Towards a metallo-catenane

Transmetallation reactions

Preparation of **Rh-33o**

A solution of tridec-1-en-12-yne (16.1 mg, 90.0 μmol, 4.5 eq) in THF (1 mL) was treated with *i*PrMgCl (40 μL, 2 M, 80 μmol, 4 eq) and heated at 80 °C for 30 minutes. The solution was allowed to cool to room temperature and was added to a solution of **Rh-19o** (13.6 mg, 20.0 μmol, 1 eq) in THF (1 mL). The reaction mixture was left to stir at room temperature for 18 h. In air, the excess Grignard was quenched with water (0.2 mL) and the volatiles were removed in vacuo. The crude was extracted with hexane (3 × 2 mL) and dried. Purification by flash column chromatography (neutralized silica, HMDSO, R_f = 0.15) afforded the title compound as a colourless oil. Yield 18.3 mg (95%).

^{1}H NMR (600 MHz, toluene-d_8): δ 6.75 (t, $^3J_{HH}$ = 7.9, 1H, Ar), 6.58 (d, $^3J_{HH}$ = 7.9, 2H, Ar), 5.78 (app ddt, $^3J_{HH}$ = 16.9, 10.2, 6.7, 2H, C<u>H</u>=CH$_2$), 5.02 (app dq, $^3J_{HH}$ = 17.1, J_{HH} = 1.8, 2H, CH=C<u>H</u>$_2$), 4.97 (app dq, $^3J_{HH}$ = 10.2, J_{HH} = 1.8, 2H, CH=C<u>H</u>$_2$), 3.95 (app dp, $^2J_{HH}$ = 14.2, J = 7.3, 2H, PCH$_2$), 2.31 – 2.15 (m, 6H, CH$_2$), 1.99 (q, $^3J_{HH}$ = 7,2, 4H, C<u>H</u>$_2$-CH=CH$_2$), 1.92 – 1.85 (m, 2H, CH$_2$), 1.72 – 1.60 (m, 6H, CH$_2$), 1.60 – 1.49 (m, 4H, CH$_2$), 1.48 – 1.38 (m, 28H, 2 × P*t*Bu + CH$_2$), 1.38 – 1.29 (m, 11H, CH$_2$), 1.29 – 1.20 (m, 19H, CH$_2$).

^{13}C{^{1}H} NMR (151 MHz, toluene-d_8): δ 189.6 (dt, $^1J_{RhC}$ = 43, $^2J_{PC}$ = 6, CO), 162.7 (vt, J_{PC} = 5, Ar{C}), 139.3 (s, alkene{CH}), 136.4 (dt, $^1J_{RhC}$ = 22, $^2J_{PC}$ = 6, Ar{CRh}), 126.6 (s, Ar{CH}), 114.5 (s, alkene{CH$_2$}), 107.8 (d, $^2J_{RhC}$ = 7, RhC≡<u>C</u>), 106.6 (vt, J_{PC} = 6, Ar{CH}), 80.4 (dt, $^1J_{RhC}$ = 33, $^2J_{PC}$ = 15, Rh<u>C</u>≡C), 40.0 (vt, J_{PC} = 12, P*t*Bu{C}), 34.3 (s, <u>C</u>H$_2$-CH=CH$_2$), 30.8 (vt, $^2J_{PC}$ = 6, CH$_2$), 30.5 (s, CH$_2$), 30.2 (s, CH$_2$), 30.1 (s, CH$_2$), 29.9 (s, CH$_2$), 29.7 (s, CH$_2$), 29.62 (s, CH$_2$), 29.58 (s, CH$_2$), 29.49 (s, CH$_2$), 29.47 (s, CH$_2$), 29.3 (s, CH$_2$), 28.5 (s, CH$_2$), 27.8 (vt, J_{PC} = 14, PCH$_2$), 26.1 (s, P*t*Bu{CH$_3$}), 24.7 (br, CH$_2$), 22.3 (s, CH$_2$).

^{31}P{^{1}H} NMR (243 MHz, toluene-d_8): δ 188.4 (d, $^1J_{RhP}$ = 94).

Preparation of **Ir-33o**

A solution of tridec-1-en-12-yne (31.5 mg, 176 μmol, 4.5 eq) in THF (1 mL) was treated with *i*PrMgCl (79 μL, 2 M, 0.16 mmol, 4 eq) and heated at 80 °C for 30 minutes. The solution was allowed to cool to room temperature and was added to a solution of **Ir-19o** (30.3 mg, 39.3 μmol, 1 eq) in THF (1 mL). The reaction mixture was stirred at 120 °C for 2 days. In air, the excess Grignard was quenched with water (0.2 mL) and the volatiles were removed in vacuo. The crude was extracted with hexane (3 × 3 mL) and dried. Purification by flash column chromatography (Al_2O_3, 10% DCM-hexane, R_f = 0.33) afforded the title compound as a colourless oil. Yield 22.3 mg (54%).

^{1}H NMR (400 MHz, C_6D_6): δ 6.82 (t, $^3J_{HH}$ = 7.8, 1H, Ar), 6.69 (d, $^3J_{HH}$ = 7.9, 2H, Ar), 5.80 (app ddt, $^3J_{HH}$ = 16.8, 10.6, 5.3, 2H, C<u>H</u>=CH$_2$), 5.06 (d, $^3J_{HH}$ = 17.0, 2H, CH=C<u>H</u>$_2$), 4.97 (d, $^3J_{HH}$ = 10.2, 2H, CH=C<u>H</u>$_2$), 4.08 (app dp, $^2J_{HH}$ = 15.1, J = 7.8, 2H, PCH$_2$), 2.39 – 2.22 (m, 6H, CH$_2$), 2.01 (q, $^3J_{HH}$ = 7,2, 4H, C<u>H</u>$_2$-CH=CH$_2$), 1.92 – 1.56 (m, 8H, CH$_2$), 1.53 – 1.16 (m, 44H, CH$_2$), 1.43 (vt, J = 7.8, 18H, P*t*Bu).

^{31}P{^{1}H} NMR (162 MHz, C_6D_6): δ 147.0 (s).

Preparation of **Ir-33c**

A solution of tridec-1-en-12-yne (12.0 mg, 67 μmol, 4.5 eq) in THF (1 mL) was treated with *i*PrMgCl (30 μL, 2 M, 60 μmol, 4 eq) and heated at 80 °C for 30 minutes. The solution was allowed to cool to room temperature and was added to a solution of **Ir-19c** (11.4 mg, 14.9 μmol, 1 eq) in THF (1 mL). The reaction mixture was stirred at 120 °C for 2 days. In air, the excess Grignard was quenched with water (0.2 mL) and the volatiles were removed in vacuo. The crude was extracted with hexane (3 × 3 mL) and dried. Purification by flash column chromatography (Al_2O_3, 8% DCM-hexane, R_f = 0.41) afforded the title compound as a colourless oil. Yield 22.3 mg (54%).

^{1}H NMR (400 MHz, $CDCl_3$): δ 6.89 (d, $^3J_{HH}$ = 7.4, 1H, Ar), 6.82 (t, $^3J_{HH}$ = 7.4, 2H, Ar), 5.81 (app ddt, $^3J_{HH}$ = 16.7, 11.0, 5.7, 2H, C<u>H</u>=CH$_2$), 4.99 (d, $^3J_{HH}$ = 17.2, 2H, CH=C<u>H</u>$_2$), 4.93 (d, $^3J_{HH}$ = 10.3, 2H, CH=C<u>H</u>$_2$), 3.75 (dt, $^2J_{HH}$ = 15.5, $^2J_{PH}$ = 5.2, 2H, ArCH$_2$P), 3.40 (br d, $^2J_{HH}$ = 15.4, 2H, ArCH$_2$P), 3.21 (app ddt, $^2J_{HH}$ = 14.2, J = 10, 5, 2H, PCH$_2$), 2.11

(t, $^3J_{HH}$ = 7.2, 4H, CH_2), 2.04 (q, $^3J_{HH}$ = 7.3, 4H, C<u>H</u>$_2$-CH=CH_2), 2.09 – 1.97 (m, 2H, CH_2), 1.92 – 1.80 (m, 2H, CH_2), 1.79 – 1.04 (m, 68H, CH_2 + P*t*Bu).

^{31}P{^{1}H} NMR (162 MHz, $CDCl_3$): δ 37.3 (s).

Ring closing metathesis reactions – General procedure.

A solution of Grubbs' 2nd generation catalyst (5mol%) in fluorobenzene (2 mL, from a freshly prepared stock solution) was added to a solution of Rh-33o/Ir-33o/Ir-33c in fluorobenzene (conc. 1 mM). The reaction mixture was left to stir for 24 h with periodic Ar bubbling and monitoring by TLC. The volatiles were removed *in vacuo* and purification by flash chromatography (Al_2O_3, DCM-hexane, Ir; neutralized SiO_2 – HMDSO, Rh) afforded **M-34o,c** as a colourless oil.

Preparation of **Rh-34o**

Following the general procedure and using **Rh-33o** (18.3 mg, 19.0 μmol) and Grubbs' 2nd generation catalyst (0.8 mg, 0.9 μmol) (neutralized SiO_2, HMDSO, R_f = 0.35). Yield 10.0 mg (56%).

^{1}H NMR (400 MHz, $CDCl_3$): δ 6.79 (t, $^3J_{HH}$ = 8.2, 1H, Ar), 6.45 (d, $^3J_{HH}$ = 7.9, 2H, Ar), 5.54 (br, 2H, alkene), 3.81 – 3.64 (m, 2H, PC<u>H$_a$</u>H$_b$), 2.26 – 2.14 (m, 2H, PCH$_a$<u>H$_b$</u>), 2.14 – 1.94 (m, 8H, CH_2), 1.85 – 1.57 (m, 10H, CH_2), 1.52 – 0.87 (m, 42H, CH_2 + P*t*Bu), 1.37 (vt, *J* = 7.7, 18H, P*t*Bu).

^{31}P{^{1}H} NMR (162 MHz, $CDCl_3$): δ 147.3 (d, $^1J_{RhP}$ = 93).

Preparation of **Ir-34o**

Following the general procedure and using **Ir-33o** (22.3 mg, 21.1 μmol) and Grubbs' 2nd generation catalyst (0.9 mg, 1 μmol) (Al_2O_3, 5% DCM-hexane, R_f = 0.35). Yield 18.1 mg (84%).

^{1}H NMR (400 MHz, C_6D_6): δ 6.84 (t, $^3J_{HH}$ = 7.7, 1H, Ar), 6.77 (d, $^3J_{HH}$ = 7.7, 2H, Ar), 5.67 (br, 2H, alkene), 4.08 – 3.94 (m, 2H, PCH_2), 2.51 – 2.34 (m, 4H, CH_2), 2.29 – 2.17 (m, 2H, CH_2), 2.16 – 2.04 (m, 4H, CH_2), 1.90 – 1.11 (m, 70H, CH_2 + P*t*Bu).

^{31}P{^{1}H} NMR (162 MHz, C_6D_6): δ 147.3 (s).

Preparation of **Ir-34c**

Following the general procedure and using **Ir-33c** (11.8 mg, 11.2 μmol) and Grubbs' 2nd generation catalyst (0.9 mg, 1 μmol) (Al_2O_3, 5% DCM-hexane, R_f = 0.45). Yield 7.1 mg (62%).

^{1}H NMR (400 MHz, $CDCl_3$): δ 6.87 (d, $^3J_{HH}$ = 7.3, 1H, Ar), 6.80 (t, $^3J_{HH}$ = 7.3, 2H, Ar), 5.57 (br s, $^3J_{HH}$ = 17.2, 2H, alkene), 3.77 (dt, $^2J_{HH}$ = 15.4, $^2J_{PH}$ = 5.0, 2H, $ArCH_2P$), 3.38 (br d, $^2J_{HH}$ = 15.4, 2H, $ArCH_2P$), 3.27 – 3.13 (m, 2H, PCH_2), 2.21 – 1.93 (m, 11H, CH_2), 1.92 – 0.77 (m, 51H, CH_2). 1.25 (vt, J = 7.2, 18H, P*t*Bu).

^{31}P{^{1}H} NMR (162 MHz, $CDCl_3$): δ 36.6 (s).

Attempts to decarbonylate **Ir-34o,c**

All methods described in section 5.3.8 were trialled with **Ir-34o,c** and afforded identical outcomes.

Decarbonylation and hydrogenation of **Rh-34o**

In a J Young NMR tube, a solution of **Rh-34o** (10.0 mg, 10.7 μmol) and Me_3NO (16.1 mg, 21.4 μmol) in fluorobenzene (0.5 mL) was heated at 85 °C for 3 days, after which monitoring by ^{31}P NMR spectroscopy showed complete consumption of the starting material and formation of **Rh-18o** and **Rh-35o**. The volatiles were removed *in vacuo* and the crude was extracted with hexane (3 × 1 mL) and dried. The mixture was dissolved in toluene-d_8 and the resulting solution was freeze-pump-thaw degassed and placed under an atmosphere of H_2 (1 atm). The solution was heated at 85 °C for 4 days, resulting in the formation of **Rh-15o** and **Rh-36o**.

5.3.10. Computational details

All molecular dynamics (MD) runs were carried out employing the Grimme group's XTB software and implemented MD module. Specifically, the GFN2-xTB method was initially used to optimise **Rh-25o** from the solid-state structure. Subsequent MD runs were carried out with a large time step for propagation of 2 fs, allowed by hydrogen mass repartitioning to four times.[24] The calculations were performed in the NVT ensemble at the chosen thermostat temperature [293, 373, 473, 573] K three times for a total duration of 2 ns, with an interval of 50 fs for trajectory printout. The SHAKE algorithm to constrain bonds was turned off to allow for full conformational freedom during the run. All other parameters were used as default.

All DFT-based calculations were carried out using ORCA 4.1.2.[25,26] Three functionals were included in an early benchmark, BP86 and B3LYP, both with the D3BJ dispersion correction and wB97X-D3. After geometry optimisation of **Rh-24o** with the def2-SV(P) basis set (and associated def2-ECP), the three geometries were compared to the experimentally determined crystal structure. Functional wB97X-D3 was found to be the closest to experiment in terms of reproducing the distorted octahedral geometry, particularly with a P-Rh-C_{alkyne} angle of 85.5 ° (*vs* 86.1, XRD; 85.2, B3LYP-D3BJ; 84.9, BP86-D3BJ). In addition both methods featuring the D3BJ dispersion correction showed exaggerated distortion of the alkyne+stopper group half axle away from linearity, which was not the case with wB97X-D3. Finally, the choice of wB97X-D3 for this study was further consolidated by its previous successful application in modelling the thermodynamics in various related projects in the group involving the same transition metals and ligand types.[27–30] With a view to accurately capturing the steric properties of the system, the full Ar' groups were kept without any truncation. To compensate for the significant computational expense associated with a 156 atoms structure featuring a transition metal, the def2-SV(P) basis set was chosen, as optimisation with a heavier basis set, def2-TZVP, resulted in only minor geometrical differences (*e.g.* P-Rh-C_{alkyne} angle: 85.5 ° for def2-SV(P), 85.7 ° for def2-TZVP; d(C-O): 1.136 for def2-SV(P) and 1.133 for def2-TZVP). All compounds in this study are neutral, therefore the effect of solvation models was assumed to be minimal and was not investigated.

Geometries were optimised using the tightopt and tightscf settings starting from the XTB generated structures and employing Grimme's dispersion corrected wB97X-D3 functional,[31,32] the def2-SV(P) basis set[33] on all atoms and the associated def2-ECP effective core potential on Rh/Ir.[34] Analytical vibrational frequency calculations were carried out at the same level of theory in order to verify the nature of minima as well as to help compute the thermodynamics. The optimizations were followed by single point energy evaluation with the same functional and the def2-TZVP(-f) basis set on all atoms,[33] and the associated def2-ECP effective core potential on Rh/Ir.[34] The RIJCOSX approximation was used to reduce the computational cost of calculations using the def2/J auxiliary basis set and integration grids set to Grid5 and GridX7.[35,36]

TDDFT calculations were carried out using ORCA 4.1.2 at the wB97X-D3/def2-TZVP//wb97X-D3/def2-SV(P) level of theory to compute the first 10 singlet excitations. The Tamm-Dancoff Approximation (TDA) was turned off, and the Natural Transition Orbitals (NTOs) were computed to aid in the identification of the excitations.

Calculated thermodynamics

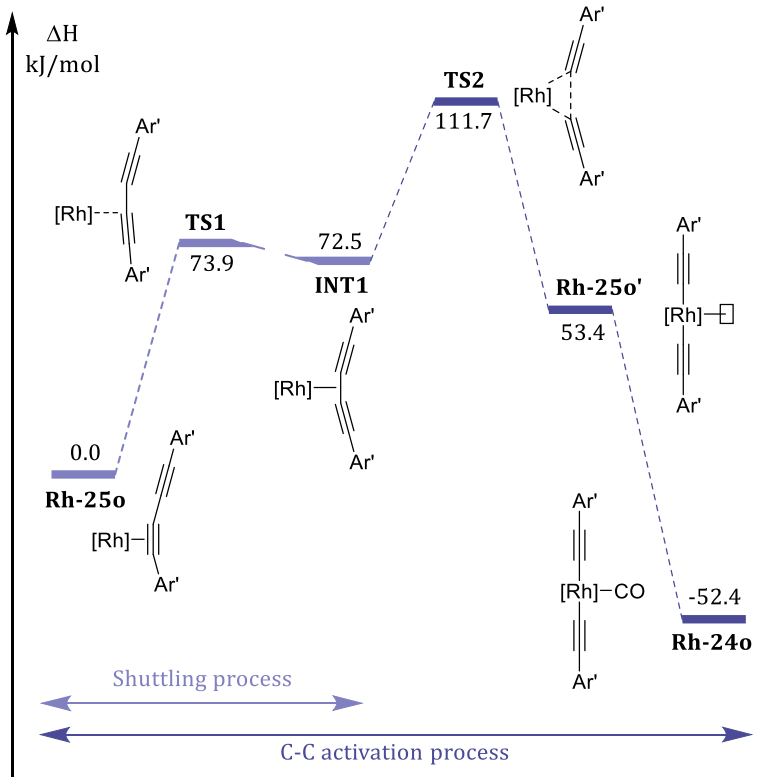

Figure 5.16. Computed energy profile for the shuttling and C(sp)-C(cp) activation processes observed in **Rh-25o**.

Table 5.6. Calculated thermodynamics

Compound	E (a. u.)	H (a. u.)	T x S (a. u.)	G (a. u.)	
Rh-25o	-3285.337022	-3283.872089	0.166181	-3284.038270	
		-3283.872448	0.166299	-3284.038747	**^{13}C**
Rh-26o	-3398.700595	-3397.222921	0.168991	-3397.391912	
INT1	-3285.308929	-3283.844483	0.166599	-3284.011082	
TS1	-3285.308155	-3283.843924	0.167778	-3284.011702	
		-3283.844258	0.167904	-3284.012162	**^{13}C**
TS2	-3285.293760	-3283.829558	0.166241	-3283.995799	
		-3283.829848	0.166347	-3283.996195	**^{13}C**
Rh-25o'	-3285.317891	-3283.851749	0.168384	-3284.020133	
Rh-24o	-3398.687166	-3397.210785	0.170622	-3397.381407	
Ir-25o	-3279.142222	-3277.675911	0.167452	-3277.843362	
Ir-25o'	-3279.140334	-3277.675217	0.167157	-3277.842374	
Ir-25c	-3207.273323	-3205.758778	0.168811	-3205.927588	
Ir-25c'	-3207.277284	-3205.764808	0.166262	-3205.931069	
CO	-113.327227	-113.318740	0.022428	-113.341168	

5.4. Crystallographic data

Data were collected on a Rigaku Oxford Diffraction SuperNova AtlasS2 CCD diffractometer using graphite monochromated MoKα (λ = 0.71073 Å) or CuKα (λ = 1.54184 Å) radiation and an Oxford Cryosystems N-HeliX low temperature device [150(2) K] and all associated data are summarised in the tables below.

Data were collected and reduced using CrysAlisPro and refined using SHELXL,[37] through the Olex2 interface.[38] Hydrogen atoms were placed in calculated positions using the riding model.

Full details about the collection, solution, and refinement for compounds **syn-6**, **anti-6**, **Rh-18o**, **Rh-18c**, **Ir-18o**, **Ir-18c, Rh-19o, Rh-19c**, **Ir-19o** and **Ir-19c** are documented in CIF format, which have been deposited with the Cambridge Crystallographic Data Centre under CCDC 1972811 – 1972820.

Table 5.7	***syn*-6**	***anti*-6**	**Rh-18o**
Empirical formula	$C_{28}H_{56}B_2O_2P_2$	$C_{28}H_{56}B_2O_2P_2$	$C_{29}H_{49}O_3P_2Rh$
Formula weight	508.28	508.28	610.53
Temperature/K	150(2)	150(2)	150(2)
Crystal system	orthorhombic	monoclinic	orthorhombic
Space group	$Pca2_1$	$P2_1/c$	$Pca2_1$
a/Å	36.2517(2)	15.09343(9)	20.85015(15)
b/Å	6.78334(5)	12.86467(7)	10.67243(11)
c/Å	13.08712(7)	32.65837(16)	13.58703(12)
α/°	90	90	90
β/°	90	90.5535(5)	90
γ/°	90	90	90
Volume/Å³	3218.23(4)	6341.04(6)	3023.41(5)
Z	4	8	4
ρ_{calc}g/cm³	1.049	1.065	1.341
μ/mm⁻¹	1.368	1.388	5.77
F(000)	1120	2240	1288
Crystal size/mm³	0.264 × 0.234 × 0.072	0.653 × 0.24 × 0.087	0.356 × 0.186 × 0.064
Radiation	CuKα (λ = 1.54184)	CuKα (λ = 1.54184)	CuKα (λ = 1.54184)
2Θ range for data collection/°	13.052 to 140.098	5.412 to 147.224	13.032 to 140.142
Index ranges	-44 ≤ h ≤ 44, -7 ≤ k ≤ 8, -15 ≤ l ≤ 15	-18 ≤ h ≤ 17, -15 ≤ k ≤ 15, -40 ≤ l ≤ 33	-25 ≤ h ≤ 25, -12 ≤ k ≤ 11, -16 ≤ l ≤ 14
Reflections collected	39875	68205	19287
Independent reflections	6086 [R_{int} = 0.0240, R_{sigma} = 0.0137]	12666 [R_{int} = 0.0395, R_{sigma} = 0.0215]	4830 [R_{int} = 0.0556, R_{sigma} = 0.0360]
Data/restraints/parameters	6086/1187/503	12666/573/706	4830/1/322
Goodness-of-fit on F²	1.034	1.021	1.063
Final R indexes [I>=2σ (I)]	R_1 = 0.0711, wR_2 = 0.2063	R_1 = 0.0388, wR_2 = 0.1031	R_1 = 0.0474, wR_2 = 0.1283
Final R indexes [all data]	R_1 = 0.0721, wR_2 = 0.2077	R_1 = 0.0442, wR_2 = 0.1082	R_1 = 0.0482, wR_2 = 0.1297
Largest diff. peak/hole / e Å⁻³	0.56/-0.35	0.46/-0.35	1.54/-1.36
Flack parameter	0.011(7)	-	-0.016(13)

Table 5.8	Rh-18c	Ir-18o	Ir-18c
Empirical formula	$C_{28}H_{56}B_2O_2P_2$	$C_{29}H_{49}IrO_3P_2$	$C_{31}H_{53}IrOP_2$
Formula weight	508.28	699.82	695.87
Temperature/K	150(2)	150(2)	150(2)
Crystal system	monoclinic	orthorhombic	orthorhombic
Space group	$P2_1/c$	$Pca2_1$	$P2_12_12_1$
a/Å	15.09343(9)	20.8772(2)	10.91013(11)
b/Å	12.86467(7)	10.65296(8)	13.58277(17)
c/Å	32.65837(16)	13.56659(11)	20.9292(2)
α/°	90	90	90
β/°	90.5535(5)	90	90
γ/°	90	90	90
Volume/Å³	6341.04(6)	3017.26(4)	3101.49(6)
Z	8	4	4
ρ_{calc}g/cm³	1.065	1.541	1.49
μ/mm⁻¹	1.388	9.772	4.429
F(000)	2240	1416	1416
Crystal size/mm³	0.653 × 0.24 × 0.087	0.304 × 0.224 × 0.088	0.4 × 0.2 × 0.2
Radiation	CuKα (λ = 1.54184)	CuKα (λ = 1.54184)	MoKα (λ = 0.71073)
2Θ range for data collection/°	5.412 to 147.224	13.052 to 140.146	6.172 to 59.146
Index ranges	$-18 \le h \le 17$, $-15 \le k \le 15$, $-40 \le l \le 33$	$-22 \le h \le 25$, $-12 \le k \le 12$, $-16 \le l \le 16$	$-15 \le h \le 15$, $-18 \le k \le 18$, $-29 \le l \le 29$
Reflections collected	68205	25010	120512
Independent reflections	12666 [R_{int} = 0.0395, R_{sigma} = 0.0215]	5667 [R_{int} = 0.0356, R_{sigma} = 0.0261]	8680 [R_{int} = 0.0529, R_{sigma} = 0.0209]
Data/restraints/parameters	12666/573/706	5667/1/323	8680/0/322
Goodness-of-fit on F²	1.021	1.075	1.07
Final R indexes [I>=2σ (I)]	R_1 = 0.0388, wR_2 = 0.1031	R_1 = 0.0192, wR_2 = 0.0464	R_1 = 0.0154, wR_2 = 0.0338
Final R indexes [all data]	R_1 = 0.0442, wR_2 = 0.1082	R_1 = 0.0205, wR_2 = 0.0467	R_1 = 0.0166, wR_2 = 0.0343
Largest diff. peak/hole / e Å⁻³	0.46/-0.35	0.60/-0.48	0.80/-0.36
Flack parameter	-	0.234(9)	-0.0172(19)

Table 5.9	**Rh-19o**	**Rh-19c**	**Ir-19o**
Empirical formula	$C_{29}H_{49}Cl_2O_3P_2Rh$	$C_{31}H_{53}Cl_2OP_2Rh$	$C_{29}H_{49}Cl_2O_3P_2Ir$
Formula weight	681.43	677.48	770.72
Temperature/K	150(2)	150(2)	150(2)
Crystal system	orthorhombic	orthorhombic	orthorhombic
Space group	Pbca	$P2_12_12_1$	Pbca
a/Å	12.40495(16)	11.62738(6)	12.4393(2)
b/Å	13.12123(13)	11.80036(5)	13.2278(2)
c/Å	39.3620(5)	24.50061(12)	39.2327(7)
α/°	90	90	90
β/°	90	90	90
γ/°	90	90	90
Volume/Å³	6406.88(13)	3361.66(3)	6455.6(2)
Z	8	4	8
ρ_{calc}g/cm³	1.413	1.339	1.586
μ/mm⁻¹	7.004	6.624	10.681
F(000)	2848	1424	3104
Crystal size/mm³	0.146 × 0.089 × 0.023	0.174 × 0.147 × 0.069	0.168 × 0.092 × 0.024
Radiation	CuKα (λ = 1.54184)	CuKα (λ = 1.54184)	CuKα (λ = 1.54184)
2Θ range for data collection/°	13.32 to 140.136	12.902 to 140.13	13.578 to 140.14
Index ranges	$-14 \leq h \leq 15$, $-16 \leq k \leq 15$, $-37 \leq l \leq 48$	$-14 \leq h \leq 14$, $-14 \leq k \leq 14$, $-29 \leq l \leq 28$	$-15 \leq h \leq 15$, $-16 \leq k \leq 16$, $-47 \leq l \leq 47$
Reflections collected	54793	29314	68739
Independent reflections	6061 [R_{int} = 0.0616, R_{sigma} = 0.0289]	6376 [R_{int} = 0.0314, R_{sigma} = 0.0209]	6116 [R_{int} = 0.0731, R_{sigma} = 0.0357]
Data/restraints/parameters	6061/258/377	6376/354/395	6116/258/377
Goodness-of-fit on F²	1.267	1.053	1.445
Final R indexes [I>=2σ (I)]	R_1 = 0.0514, wR_2 = 0.1078	R_1 = 0.0170, wR_2 = 0.0404	R_1 = 0.0677, wR_2 = 0.1237
Final R indexes [all data]	R_1 = 0.0564, wR_2 = 0.1100	R_1 = 0.0181, wR_2 = 0.0408	R_1 = 0.0748, wR_2 = 0.1260
Largest diff. peak/hole / e Å⁻³	0.80/-1.03	0.34/-0.21	2.32/-3.87
Flack parameter	-	-0.021(2)	-0.021(2)

Table 5.10	Ir-19c	Rh-24o	Rh-25o
Empirical formula	$C_{31}H_{53}Cl_2IrOP_2$	$C_{64}H_{100}O_{3.5}P_2RhSi$	$C_{60}H_{91}O_2P_2Rh$
Formula weight	766.77	1118.37	1009.17
Temperature/K	150(2)	150(2)	150(2)
Crystal system	orthorhombic	monoclinic	triclinic
Space group	$P2_12_12_1$	$P2_1/c$	P-1
a/Å	11.6548(2)	16.59803(8)	13.3283(5)
b/Å	11.78332(18)	12.01061(7)	21.5473(6)
c/Å	24.5327(4)	32.98791(18)	23.0673(9)
α/°	90	90	64.912(3)
β/°	90	102.9884(5)	74.571(3)
γ/°	90	90	72.701(3)
Volume/Å³	3369.14(10)	6407.97(6)	5652.8(4)
Z	4	4	4
ρ_{calc}g/cm³	1.512	1.159	1.186
μ/mm⁻¹	4.238	3.116	3.264
F(000)	1552	2404	2168
Crystal size/mm³	0.326 × 0.324 × 0.08	0.569 × 0.141 × 0.067	0.179 × 0.038 × 0.01
Radiation	MoKα (λ = 0.71073)	CuKα (λ = 1.54184)	CuKα (λ = 1.54184)
2Θ range for data collection/°	5.934 to 59.146	12.97 to 140.14	12.724 to 140.148
Index ranges	$-16 \le h \le 16$, $-16 \le k \le 16$, $-34 \le l \le 34$	$-20 \le h \le 20$, $-13 \le k \le 14$, $-40 \le l \le 40$	$-15 \le h \le 16$, $-26 \le k \le 25$, $-27 \le l \le 28$
Reflections collected	79384	102956	78067
Independent reflections	9431 [R_{int} = 0.0430, R_{sigma} = 0.0240]	12147 [R_{int} = 0.0418, R_{sigma} = 0.0211]	21412 [R_{int} = 0.0796, R_{sigma} = 0.0808]
Data/restraints/parameters	9431/270/395	12147/699/770	21412/213/1238
Goodness-of-fit on F²	1.058	1.032	1.01
Final R indexes [I>=2σ (I)]	R_1 = 0.0180, wR_2 = 0.0377	R_1 = 0.0294, wR_2 = 0.0719	R_1 = 0.0519, wR_2 = 0.1203
Final R indexes [all data]	R_1 = 0.0200, wR_2 = 0.0384	R_1 = 0.0333, wR_2 = 0.0747	R_1 = 0.0821, wR_2 = 0.1362
Largest diff. peak/hole / e Å⁻³	0.75/-0.40	0.60/-0.50	0.75/-1.41
Flack parameter	-0.0206(18)	-	-

Table 5.11	***t*Bu-Rh-25o**	**Rh-26o**
Empirical formula	$C_{54}H_{81}O_2P_2Rh$	$C_{65}H_{103}O_3P_2RhSi$
Formula weight	927.03	1125.41
Temperature/K	150(2)	150(2)
Crystal system	orthorhombic	monoclinic
Space group	Pccn	$P2_1/c$
a/Å	19.67019(8)	16.55669(14)
b/Å	27.30087(9)	10.34632(11)
c/Å	19.74945(7)	38.3373(3)
α/°	90	90
β/°	90	100.0175(8)
γ/°	90	90
Volume/Å³	10605.71(7)	6467.09(10)
Z	8	4
ρ_{calc}g/cm³	1.161	1.156
μ/mm⁻¹	3.438	3.083
F(000)	3968	2424
Crystal size/mm³	0.256 × 0.144 × 0.05	0.196 × 0.062 × 0.035
Radiation	CuKα (λ = 1.54184)	CuKα (λ = 1.54184)
2Θ range for data collection/°	12.704 to 140.146	12.696 to 140.144
Index ranges	$-22 \leq h \leq 23$, $-33 \leq k \leq 33$, $-24 \leq l \leq 24$	$-18 \leq h \leq 20$, $-11 \leq k \leq 12$, $-46 \leq l \leq 46$
Reflections collected	122452	50357
Independent reflections	10058 [R_{int} = 0.0396, R_{sigma} = 0.0146]	12248 [R_{int} = 0.0374, R_{sigma} = 0.0319]
Data/restraints/parameters	10058/1203/636	12248/475/750
Goodness-of-fit on F²	1.072	1.049
Final R indexes [I>=2σ (I)]	R_1 = 0.0358, wR_2 = 0.0829	R_1 = 0.0303, wR_2 = 0.0714
Final R indexes [all data]	R_1 = 0.0389, wR_2 = 0.0850	R_1 = 0.0359, wR_2 = 0.0741
Largest diff. peak/hole / e Å⁻³	0.80/-0.47	0.52/-0.57
Flack parameter	-	-

References

[1] T. R. Hoye, B. M. Eklov, M. Voloshin, *Org. Lett.* **2004**, *6*, 2567–2570.
[2] E. Salomó, S. Orgué, A. Riera, X. Verdaguer, *Synthesis* **2016**, *48*, 2659–2663.
[3] S. Orgué, A. Flores-Gaspar, M. Biosca, O. Pàmies, M. Diéguez, A. Riera, X. Verdaguer, *Chem. Commun.* **2015**, *51*, 17548–17551.
[4] T. León, A. Riera, X. Verdaguer, *J. Am. Chem. Soc.* **2011**, *133*, 5740–5743.
[5] Y. Chen, T. P. Clark, B. A. Jazdzewski, S. B. Klamo, T. T. Wenzel, *Polyhedron* **2014**, *84*, 32–36.
[6] T. M. Hood, M. R. Gyton, A. B. Chaplin, *Dalton Trans.* **2020**, DOI 10.1039/C9DT04474D.
[7] M. S. Carle, G. K. Shimokura, G. K. Murphy, *Eur. J. Org. Chem.* **2016**, *2016*, 3930–3933.
[8] J. A. Osborn, G. Wilkinson, J. J. Mrowca, in *Inorg. Synth.* (Ed.: R.J. Angelici), John Wiley & Sons, Inc., Hoboken, NJ, USA, **2007**, pp. 77–79.
[9] A. L. Onderdelinden, R. A. Schunn, van der Ent, A., in *Inorg. Synth.*, John Wiley & Sons, Inc., **1973**, pp. 92–95.
[10] J. L. Herde, J. C. Lambert, C. V. Senoff, M. A. Cushing, in *Inorg. Synth.* (Ed.: G.W. Parshall), John Wiley & Sons, Inc., **1974**, pp. 18–20.
[11] C. J. Moulton, B. L. Shaw, *J. Chem. Soc., Dalton Trans.* **1976**, 1020–1024.
[12] D. Morales-Morales, R. Redón, Z. Wang, D. W. Lee, C. Yung, K. Magnuson, C. M. Jensen, *Can. J. Chem.* **2001**, *79*, 823–829.
[13] S. Nemeh, C. Jensen, E. Binamira-Soriaga, W. C. Kaska, *Organometallics* **1983**, *2*, 1442–1447.
[14] I. Göttker-Schnetmann, P. S. White, M. Brookhart, *Organometallics* **2004**, *23*, 1766–1776.
[15] A. V. Polezhaev, S. A. Kuklin, D. M. Ivanov, P. V. Petrovskii, F. M. Dolgushin, M. G. Ezernitskaya, A. A. Koridze, *Russ. Chem. Bull.* **2009**, *58*, 1847–1854.
[16] M. Brookhart, B. Grant, A. F. Volpe, *Organometallics* **1992**, *11*, 3920–3922.
[17] R. Zhang, X. Hao, X. Li, Z. Zhou, J. Sun, R. Cao, *Cryst. Growth Des.* **2015**, *15*, 2505–2513.
[18] M. H. Vilhelmsen, J. Jensen, C. G. Tortzen, M. B. Nielsen, *Eur. J. Org. Chem.* **2013**, *2013*, 701–711.
[19] J. Y. C. Lim, N. Yuntawattana, P. D. Beer, C. K. Williams, *Angew. Chem. Int. Ed.* **2019**, *58*, 6007–6011.
[20] G. R. Fulmer, A. J. M. Miller, N. H. Sherden, H. E. Gottlieb, A. Nudelman, B. M. Stoltz, J. E. Bercaw, K. I. Goldberg, *Organometallics* **2010**, *29*, 2176–2179.
[21] C. R. Hilliard, N. Bhuvanesh, J. A. Gladysz, J. Blümel, *Dalton Trans* **2012**, *41*, 1742–1754.
[22] In *Solubility Data Ser.*, Elsevier, **1990**, pp. 110–151.
[23] J.-H. Ulises-Javier, E. J. Pardillo-Fontdevila, A. M. Wilhelm, H. Delmas, *Lat Am Appl Res* **2004**, *34*, 71–74.
[24] C. W. Hopkins, S. Le Grand, R. C. Walker, A. E. Roitberg, *J. Chem. Theory Comput.* **2015**, *11*, 1864–1874.
[25] F. Neese, *Wiley Interdiscip. Rev. Comput. Mol. Sci.* **2012**, *2*, 73–78.
[26] F. Neese, *Wiley Interdiscip. Rev. Comput. Mol. Sci.* **2018**, *8*, e1327.
[27] S. L. Apps, R. E. Alflatt, B. Leforestier, C. M. Storey, A. B. Chaplin, *Polyhedron* **2017**, DOI 10.1016/j.poly.2017.08.001.
[28] M. R. Gyton, B. Leforestier, A. B. Chaplin, *Organometallics* **2018**, *37*, 3963–3971.
[29] T. M. Hood, B. Leforestier, M. R. Gyton, A. B. Chaplin, *Inorg. Chem.* **2019**, *58*, 7593–7601.
[30] G. L. Parker, S. Lau, B. Leforestier, A. B. Chaplin, *Eur. J. Inorg. Chem.* **2019**, *2019*, 3791–3798.
[31] S. Grimme, J. Antony, S. Ehrlich, H. Krieg, *J. Chem. Phys.* **2010**, *132*, 154104.
[32] Y.-S. Lin, G.-D. Li, S.-P. Mao, J.-D. Chai, *J. Chem. Theory Comput.* **2013**, *9*, 263–272.
[33] F. Weigend, R. Ahlrichs, *Phys. Chem. Chem. Phys.* **2005**, *7*, 3297–3305.
[34] T. Leininger, A. Nicklass, W. Küchle, H. Stoll, M. Dolg, A. Bergner, *Chem. Phys. Lett.* **1996**, *255*, 274–280.
[35] F. Weigend, *Phys. Chem. Chem. Phys.* **2006**, *8*, 1057–1065.
[36] F. Neese, F. Wennmohs, A. Hansen, U. Becker, *Chem. Phys.* **2009**, *356*, 98–109.
[37] G. M. Sheldrick, *Acta Crystallogr. Sect. C Struct. Chem.* **2015**, *71*, 3–8.
[38] O. V. Dolomanov, L. J. Bourhis, R. J. Gildea, J. A. K. Howard, H. Puschmann, *J. Appl. Crystallogr.* **2009**, *42*, 339–341.

Chapter 6

Summary of findings

The preparation and organometallic chemistry of macrocyclic phosphine-based anionic pincer ligands derived from resorcinol (**POCOP-14**) and *m*-xylene (**PCP-14**) has been described, with a view to studying the rhodium- and iridium-mediated activation of alkanes mechanically entrapped within the ligand scaffold.

Synthesis of the proligand **POCOP-14'** was achieved following an eight-step racemic procedure starting from *tert*-butyldichlorophosphine and involving borane protection, ring-closing olefin metathesis, hydrogenation, chromatographic separation from the *syn*-substituted diastereomer, and borane deprotection (Scheme 6.1). Whilst **POCOP-14'** was obtained in a respectable overall yield of 29%, the formation of an equal amount of the undesired *syn* isomer during the procedure makes it inherently atom-inefficient, and the separation of the diastereomers is very tedious and time consuming.

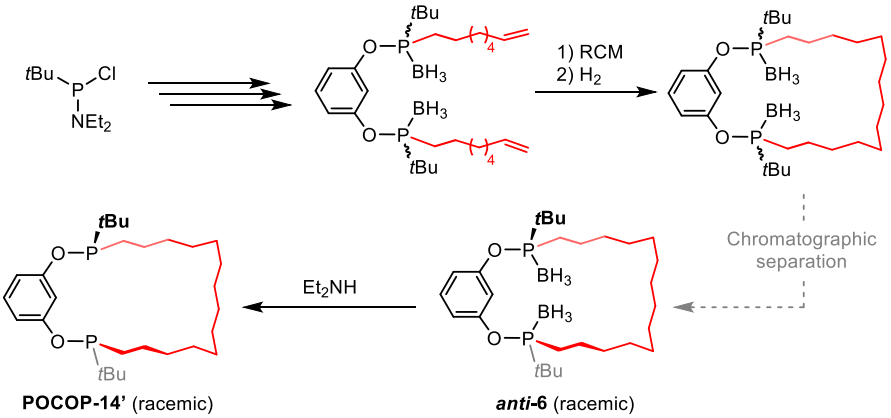

Scheme 6.1. Preparation of *rac*-**POCOP-14'**.

As a more attractive alternative, an asymmetric variant employing (-)-*cis*-1-amino-2-indanol as a chiral auxiliary was developed for the synthesis of the proligand **PCP-14'**. This procedure exploits the stereoselective ring-opening of a known oxazaphospholidine borane by octen-7-yl-magnesium bromide, with cleavage of the chiral auxiliary effected by acidolysis to afford a phosphinous acid that can, in turn, be converted to a chiral phosphine borane intermediate. Whilst the phosphine borane was found to be unstable, it can be deprotected to afford the PCP backbone in the desired *anti*-configuration selectively. In this way, **PCP-14'** was ultimately obtained in an overall yield of 48% and > 95% ee (Scheme 6.2).

Unfortunately, and despite considerable effort, this methodology could not be extended to the asymmetric synthesis of **POCOP-14'**.

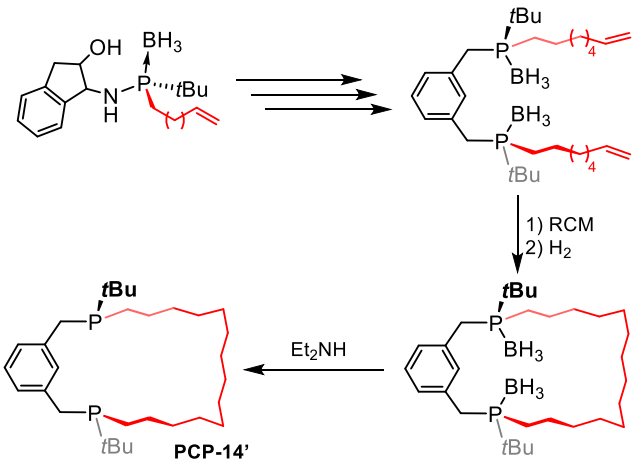

Scheme 6.2. Preparation of (*R*,*R*)-**PCP-14'**.

The macrocyclic pincer proligands are readily metallated using rhodium and iridium diene precursors, but careful tuning of the reaction conditions was required to avoid formation of polymeric derivatives and intramolecular C–H bond activation of the tetradecamethylene linker. The optimised procedures all involved metallation and dehydrohalogenation under hydrogen and generated hydride complexes **M-15o,c** (ML_n = $Rh(H_2)$, $IrH_2(H_2)$/IrH_4; Scheme 6.3). From these hydride species, the corresponding $M^{I}(CO)$ (**M-18o,c**) and $M^{III}Cl_2(CO)$ (**M-19o,c**) derivates can be obtained *in situ*, but only the latter are sufficiently air and silica stable to allow their isolation as analytically pure compounds. The $M^{I}(CO)$ derivatives can, however, be obtained as clean materials by reduction of **M-19o,c** and enable quantification of the donor properties of the new ligands by measurement of the carbonyl stretching frequencies by IR spectroscopy. In this way, **PCP-14** and **POCOP-14** were found to be marginally weaker donors than the corresponding acyclic congeners *t*Bu$_4$-PCP and *t*Bu$_4$-POCOP, respectively, consistent with changes in the phosphine/phosphinite substituents alone.

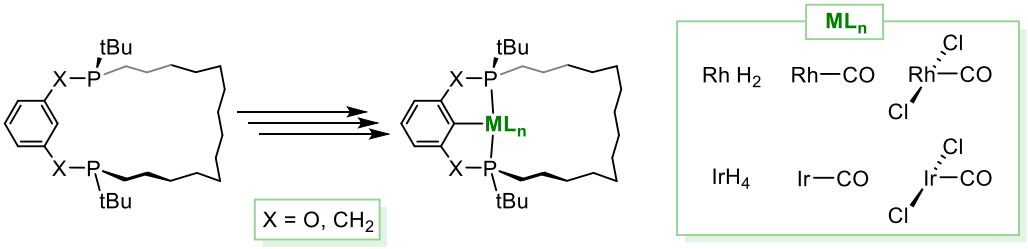

Scheme 6.3. Preparation of Rh and Ir complexes of **POCOP-14** and **PCP-14**.

The isolation of **M-19o,c** proved to be an important milestone in the project, not only as means to generate **M-18o,c,** but also as a template for constructing interlocked architectures. Methods starting alternatively from M(I) 14VE derivatives, for instance, were discounted as reactions between the hydride complexes and **M-15o,c** and the sacrificial hydrogen acceptor *tert*-butylethylene resulted in rapid intramolecular C–H bond activation.

With a view to capturing interlocked topologies, C(sp)–C(sp) bond formation through the cavity of the bound PXCXP ligands was targeted. This approach was first evaluated by installation of alkynyl ligands bearing the bulky 3,5-tBu$_2$C$_6$H$_3$ "stoppering" substituent (Ar'), by reaction of **M-19o,c** with the corresponding Grignard reagent to afford [M(PXCXP-14)(C$_2$Ar')$_2$(CO)] (**M-24o,c**). Subsequent decarbonylation was anticipated to induce reductive elimination and formation of the corresponding interlocked diyne derivatives, however, only in the case of **Rh-24o**, did this strategy prove effective. The resulting diyne complex [Rh(POCOP-14)(Ar'C$_4$Ar')] (**Rh-25o**) was found to exhibit interesting dynamic behaviour, involving alkyne π-complex shuttling, which was studied in detail by VT-NMR spectroscopy, GFN2-xTB based molecular dynamics and DFT calculations (Figure 6.1). More interestingly, reactions of **Rh-25o** with H_2 or CO at high temperature evidenced activation of the formidably robust C(sp)–C(sp) bond. Kinetic analysis of the latter using VT UV-vis spectroscopy, where **Rh-24o** was formed, confirmed that C–C bond scission step was rate-determining. This conclusion was further supported by measurement of a KIE of 1.08 ± 0.02 as well as a DFT-based analysis.

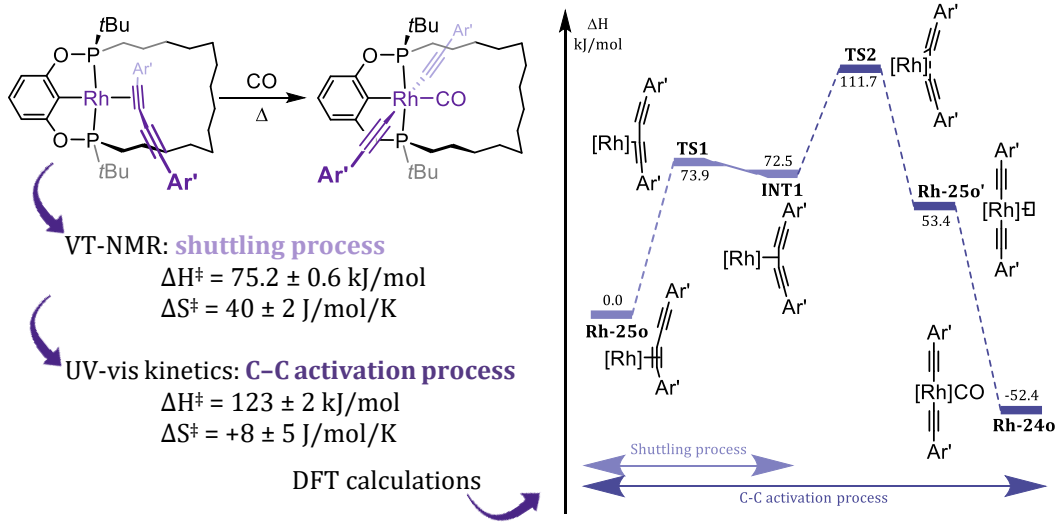

Figure 6.1. C(sp)–C(sp) bond cleavage observed for **Rh-25o**.

Whilst facile C(sp)–C(sp) bond hydrogenolysis prevented hydrogenation of the diyne axle component of **Rh-25o** by reaction with dihydrogen, a stepwise protocol was developed and that enabled preparation of the *E*-enyne (**Rh-28o**) and ultimately but-1-ene (**Rh-32o**) derivatives (Scheme 6.4).

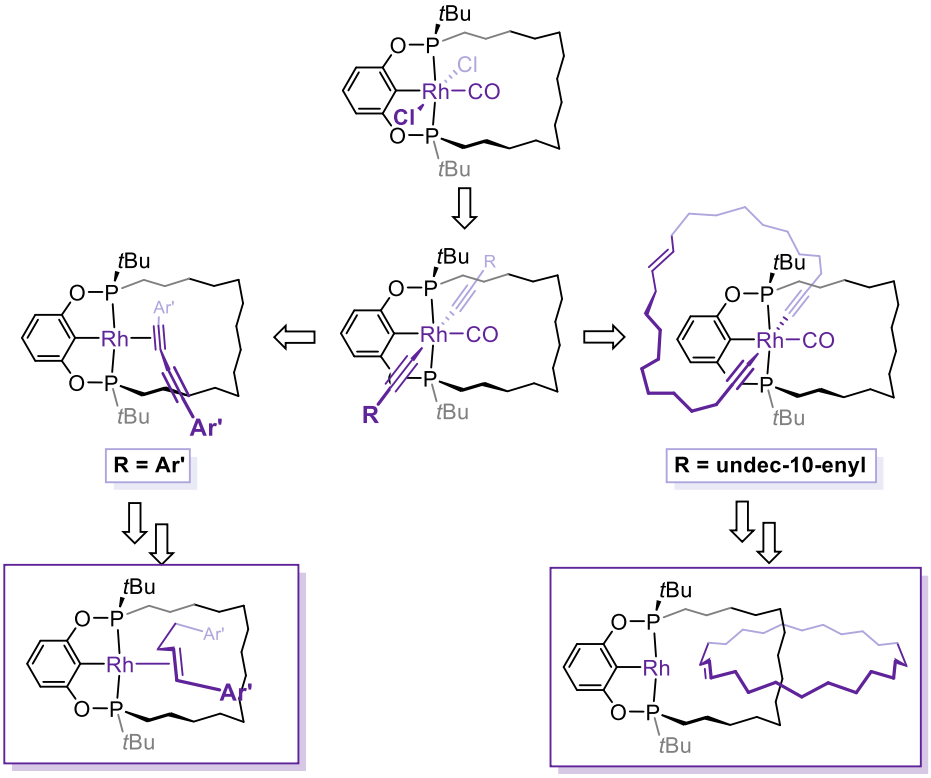

Scheme 6.4. η^2-alkene complexes **Rh-32o** and **Rh-36o**.

Extension of the bis(alkynyl)carbonyl-complex-based method to the synthesis of metallo-catenanes was also evaluated using **Ir-19o,c** and **Rh-19o**, by installation of alkynyl ligands bearing undec-10-enyl substituents and subsequent ring-closing olefin metathesis, catalysed by Grubbs' 2nd generation catalyst in fluorobenzene under high dilution conditions. Spectroscopic data was consistent with formation of the new metallocycle in all cases and verified for the iridium products **Ir-34o,c** by X-ray diffraction. Paralleling the reaction described above, only for the rhodium system was evidence for capture of a [2]catenate obtained, however, additional work is required to verify this promising preliminary finding (Scheme 6.4).

Combined, the work presented in this thesis demonstrates that the synthesis of macrocyclic pincer complexes featuring mechanically interlocked hydrocarbon substrates is, whilst incredibly challenging, possible. These methodological developments provide a strong foundation for future work towards the ultimate goal of using these systems to study the activation and dehydrogenation of alkanes.